

© 2019 by Huiying Liu. All rights reserved.

DYNAMIC REMODELING AND RAPID MANUFACTURING OF FUNCTIONAL
MATERIALS BY RING-OPENING METATHESIS POLYMERIZATION

BY

HUIYING LIU

DISSERTATION

Submitted in partial fulfillment of the requirements
for the degree of Doctor of Philosophy in Chemistry
in the Graduate College of the
University of Illinois at Urbana-Champaign, 2019

Urbana, Illinois

Doctoral Committee:

Professor Jeffrey S. Moore, Chair
Professor Scott K. Silverman
Associate Professor Yang Zhang
Professor Steven C. Zimmerman

Abstract

Ring-opening metathesis polymerization (ROMP) is a powerful and broadly applicable method to synthesize polymeric materials with unique architectures and useful functions. Remarkable progress has been made on the molecular design of catalysts and monomers that allows precise control over ROMP. The research presented in this dissertation investigates ROMP behavior of cyclic olefins with different ring nature in the bulk state, which is much less explored in the literature compared to solution ROMP. Structure-property relationships were constructed to advance fundamental understanding and provide guidance for further monomer design. Potential applications of these monomers in dynamic remodeling and rapid manufacturing were also demonstrated.

As ROMP is driven by the release of ring strain, a monomer-polymer equilibrium would be established for monomers with low ring strain energy. Chapter 2 investigates the reversibility of equilibrium ROMP and explores the feasibility of depolymerization in the bulk state upon a mild thermal stimulus. We conducted a systematic study on ceiling temperatures (T_c) of substituted cyclopentenes to quantitatively describe the polymerizability of the low-strain monomers both in solution and in the bulk state. This study also identified the important role of anchor group effect in T_c . With the establishment of tunable T_c s, Chapter 3 focuses on the development of thermally reversible networks for remodeling applications by employing multifunctional cyclopentenes. These neat monomers undergo ROMP at room temperature to afford mechanically robust, cross-linked polymers; at slightly elevated temperatures, the resulting polymers readily depolymerize to a free-flowing liquid. This polymerization-depolymerization process, characterized by thermal analysis and rheological tests, is triggered solely by temperature changes and is reversible for several cycles.

When cyclic olefins with large ring strain energy are polymerized, ROMP becomes irreversible and highly exothermic. The heat generated can be utilized as the energy source to trigger further polymerization; ultimately, a propagating reaction wave is produced to convert the available monomer to polymer. This process is termed as frontal ring-opening metathesis polymerization (FROMP) which has great potential in manufacturing large parts of thermosets and composites in a rapid and energy-efficient manner. Since only *exo*- and *endo*-dicyclopentadiene have been reported as FROMP monomers, Chapter 4 expands the scope of monomers and builds the structure-property relationship to guide functional materials design. We

investigated 30 strained cyclic olefins and correlated FROMP reactivity with the thermodynamic, kinetic and physical properties of the monomer using linear regression analysis. Due to the complexity of FROMP, linear regression did not perform well for structurally disparate monomers. Thus, machine learning approaches were applied with structural parameters of the monomer as inputs and FROMP-related properties (heat released and frontal velocity) as outputs. Models by random forest algorithm with reasonable predictability were constructed, and important features that determine FROMP behavior were also identified. With the expansion of FROMP toolbox, Chapter 5 examines the copolymerization behavior in FROMP. An unexpected non-monotonic increase in frontal velocity was observed in copolymerization with di-norbornenyl cross-linkers, which is counterintuitive to the mixing rules. We believe that the degree of cross-linking is the main contributor to this unusual behavior, which is supported by a series of copolymerization experiments with mono-norbornenyl derivatives. The copolymerization study not only provides a strategy to systematically modify materials properties (such as interfacial shear strength and mechanical properties) but also strengthens further understanding of the FROMP process.

To my family and friends

Acknowledgements

Graduate school has been an incredible adventure for me, filled with many ups and downs. I cannot picture myself crossing the finish line without the help and support from many people in my life. First and foremost, I would like to express my sincere gratitude to my fantastic advisor and mentor, Prof. Jeffrey S. Moore, for his support and guidance. He has been a constant inspiration and taught me many invaluable lessons about chemistry and life. I always felt so energized and unstoppable after meeting with him. His laissez-faire management style really made me grow as an independent and creative scientist, which is truly the goal of a Ph.D.

I would also like to thank my committee members: Prof. Scott K. Silverman, Prof. Yang Zhang, Prof. Steven C. Zimmerman, Prof. Catherine J. Murphy, and Prof. Kami L. Hull. Their constructive feedback and encouragement have been very helpful throughout my journey at UIUC. Additionally, I want to thank Prof. Randy H. Ewoldt, Prof. Narayana R. Aluru and Prof. Jeremy E. Wulff for providing insightful discussions and suggestions on the collaborated projects.

The work described here would not be possible without the efforts of my amazing collaborators including Dr. Arif Z. Nelson, Dr. Yi Ren, Dr. Ke Yang, Dr. Shijia Tang, Dr. Haibing Wei, Dr. Pikee Priya, and Tong Li. It is a great pleasure to work with them, and I am truly grateful for our interactions through all these years. Financial support for this work was provided by the Air Force Office of Scientific Research with award FA9550-16-1-0017.

I've received countless help from the Moore group members. First, I want to thank Dr. Nagamani Chikkannagari, my mentor in my first year. We worked together on the mechanoacid project which really got me started in graduate school. I thank Dr. Olivia Lee and Dr. Anna Yang for always taking care of me and offering lots of positive thoughts on research, writing, and life in general. Thanks to Dr. Joshua Grolman for being a wonderful team member in National Science Foundation I-Corps program where I learned a lot about entrepreneurship and commercialization. I am grateful for all the insightful discussions and suggestions from Dr. Joshua Kaitz, Dr. Jun Li, Dr. Eric Epstein, Dr. Maxwell Robb, Dr. Ian Robertson, Dr. Xing Jiang, Dr. Xiaocun Lu, Dr. Yu Cao, Dr. Etienne Chenard, Dr. Kristin Hutchins, Dr. Vivian Lau, Dr. Semin Lee, Dr. Kenneth Schwieter, Dr. Lily Robertson, Dr. Gabe Rudebusch, Dr. Adam Feinberg, Dr. Qian Hai and Dr. Qiong Wu.

I thank everyone from the Moore group, both current members and alumni, for providing an open and supportive environment. I sincerely enjoyed my time here and thank you all for your company: Dr. Nina Sekerak, Dr. Catherine Possanza Casey, Dr. Shawn Miller, Dr. Yang Song, Kevin Cheng, Dr. Nagarjuna Gavvalapalli, Dr. Timothy Money Penny, Anderson Coates, Chengtian Shen, Abigail Halmes, Jose Zavala, Hao Yu, Morgan Cencer, Oleg Davydovich, Liuyan Tang, Dr. Yingxian Ma, Dr. Po Yang, Dr. Yun Liu, Dr. Kevin Schwarz, Chris Pattillo, Summer Laffoon, Evan Lloyd, Katherine Stawiasz and Andrew Greenlee. I would also like to acknowledge the entire AMS group for providing an incredible multidisciplinary environment.

Special thanks to Ashley Trimmell, who has been phenomenal in keeping the Moore group organized. I am also grateful to the administrative/supporting staff who helped me during graduate school: Dr. Dean Olson, Dr. Lingyang Zhu, Dr. Andre Sutrisno, Dr. Dianwen Zhang, Erica Malloch, Dorothy Loudermilk, Dawn Goeddel, Lori Johnson, Jamison Lowe, Kara Metcalf, Jason Madden, Connie Knight, Patricia Simpson, and Karen Watson. They made many processes at UIUC smooth for me.

Finally, I want to acknowledge my friends and family for their encouragement and help throughout my life. In particular, I want to thank my parents for their unconditional love. I would also like to thank my dear husband Neng Xiao who is also a brilliant chemist. Neng, thank you for always supporting and trusting me even though we are not doing graduate school in the same city. You are my best friend and I love you!

Table of Contents

Chapter 1: Introduction	1
1.1 Overview of Ring-Opening Metathesis Polymerization.....	1
1.2 ROMP Catalyst Development.....	3
1.3 ROMP Monomer Selection.....	4
1.3.1 Monomer with High Ring Strain	5
1.3.2 Monomer with Low Ring Strain	8
1.4 Applications of ROMP	9
1.5 Conclusion	9
1.6 References.....	10
Chapter 2: Ceiling Temperature of Cyclopentene Derivatives in Ring-Opening Metathesis Polymerization	17
2.1 Abstract	17
2.2 Introduction.....	17
2.3 Theoretical Calculations of Polymerization Enthalpy	18
2.4 Ceiling Temperature of Cyclopentene Derivatives.....	19
2.5 Evaluation of Reversibility	23
2.6 Conclusion	24
2.7 Experimental Details.....	24
2.7.1 Materials and General Methods.....	24
2.7.2 Synthesis of Cyclopentene Derivatives	25
2.7.3 Ceiling Temperature Measurement.....	32
2.7.4 DSC Characterization	36
2.7.5 Evaluation of Reversibility	37
2.8 Notes and References.....	39
Chapter 3: Dynamic Remodeling of Network Polymers via Ring-Opening Metathesis Polymerization	42
3.1 Abstract.....	42

3.2 Introduction.....	42
3.3 Design of Multifunctional Cyclopentene Derivatives	43
3.4 Tuning Depolymerization Behavior by Copolymerization.....	46
3.5 Evaluation of Reversibility by Rheological Characterization	47
3.6 Conclusion	48
3.7 Experimental Details.....	49
3.7.1 Materials and General Methods.....	49
3.7.2 Synthesis of Multifunctional Cyclopentene Derivatives	50
3.7.3 DSC Characterization	57
3.7.4 Raman Characterization.....	59
3.7.5 Rheological Characterization.....	60
3.7.6 Evaluation of Reversibility	63
3.8 Notes and References.....	64
Chapter 4: Monomer Design in Frontal Ring-Opening Metathesis Polymerization.....	66
4.1 Abstract.....	66
4.2 Introduction.....	66
4.3 Structure-Property Relationship by Linear Regression	67
4.3.1 Constitutive Equation.....	69
4.3.2 Effect of Molecular Weight	71
4.3.3 Correlation with Thermodynamic Properties.....	72
4.3.4 Effect of Substituents.....	73
4.4 Structure-Property Relationship by Machine Learning	74
4.5 Gel Time of Functionalized Monomers.....	78
4.6 Cross-Linking Mechanism of DCPD.....	80
4.7 FROMP of TCND.....	82
4.8 Conclusion	83
4.9 Experimental Details.....	84
4.9.1 Materials and General Methods.....	84
4.9.2 Synthesis of Strained Monomers	84
4.9.3 Frontal Velocity Measurement	106

4.9.4 DSC Characterization	107
4.9.5 Kinetic Experiments.....	109
4.9.6 Machine Learning Model.....	110
4.9.7 Gel Time Measurement.....	112
4.10 References.....	113

Chapter 5: Non-Monotonic Acceleration in Frontal Ring-Opening Metathesis

Copolymerization	117
5.1 Abstract.....	117
5.2 Introduction.....	117
5.3 Design of Cross-Linkers	119
5.4 Mixing Rule in Copolymerization	120
5.5 Copolymerization with Cross-Linkers.....	121
5.6 Role of Cross-Linking.....	124
5.7 Conclusion	127
5.8 Experimental Details.....	127
5.8.1 Materials and General Methods	127
5.8.2 Frontal Velocity Measurement	128
5.8.3 DSC Characterization	129
5.9 References.....	132

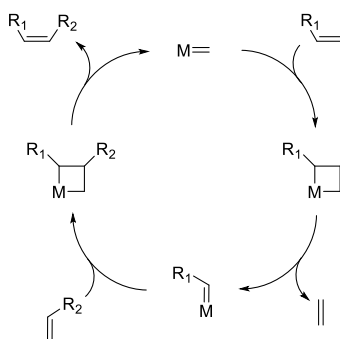
Chapter 6: Summary and Outlook..... 134

6.1 Summary.....	134
6.2 Outlook	136

Chapter 1: Introduction

1.1 Overview of Ring-Opening Metathesis Polymerization

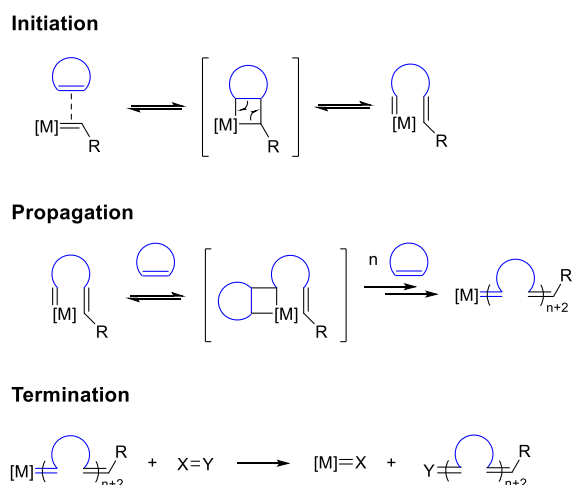
Olefin metathesis reactions are metal-mediated carbon-carbon double bond (C=C) exchange process, which were discovered in the mid-1950s by industrial chemists at DuPont, Standard Oil and Phillips Petroleum who reported that propene reacted to generate ethylene and 2-butene when passed over a molybdenum-on-alumina catalyst at high temperature.^{1,2} The generally accepted mechanism which involves the formation of metallacyclobutane intermediates was originally proposed by Chauvin, as illustrated in Scheme 1.1.³ In the early stages, transition metal chlorides (such as $WCl_6/EtAlCl_2$) were employed as catalysts for the reaction, but the well-defined transition metal carbene catalysts developed by Schrock and Grubbs have remarkably advanced the mechanistic understanding and control of catalytic activity, which enabled the synthesis of a wide range of polymers with complex architectures and useful functions. Thus, the 2005 Nobel Prize in Chemistry was awarded to Yves Chauvin, Robert H. Grubbs and Richard R. Schrock for “development of metathesis method in organic synthesis”.²



Scheme 1.1 Mechanism of a typical olefin metathesis reaction.

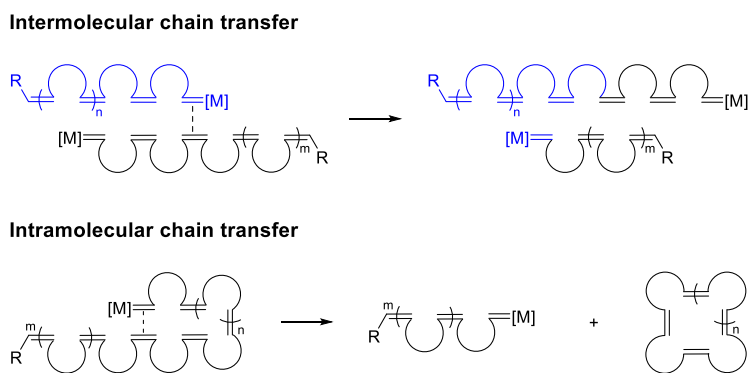
Ring-opening metathesis polymerization (ROMP) is an application of olefin metathesis to polymer synthesis.⁴⁻⁸ It is a chain growth polymerization process that converts cyclic olefins into polymers comprised of C=C repeating units. As a result, the unsaturation associated with the monomer is retained after polymerization, which is different from typical olefin addition polymerizations. The metal-mediated ROMP mechanism is shown in Scheme 1.2. The initiation step involves the coordination of a cyclic olefin to the metal alkylidene complex to afford a four-membered metallacyclobutane intermediate by [2+2] cycloaddition. This intermediate

subsequently undergoes cycloreversion to generate a new metal alkylidene. Although the resulting complex has increased in size due to the incorporation of monomers, its reactivity is similar compared to the initiator. Hence, analogous steps are repeated during the propagation stage until the reaction is terminated either due to the complete consumption of the monomer or quenching of the catalyst. Living ROMP is commonly quenched through the addition of a specialized reagent to selectively remove the transition metal from the chain end or install functional groups at the chain end for further modification.^{9–11} Other than metal-mediated ROMP, Boydston and coworkers developed photoredox-mediated metal-free ROMP that undergoes inherently distinct mechanism.^{12–15}



Scheme 1.2 A general mechanism of metal-mediated ROMP.

ROMP is commonly accompanied by intermolecular and intramolecular chain transfer reactions as illustrated in Scheme 1.3.^{6,16} The carbene moiety at a growing polymer chain might react with a C=C from another polymer chain or from its own polymer chain, which is detrimental for obtaining polymers with narrow dispersity and synthesizing precision polymers. To achieve living polymerization where ROMP proceeds without any side reactions, a fast-initiating catalyst is desired, and the monomer is preferably sterically bulky enough to prevent chain transfer reactions. Other approaches were also reported such as adding phosphine ligands¹⁷ or using variable temperature techniques.¹⁸



Scheme 1.3 Chain transfer reactions in ROMP.

1.2 ROMP Catalyst Development

Early catalyst systems were heterogeneous mixtures that were extremely sensitive toward air and moisture, which makes the structural characterization and systematic optimization quite challenging. Therefore, tremendous efforts have been made in the development of well-defined, functional-group-tolerant catalysts which are based on titanium,^{19–21} tantalum,^{22–24} tungsten,^{25,26} molybdenum^{27–30} and ruthenium.^{31,32} Unlike early transition-metal catalysts, ruthenium shows low oxophilicity, which makes it more stable toward oxygen, water and many polar functional groups such as alcohols, amides, aldehydes, and carboxylic acids.³¹ As a result, hundreds of ruthenium olefin metathesis catalysts have been prepared, and they offer a wide array of structures and activities that benefit specific applications such as aqueous and asymmetric reactions. In addition, for most applications, a few structures will provide excellent results.

Various metathesis-active ruthenium catalysts are commonly used and commercially available as shown in Figure 1.1. Substitution of one tricyclohexylphosphine (PCy₃) ligand on Grubbs first-generation catalyst (Grubbs I) with the bulky *N*-heterocyclic carbene (NHC) ligand affords Grubbs second-generation catalyst (Grubbs II).³³ Grubbs II displays higher catalytic reactivity than Grubbs I while maintaining the excellent functional group tolerance and thermal stability. This improvement was rationalized on the basis of an increased affinity of the NHC-substituted Ru center for π -acidic olefins relative to σ -donating phosphines.^{34,35} Furthermore, substitution of the PCy₃ for a bidentate alkylidene forms isopropoxystyrene-coordinated Hoveyda-Grubbs second-generation catalyst (HG II) that exhibits improved thermal stability, oxygen- and moisture-tolerance.³⁶ However, it has a decreased initiation rate which is a major

disadvantage in living polymerization or block copolymer synthesis. Due to the lability of pyridine ligands, one of the most famous fast-initiating catalysts is Grubbs third-generation catalyst (Grubbs III). Its initiation rate is at least six orders of magnitude higher than Grubbs II, which enables its application in synthesizing monodisperse polymers.^{37,38}

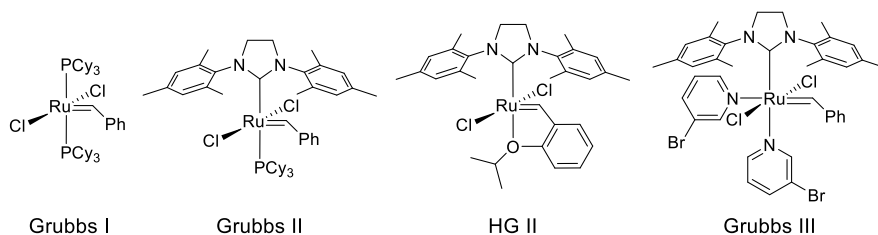


Figure 1.1 Common ruthenium metathesis catalysts.

To ensure catalyst efficiency in solution polymerization, the most common solvents for ROMP are non-coordinating, including chloroform, dichloromethane and toluene. However, coordinating solvents such as tetrahydrofuran are also used in some cases, and they have been shown to limit or even prevent secondary metathesis.^{17,39–41}

1.3 ROMP Monomer Selection

With the development of well-defined catalysts, a large variety of monomers have been successfully polymerized using ROMP.¹⁶ Ring strain is not the only driving force for ROMP, and the thermodynamics of ROMP in terms of Gibbs-Helmholtz equation $\Delta G = \Delta H - T\Delta S$ also needs to be considered. For highly strained monomers such as norbornene (NBE) (Table 1.1),⁴² ΔH term is negative and dominant, arising mainly from distortion of the bond angles and stretching of the bonds in the ring. As a result, such monomers generally polymerize to high conversion or completion by a number of catalysts. For low-strain monomers (Table 1.2),^{42,43} ΔH and ΔS are more delicately balanced. ROMP of these monomers is then critically dependent on the nature of the ring and the presence of the substituents. Highly active catalysts are usually required, and polymerization rarely reaches full conversion. When the ring size is large enough (> 14 atoms), changes in enthalpy upon ring opening are minimal, and ROMP becomes entropy-driven through an increase in conformational freedom.^{44,45} My graduate work mainly focused on cyclopentene and NBE derivatives, and thus the entropy-driven ROMP is not further discussed here.

Table 1.1 Ring strain energy of high-strain monomers.⁴²







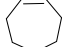
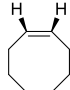
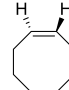
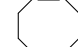
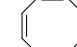
Monomer				
Ring Strain (kcal/mol)	54.5	30.6	27.2	34.7

Table 1.2 Ring strain energy of low-strain monomers.^{42,43}

Monomer							
Ring Strain (kcal/mol)	6.8	2.5	6.7	7.4	16.7	13.3	2.5

1.3.1 Monomer with High Ring Strain

The most commonly used monomer in ROMP is NBE derivatives because of their high ring strain and synthetic accessibility. NBE derivatives could be prepared by [2+4] cycloaddition of cyclopentadiene and an electron-deficient olefin. Moreover, a variety of substituted NBEs are commercially available. Figure 1.2 shows a few common starting materials for the synthesis of functionalized monomers by esterification or imidation.^{16,46}

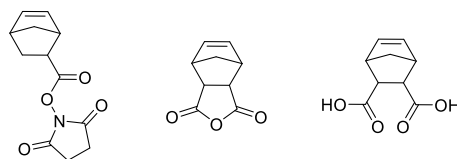


Figure 1.2 Examples of common norbornene-based starting materials.

The resulting monomer is composed of a polymerizable group (C=C) and a functional unit that is attached via an anchor group. The anchor group not only provides a synthetically feasible connection to the functional unit but also affects the reactivity of the monomer during ROMP. It has been suggested that the anchor group effect originates from the chelating abilities with Ru center during the resting state of propagation.⁴⁷⁻⁵¹ Slugovc et al. investigated the influence of oxygen-containing anchor groups on the polymerization rate and found that the rate constant decreased in the order of **2** > **3** > **1** >> **4** (Figure 1.3 (a)).⁴⁷ They attributed this difference to the increasing ability to form a six-membered chelate with [Ru] (ester ≈ ether < ketone) which were identified by nuclear magnetic resonance (NMR) spectroscopy (Figure 1.3

(b)). Another study by Radzinski et al. demonstrated that the anchor group effect resulted from a combination of varying steric demands and electronic structure among the different functional groups.⁵² They proposed that monomers with anchor groups that raise the HOMO energy lead to a larger overall polymerization rate, which is supported by theoretical calculations. Even though the origin of the anchor group effect is not thoroughly understood, the overall ROMP reactivity could be modulated by installing different anchor groups.

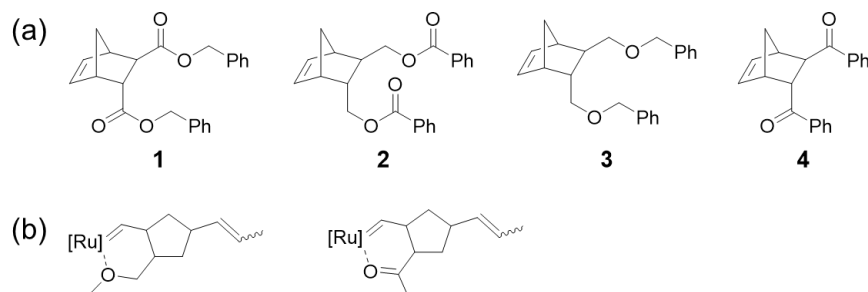


Figure 1.3 (a) Norbornene monomers with oxygen-containing anchor groups.⁴⁷ (b) Possible chelate structures generated between the anchor group and [Ru].

ROMP reactivity is also affected by the stereochemistry and the size of the substituents. *exo*-isomer reacts faster than *endo*-isomer mainly due to steric interactions;⁵³ thus, in di-substituted NBE monomers, the rate decreases in the order of *exo,exo* > *exo,endo* > *endo,endo* (Figure 1.4).⁵⁰ For the analogous *exo,exo*-norbornendicarboxylates, elongation of the aliphatic ester has no impact on rate constant but leads to an increase of the activation parameter.⁵⁰ This could be explained by the enhancement in the donor properties of carbonyl oxygen which strengthens the coordination with [Ru]. Since Ru center and the oxygen should be positioned in proximity to effectively form an intramolecular chelate, increasing the steric hindrance by branching the substituent from *n*-butyl to *i*-butyl lowers the activation parameter. However, the bulkier *i*-butyl also impedes the approaching of another monomer to reactive [Ru] carbene, which reduces the reactivity of this ester.

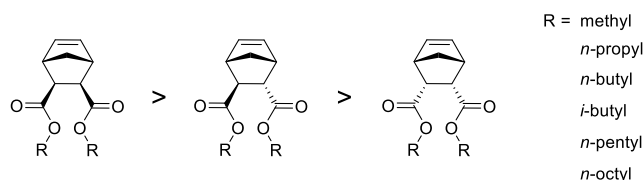


Figure 1.4 Norbornendicarboxylate monomers with different stereochemistry.

Cyclobutene has a higher ring strain energy than NBE, so its derivatives are also a valuable addition to the ROMP monomer toolbox. ROMP of 3,4-disubstituted cyclobutene

affords polymers with a high density of pendant functionalities and a 1,4-linked polybutadiene backbone, which is not accessible with other polymerization techniques. ROMP of *cis*-isomer **5** is faster than *trans*-isomer **6** owing to the steric effect (Figure 1.5 (a)).⁵⁴ When the substitution is at 1-position (Figure 1.5 (b)), ROMP becomes even slower. Furthermore, stereoselectivity and reactivity are highly sensitive to substituents. ROMP of **7** generated functionalized polymers with excellent regioselectivity and stereoselectivity while ROMP of **8** exhibited no control.⁵⁵ Calculations on the relative free energy profiles suggested that the *cis*-pathway is favored for secondary amide monomer **7**, but the activation energies in both *cis*- and *trans*-pathways are nearly equivalent for carbinol ester monomer **8**. When tertiary amide monomer **9** was polymerized, only ring-opened products were observed, which presumably results from the steric hindrance by the *N*-methyl group that blocks the incoming cyclobutene. In addition, ester monomer **10** was not able to homopolymerize due to the formation of stable enoic carbene chelate structure.

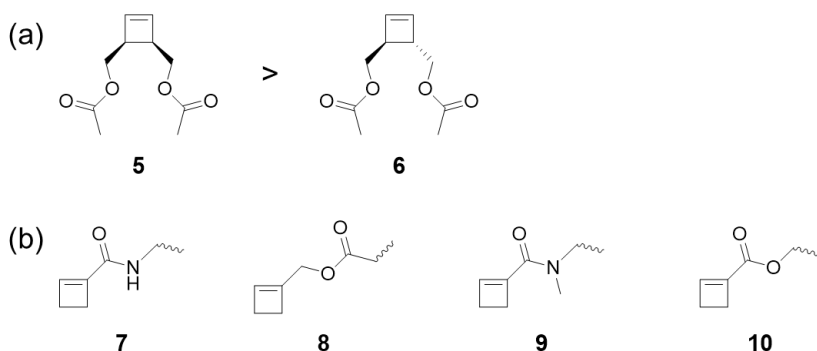


Figure 1.5 (a) 3,4-disubstituted cyclobutene monomers.⁵⁴ (b) 1-substituted cyclobutene monomers.⁵⁵

Only a few examples of cyclopropene derivatives, despite being the most strained cyclic olefins, were reported on their ROMP behavior. Usually, disubstitution is required for cyclopropene monomers to be stable at ambient conditions. For 1,1-disubstituted cyclopropenes, the steric bulk introduced from both faces of the olefin dramatically reduces their tendency to homopolymerize. This characteristic, however, enables the synthesis of a rigorously alternating sequence when copolymerizing with unhindered, low-strain monomers.⁵⁶ For 1,2-disubstituted cyclopropenes, the electronic nature of the substituents has a noticeable effect on polymerization rates.⁵⁷ With carefully optimized conditions, polymers with controlled molecular weight and dispersity were obtained.

1.3.2 Monomer with Low Ring Strain

While ROMP of high-strain monomers has been largely explored, there are much fewer examples on low-strain monomers. According to $\Delta G = \Delta H - T\Delta S$, ROMP is more reversible for monomers with slightly negative ΔH , such as cyclopentene, cyclohexene, and cycloheptene. Since $-T\Delta S$ term is small and positive due to the loss in translational entropy upon polymerization, ΔG changes its sign from negative to positive as T increases. Hence, ROMP of low-strain monomers is much more sensitive to reaction conditions such as temperature, pressure and concentration. In addition, the competition between chain transfer and ROMP makes the control over polymerization (such as molecular weight and dispersity) challenging.

Cyclohexene is relatively inert to ROMP due to the thermodynamic stability of its six-membered ring. Polymerization of cyclohexene at $-60\text{ }^{\circ}\text{C}$ only afforded ring-opened products (i.e., dimers and oligomers) instead of polymers.⁵⁸ However, its inability of homopolymerization at ambient conditions facilitates the synthesis of alternating sequences by copolymerization with bulky, strained monomers.^{56,59}

Cyclopentene and cycloheptene have similar ring strain; therefore, they exhibit similar behavior in ROMP. Higher monomer conversion is achieved when ROMP is performed at lower temperatures or higher initial monomer concentration.^{60,61} While the equilibrium time, polymer molecular weight, and dispersity are influenced by the catalyst loading and catalyst activity, the overall monomer conversion is determined only by the applied temperature.⁶¹ Further control over molecular weight and dispersity could be achieved by variable temperature ROMP where the initiation is performed at warm temperatures followed by propagation at low temperatures.¹⁸ These procedures lead to a living-like polymerization due to the suppression of chain transfer events. Substitution on the ring also affects ROMP, which is explained by the Thorpe-Ingold effect where substituents stabilize the ring-closed form relative to its linear counterpart.⁶² As a result, lower or even zero conversion was observed with bulky substituents owing to lack of ring strain.⁶⁰

Compared to five to seven-membered cyclic alkenes, cyclooctene and cyclooctadiene have appreciable ring strain energy and polymerize to relatively high conversion.^{17,43} For *trans*-cyclooctene, it polymerizes in a living fashion due to an even larger ring strain.¹⁷ Thus, the

substituent effect in eight-membered rings is less prominent. With the development of highly active and functional group tolerant catalysts, cyclooctene and cyclooctadiene with a wide range of functionalities (such as amino, thiol, halogen, nitrile, epoxy, hydroxyl, alkoxy and carbonyl substituents) have been reported to generate polymers with desirable properties in high yields.⁴³ The use of different catalysts and diverse functionalized monomers allows for control over stereo- and regio-selectivity, which leads to the synthesis of precision polymers that were not previously attainable. Despite the low strain energy, ROMP of cyclooctatetrene seems driven by the formation of highly conjugated poly(acetylene) product. Copolymerization with olefin-terminated chain transfer agents affords block copolymers up to 82% yield.⁶³

1.4 Applications of ROMP

One of the most attractive attributes of ROMP is its potential for living polymerization under mild conditions. The living characteristic allows for the synthesis of highly functional, narrowly dispersed polymers with defined length, controlled composition, and unique structural features. In addition, with the development of ruthenium catalysts that are tolerant toward various functionalities, a wide variety of chemical groups can be incorporated into the monomer unit without post-polymerization modification. Thus, biologically-relevant polymers,^{6,64,65} self-healing materials,^{66,67} organoelectronics,⁶⁸⁻⁷⁰ and highly porous materials⁷ have been prepared via ROMP.

1.5 Conclusion

In the past few decades, remarkable progress has been made in the molecular design of ROMP catalysts and monomers, which enables the development of unique and useful polymeric materials with a broad range of applications. Compared to other polymerization techniques, Ru-based ROMP demonstrates exceptional stability toward moisture, oxygen, and numerous functional groups.

As the main driving force is the release of ring strain, the nature of the ring is the primary factor that determines ROMP performance, but the substituent in the monomer also plays an important role. For highly strained monomers, substituents on the ring have minimal impact on

the thermodynamics but dramatically alter the kinetic behavior. However, for low-strain monomers, ROMP is in an equilibrium where substituent effect is much more prominent in terms of thermodynamic behavior. Therefore, precision polymers with unique microstructures and interesting properties have been synthesized by judiciously modulating the ring nature and substituents.

1.6 References

- (1) Calderon, N. Olefin Metathesis Reaction. *Acc. Chem. Res.* **2005**, *5*, 127–132.
- (2) Casey, C. P. 2005 Nobel Prize in Chemistry. Development of the Olefin Metathesis Method in Organic Synthesis. *J. Chem. Educ.* **2009**, *83*, 192.
- (3) Jean-Louis, P.; Hérisson Chauvin, Y. Catalyse de Transformation Des Oléines Par Les Complexes Du Tungstène. *Die Makromol. Chemie* **1970**, *141*, 161–176.
- (4) Bielawski, C. W.; Grubbs, R. H. Living Ring-Opening Metathesis Polymerization. *Prog. Polym. Sci.* **2007**, *32*, 1–29.
- (5) Slugovc, C. The Ring Opening Metathesis Polymerisation Toolbox. *Macromol. Rapid Commun.* **2004**, *25*, 1283–1297.
- (6) Sutthasupa, S.; Shiotsuki, M.; Sanda, F. Recent Advances in Ring-Opening Metathesis Polymerization, and Application to Synthesis of Functional Materials. *Polym. J.* **2010**, *42*, 905–915.
- (7) Leitgeb, A.; Wappel, J.; Slugovc, C. The ROMP Toolbox Upgraded. *Polymer (Guildf)*. **2010**, *51*, 2927–2946.
- (8) Nelson, D. J.; Manzini, S.; Urbina-Blanco, C. A.; Nolan, S. P. Key Processes in Ruthenium-Catalysed Olefin Metathesis. *Chem. Commun.* **2014**, *50*, 10355–10375.
- (9) Hilf, S.; Kilbinger, A. F. M. Functional End Groups for Polymers Prepared Using Ring-Opening Metathesis Polymerization. *Nat. Chem.* **2009**, *1*, 537–546.
- (10) Elling, B. R.; Xia, Y. Efficient and Facile End Group Control of Living Ring-Opening Metathesis Polymers via Single Addition of Functional Cyclopropenes. *ACS Macro Lett.* **2018**, *7*, 656–661.
- (11) Owen, R. M.; Gestwicki, J. E.; Young, T.; Kiessling, L. L. Synthesis and Applications of End-Labeled Neoglycopolymers. *Org. Lett.* **2002**, *4*, 2293–2296.

- (12) Goetz, A. E.; Boydston, A. J. Metal-Free Preparation of Linear and Cross-Linked Polydicyclopentadiene. *J. Am. Chem. Soc.* **2015**, *137*, 7572–7575.
- (13) Ogawa, K. A.; Goetz, A. E.; Boydston, A. J. Metal-Free Ring-Opening Metathesis Polymerization. *J. Am. Chem. Soc.* **2015**, *137*, 1400–1403.
- (14) Ogawa, K. A.; Dunford, D. G.; Goetz, A. E.; Knorr, D. B.; Pascual, L. M. M.; Boydston, A. J. Expanded Functionality of Polymers Prepared Using Metal-Free Ring-Opening Metathesis Polymerization. *ACS Macro Lett.* **2016**, *5*, 579–582.
- (15) Pascual, L. M. M.; Goetz, A. E.; Roehrich, A. M.; Boydston, A. J. Investigation of Tacticity and Living Characteristics of Photoredox-Mediated Metal-Free Ring-Opening Metathesis Polymerization. *Macromol. Rapid Commun.* **2017**, *38*, 1–6.
- (16) Slugovc, C. *Handbook of Metathesis, Volume 3: Polymer Synthesis*; Grubbs, R. H., Khosravi, E., Eds.; Wiley-VCH, 2015.
- (17) Walker, R.; Conrad, R. M.; Grubbs, R. H. The Living ROMP of *Trans* -Cyclooctene. *Macromolecules* **2009**, *42*, 599–605.
- (18) Neary, W. J.; Kennemur, J. G. Variable Temperature ROMP: Leveraging Low Ring Strain Thermodynamics to Achieve Well-Defined Polypentenamers. *Macromolecules* **2017**, *50*, 4935–4941.
- (19) Tebbe, F. N.; Parshall, G. W.; Reddy, G. S. Olefin Homologation with Titanium Methylene Compounds. *J. Am. Chem. Soc.* **1978**, *100*, 3611–3613.
- (20) Tebbe, F. N.; Parshall, G. W.; Ovenall, D. W. Titanium-Catalyzed Olefin Metathesis. *J. Am. Chem. Soc.* **1979**, *101*, 5074–5075.
- (21) Howard, T. R.; Lee, J. B.; Grubbs, R. H. Titanium Metallacarbene-Metallacyclobutane Reactions: Stepwise Metathesis. *J. Am. Chem. Soc.* **1980**, *102*, 6876–6878.
- (22) Wallace, K. C.; Schrock, R. R. Ring-Opening Polymerization of Norbornene by a Tantalum Catalyst: A Living Polymerization. *Macromolecules* **1987**, *20*, 448–450.
- (23) Wallace, K. C.; Liu, A. H.; Dewan, J. C.; Schrock, R. R. Preparation and Reactions of Tantalum Alkylidene Complexes Containing Bulky Phenoxide or Thiolate Ligands. Controlling Ring-Opening Metathesis Polymerization Activity and Mechanism through Choice of Anionic Ligand. *J. Am. Chem. Soc.* **1988**, *110*, 4964–4977.
- (24) Schrock, R. R.; Fellmann, J. D. Multiple Metal-Carbon Bonds. 8.1a Preparation, Characterization, and Mechanism of Formation of the Tantalum and Niobium

- Neopentylidene Complexes, $M(\text{CH}_2\text{CMe}_3)_3$ (CHCMe_3). *J. Am. Chem. Soc.* **1978**, *100*, 3359–3370.
- (25) J. Kress, J.A. Osborn, R.M.E. Greene, K.J. Ivin, J. J. R. The Detection of ‘Living’ Propagating Tungsten–carbene Complexes in the Ring-Opening Polymerization of Bicycloalkenes. *J Chem Soc Chem Commun* **1985**, No. 13, 874–876.
- (26) Ivin, K. J.; Kress, J.; Osborn, J. A. Kinetics of Initiation and Propagation of the Metathesis Polymerization of the Exo Diels-Alder Adduct of Cyclopentadiene and Maleic Anhydride Initiated by the Tungsten-Carbene Complex $\text{W}[\text{H}_2](\text{OCH}_2\text{CMe}_3)_2\text{Br}_2$. *J Mol Catal* **1988**, *46*, 351–358.
- (27) Cho, H. N.; Oskam, J. H.; Schrock, R. R.; Park, L. Y.; Bazan, G. C. Living Ring-Opening Metathesis Polymerization of 2,3-Difunctionalized 7-Oxanorbornenes and 7-Oxanorbornadienes by $\text{Mo}(\text{CHCMe}_2\text{R})(\text{NC}_6\text{H}_3\text{-Iso-Pr}_2\text{-2,6})(\text{O-Tert-Bu})_2$ and $\text{Mo}(\text{CHCMe}_2\text{R})(\text{NC}_6\text{H}_3\text{-Iso-Pr}_2\text{-2,6})(\text{OCMe}_2\text{CF}_3)_2$. *J. Am. Chem. Soc.* **2005**, *113*, 6899–6907.
- (28) Bazan, G. C.; Schrock, R. R.; Cho, H. N.; Gibson, V. C. Polymerization of Functionalized Norbornenes Employing $\text{Mo}(\text{CH-t-Bu})(\text{NAr})(\text{O-t-Bu})_2$ as the Initiator. *Macromolecules* **1991**, *24*, 4495–4502.
- (29) Bazan, G. C.; Schrock, R. R.; O’Regan, M. B.; Thomas, J. K.; Davis, W. M.; Khosravi, E.; Feast, W. J.; Gibson, V. C. Living Ring-Opening Metathesis Polymerization of 2,3-Difunctionalized Norbornadienes by $\text{Mo}(\text{CH-t-Bu})(\text{N-2,6-C}_6\text{H}_3\text{-i-Pr}_2)(\text{O-t-Bu})_2$. *J. Am. Chem. Soc.* **1990**, *112*, 8378–8387.
- (30) Schrock, R. R. Synthesis of Stereoregular Polymers through Ring-Opening Metathesis Polymerization. *Acc. Chem. Res.* **2014**, *47*, 2457–2466.
- (31) Trnka, T. M.; Grubbs, R. H. The Development of $\text{L}_2\text{X}_2\text{RU}=\text{CHR}$ Olefin Metathesis Catalysts: An Organometallic Success Story. *Acc. Chem. Res.* **2001**, *34*, 18–29.
- (32) Vougioukalakis, G. C.; Grubbs, R. H. Ruthenium-Based Heterocyclic Carbene-Coordinated Olefin Metathesis Catalysts. *Chem. Rev.* **2010**, *110*, 1746–1787.
- (33) Scholl, M.; Ding, S.; Lee, C. W.; Grubbs, R. H. Synthesis and Activity of a New Generation of Synthesis and Activity of a New Generation of Ruthenium-Based Olefin Metathesis Catalysts Coordinated with 1,3-Dimesityl-4,5-Dihydroimidazol-2-Ylidene Ligands. *Org. Lett.* **1999**, *1*, 2518–2519.

- (34) Sandford, M. S.; Love, J. A.; Grubbs, R. H. Mechanism and Activity of Ruthenium Olefin Metathesis Catalysts. *J. Am. Chem. Soc.* **2001**, *123*, 6543–6554.
- (35) Sanford, M. S.; Ulman, M.; Grubbs, R. H. New Insights into the Mechanism of Ruthenium-Catalyzed Olefin Metathesis Reactions [9]. *J. Am. Chem. Soc.* **2001**, *123*, 749–750.
- (36) Garber, S. B.; Kingsbury, J. S.; Gray, B. L.; Hoveyda, A. H. Efficient and Recyclable Monomeric and Dendritic Ru-Based Metathesis Catalysts. *J. Am. Chem. Soc.* **2000**, *122*, 8168–8179.
- (37) Sanford, M. S.; Love, J. A.; Grubbs, R. H. A Versatile Precursor for the Synthesis of New Ruthenium Olefin Metathesis Catalysts. *Organometallics* **2001**, *20*, 5314–5318.
- (38) Choi, T. L.; Grubbs, R. H. Controlled Living Ring-Opening-Metathesis Polymerization by a Fast-Initiating Ruthenium Catalyst. *Angew. Chemie - Int. Ed.* **2003**, *42*, 1743–1746.
- (39) Nguyen, S. B. T.; Grubbs, R. H.; Ziller, J. W. Syntheses and Activities of New Single-Component, Ruthenium-Based Olefin Metathesis Catalysts. *J. Am. Chem. Soc.* **1993**, *115*, 9858–9859.
- (40) Bielawski, C. W.; Grubbs, R. H. Increasing the Initiation Efficiency of Ruthenium-Based Ring-Opening Metathesis Initiators: Effect of Excess Phosphine. *Macromolecules* **2001**, *34*, 8838–8840.
- (41) Matson, J. B.; Grubbs, R. H. ROMP-ATRP Block Copolymers Prepared from Monotelechelic Poly(Oxa)Norborenanes Using a Difunctional Terminating Agent. *Macromolecules* **2008**, *41*, 5626–5631.
- (42) Schleyer, P. V. R.; Williams, J. E.; Blanchard, K. R. The Evaluation of Strain in Hydrocarbons. The Strain in Adamantane and Its Origin. *J. Am. Chem. Soc.* **1970**, *92*, 2377–2386.
- (43) Martinez, H.; Ren, N.; Matta, M. E.; Hillmyer, M. A. Ring-Opening Metathesis Polymerization of 8-Membered Cyclic Olefins. *Polym. Chem.* **2014**, *5*, 3507–3532.
- (44) Hodge, P.; Kamau, S. D. Entropically Driven Ring-Opening-Metathesis Polymerization of Macrocyclic Olefins with 21-84 Ring Atoms. *Angew. Chemie - Int. Ed.* **2003**, *42*, 2412–2414.
- (45) Strandman, S.; Gautrot, J. E.; Zhu, X. X. Recent Advances in Entropy-Driven Ring-Opening Polymerizations. *Polym. Chem.* **2011**, *2*, 791–799.

- (46) Michael A. Tallon. *Handbook of Maleic Anhydride Based Materials: Syntheses, Properties and Applications*; Musa, O. M., Ed.; Springer: Switzerland, **2016**.
- (47) Slugovc, C.; Demel, S.; Riegler, S.; Hobisch, J.; Stelzer, F. The Resting State Makes the Difference: The Influence of the Anchor Group in the ROMP of Norbornene Derivatives. *Macromol. Rapid Commun.* **2004**, *25*, 475–480.
- (48) Haigh, D. M.; Kenwright, A. M.; Khosravi, E. Nature of the Propagating Species in Ring-Opening Metathesis Polymerizations of Oxygen-Containing Monomers Using Well-Defined Ruthenium Initiators. *Macromolecules* **2005**, *38*, 7571–7579.
- (49) Czelusniak, I.; Heywood, J. D.; Kenwright, A. M.; Khosravi, E. Investigation of Factors Affecting Ruthenium Complexation in ROMP Reactions of Oxygen-Containing Norbornene Derivatives Using Grubbs First Generation Initiator. *J. Mol. Catal. A Chem.* **2008**, *280*, 29–34.
- (50) Lenev, D. A.; Ashirov, R. V.; Semakin, S. V.; Bozhenkova, G.; Kiselev, S. A.; Verpoort, F.; Lyapkov, A. A. Reactivity of Norbornene Esters in Ring-Opening Metathesis Polymerization Initiated by a N-Chelating Hoveyda II Type Catalyst. *RSC Adv.* **2016**, *6*, 5177–5183.
- (51) Kumar, D. R.; Lidster, B. J.; Adams, R. W.; Turner, M. L. Mechanistic Investigation of the Ring Opening Metathesis Polymerisation of Alkoxy and Alkyl Substituted Paracyclophanedienes. *Polym. Chem.* **2017**, *8*, 3186–3194.
- (52) Radzinski, S. C.; Foster, J. C.; Chapleski, R. C.; Troya, D.; Matson, J. B. Bottlebrush Polymer Synthesis by Ring-Opening Metathesis Polymerization: The Significance of the Anchor Group. *J. Am. Chem. Soc.* **2016**, *138*, 6998–7004.
- (53) Rule, J. D.; Moore, J. S. ROMP Reactivity of Endo- and Exo-Dicyclopentadiene. *Macromolecules* **2002**, *35*, 7878–7882.
- (54) Lapinte, V.; De Frémont, P.; Montembault, V.; Fontaine, L. Ring Opening Metathesis Polymerization (ROMP) of Cis- and Trans-3,4-Bis(Acetyloxymethyl)Cyclobut-1-Enes and Synthesis of Block Copolymers. *Macromol. Chem. Phys.* **2004**, *205*, 1238–1245.
- (55) Song, A.; Lee, J. C.; Parker, K. A.; Sampson, N. S. Scope of the Ring-Opening Metathesis Polymerization (ROMP) Reaction of 1-Substituted Cyclobutenes. *J. Am. Chem. Soc.* **2010**, *132*, 10513–10520.
- (56) Elling, B. R.; Xia, Y. Living Alternating Ring-Opening Metathesis Polymerization Based

- on Single Monomer Additions. *J. Am. Chem. Soc.* **2015**, *137*, 9922–9926.
- (57) Elling, B. R.; Su, J. K.; Xia, Y. Ring-Opening Metathesis Polymerization of 1,2-Disubstituted Cyclopropenes. *Chem. Commun.* **2016**, *52*, 9097–9100.
- (58) Hlil, A. R.; Bazzi, H. S.; Tuba, R.; Brothers, E. N.; Balogh, J.; Su, H.-L.; Moncho, S.; Al-Hashimi, M. Ring Opening Metathesis Polymerization (ROMP) of Five- to Eight-Membered Cyclic Olefins: Computational, Thermodynamic, and Experimental Approach. *J. Polym. Sci. Part A Polym. Chem.* **2017**, *55*, 3137–3145.
- (59) Tan, L.; Parker, K. A.; Sampson, N. S. A Bicyclo[4.2.0]Octene-Derived Monomer Provides Completely Linear Alternating Copolymers via Alternating Ring-Opening Metathesis Polymerization (AROMP). *Macromolecules* **2014**, *47*, 6572–6579.
- (60) Hejl, A.; Scherman, O. A.; Grubbs, R. H. Ring-Opening Metathesis Polymerization of Functionalized Low-Strain Monomers with Ruthenium-Based Catalysts. *Macromolecules* **2005**, *38*, 7214–7218.
- (61) Tuba, R.; Grubbs, R. H. Ruthenium Catalyzed Equilibrium Ring-Opening Metathesis Polymerization of Cyclopentene. *Polym. Chem.* **2013**, *4*, 3959–3962.
- (62) Allinger, N. L.; Zalkow, V. Conformational Analysis. IX. The Gem-Dimethyl Effect^{1,2}. *J. Org. Chem.* **1960**, *25*, 701–704.
- (63) Scherman, O. A.; Rutenberg, I. M.; Grubbs, R. H. Direct Synthesis of Soluble, End-Functionalized Polyenes and Polyacetylene Block Copolymers. *J. Am. Chem. Soc.* **2003**, *125*, 8515–8522.
- (64) Lee, Y.; Sampson, N. S. Romping the Cellular Landscape: Linear Scaffolds for Molecular Recognition. *Curr. Opin. Struct. Biol.* **2006**, *16*, 544–550.
- (65) Smith, D.; Pentzer, E. B.; Nguyen, S. T. Bioactive and Therapeutic ROMP Polymers. *Polym. Rev.* **2007**, *47*, 419–459.
- (66) White, S. R.; Sottos, N. R.; Geubelle, P. H.; Moore, J. S.; Kessler, M. R.; Sriram, S. R.; Brown, E. N.; Viswanathan, S. Autonomic Healing of Polymer Composites. *Nature* **2001**, *409*, 794–797.
- (67) Toohey, K. S.; Sottos, N. R.; Lewis, J. A.; Moore, J. S.; White, S. R. Self-Healing Materials with Microvascular Networks. *Nat. Mater.* **2007**, *6*, 581–585.
- (68) Kang, H. A.; Bronstein, H. E.; Swager, T. M. Conductive Block Copolymers Integrated into Polynorbornene-Derived Scaffolds. *Macromolecules* **2008**, *41*, 5540–5547.

- (69) Feng, K.; Zuniga, C.; Zhang, Y. D.; Kim, D.; Barlow, S.; Marder, S. R.; Brédas, J. L.; Weck, M. Norbornene-Based Copolymers Containing Platinum Complexes and Bis(Carbazolyl)Benzene Groups in Their Side-Chains. *Macromolecules* **2009**, *42*, 6855–6864.
- (70) Niedermair, F.; Sandholzer, M.; Kremser, G.; Slugovc, C. Solution Self-Assembly and Photophysics of Platinum Complexes Containing Amphiphilic Triblock Random Copolymers Prepared by Romp. *Organometallics* **2009**, *28*, 2888–2896.

Chapter 2: Ceiling Temperature of Cyclopentene Derivatives in Ring-Opening Metathesis Polymerization

2.1 Abstract

The reversible transition between monomer and polymer is usually accomplished by chemical catalysis in organic solvents with appropriate temperature control. When it comes to applications without the presence of solvents, depolymerization often leads to irreversible degradation of the bulk materials since $T_c(\text{neat})$ is typically high. Here, we systematically studied the T_c phenomenon in ROMP of cyclopentene derivatives and demonstrated the reversibility of bulk polypentenamers under mild temperature stimulus. By introducing different substituents into cyclopentene ring, $T_c(\text{solution})$ and $T_c(\text{neat})$ are tunable within a wide temperature range. As a result, the neat cyclopentene derivatives polymerize at room temperature to afford polypentenamers which readily depolymerize at slightly elevated temperatures without addition of any reagent. This polymerization-depolymerization process is reversible after multiple cycles without significant catalyst deactivation.

2.2 Introduction

Materials with reversible polymerizability are of great importance to achieve their full sustainability and have great potential in many applications such as chemical recycling and remodeling.¹⁻³ Diels-Alder reactions and equilibrium polymerizations have been frequently utilized to achieve reversible transformation.⁴⁻¹⁰ However, Diels-Alder and retro-Diels-Alder reactions often require high temperatures for the interconversion between monomer and polymer.⁸⁻¹⁰ For most equilibrium polymerizations, reversibility is typically achieved by varying reaction conditions (such as concentration and temperature)^{5,7} or applying different chemical reagents.^{4,6,11} Both scenarios require the use of organic solvents, which hinders the application of these materials. From a practical standpoint, temperature control in equilibrium polymerizations is a more straightforward and facile approach to achieve reversibility of bulk polymers.

Ceiling temperature (T_c) is a thermodynamic parameter to quantify monomer polymerizability in equilibrium polymerizations and represents a threshold at which the

depropagation rate equals the propagation rate.^{12,13} At each temperature, there is a monomer-polymer equilibrium at which

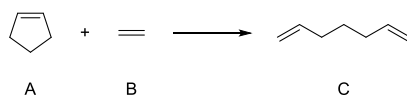
$$\Delta G_p = \Delta G_p^0 + RT \ln \frac{1}{[M]_e} = 0$$

T_c is concentration-dependent since higher equilibrium monomer concentration ($[M]_e$) biases the equilibrium toward the polymer.¹³ Thus, T_c reaches its maximum value $T_c(\text{neat})$ in bulk polymerization. The T_c phenomenon discussed in the literature mostly focuses on solution polymerization.^{2,14} However, most bulk materials contain minimal solvents; hence, determining T_c in the bulk state is the first step to enable development of bulk materials with reversible polymerizability.

Inspired by work from the Grubbs group,^{15,16} ruthenium-catalyzed ROMP of cyclopentene is a promising system to achieve this goal for two main reasons. First, previous studies suggest that the conversion from cyclopentene monomer to polypentenamer is dramatically affected by the applied temperature due to the small absolute value of ΔH_p .¹⁵⁻¹⁷ Thus, the polymerization-depolymerization equilibrium is readily shifted by mild temperature changes. Second, Grubbs' catalysts are stable toward polar functional groups, which allows modification of monomers without deactivation of the catalysts.¹⁸ Despite these advantages, the polypentenamers demonstrated in previous examples cannot be depolymerized without the use of solvents since $T_c(\text{neat})$ of cyclopentene (**1a**) or 3-cyclopentene-1-ol (**1b**) is much higher than the boiling point of the monomer or the decomposition temperature of Grubbs II. We envisioned that incorporating bulky substituents into the cyclopentene ring reduces the ring strain and lowers the T_c to a desirable range.¹⁹ The ideal monomer will efficiently polymerize at room temperature, and the resulting polypentenamer would readily depolymerize upon a mild thermal stimulus.

2.3 Theoretical Calculations of Polymerization Enthalpy

As ring strain largely contributes to the enthalpy of polymerization (ΔH_p),^{13,15,16} we estimated the ΔH_p of several cyclopentene derivatives using Density Functional Theory (DFT) at B3LYP/6-31G(d) level, which provides a theoretical insight into their relative polymerizability. An example for cyclopentene ΔH_p (kcal/mol) calculation is shown below.



$$H_A = -195.204254, H_B = -78.532244, H_C = -273.787519 \text{ (Unit: Hartree)}$$

$$\Delta H = H_C - (H_A + H_B) = -0.008314 \text{ Hartree} = -5.22 \text{ kcal/mol}$$

We focused on homoallylic-substituted cyclopentene derivatives as the allylic substituent might adversely affect the catalyst reactivity through steric hindrance that prevents the catalyst from approaching the alkene or through irreversible coordination with the active [Ru] carbene.²⁰ A smaller absolute value of ΔH_p is desired to reduce the polymerizability of cyclopentene, thereby lowering the T_c . However, if the absolute ΔH_p value is too small, it may not possess enough ring strain to undergo homopolymerization under ambient conditions. Based on the calculation results, cyclopentene has a ΔH_p of -5.22 kcal/mol, and incorporating substituents such as $-\text{CH}_2\text{OH}$, $-\text{COOMe}$ and $-\text{CH}_2\text{OTBS}$ at the homoallylic position reduces the absolute ΔH_p value to -3.47 kcal/mol, -3.16 kcal/mol, and -2.66 kcal/mol, respectively (Table 2.1).

Table 2.1 A summary of the calculated ΔH_p for cyclopentene derivatives.

Monomers									
ΔH_p (kcal/mol)	-5.86	-5.26	-5.22	-4.38	-3.55	-3.47	-3.24	-3.16	-2.66

2.4 Ceiling Temperature of Cyclopentene Derivatives

With the feasibility assessed by DFT calculations, we first investigated T_c of methyl 3-cyclopentenecarboxylate (**1f**). $T_c(\text{solution})$ was determined by variable-temperature nuclear magnetic resonance (VT-NMR). The catalyst loading and type of the catalyst have negligible effects on the thermodynamics.¹³ Grubbs II was selected due to its excellent solubility in the neat cyclopentene monomers. At 0, 10, 15 and 20 °C, $[M]_e$ was obtained by ¹H NMR spectroscopy using toluene as the internal standard. By plotting $\ln([M]_e)$ against $1/T$, ΔH_p and entropy of polymerization (ΔS_p) were determined based on the slope and y-intercept. For **1f**, T_c was calculated as $T_c(\text{solution}) = \Delta H_p / \Delta S_p = -26$ °C. This $T_c(\text{solution})$ is extrapolated to bulk

polymerization according to $T_c(\text{neat}) = \Delta H_p / (\Delta S_p + R \ln[M]_{\text{max}})$ where $[M]_{\text{max}}$ is the molarity of neat **1f**. As shown in Figure 2.1(a), $T_c(\text{neat})$ is calculated to be 63 °C, which implies that depolymerization is more favorable above this temperature.

To validate the extrapolated value from VT-NMR, we further characterized the depolymerization behavior of the poly(**1f**) by DSC. Gratifyingly, as shown in Figure 2.1(b), the endothermic depolymerization peak of 62 °C was observed, matching well with the extrapolated $T_c(\text{neat})$ value. Thus, introducing a bulky –COOMe to the cyclopentene ring effectively lower the ring strain and T_d compared to **1a** and **1b**.

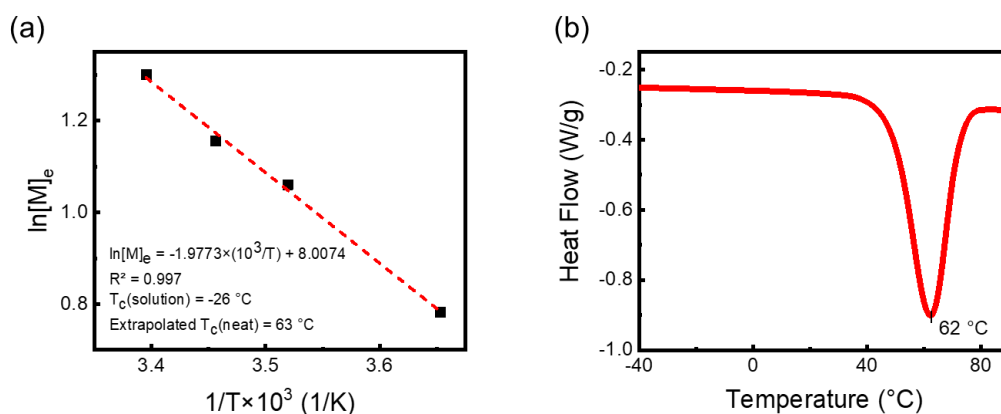
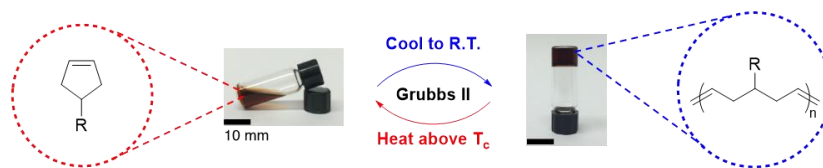


Figure 2.1 (a) Thermodynamics of equilibrium ROMP of **1f**. The polymerization was performed in *d*₈-THF with 0.22 mol % Grubbs II loading. (b) Depolymerization peak maximum of poly(**1f**) with a ramping rate of 10 °C/min. The poly(**1f**) sample was a monomer-polymer equilibrated mixture from bulk polymerization with 0.22 mol % Grubbs II loading at room temperature.

Encouraged by the results from **1f**, we then evaluated the polymerizability of other cyclopentene derivatives both in solution and in the bulk state. Similar to **1f**, monomers with different bulky substituents (**1c-1i**) possess much lower T_c values than **1a** and **1b** as summarized in Table 2.2. These results suggest that equilibrium ROMP is readily tunable by varying the substituent and the bulk poly(pentenamers) is depolymerizable upon a mild temperature stimulus. Except for **1e** and **1h** that form hydrogen-bonding which leads to higher a T_d than the extrapolated $T_c(\text{neat})$, T_d agreed well with $T_c(\text{neat})$ (Figure 2.2). This not only confirms the reliability of extrapolation from VT-NMR but also implies DSC as a straightforward empirical method to estimate the $T_c(\text{neat})$ of low-strain monomers.

Table 2.2 Reversible polymerization of cyclopentene monomers.



Entry	1a	1b	1c	1d	1e	1f	1g	1h	1i
Monomer									
$T_c(\text{solution})^a$ (°C)	35 ± 2	49 ± 1	31 ± 1	-14 ± 2	-35 ± 3	-25 ± 1	-15 ± 1	-25 ± 1	-15 ± 2
Extrapolated $T_c(\text{neat})^b$ (°C)	185 ± 3	386 ± 3	92 ± 5	67 ± 5	70 ± 3	59 ± 4	45 ± 3	48 ± 1	55 ± 2
T_d^c (°C)	not obsd ^d	not obsd ^d	82 ± 4	62 ± 1	82 ± 2	60 ± 3	51 ± 2	68 ± 2	52 ± 2
Monomer conversion ^e (%)	92 ± 2	84 ± 1	78 ± 4	84 ± 3	69 ± 2	63 ± 2	55 ± 3	68 ± 5	24 ± 2

^a Calculated as $T_c(\text{solution}) = \Delta H_p / \Delta S_p$ where ΔH_p and ΔS_p were obtained from VT-NMR. The polymerization was performed in *ds*-THF with 0.22 mol % Grubbs II loading. ^b Calculated as $T_c(\text{neat}) = \Delta H_p / (\Delta S_p + R \ln[M]_{\text{max}})$ where $[M]_{\text{max}} = \rho(\text{g/L}) / M(\text{g/mol})$. ^c Determined by DSC with a ramping rate of 10 °C/min. ^d Degradation of the polymer backbone occurred before depolymerization. ^e Monomer conversion of bulk polymerization determined by ¹H NMR after equilibrium.

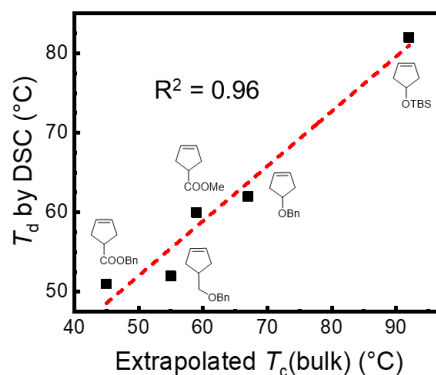


Figure 2.2 Correlation between T_d by DSC and extrapolated $T_c(\text{neat})$.

While ring size is often considered as the main contributor to the ring strain energy, substituents also have a large influence on the thermodynamics of ROMP. Functional groups that directly attach to the cyclopentene ring are a key determinant of ring strain and polymerizability. In general, polymerizability decreases in the order of, $-\text{OR} > -\text{COOR} > -\text{CH}_2\text{OR}$. For example, polymers resulting from **1d** depolymerize at a higher temperature than those from **1g** and **1i**.

While **1g** and **1i** possess similar T_d around 50 °C, **1i** has a much lower monomer conversion. Monomer **1j** with $-\text{CH}_2\text{OTBS}$ substituent showed no evidence of polymerization under neat conditions at room temperature, which further confirms the lower polymerizability of monomers with $-\text{CH}_2\text{OR}$ (Figure 2.7). Molecular weight also plays a role in the polymerizability. While $T_c(\text{solution})$ value reflects the ring strain in a monomer, $T_c(\text{neat})$ value is a combination of ring strain, molecular weight and density of the monomer. Monomers with lower densities or larger molecular weights tend to have lower $T_c(\text{neat})$ values than those with similar ring strain. For example, as the substituent size increases from $\text{R} = \text{COOH}$ to $\text{R} = \text{COOBn}$, $T_c(\text{neat})$ and monomer conversion of **1e**, **1f** and **1g** decrease accordingly. This phenomenon is likely due to the fact that larger substituents result in decreased ΔS , which decreases the propensity of polymerization.

With the experimental $T_c(\text{solution})$ values determined, we further investigated the predictability of a model that correlates experimental and theoretical $T_c(\text{solution})$. Since ΔS_p for ROMP of the analogous cyclopentenenes are similar, $T_c(\text{solution})$ is estimated to be ΔH_p divided by a previously reported ΔS_p for ROMP of cyclopentene $-18.5 \text{ cal}/(\text{mol}\cdot\text{K})$.¹⁵ Thus, a correlation was constructed by plotting the experimental $T_c(\text{solution})$ values against theoretical $T_c(\text{solution})$ values that were calculated from ΔH_p shown in Table 2.1. A linear relationship with $R^2 = 0.988$ was observed even when using a simplified model that considers the same ΔS_p value for all other derivatives (Figure 2.3). In general, theoretical $T_c(\text{solution})$ values predict the depolymerization behavior of low-strain monomers with acceptable accuracy.

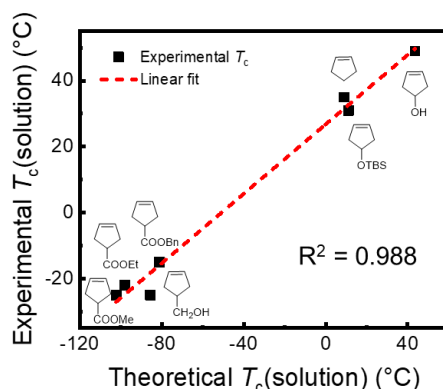


Figure 2.3 Correlation between experimental and theoretical $T_c(\text{solution})$.

2.5 Evaluation of Reversibility

With the establishment of tunable T_{AS} , reversibility of the polymerization-depolymerization process was evaluated. We first employed **1f** monomer as it possesses a mild $T_c(\text{neat})$ and solubilizes the catalyst well. Equilibrium monomer conversion was quantified by ^1H NMR, and number-average molecular weight (M_n) of the monomer-polymer mixture in the heating-cooling cycle was monitored by gel permeation chromatography (GPC). As shown in Figure 2.4 (a), after heating at 50 °C for 10 min and subsequent cooling at 25 °C for 2 h, the monomer conversion increased from 32% to 64%. The same trend was observed for M_n . However, the system gradually lost its reversibility in the second and third heating-cooling cycles where monomer conversion and M_n remained almost unchanged. We hypothesized that a six-membered chelate forms between carboxylate and ruthenium, resulting in an inactive ruthenium species.^{20,23}

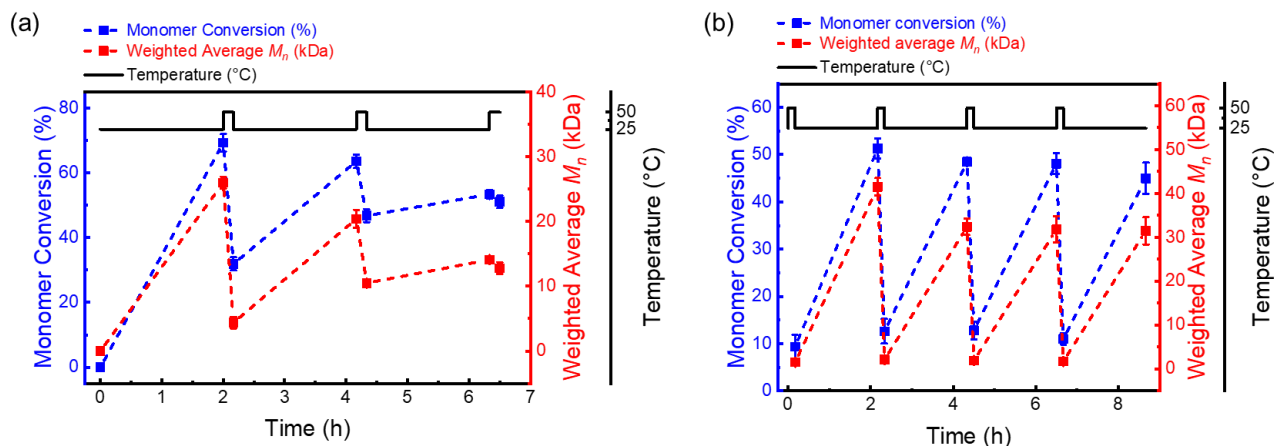


Figure 2.4 Multiple depolymerization-repolymerization cycles of (a) **1f** and (b) **1g**. Monomer and catalyst (0.22 mol %) were mixed and cycled between 50 °C and 25 °C.

Thus, we tested the reversibility of **1g** which possesses a similar T_c but contains a bulkier substituent that potentially prevents the formation of the proposed six-membered chelate. After initiation at 50 °C and subsequent polymerization at 25 °C of **1g** for 2 h, the monomer conversion and M_n increased to 51% and 41 kDa, respectively (Figure 2.4 (b)). Upon heating to 50 °C, depolymerization reduced monomer conversion and M_n to 13% and 2.1 kDa, respectively. Compared to **1f**, **1g** exhibits a more prominent change in monomer conversion and M_n with much improved reversibility. Thus, equilibrium ROMP of **1g** is highly temperature-sensitive, and this depolymerization-repolymerization is reversible for three more cycles. The slight decrease in

reversibility is likely a result of side reactions²¹ and shortened catalyst lifetime²² at elevated temperatures, which leads to less active Ru carbene species.

2.6 Conclusion

We demonstrated that varying the substituents on the cyclopentene ring affords tunable $T_c(\text{neat})$ in ROMP ranging from 40 °C to 90 °C. These neat cyclopentene monomers are polymerizable at room temperature, and the resulting polymers are readily depolymerized at elevated temperatures. This polymerization-depolymerization process is triggered solely by temperature changes and is reversible up to four cycles without substantial decomposition of the catalyst. These results indicate the first step towards the engineering of reversibly polymerizable materials as only a mild temperature stimulus is needed to depolymerize the polymers into liquid monomers, which are transported and repolymerized to remodel the materials system at room temperature.

2.7 Experimental Details

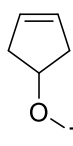
2.7.1 Materials and General Methods

All air or moisture-sensitive experiments were performed under argon atmosphere in the glove box (MBRAUN UNIlab Plus). Unless otherwise stated, all starting materials and reagents were purchased from commercial suppliers (Sigma-Aldrich, Enamine, Oakwood Chemical, Alfa Aesar, and TCI America) and were used without further purification. ¹H and ¹³C NMR spectra were recorded on a Varian Unity 500 MHz spectrometer or a Varian Unity 600 MHz spectrometer in the VOICE NMR laboratory at the University of Illinois. Chemical shifts are reported in δ (ppm) relative to the residual solvent peak (CDCl₃: 7.26, THF-*d*₈: 1.73 for ¹H; CDCl₃: 77.16 for ¹³C). Coupling constants (*J*) are reported in Hertz (Hz). Splitting patterns are designated as s (singlet), d (doublet), t (triplet), q (quartet), quint (quintet), dd (doublet of doublets) and m (multiplet). The temperatures of Variable Temperature NMR (VT-NMR) experiments were calibrated by neat methanol (low-temperature calibration) and neat ethylene glycol (high-temperature calibration). High-resolution ESI mass spectra were recorded on a

Micromass 70-VSE spectrometer through the Mass Spectrometry Facility, SCS at University of Illinois. The DSC measurement was performed using TA Instrument Q20 Differential Scanning Calorimeter equipped with a Liquid Nitrogen Cooling System (LNCS). Tzero hermetic aluminum pans and lids were used as sample testing containers. Nitrogen was used as sample purge gas. Analytical gel permeation chromatography (GPC) analyses were performed with a Waters1515 Isocratic HPLC pump, a Waters (2998) Photodiode Array Detector, a Waters (2414) Refractive Index Detector, a Waters (2707) 96-well autosampler, and a series of 4 Waters HR Styragel columns (7.8 × 300 mm, HR1, HR3, HR4, and HR5) in THF at 30 °C. The GPC was calibrated using monodisperse polystyrene standards.

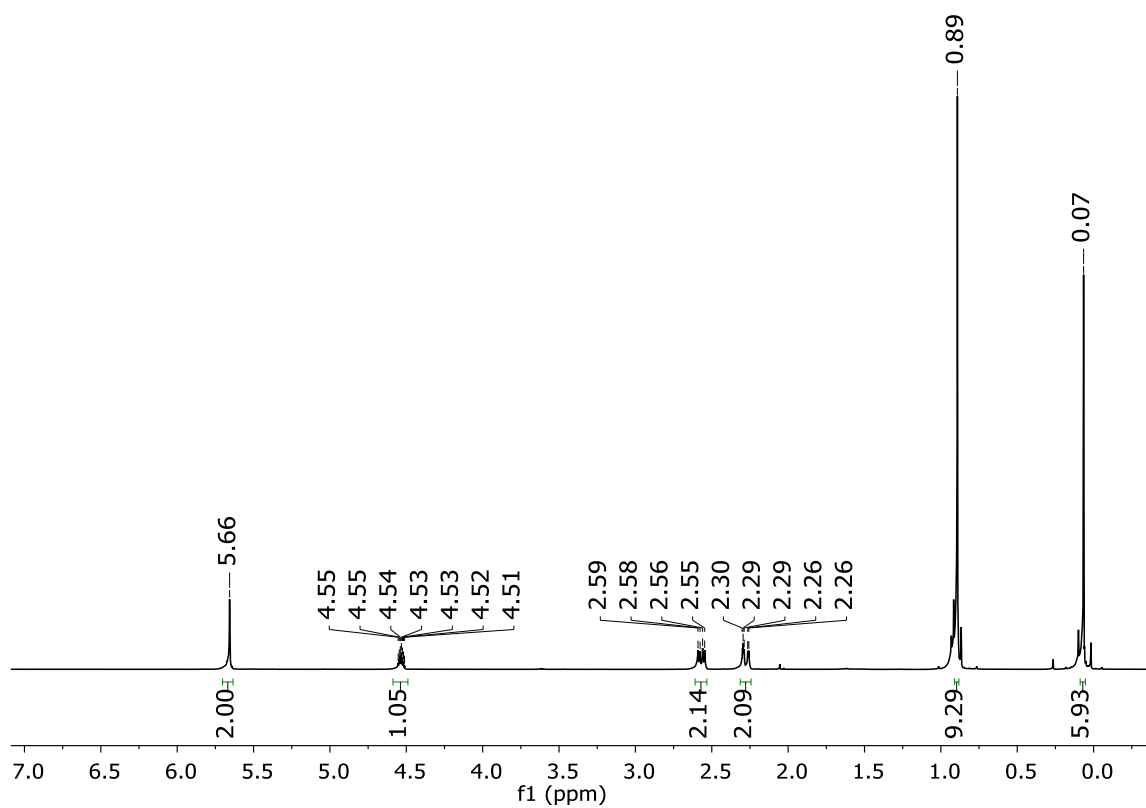
2.7.2 Synthesis of Cyclopentene Derivatives

Synthesis of *tert*-butyl(cyclopent-3-en-1-yloxy)dimethylsilane²⁴ (1c)

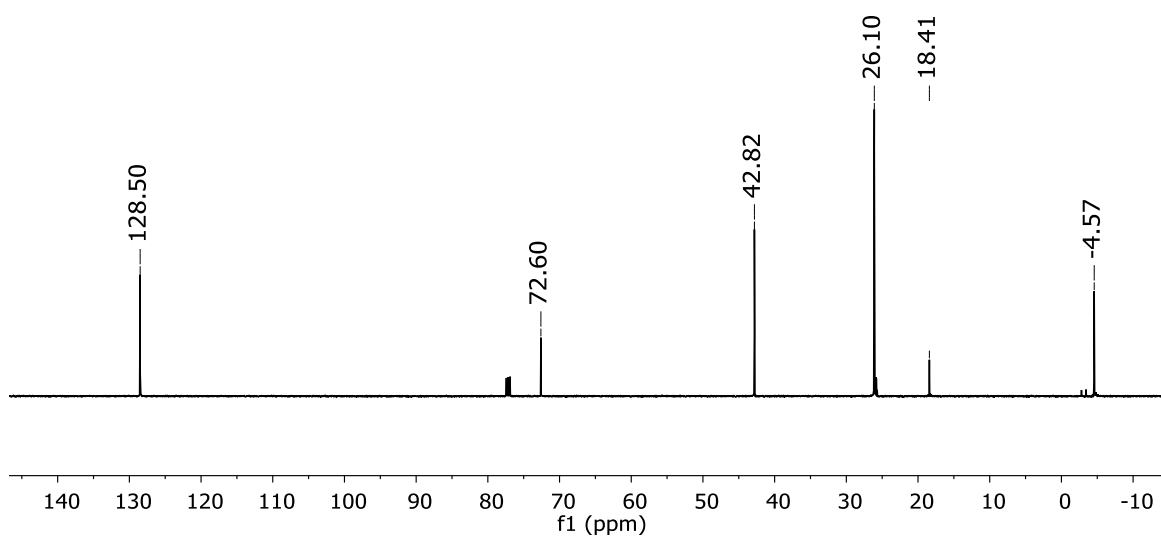


A solution of 3-cyclopentene-1-ol (1.0 g, 11.9 mmol, 1.0 equiv.) in 30 mL of dry DCM was stirred at 0 °C under a nitrogen atmosphere. To this solution was added TBSCl (2.15 g, 14.3 mmol, 1.2 equiv.) and imidazole (1.62 g, 23.8 mmol, 2.0 equiv.). The turbid reaction mixture was allowed to stir overnight at room temperature. Water (15 mL) was added, and the organic layer was reserved. The aqueous layer was further extracted with DCM (2×15 mL). The combined organic layer was washed with brine (15 mL), dried with anhydrous sodium sulfate, and then concentrated. The crude product was purified by passing a short silica column, eluting with DCM, to afford the desired product as a colorless oil (2.04 g, 87%). ¹H NMR (CDCl₃, 500 MHz) δ 5.66 (s, 2H), 4.53 (sept, *J* = 3.5 Hz, 1H), 2.57 (dd, *J* = 15 Hz and 6.5 Hz, 2H), 2.28 (dd, *J* = 15 Hz and 3.5 Hz, 2H), 0.89 (s, 9H), 0.07 (s, 6H); ¹³C NMR (CDCl₃, 125 MHz) δ 128.5, 72.6, 42.8, 26.1, 18.4, -4.6. HRMS-ESI (*m/z*): calculated for C₁₁H₂₁OSi [M+H]⁺, 197.1362; Found, 197.1361.

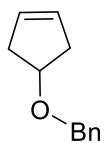
^1H NMR of 1c



^{13}C NMR of 1c

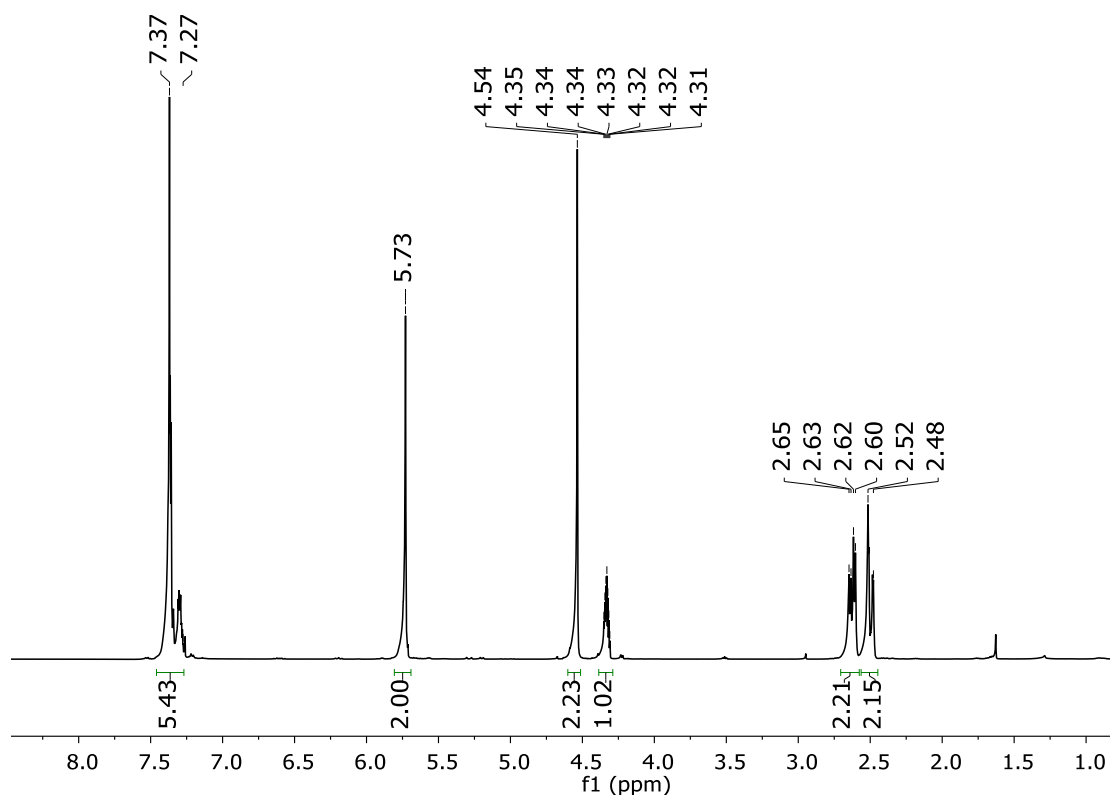


Synthesis of ((cyclopent-3-en-1-yloxy)methyl)benzene²⁵ (1d)

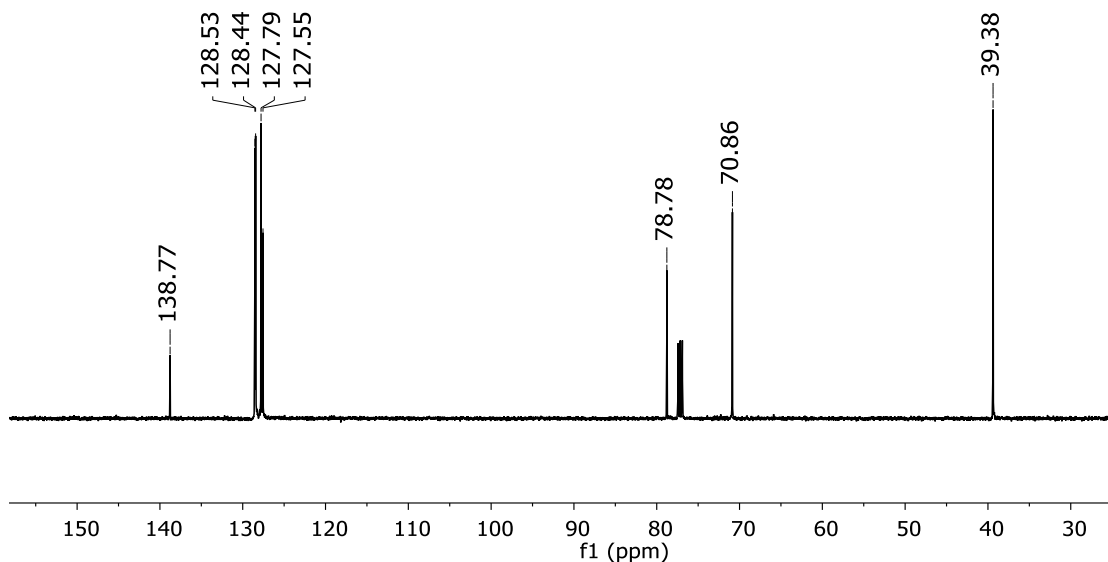


NaH (60% dispersion in mineral oil, 0.48 g, 11.9 mmol, 1.5 equiv.) was added to a solution of 3-cyclopentene-1-ol (1.0 g, 11.9 mmol, 1.0 equiv.) in 30 mL of dry THF at room temperature under a nitrogen atmosphere. After effervescence had ceased, benzyl bromide (1.36 g, 1.0 equiv.) was added dropwise and the resulting mixture was heated to 40 °C for 4 hours. Excess NaH was carefully quenched by H₂O. After removing all the volatiles from the reaction mixture, water (15 mL) was added and further extracted with EtOAc (2×15 mL). The combined organic layer was washed with brine (15 mL), dried with anhydrous sodium sulfate, and then concentrated. The crude product was purified by flash chromatography to give the desired product as a colorless oil (1.03 g, 74%). ¹H NMR (CDCl₃, 500 MHz) δ 7.37-7.27 (m, 5 H), 5.73 (s, 2H), 4.54 (s, 2H), 4.33 (sept, *J* = 3.5 Hz, 1H), 2.65-2.60 (m, 2H), 2.52-2.48 (m, 2H); ¹³C NMR (CDCl₃, 125 MHz) δ 138.8, 128.5, 128.4, 127.8, 127.6, 78.8, 70.9, 39.4. HRMS-ESI (*m/z*): calculated for C₁₂H₁₄ONa [M+Na]⁺, 197.0942; Found, 197.0945.

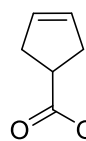
¹H NMR of 1d



^{13}C NMR of 1d

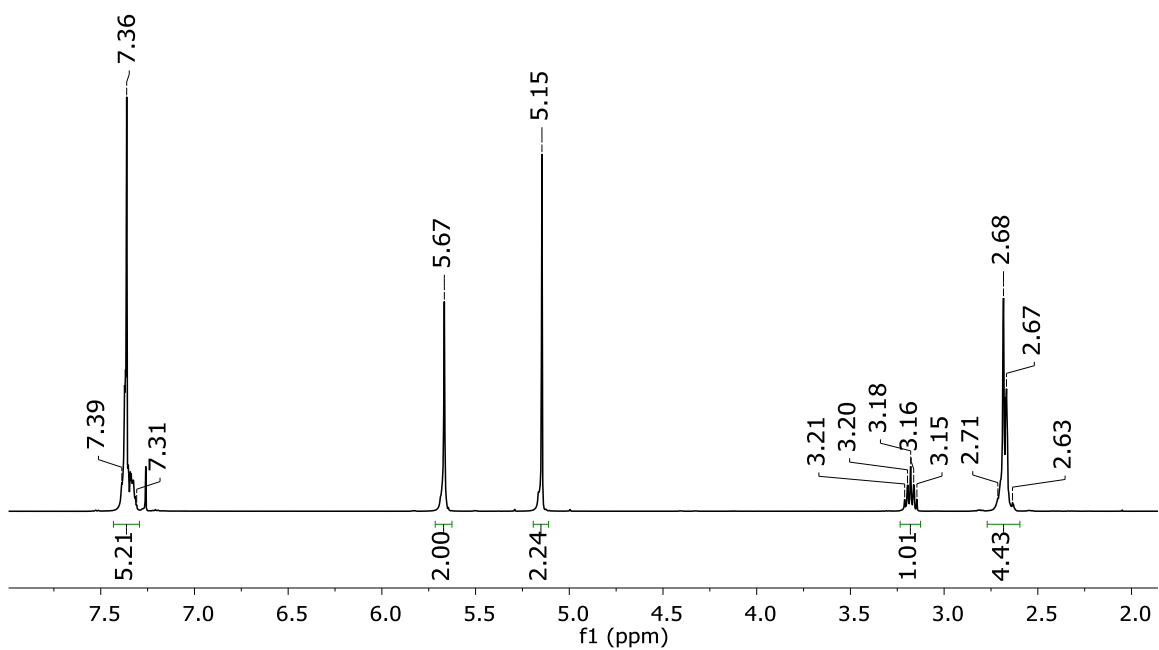


Synthesis of Benzyl cyclopent-3-ene-1-carboxylate²⁶ (1g)

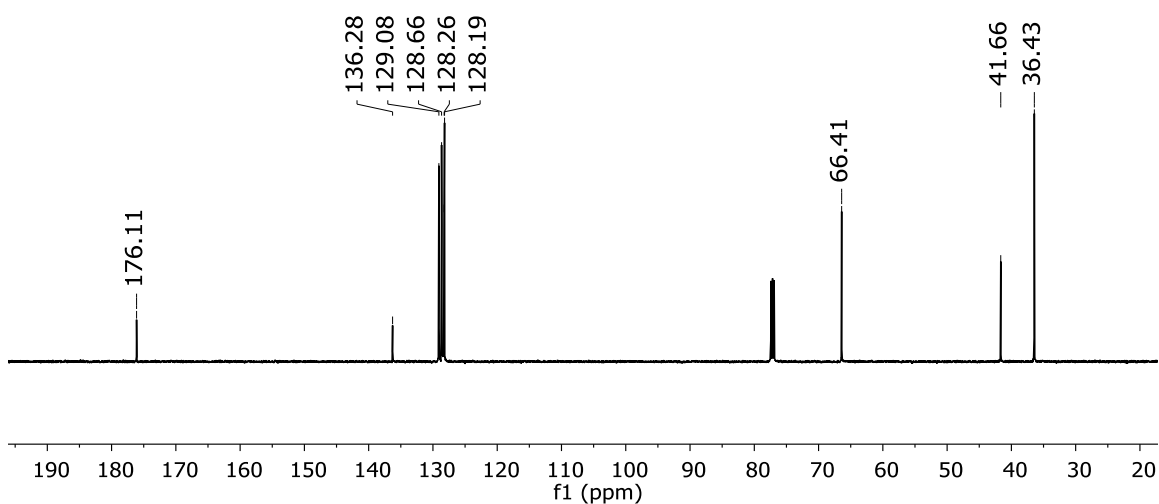


To a mixture of cyclopent-3-enecarboxylic acid (1.3 g, 11.6 mmol, 1.0 equiv.) and K_2CO_3 (2.46 g, 17.9 mmol, 1.5 equiv.) in acetone (20 mL) was added BnBr (1.54 g, 9.0 mmol, 0.8 equiv.). The mixture was stirred at 60 °C for 2 h. The resulting mixture was filtered. The filtrate was concentrated. 20 mL EtOAc was added to the residue and washed with brine (2×15 mL), dried with anhydrous sodium sulfate, and then concentrated. The crude product was purified by flash chromatography to give the desired product as colorless oil (1.36 g, 75%). ^1H NMR (CDCl_3 , 500 MHz) δ 7.39-7.31 (m, 5H), 5.67 (s, 2H), 5.15 (s, 2H), 3.18 (q, $J = 8.6$ Hz, 1H), 2.71-2.63 (m, 4H); ^{13}C NMR (CDCl_3 , 125 MHz) δ 176.1, 136.3, 129.1, 128.7, 128.3, 128.2, 66.4, 41.7, 36.4. HRMS-ESI (m/z): calculated for $\text{C}_{13}\text{H}_{14}\text{O}_2$ [M] $^+$, 202.0994; Found, 202.0994.

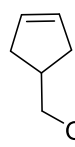
^1H NMR of **1g**



^{13}C NMR of **1g**



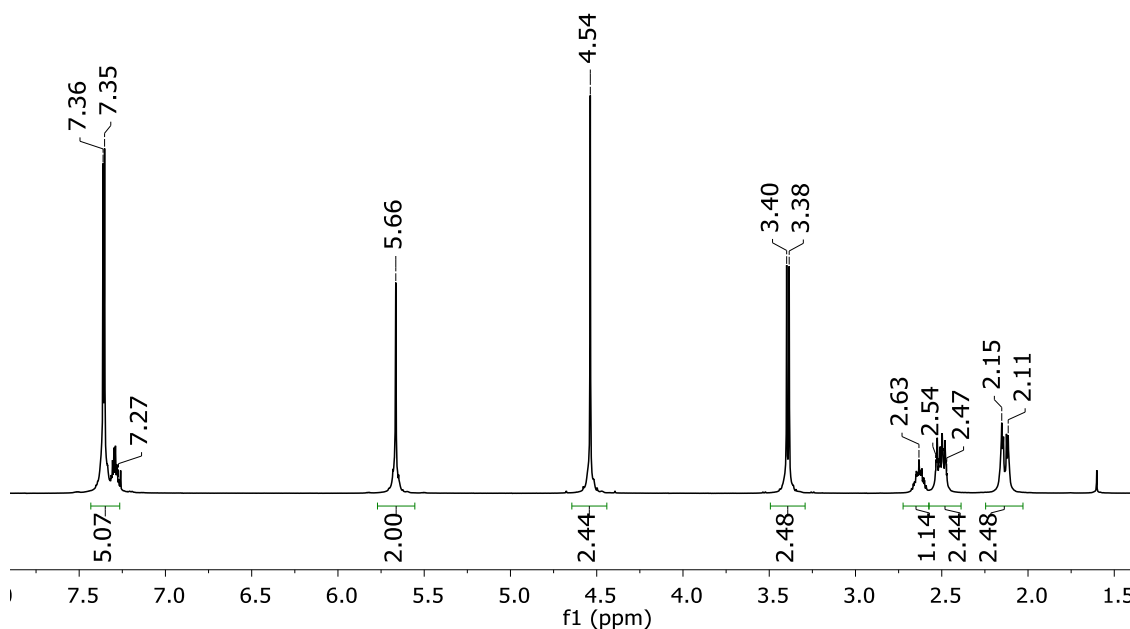
Synthesis of ((cyclopent-3-en-1-ylmethoxy)methyl)benzene²⁵ (**1i**)



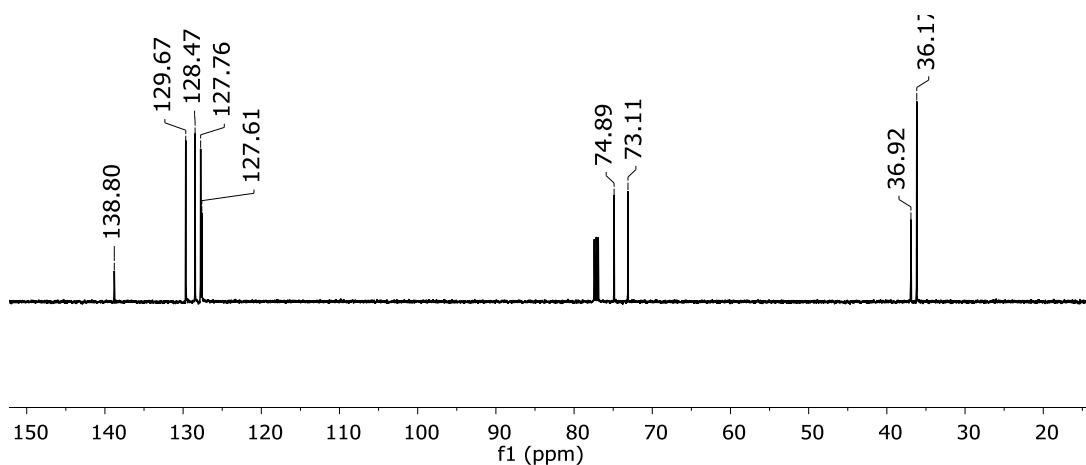
NaH (60% dispersion in mineral oil, 0.41 g, 10.2 mmol, 1.5 equiv.) was added to a solution of cyclopent-3-en-1-ylmethanol (1.0 g, 10.2 mmol, 1.5 equiv.) in 30 mL of dry THF at room temperature under a nitrogen atmosphere. After effervescence had ceased, benzyl bromide (1.16 g, 1.0 equiv.) was added dropwise and the resulting mixture was allowed to heat at 40 °C for 4 hours. Excess NaH was carefully quenched by H₂O. After

removing all the volatiles from the reaction mixture, water (15 mL) was added and further extracted with EtOAc (2×15 mL). The combined organic layer was washed with brine (15 mL), dried with anhydrous sodium sulfate, and then concentrated. The crude product was purified by passing a short silica column to afford the desired product as a colorless oil (0.90 g, 70%). ^1H NMR (CDCl_3 , 500 MHz) δ 7.36-7.27 (m, 5H), 5.66 (s, 2H), 4.54 (s, 2H), 3.39 (d, $J = 7.5$ Hz, 2H), 2.63 (m, 1H), 2.54-2.47 (m, 2 H), 2.15-2.11 (m, 2 H); ^{13}C NMR (CDCl_3 , 125 MHz) δ 138.8, 129.7, 128.5, 127.8, 127.6, 74.9, 73.1, 36.9, 36.2. HRMS-ESI (m/z): calculated for $\text{C}_{13}\text{H}_{17}\text{O}$ $[\text{M}+\text{H}]^+$, 188.1201; Found, 188.1199.

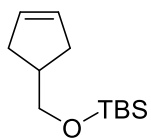
^1H NMR of **1i**



^{13}C NMR of **1i**

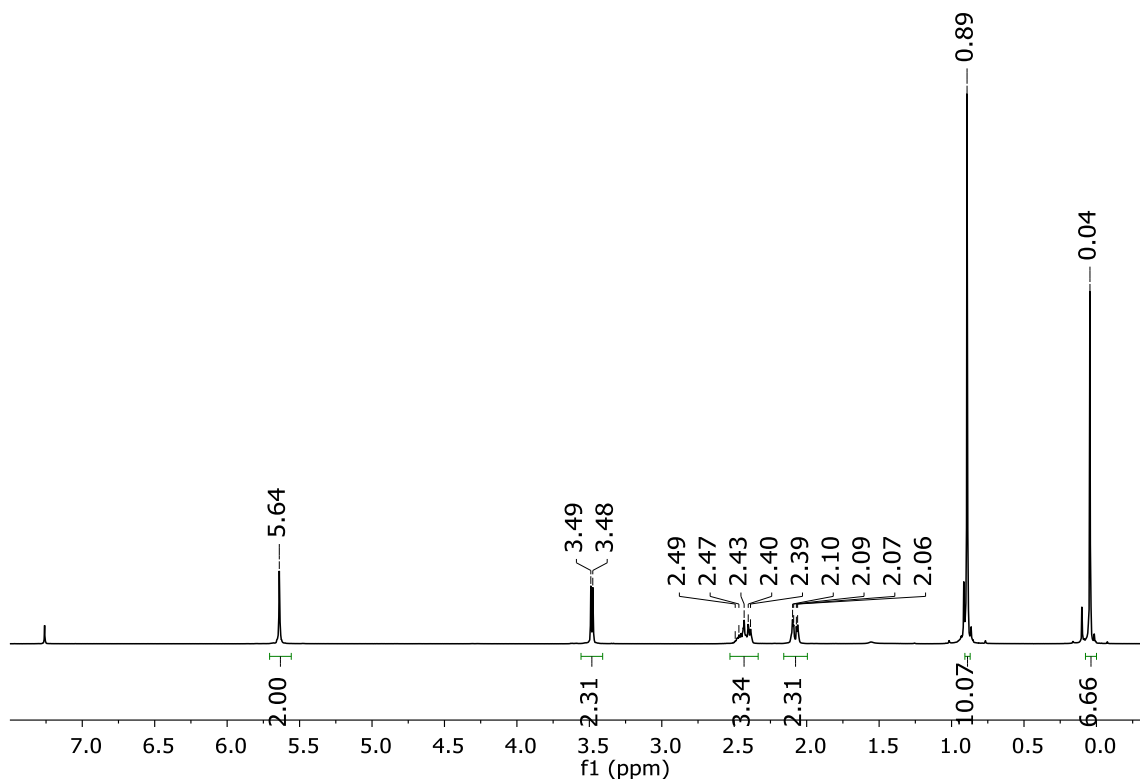


Synthesis of *tert*-butyl(cyclopent-3-en-1-ylmethoxy)dimethylsilane²⁴ (**1j**)

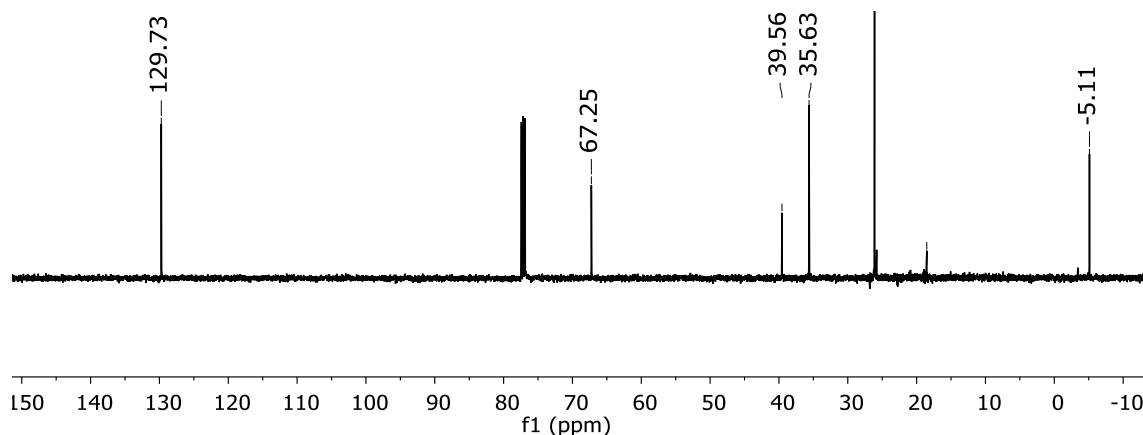


A solution of cyclopent-3-en-1-ylmethanol (1.0 g, 10.2 mmol, 1.0 equiv.) in 30 mL of dry DCM was stirred at 0 °C under nitrogen atmosphere. To this solution was added TBSCl (1.84 g, 12.2 mmol, 1.2 equiv.) and imidazole (1.39 g, 20.4 mmol, 2.0 equiv.). The turbid reaction mixture was allowed to stir overnight at room temperature. Water (15 mL) was added, and the organic layer was reserved. The aqueous layer was further extracted with DCM (2×15 mL). The combined organic layer was washed with brine (15 mL), dried with anhydrous sodium sulfate, and then concentrated. The crude product was purified by passing a short silica column, eluting with DCM, to afford the desired product as a colorless oil (1.9 g, 90%). ¹H NMR (CDCl₃, 500 MHz) δ 5.64 (s, 2H), 3.48 (d, *J* = 7 Hz, 2H), 2.49-2.39 (m, 3H), 2.10-2.06 (m, 2H), 0.89 (s, 9H), 0.04 (s, 6 H); ¹³C NMR (CDCl₃, 125 MHz) δ 129.7, 67.2, 39.6, 35.6, 26.1, 18.5, -5.1. HRMS-ESI (*m/z*): calculated for C₁₂H₂₅OSi [M+H]⁺, 213.1675; Found, 213.1678.

¹H NMR of **1j**



¹³C NMR of 1j



2.7.3 Ceiling Temperature Measurement

Definition: T_c represents a threshold where the depropagation rate equals the propagation rate. At each temperature, there is a monomer-polymer equilibrium and T_c in solution is defined as the temperature where the equilibrium monomer concentration ($[M]_e$) is 1 M.

$$\ln[M]_e = \frac{\Delta H_p}{R} \left(\frac{1}{T} \right) - \frac{\Delta S_p}{R} \quad \text{or} \quad T = \frac{\Delta H_p}{\Delta S_p + R \ln[M]_e}$$

$$\text{At } T_c, [M]_e = 1 \text{ M and } T_c(\text{solution}) = \frac{\Delta H_p}{\Delta S_p}$$

T_c measurement in solution polymerization: In the glove box, a low pressure/vacuum NMR tube was charged with the cyclopentene monomer (initial monomer concentration varied with different monomers in consideration of NMR integration error, see Table 2.3-2.11), THF- d_8 , 0.22 mol % Grubbs II and toluene or mesitylene (~50 mg) as the internal standard. The tube was placed in the NMR spectrometer at four different temperatures. At each temperature, an equilibration time of 1-3 h ensured that equilibrium was reached. The equilibrium monomer concentration $[M]_e$ was calculated according to the internal standard (Figure 2.5). By plotting $\ln[M]_e$ against $1/T$, ΔH_p and ΔS_p were determined based on the slope and y-intercept. For solution polymerization, ceiling temperature was calculated as $T_c(\text{solution}) = \Delta H_p / \Delta S_p$.

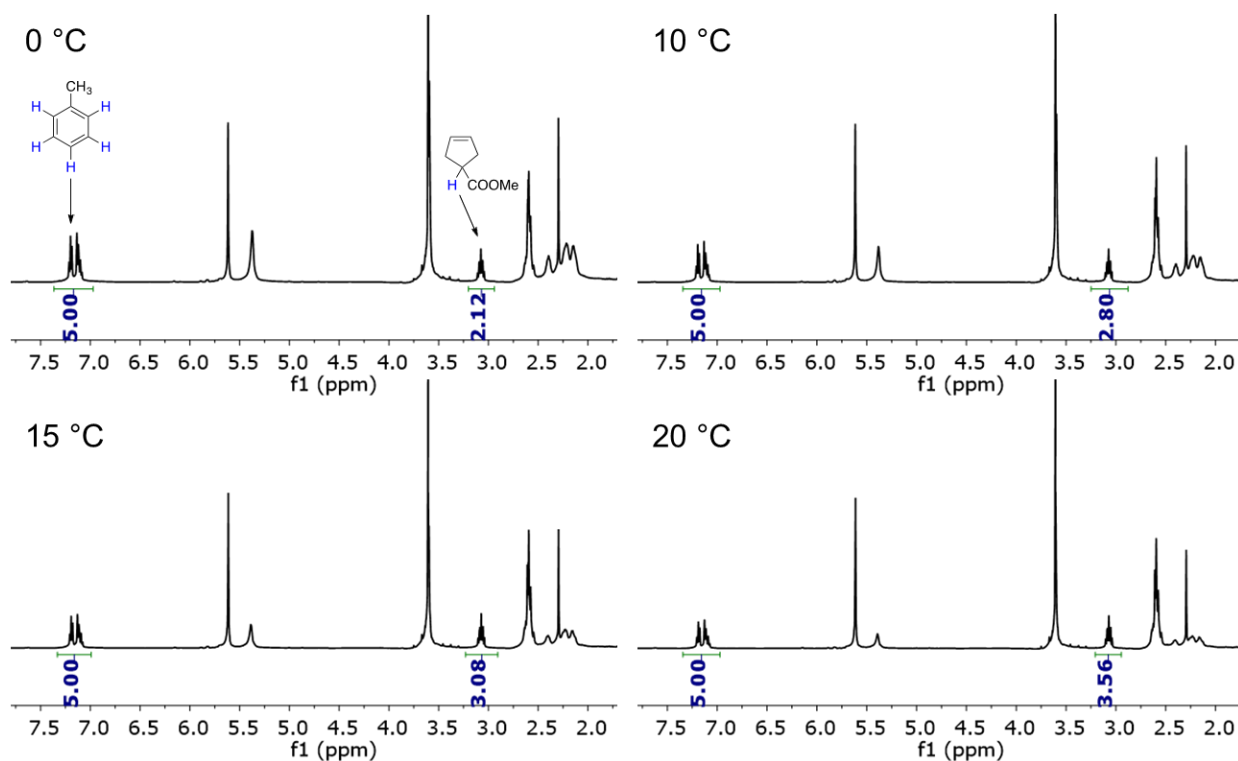


Figure 2.5 ^1H NMR spectra of **1f** in $\text{THF-}d_8$ at 0, 10, 15 and 20 °C (setting temperature) upon ROMP. $[M]_0 = 5\text{ M}$. Equilibrium time for each temperature is 1.5 h.

Table 2.3 A summary for $[M]_e$ of **1a** at 20, 30, 35 and 40 °C. $[M]_0 = 2\text{ M}$.

Setting Temp. (°C)	20	30	35	40
$[M]_e$ (mol/L)	0.68 ± 0.04	0.87 ± 0.04	0.95 ± 0.04	1.06 ± 0.05

Table 2.4 A summary for $[M]_e$ of **1b** at 15, 20, 25 and 30 °C. $[M]_0 = 2\text{ M}$.

Setting Temp. (°C)	15	20	25	30
$[M]_e$ (mol/L)	0.58 ± 0.006	0.64 ± 0.003	0.68 ± 0.01	0.74 ± 0.006

Table 2.5 A summary for $[M]_e$ of **1c** at 10, 20, 30 and 40 °C. $[M]_0 = 2\text{ M}$.

Setting Temp. (°C)	10	20	30	40
$[M]_e$ (mol/L)	0.64 ± 0.02	0.82 ± 0.006	1.06 ± 0.06	1.3 ± 0.05

Table 2.6 A summary for $[M]_e$ of **1d** at 0, 10, 20 and 30 °C. $[M]_0 = 3.3\text{ M}$.

Setting Temp. (°C)	0	10	20	30
$[M]_e$ (mol/L)	1.56 ± 0.01	1.94 ± 0.01	2.44 ± 0.03	3.03 ± 0.17

Table 2.7 A summary for $[M]_e$ of **1e** at 0, 10, 15 and 20 °C. $[M]_0 = 5 M$.

Setting Temp. (°C)	0	10	15	20
$[M]_e$ (mol/L)	3.16 ± 0.08	3.81 ± 0.03	4.18 ± 0.02	4.66 ± 0.02

Table 2.8 A summary for $[M]_e$ of **1f** at 0, 10, 15 and 20 °C. $[M]_0 = 5 M$.

Setting Temp. (°C)	0	10	15	20
$[M]_e$ (mol/L)	2.58 ± 0.02	3.24 ± 0.05	3.62 ± 0.08	4.03 ± 0.12

Table 2.9 A summary for $[M]_e$ of **1g** at 0, 10, 15 and 20 °C. $[M]_0 = 5 M$.

Setting Temp. (°C)	0	10	15	20
$[M]_e$ (mol/L)	1.73 ± 0.13	2.34 ± 0.06	2.75 ± 0.03	3.27 ± 0.05

Table 2.10 A summary for $[M]_e$ of **1h** at 10, 15, 20 and 30 °C. $[M]_0 = 7.3 M$.

Setting Temp. (°C)	10	15	20	30
$[M]_e$ (mol/L)	3.72 ± 0.04	4.21 ± 0.01	4.83 ± 0.05	6.21 ± 0.02

Table 2.11 A summary for $[M]_e$ of **1i** at -10, -5, 0 and 5 °C. $[M]_0 = 4.6 M$.

Setting Temp. (°C)	-10	-5	0	5
$[M]_e$ (mol/L)	1.19 ± 0.08	1.47 ± 0.02	1.63 ± 0.1	1.86 ± 0.03

Extrapolation to bulk polymerization: Maximum equilibrium monomer concentration $[M]_{\max}$ (i.e. neat monomer concentration) is calculated as $[M]_{\max} = \frac{\rho(\text{g/L})}{M(\text{g/mol})}$ (ρ is the density of the liquid monomer and M is its molar mass). Extrapolated $T_c(\text{neat}) = \frac{\Delta H_p}{\Delta S_p + R \ln[M]_{\max}}$ (R is the ideal gas constant).

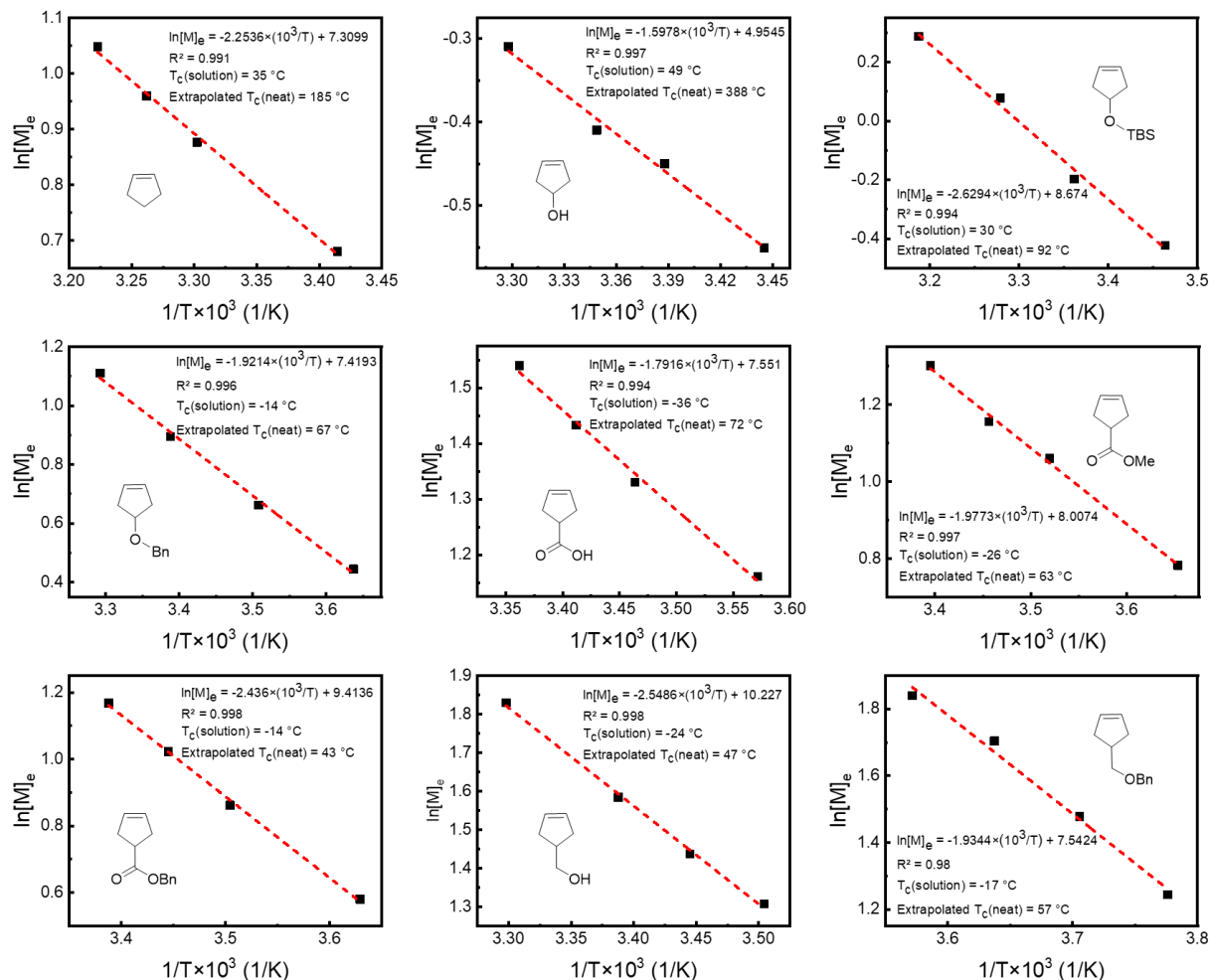


Figure 2.6 Thermodynamics of equilibrium ROMP of cyclopentene derivatives **1a-1i**.

Bulk polymerization of 1j (tert-butyl(cyclopent-3-en-1-ylmethoxy)dimethylsilane): In the glovebox, a vial was charged with 100 mg **1j** and 0.88 mg (0.22 mol %) Grubbs II catalyst. After 24 h, 0.05 mL ethyl vinyl ether was added to quench the catalyst. The resulting mixture was dissolved in THF- d_8 . No noticeable polymer peak was observed according to ^1H NMR.

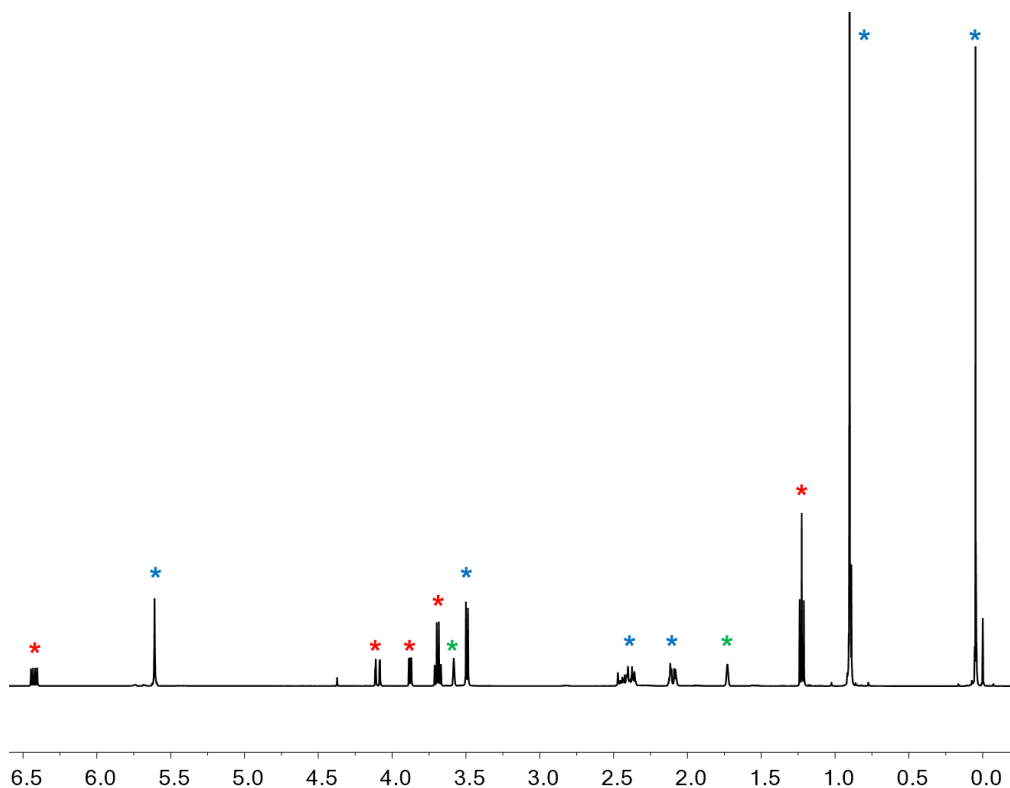


Figure 2.7 ^1H NMR spectrum of 24 h bulk polymerization of **1j**. (*monomer **1j**, *ethyl vinyl ether, *THF- d_8 solvent residue)

2.7.4 DSC Characterization

The DSC specimen was encapsulated using Tzero hermetic aluminum pan with 5-15 mg loading of polymerization mixture (neat monomer and 0.22 mol % Grubbs II reacting for 2 h). Typical DSC measurement was done by heating specimen from $-50\text{ }^\circ\text{C}$ to $120\text{ }^\circ\text{C}$ with a ramping rate of $10\text{ }^\circ\text{C}/\text{min}$. For all samples, the significant exothermic peaks in heating cycle are identified as depolymerization peaks, which was further confirmed by ^1H NMR. Peak maximum is reported as T_d and compared with extrapolated $T_c(\text{neat})$ values obtained from VT-NMR results.

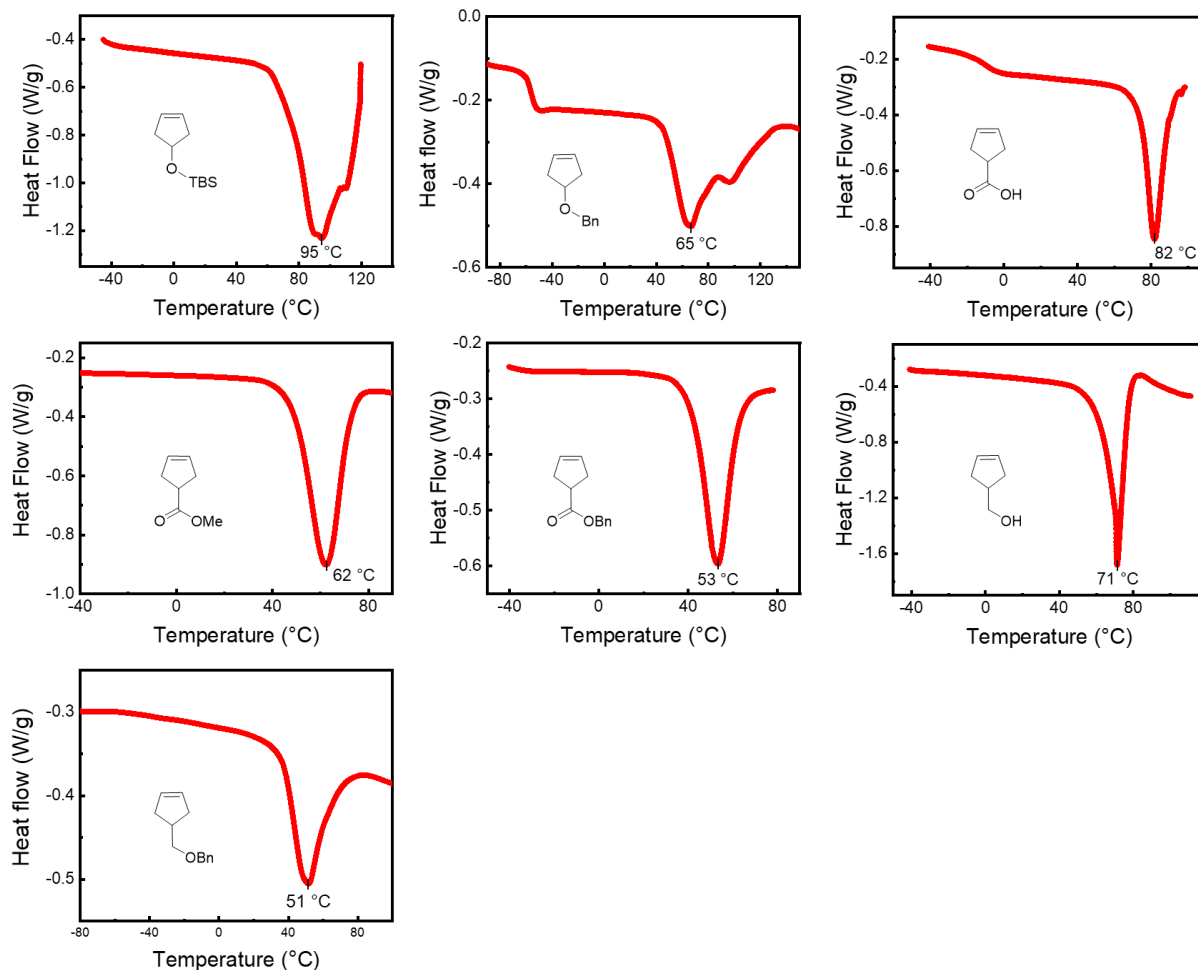


Figure 2.8 Depolymerization peak maximums of polymerization mixture of cyclopentene derivatives **1c-1i**. The samples were a monomer-polymer equilibrated mixture from bulk polymerization at room temperature.

2.7.5 Evaluation of Reversibility

Depolymerization-repolymerization cycle for monomer 1g: A mixture of 9.23 mg Grubbs II (0.011 mmol, 0.22 mol%) and 1 g neat monomer **1g** (4.94 mmol, 1.0 equiv.) was evenly distributed in eight separate vials (A-H) under Ar atmosphere in the glove box. Monomer conversion and M_n of the obtained polymer were determined by ^1H NMR and GPC, respectively. All vials were first heated to 50 °C for 10 min and 0.1 mL ethyl vinyl ether was added to vial A which is referred as “heating cycle #1”. Vial B-H were brought back to room temperature for 2 h; 0.1 mL ethyl vinyl ether was added to vial B which is “cooling cycle #1”. The reversibility was evaluated for another three cycles. M_n of the equilibrated polymer-monomer mixture was

calculated according to the equation: $M_n(\text{polymer-monomer mixture}) = \text{monomer conversion} \cdot M_n(\text{polymer}) + (1 - \text{monomer conversion}) \cdot M(\text{monomer molar mass})$

Other catalysts such as HG II and Grubbs III catalysts were also tested. However, they both exhibited worse reversibility compared to Grubbs II.

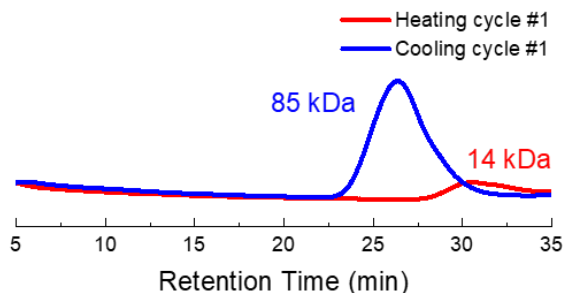


Figure 2.9 Representative GPC traces of first heating-cooling cycle of **1g**.

Table 2.12 Depolymerization-repolymerization cycle of **1f**.

Cycle	Monomer conversion (%)	M_n (polymer) (kDa)	M_n (polymer-monomer mixture) (kDa)
Heating cycle #1	9 ± 2	13 ± 4	1.5 ± 0.6
Cooling cycle #1	51 ± 2	81 ± 3	41 ± 2
Heating cycle #2	13 ± 3	15 ± 1	2.1 ± 0.5
Cooling cycle #2	48 ± 1	67 ± 4	32 ± 2
Heating cycle #3	13 ± 2	14 ± 2	1.9 ± 0.1
Cooling cycle #3	48 ± 2	66 ± 3	32 ± 3
Heating cycle #4	11 ± 1	14 ± 4	1.7 ± 0.6
Cooling cycle #4	45 ± 3	70 ± 3	31 ± 3

Table 2.13 Depolymerization-repolymerization cycle of **1g**.

Cycle	Monomer conversion (%)	M_n (polymer) (kDa)	M_n (polymer-monomer mixture) (kDa)
Heating cycle #1	32 ± 2	13 ± 2	4 ± 1
Cooling cycle #1	64 ± 2	32 ± 1	20 ± 1
Heating cycle #2	47 ± 2	22 ± 1	10 ± 1
Cooling cycle #2	53 ± 1	26 ± 1	14 ± 1
Heating cycle #3	51 ± 2	25 ± 1	13 ± 1

2.8 Notes and References

Notes:

Portions of this chapter have been published: Liu, H.; Nelson, A. Z.; Ren, Y.; Yang, K.; Ewoldt, R. H.; Moore, J. S. “Dynamic Remodeling of Covalent Networks via Ring-Opening Metathesis Polymerization” *ACS Macro Lett.* **2018**, *7*, 933-937. They are reproduced/adapted with permission. Copyright 2018 American Chemical Society.

References:

- (1) Nishida, H. Development of Materials and Technologies for Control of Polymer Recycling. *Polymer Journal*. Nature Publishing Group **2011**, 435–447.
- (2) Diesendruck, C. E.; Peterson, G. I.; Kulik, H. J.; Kaitz, J. A.; Mar, B. D.; Boydston, A. J.; Moore, J. S.; May, P. A.; White, S. R.; Marti, T. J. Mechanically Triggered Heterolytic Unzipping of a Low-Ceiling-Temperature Polymer. *Nat. Chem.* **2014**, *6*, 624–629.
- (3) Endo, T.; Nagai, D. A Novel Construction of Ring-Opening Polymerization and Chemical Recycling System. In *Macromolecular Symposia*; 2005; Vol. 226, 79–86.
- (4) Kawaguchi, A. W.; Sudo, A.; Endo, T. Polymerization-Depolymerization System Based on Reversible Addition-Dissociation Reaction of 1,3-Benzoxazine with Thiol. *ACS Macro Lett.* **2013**, *2*, 1–4.
- (5) Endo, T.; Kakimoto, K.; Ochiai, B.; Nagai, D. Synthesis and Chemical Recycling of a Polycarbonate Obtained by Anionic Ring-Opening Polymerization of a Bifunctional Cyclic Carbonate. *Macromolecules* **2005**, *38*, 8177–8182.
- (6) Miyagawa, T.; Shimizu, M.; Sanda, F.; Endo, T. Six-Membered Cyclic Carbonate Having Styrene Moiety as a Chemically Recyclable Monomer. Construction of Novel Cross-Linking-de-Cross-Linking System of Network Polymers. *Macromolecules* **2005**, *38*, 7944–7949.
- (7) Endo, T.; Suzuki, T.; Sanda, F.; Takata, T. A Novel Network Polymer \rightleftharpoons Linear Polymer Reversible System. A New Cross-Linking System Consisting of a Reversible Cross-Linking–Depolymerization of a Polymer Having a Spiro Orthoester Moiety in the Side Chain. *Macromolecules* **1996**, *29*, 4819–4819.
- (8) Chen, X.; Dam, M. A.; Ono, K.; Mal, A.; Shen, H.; Nutt, S. R.; Sheran, K.; Wudl, F. A Thermally Re-Mendable Cross-Linked Polymeric Material. *Science* **2002**, *295*, 1698–

1702.

- (9) Chen, X.; Wudl, F.; Mal, A. K.; Shen, H.; Nutt, S. R. New Thermally Remendable Highly Cross-Linked Polymeric Materials. *Macromolecules* **2003**, *36*, 1802–1807.
- (10) Liu, Y. L.; Hsieh, C. Y. Crosslinked Epoxy Materials Exhibiting Thermal Remendability and Removability from Multifunctional Maleimide and Furan Compounds. *J. Polym. Sci. Part A Polym. Chem.* **2006**, *44*, 905–913.
- (11) Baker, M. S.; Kim, H.; Olah, M. G.; Lewis, G. G.; Phillips, S. T. Depolymerizable Poly(Benzyl Ether)-Based Materials for Selective Room Temperature Recycling. *Green Chem.* **2015**, *17*, 4541–4545.
- (12) Duda, A.; Kowalski, A. Thermodynamics and Kinetics of Ring-Opening Polymerization. In *Handbook of Ring-Opening Polymerization*; **2009**; 1–51.
- (13) Ivin, K. J. Thermodynamics of Addition Polymerization. *J. Polym. Sci. Part A Polym. Chem.* **2000**, *38*, 2137–2146.
- (14) Hong, M.; Chen, E. Y. Completely Recyclable Biopolymers with Linear and Cyclic Topologies via Ring-Opening Polymerization of γ -Butyrolactone. *Nat. Chem.* **2016**, *8*, 42–49.
- (15) Tuba, R.; Grubbs, R. H. Ruthenium Catalyzed Equilibrium Ring-Opening Metathesis Polymerization of Cyclopentene. *Polym. Chem.* **2013**, *4*, 3959–3962.
- (16) Tuba, R.; Al-Hashimi, M.; Bazzi, H. S.; Grubbs, R. H. One-Pot Synthesis of Poly(Vinyl Alcohol) (PVA) Copolymers via Ruthenium Catalyzed Equilibrium Ring-Opening Metathesis Polymerization of Hydroxyl Functionalized Cyclopentene. *Macromolecules* **2014**, *47*, 8190–8195.
- (17) Tuba, R.; Balogh, J.; Hlil, A.; Barlóg, M.; Al-Hashimi, M.; Bazzi, H. S. Synthesis of Recyclable Tire Additives via Equilibrium Ring-Opening Metathesis Polymerization. *ACS Sustain. Chem. Eng.* **2016**, *4*, 6090–6094.
- (18) Hillmyer, M. A.; Laredo, W. R.; Grubbs, R. H. Ring-Opening Metathesis Polymerization of Functionalized Cyclooctenes by a Ruthenium-Based Metathesis Catalyst. *Macromolecules* **1995**, *28*, 6311–6316.
- (19) Hejl, A.; Scherman, O. A.; Grubbs, R. H. Ring-Opening Metathesis Polymerization of Functionalized Low-Strain Monomers with Ruthenium-Based Catalysts. *Macromolecules* **2005**, *38*, 7214–7218.

- (20) Fürstner, A. Olefin Metathesis and Beyond. *Angew. Chemie* **2000**, *39*, 3012–3043.
- (21) Soon, H. H.; Wenzel, A. G.; Salguero, T. T.; Day, M. W.; Grubbs, R. H. Decomposition of Ruthenium Olefin Metathesis Catalysts. *J. Am. Chem. Soc.* **2007**, *129*, 7961–7968.
- (22) Ulman, M.; Grubbs, R. H. Ruthenium Carbene-Based Olefin Metathesis Initiators: Catalyst Decomposition and Longevity. *J. Org. Chem.* **1999**, *64*, 7202–7207.
- (23) Fu, G. C.; Grubbs, R. H. The Synthesis of Nitrogen Heterocycles via Catalytic Ring-Closing Metathesis of Dienes. *J. Am. Chem. Soc.* **1992**, *114*, 7324–7325.
- (24) Knapp, S.; Younong, Y. Synthesis of the Oxygenated Pactamycin Core. *Org. Lett.* **2007**, *9*, 1359–1362.
- (25) Brookes, P. C.; Milne, D. J.; Murphy, P. J.; Spolaore, B. Epoxide Rearrangements Using Dilithiated Aminoalcohols as Chiral Bases. *Tetrahedron* **2002**, *58*, 4675–4680.
- (26) Lemieux, R. M.; Popovici-Muller, J.; Travins, J.; Cai, Z.; Cui, D. W.; Zhou, D. Therapeutically Active Compositions and Their Methods of Use. Google Patents July 25, **2013**.

Chapter 3: Dynamic Remodeling of Network Polymers via Ring-Opening Metathesis Polymerization

3.1 Abstract

Reversible transformations in bulk polymers offer numerous possibilities for materials remodeling and reprocessing. While reversible systems based on dynamic covalent chemistry such as the Diels-Alder reaction and transesterification have been intensively studied to enable local bond dissociation and formation, reports regarding the reversion from bulk network polymers to monomers are rare. Herein, we demonstrated a reversibly polymerizable system based on ROMP of multifunctional cyclopentene derivatives in the neat state. The network polymer is mechanically robust at room temperature and readily depolymerizes at elevated temperatures to yield liquid monomer which is repolymerized to cross-linked polymers by simply cooling to room temperature. This reversible process was characterized by DSC and rheological tests.

3.2 Introduction

Remodeling is an important process in biological systems for resiliency and maintenance.^{1,2} A common example is the remodeling of actin filament, a supramolecular polymer, that allows for the dynamic alterations of cellular organization.³ Upon certain chemical stimuli, actin filaments are depolymerized; the resulting monomers are repolymerized to reshape the cell to a new environment. Inspired by the biopolymers, synthetic polymers capable of remodeling have the potential to reconfigure and adapt themselves to a changing environment by removing and replacing the activated regions with newly synthesized materials.

A promising materials candidate for remodeling is covalent-adaptable networks (CANs) where reversible chemical bonds are incorporated.⁴⁻⁸ As heat is one of the simplest stimuli, thermoresponsive CANs have been widely studied for shape memory and self-healing applications. Many chemistries have been utilized, including reversible addition (or condensation) such as the Diels-Alder reaction, and reversible exchange reactions such as transesterification and transimination. These CANs are reconfigurable and recyclable while still possessing the

mechanical benefits of traditional thermosets. At elevated temperatures, CANs partially depolymerize, resulting in linear polymers or less cross-linked systems with decreased moduli. Subsequent cooling allows repolymerization which affords networks with higher moduli. While these systems are reversible, depolymerization often leads to irreversible degradation of the polymer networks since T_c is typically high.⁹ In this chapter, we demonstrate a reversibly polymerizable system based on ROMP of cyclopentene derivatives with the interconversion between network polymers and neat liquid monomers. As shown in Figure 3.1, network polymers are readily depolymerized upon heating to liquid monomers which are transported and reshaped; the subsequent repolymerization affords network polymers by simply cooling the system to room temperature.

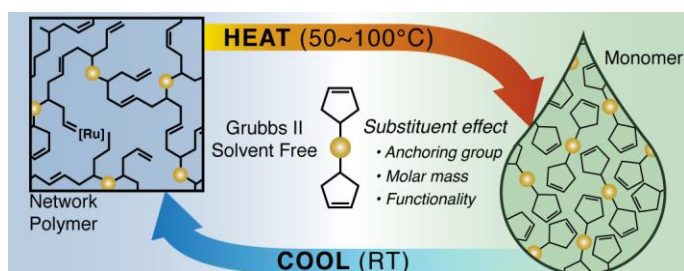


Figure 3.1 Schematic of the polymerization-depolymerization cycle of network polymers via ROMP.

ROMP is potentially an excellent system to achieve reversibility of bulk materials for two main reasons. First, dynamic covalent bond formation has been demonstrated in olefin metathesis both in solution and in the bulk state.¹⁰⁻¹² Grubbs II exhibits excellent reactivity even in the solid polymers where chain movement is limited. Second, as discussed in Chapter 2, polypentenamers are readily depolymerized under solvent-free conditions due to the low $T_c(\text{neat})$ values. The ideal monomer for remodeling purposes will efficiently polymerize at room temperature to afford mechanically robust polymers which will fully depolymerize upon a mild thermal stimulus.

3.3 Design of Multifunctional Cyclopentene Derivatives

In the last chapter, we demonstrated that introducing functional group (i.e., carbonyl or alkoxy group) at the homoallylic position effectively lower $T_c(\text{neat})$, which enables the bulk depolymerization of polypentenamers at temperatures ranging from 40-100 °C. We envisioned

that a monomer with the same functional group that links multiple cyclopentene moieties results in CANs that depolymerize at elevated temperatures, which meets the criteria for remodeling. As shown in Figure 3.2, we selected five monomers (**2a-2d** and **3a**) with different anchor groups and investigated their polymerization-depolymerization behavior.

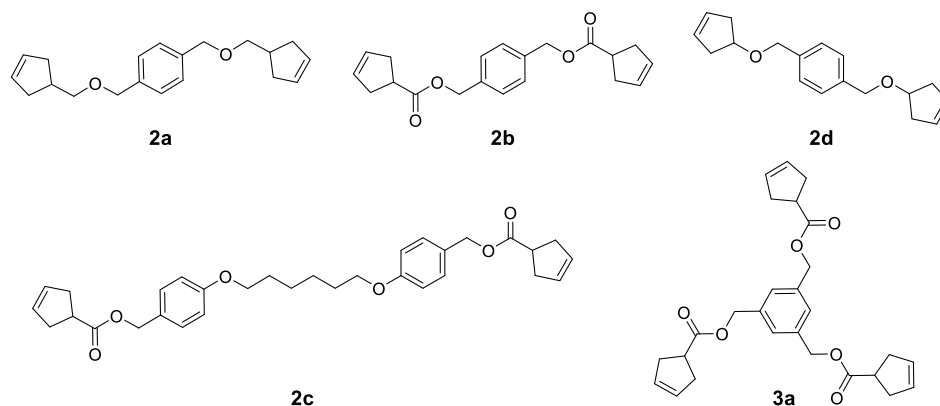


Figure 3.2 Multifunctional cyclopentene derivatives investigated in this study.

Neat multifunctional cyclopentene derivatives polymerize at a much slower rate to reach equilibrium compared to the monofunctional ones discussed in Chapter 2 due to the limited chain mobility. This is supported by the rheological data of bulk polymerization at 25 °C for 24 hours. As indicated by the change in viscoelastic storage modulus G' in Figure 3.3, bulk polymerization of **1g** initiated within 2 min while **2b** started to polymerize after 30 min. G' associated with **1g** first increased to a maximum value of 10^4 Pa due to the sluggish initiation of Grubbs II that led to the formation of high M_n of 300 kDa (theoretical M_n is 90 kDa based on monomer/catalyst ratio) at the early stage of polymerization. After 2-hour bulk polymerization at 25 °C, ROMP of **1g** reached the equilibrium with constant monomer conversion (55%) determined by ^1H NMR even though M_n and G' continued to drop owing to active chain transfer reactions. The polymerization mixture of **1g** is a monomer-swollen gel with no mechanical strength (Figure 3.14). In contrast, ROMP of **2b** afforded a network polymer with much improved mechanical properties since G' reached MPa region within 2 hours and increased slightly after 24 hours. Stress relaxation of the resulting poly(**2b**) further confirmed its mechanical integrity (Figure 3.10).

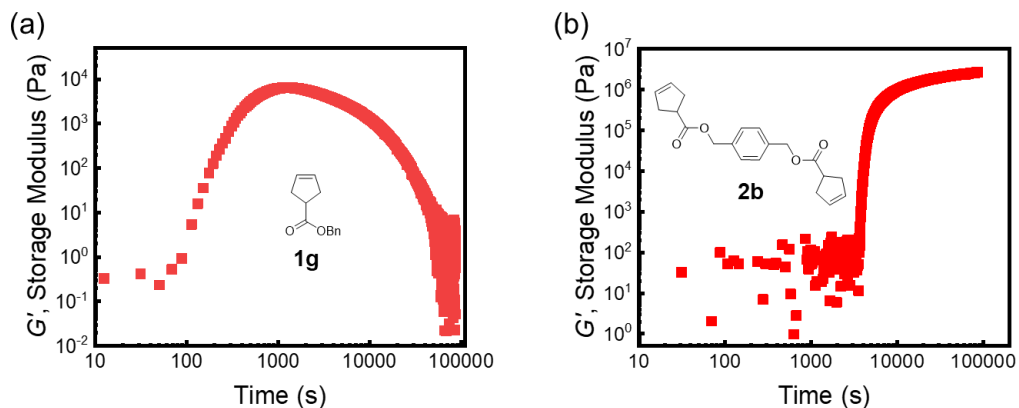


Figure 3.3 Rheological characterization of bulk polymerization of (a) **1g** and (b) **2b** at 25 °C for 24 hours.

Since the rheological data does not provide quantitative information on monomer conversion, ^1H NMR (of unreacted monomer), DSC, and Raman were employed to monitor ROMP of **2b** (Figure 3.6 and 3.9, Table 3.3-3.4). These three different methods led to similar results, and ^1H NMR was applied for quantification in the rest of the study. As shown in Table 3.1, CAN obtained from **2b** is highly sensitive to temperature. There was slight depolymerization after heating at 60 °C and near quantitative depolymerization at 75 °C. This observation is consistent with the DSC and rheological characterization (Figure 3.7 and 3.10).

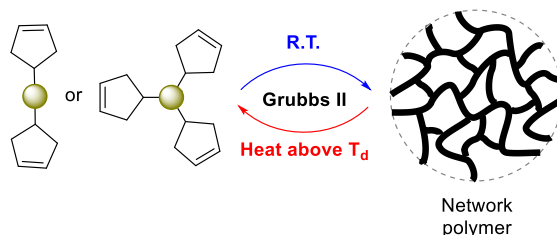
Table 3.1 Conversion of **2b** at different temperatures determined by ^1H NMR after 10-min initiation at 55 °C followed by 2-h polymerization at 25 °C.

Temperature (°C)	25	50	60	70	75
Conversion (%)	76 ± 2	74 ± 1	55 ± 6	21 ± 1	< 5

With the encouraging results from **2b**, we further investigated the polymerizability of monomers (**2a**, **2d** and **3a**) with other anchoring groups. Because **2a** and **2d** are solids at room temperature with melting points of 44 °C and 41 °C, bulk polymerization was first initiated at 50 °C for 30 min before being brought back to room temperature for 24 h. As shown in Table 3.2 and Figure 3.7, T_d and monomer conversion follow the same trend as the monofunctional monomers studied in Chapter 2: **2d** > **2b** > **2a**. To further probe the effect of anchor group, **2c** (melting point 75 °C) which has the same ester anchor group as **2b** but possesses much larger molecular weight was also examined. It was found that molecular weight has a negligible effect on polymerization and depolymerization behavior. In terms of T_d and monomer conversion under the same bulk polymerization conditions, **2b** and **2c** were nearly identical, indicating that the

anchor group effect is the main contributor to the thermodynamics. For trifunctional monomer **3a**, depolymerization occurs at a higher temperature than **2b** due to a higher degree of cross-linking, but its conversion to network polymer was the same as **2b** under the same polymerization conditions. Thus, as the functionality of cyclopentene increases (from monofunctional to trifunctional monomer), polymerizability increases accordingly.

Table 3.2 Reversible polymerization of difunctional and trifunctional monomers.



Monomer	T_d^a (°C)	Monomer conversion ^b (%)
2a	60 ± 1	79 ± 1
2b	76 ± 2	86 ± 2
	83 ± 3 ^c	78 ± 3 ^c
2c	76 ± 2 ^c	74 ± 1 ^c
2d	97 ± 2	92 ± 2
3a	89 ± 1	86 ± 1

^a Determined by DSC with a ramping rate of 10 °C/min. ^b Calculated from the unreacted monomers after 24-h bulk polymerization at room temperature by ¹H NMR using mesitylene as the internal standard. ^c Polymerization was initiated at 80 °C for 30 min and then carried out at room temperature for 24 h.

3.4 Tuning Depolymerization Behavior by Copolymerization

Besides varying T_d by different substituents, another approach to tune depolymerization behavior is by copolymerizing two monomers with disparate T_d values. To demonstrate this approach, we copolymerized **2b** and **1g**. Because the similarity of these two comonomers in structure, they formed a uniform random copolymerized CAN and its depolymerization behavior was observed as a narrow endothermic peak on DSC (Figure 3.8). By introducing different amounts of comonomer **2b**, T_d of the CAN was varied between $T_d(\mathbf{1g})$ and $T_d(\mathbf{2b})$ linearly as shown in Figure 3.4. The depolymerization behavior was further characterized by rheological measurements (Figure 3.11-3.13). Elevating the temperature near T_d significantly depolymerized

the solid network and resulted in a liquid as both viscoelastic storage modulus G' and loss modulus G'' dropped below the minimum torque resolution of the experimental setup.

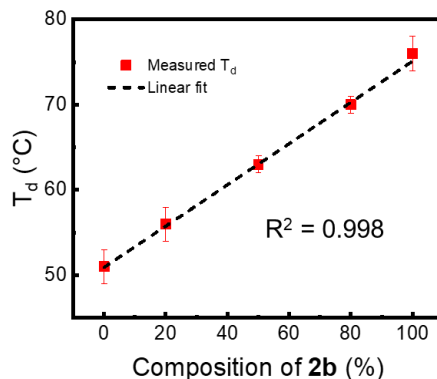


Figure 3.4 Depolymerization temperatures of CANs obtained from different **2b:1g** ratio.

3.5 Evaluation of Reversibility by Rheological Characterization

Rheological measurements were then performed to investigate the reversibility of CAN from difunctional monomer **2b** by cycling the temperature between 70 °C and 25 °C. As shown in Figure 3.5 (a), 2-h polymerization at 25 °C afforded CANs with a $G'[1] = 1.78$ MPa where [1] refers to the first polymerization cycle. This modulus is within the typical range for a rubber elastic network. When heated to 70 °C, G' fell precipitously, indicating fast depolymerization; upon cooling to 40 °C, the liquid repolymerized almost immediately and after developing at 25 °C for the same 2 hours, G' recovered to a value of $G'[2] = 0.39$ MPa (22% of $G'[1]$). After a second cycle of heating and cooling, G' was further reduced to 10% of $G'[2]$. One reason for the substantial loss of reversibility is that network polymers are much less mobile compared to the monofunctional system, which slows down the kinetics of the metathesis. Another reason is the presence of side reactions that deactivate Grubbs' catalyst at high temperatures, which is similar to the monofunctional system.

To improve the recovery behavior, we increased the loading of Grubbs II to five times while keeping the other experimental conditions the same. Following the same heating-cooling cycle procedure, G' recovered to 41% and 29% of $G'[1]$ after the first and second cooling cycles, respectively (Figure 3.15 and Table 3.5). The increased recovery efficiency supports the hypothesis of catalyst deactivation by heating. It also implies that Grubbs II partially initiated

during the first cycle of polymerization, and the higher recovery efficiency benefited from the uninitiated catalysts. Therefore, the reversibility of the second cycle significantly dropped compared to the first one. Introducing more catalysts serves as a reservoir, but this approach is not ideal for practical applications due to the cost of the catalysts.

Another approach is to avoid depolymerization at high temperatures that deactivate the catalysts. As demonstrated in Figure 3.5 (b), by copolymerizing **2b** and **1g** at a molar ratio of 1:4 with a T_d of 55 °C, recovery efficiency was greatly improved to 54% and 60% after the first and second cooling cycles, respectively. If longer time (3 h) was allowed for repolymerization at 25 °C, G' was able to recover 100% compared to the previous cycle. Therefore, we have shown that CANs based on cyclopentene derivatives are capable of reversibly transitioning between a stiff solid and a liquid with moderate recovery efficiency on repolymerization.

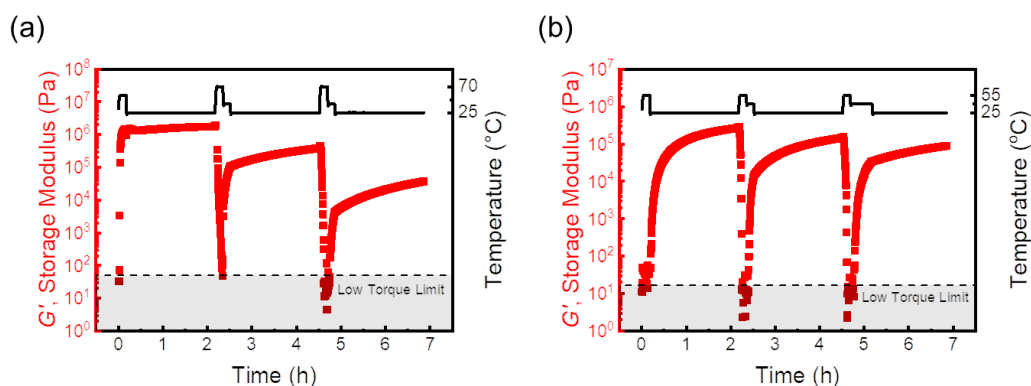


Figure 3.5 Rheological characterization at 1 rad/s of CANs from (a) **2b** and (b) 1:4 copolymerization of **2b** and **1g**. Both samples were first initiated at 55 °C and cycled between 25 °C and T_d .

3.6 Conclusion

We developed a series of CANs for remodeling applications based on ROMP. We demonstrated that varying the anchoring group on the cyclopentene ring affords tunable T_d ranging from 50 °C to 100 °C. The neat cyclopentene monomer polymerizes at room temperature with moderate to high yields, and the resulting CAN readily depolymerizes at elevated temperatures. This depolymerization-repolymerization process is modulated solely by temperature changes and is reversible for several cycles. For reversibility tests, we were able to improve the recovery performance by increasing the catalyst loading or lowering the

depolymerization temperature via copolymerization. To our best knowledge, this is the first example demonstrating highly efficient reversible transformation between cross-linked polymer (G' in MPa region) and neat liquid monomer (viscosity $\eta \approx 10^{-2}$ Pa·s) under mild temperature stimulus.

3.7 Experimental Details

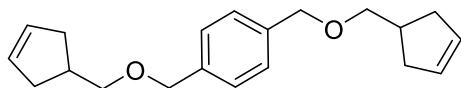
3.7.1 Materials and General Methods

All air or moisture-sensitive experiments were performed under argon atmosphere in the glove box (MBRAUN UNIlab Plus). Unless otherwise stated, all starting materials and reagents were purchased from commercial suppliers (Sigma-Aldrich, Enamine, Oakwood Chemical, Alfa Aesar, and TCI America) and were used without further purification. ^1H and ^{13}C NMR spectra were recorded on a Varian Unity 500 MHz spectrometer or a Varian Unity 600 MHz spectrometer in the VOICE NMR laboratory at the University of Illinois. Chemical shifts are reported in δ (ppm) relative to the residual solvent peak (CDCl_3 : 7.26, $\text{THF-}d_8$: 1.73 for ^1H ; CDCl_3 : 77.16 for ^{13}C). Coupling constants (J) are reported in Hertz (Hz). Splitting patterns are designated as s (singlet), d (doublet), t (triplet), q (quartet), quint (quintet), dd (doublet of doublets) and m (multiplet). The temperatures of Variable Temperature NMR (VT-NMR) experiments were calibrated by neat methanol (low temperature calibration) and neat ethylene glycol (high temperature calibration). High-resolution ESI mass spectra were recorded on a Micromass 70-VSE spectrometer through the Mass Spectrometry Facility, SCS at University of Illinois. The DSC measurement was performed using TA Instrument Q20 Differential Scanning Calorimeter equipped with a Liquid Nitrogen Cooling System (LNCS). Tzero hermetic aluminum pans and lids were used as sample testing containers. Nitrogen was used as sample purge gas. Raman spectra were collected on a Horiba LabRAM HR 3D Raman spectroscopy imaging system using a 532 nm laser line as the excitation source. Rheological characterization was conducted on an ARES-G2 rotational rheometer (separated motor-transducer) from TA Instruments using 8mm or 25mm parallel plates with a nominal gap of 1mm. A forced-convection oven was used for temperature control and to provide an inert nitrogen atmosphere. Viscoelastic moduli were characterized as a function of time at a frequency of 1 rad/s, and strain amplitudes of 1%. The relaxation modulus after polymerization was characterized with a strain

of 1% over the timescale of hundreds of seconds. The magnitude of complex viscosity after depolymerization was characterized at 1 rad/s as a function of strain amplitude.

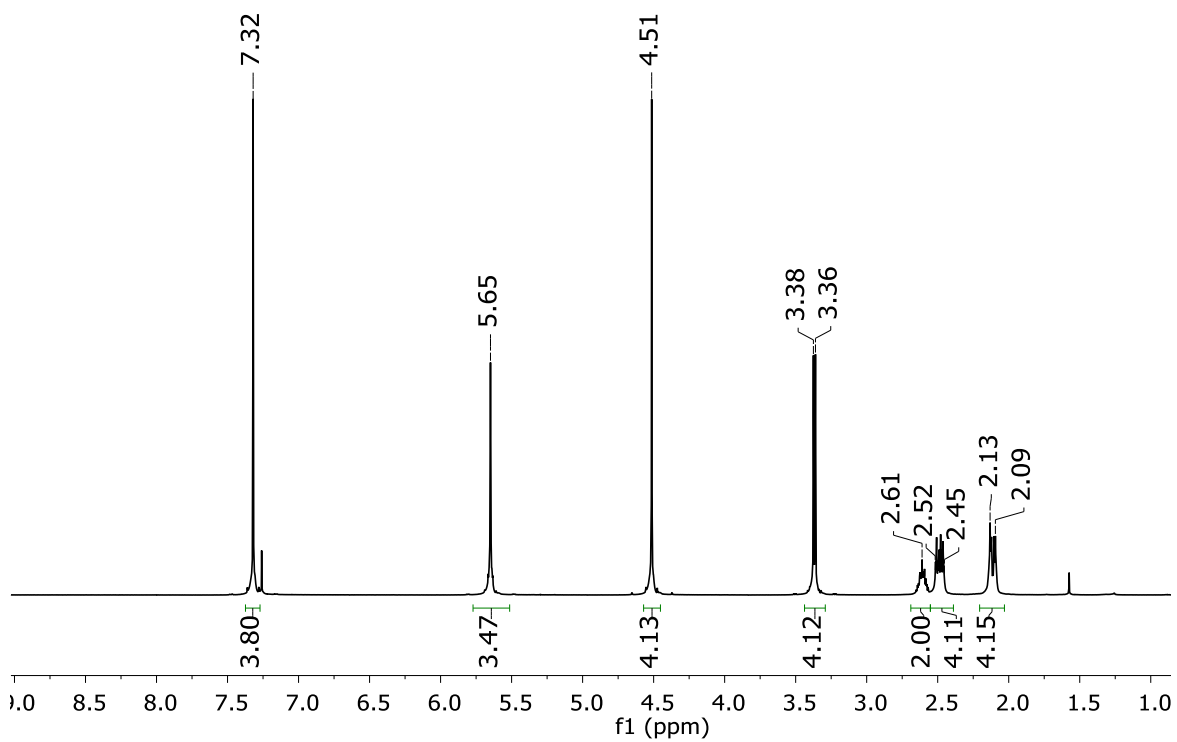
3.7.2 Synthesis of Multifunctional Cyclopentene Derivatives

Synthesis of 1,4-bis((cyclopent-3-en-1-ylmethoxy)methyl)benzene (2a)

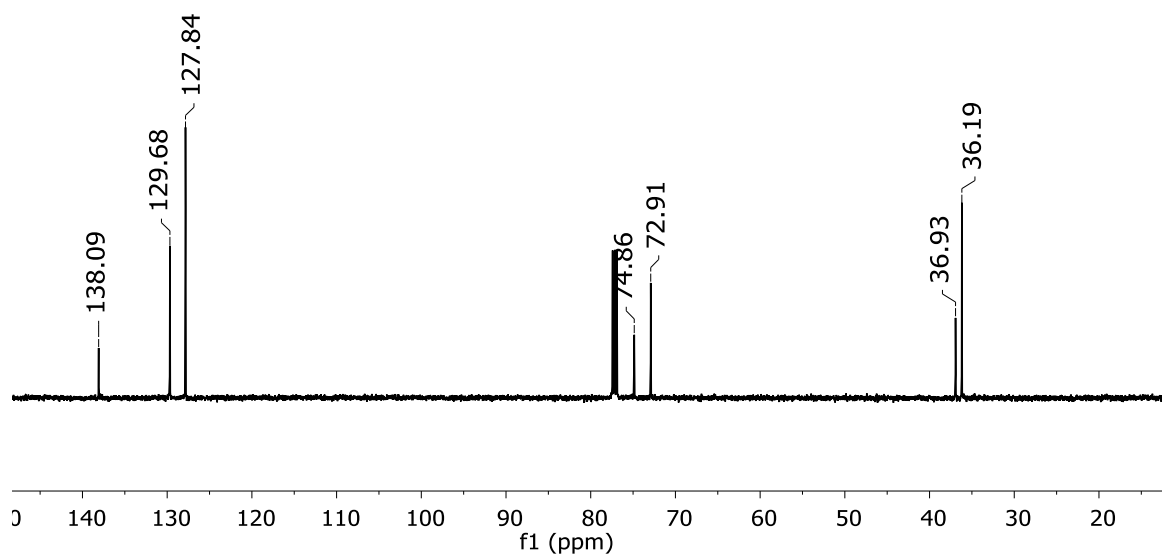


NaH (60% dispersion in mineral oil, 1.63 g, 40.8 mmol, 6.0 equiv.) was added to a solution of cyclopent-3-en-1-ylmethanol (2.0 g, 20.4 mmol, 3.0 equiv.) in 30 mL of dry THF at room temperature under a nitrogen atmosphere. After effervescence had ceased, α,α' -dibromo-*p*-xylene (1.79 g, 6.8 mmol, 1.0 equiv.) was added dropwise and the resulting mixture was allowed to heat at 40 °C for 4 hours. Excess NaH was carefully quenched by H₂O. After removing all the volatiles from the reaction mixture, water (15 mL) was added and further extracted with EtOAc (2×15 mL). The combined organic layer was washed with brine (15 mL), dried with anhydrous sodium sulfate, and then concentrated. The crude product was purified by passing a short silica column to afford the desired product as a white solid (1.56 g, 77%, m.p. 44 °C). ¹H NMR (CDCl₃, 500 MHz) δ 7.32 (s, 4H), 5.65 (s, 4H), 4.51 (s, 4H), 3.37 (d, $J = 7$ Hz, 4H), 2.61 (m, 2H), 2.52-2.45 (m, 4H), 2.13-2.09 (m, 4H); ¹³C NMR (CDCl₃, 125 MHz) δ 138.1, 129.7, 127.8, 74.9, 72.9, 36.9, 36.2. HRMS-ESI (m/z): calculated for C₂₀H₂₆O₂Na [M+Na]⁺, 321.1831; Found, 321.1833. Anal. Calcd for C₂₀H₂₆O₂: C, 80.50; H, 8.78. Found: C, 80.39; H, 8.68.

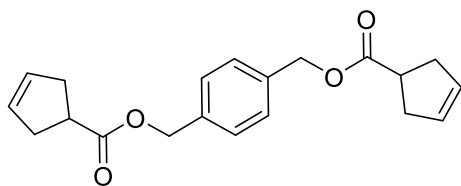
¹H NMR of 2a



¹³C NMR of 2a

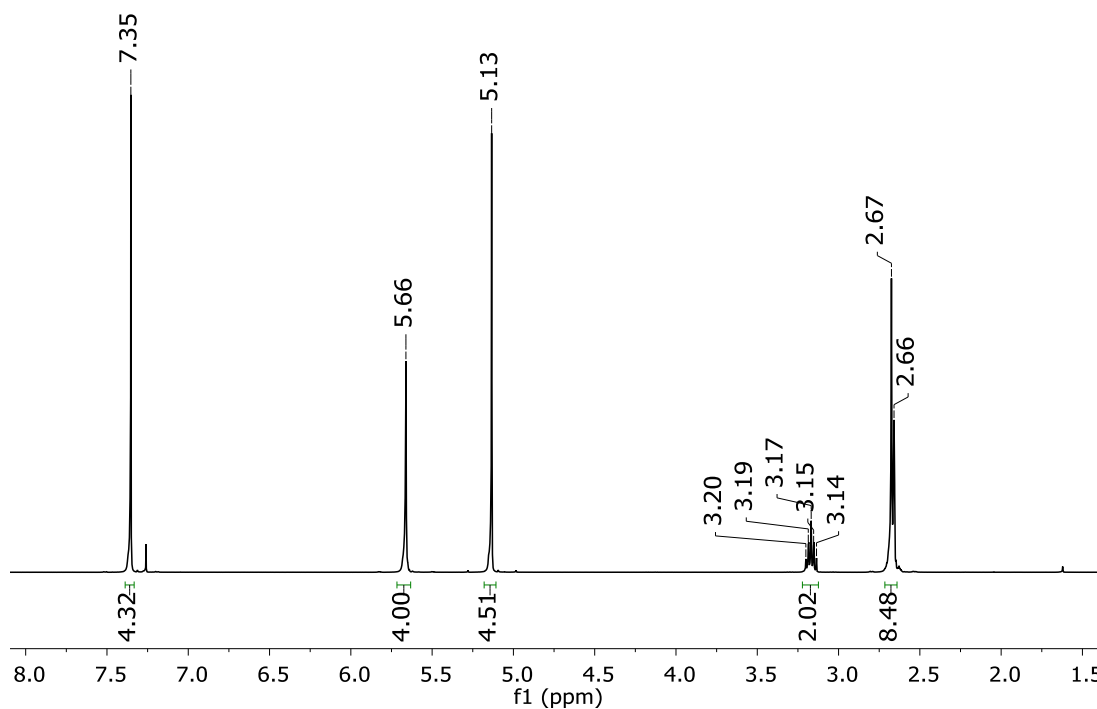


Synthesis of 1,4-phenylenebis(methylene) bis(cyclopent-3-ene-1-carboxylate) (2b)

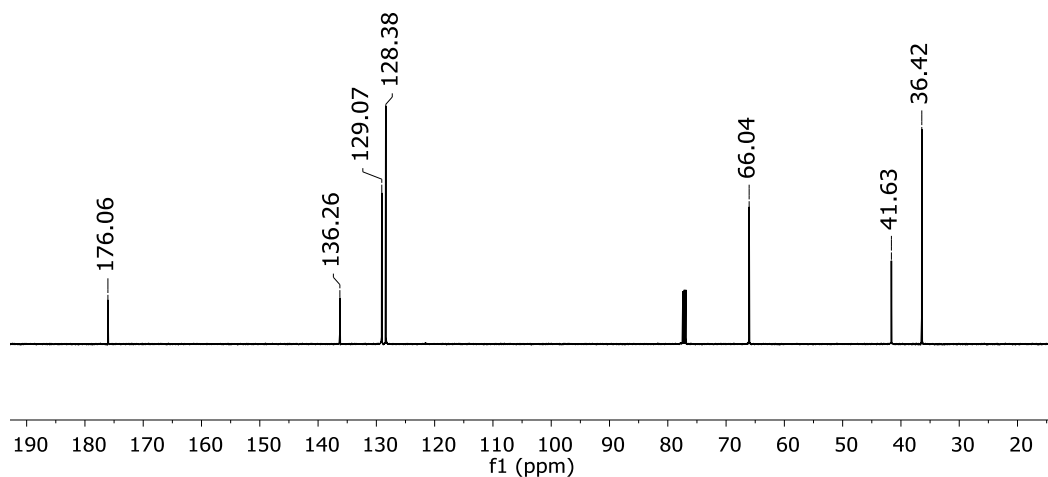


To a mixture of cyclopent-3-enecarboxylic acid (2 g, 17.8 mmol, 2.5 equiv.) and K_2CO_3 (4.93 g, 35.7 mmol, 5.0 equiv.) in acetone (30 mL) was added α,α' -dibromo-*p*-xylene (1.88 g, 7.13 mmol, 1.0 equiv.). The mixture was stirred at 60 °C for 2 h. The resulting mixture was filtered. The filtrate was concentrated. 20 mL EtOAc was added to the residue and washed with brine (2×15 mL), dried with anhydrous sodium sulfate, and then concentrated. The crude product was purified by flash chromatography to give the desired product as colorless oil (1.88 g, 81%). 1H NMR ($CDCl_3$, 500 MHz) δ 7.35 (s, 4H), 5.66 (s, 4H), 5.13 (s, 4H), 3.17 (m, 2H), 2.68-2.66 (m, 8H); ^{13}C NMR ($CDCl_3$, 125 MHz) δ 176.1, 136.3, 129.1, 128.4, 66.0, 41.6, 36.4. HRMS-ESI (m/z): calculated for $C_{20}H_{22}O_4Na$ [$M+Na$] $^+$, 349.1416; Found, 349.1412.

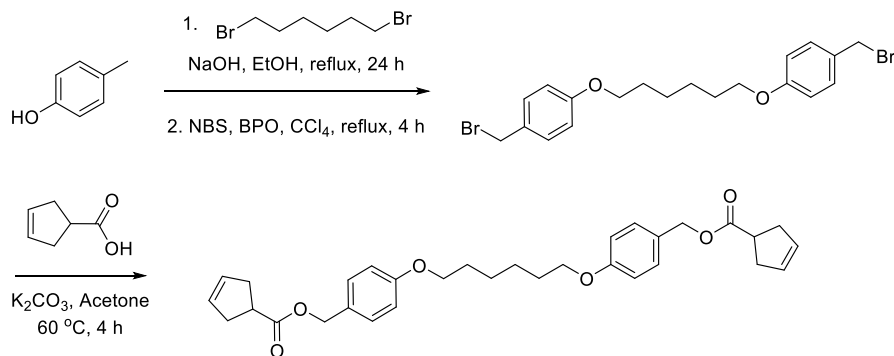
1H NMR of 2b



^{13}C NMR of 2b



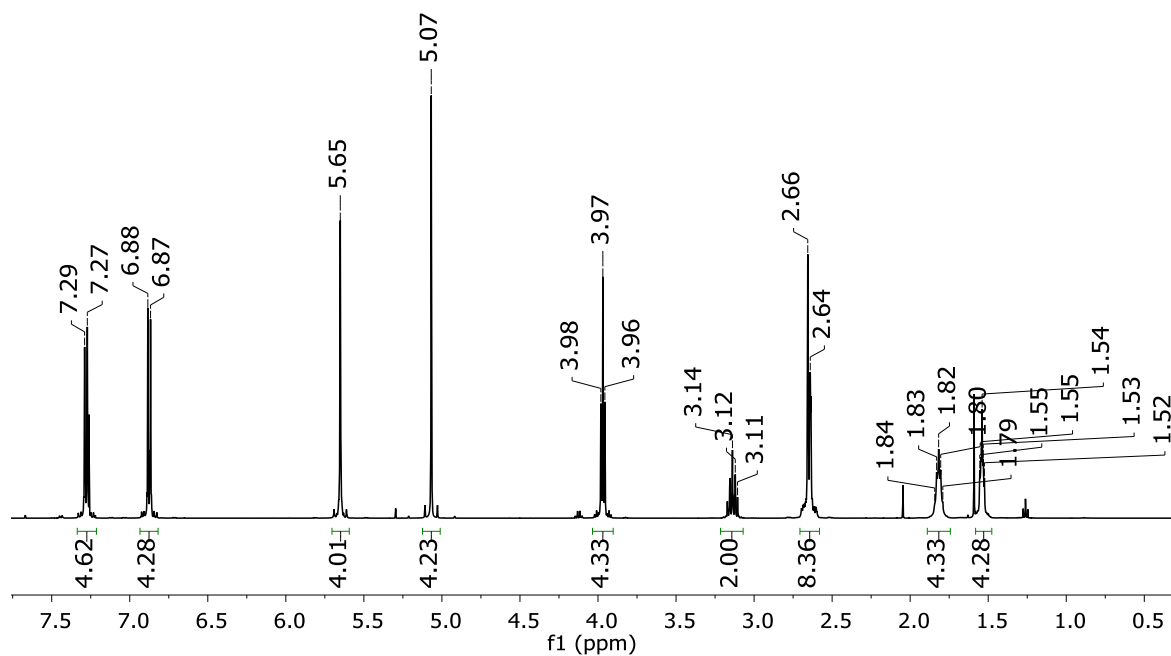
Synthesis of ((hexane-1,6-diylbis(oxy))bis(4,1-phenylene))bis(methylene)bis(cyclopent-3-ene-1-carboxylate) (2c)



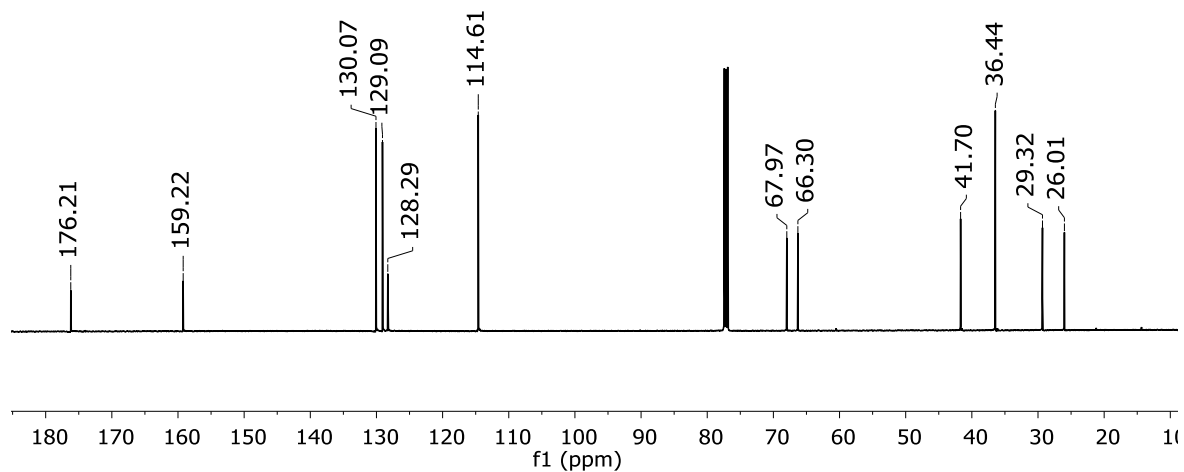
To a mixture of cyclopent-3-ene-1-carboxylic acid (1.0 g, 17.8 mmol, 2.5 equiv.) and K_2CO_3 (1.97 g, 28.5 mmol, 4.0 equiv.) in acetone (15 mL) was added 1,6-bis(4-(bromomethyl)phenoxy)hexane¹⁵ (1.63 g, 7.1 mmol, 1.0 equiv.). The mixture was stirred at $60\text{ }^\circ\text{C}$ for 4 h. The resulting mixture was filtered. The filtrate was concentrated. 20 mL EtOAc was added to the residue and washed with brine ($2 \times 15\text{ mL}$), dried with anhydrous sodium sulfate, and then concentrated. The crude product was purified by flash chromatography as eluent to give the desired product as a white solid (1.2 g, 65%, m.p. $75\text{ }^\circ\text{C}$). ^1H NMR (CDCl_3 , 500 MHz) δ 7.28 (d, $J = 8.5\text{ Hz}$, 4H), 6.88 (d, $J = 8.5\text{ Hz}$, 4H), 5.65 (s, 4H), 5.07 (s, 4H), 3.97 (t, $J = 6.5\text{ Hz}$, 2H), 3.14 (m, 2H), 2.66-2.64 (m, 8H), 1.84-1.79 (m, 4H), 1.55-1.53 (m, 4H); ^{13}C NMR (CDCl_3 , 125 MHz) δ 176.2, 159.2, 130.1, 129.1, 128.3, 114.6, 68.0, 66.3, 41.7, 36.4, 29.3, 26.0. HRMS-ESI

(m/z): calculated for $C_{32}H_{38}O_6Na [M+Na]^+$, 541.2566; Found, 541.2576. Calcd for $C_{32}H_{38}O_6$: C, 74.11; H, 7.38. Found: C, 73.76; H, 7.11.

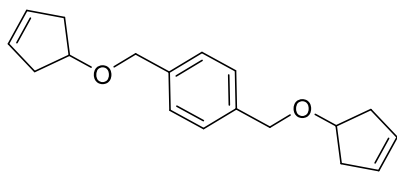
1H NMR of 2c



^{13}C NMR of 2c

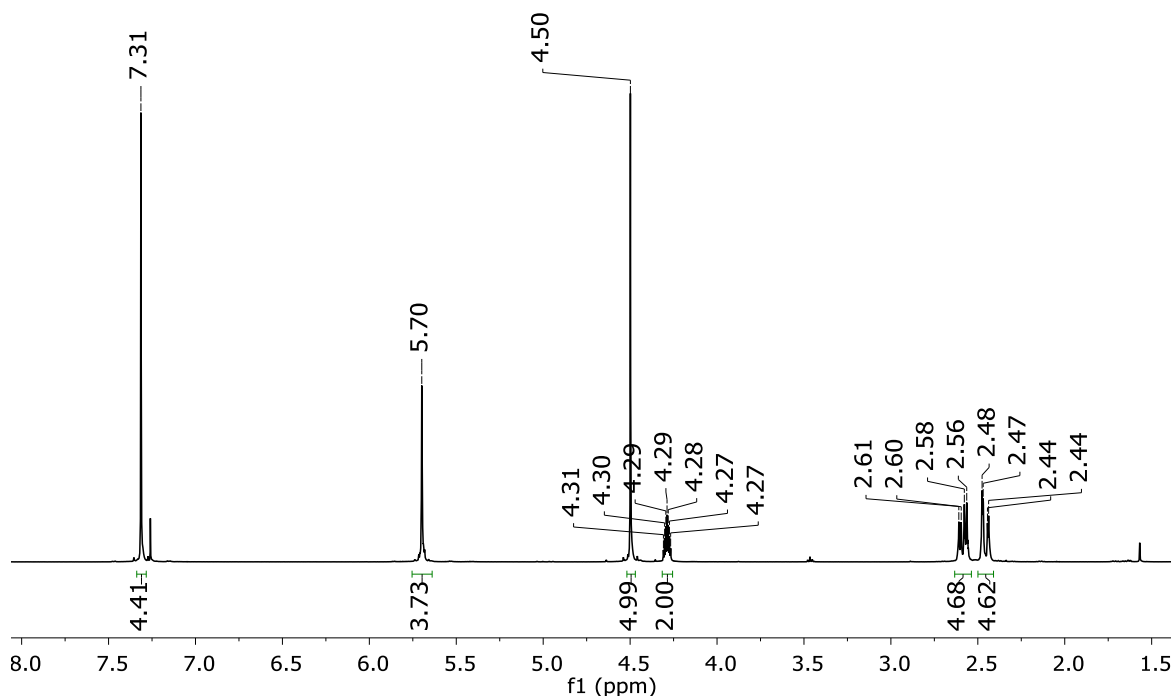


Synthesis of 1,4-bis((cyclopent-3-en-1-yloxy)methyl)benzene (2d)

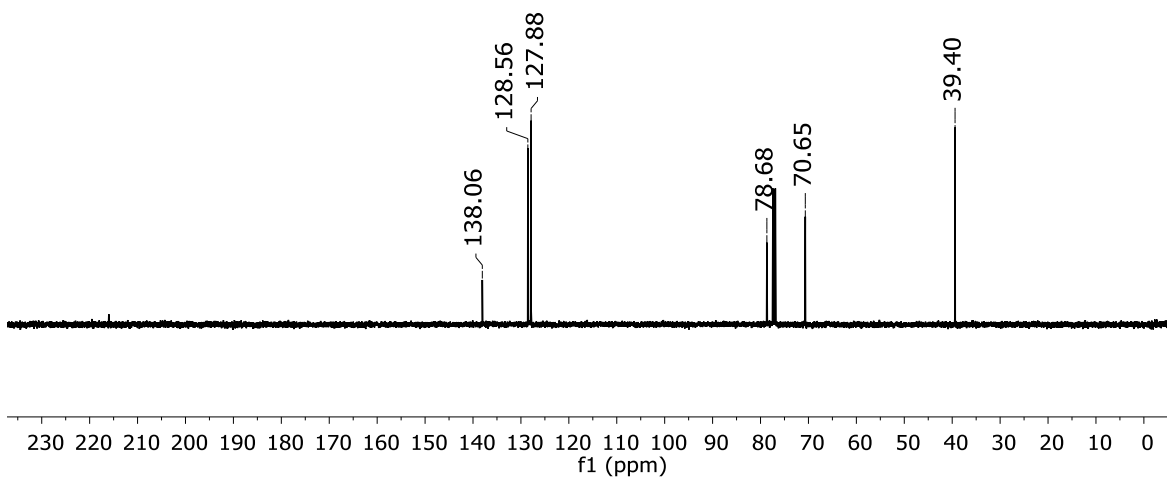


NaH (60% dispersion in mineral oil, 0.95 g, 23.8 mmol, 6.0 equiv.) was added to a solution of 3-cyclopentene-1-ol (1.0 g, 11.9 mmol, 3.0 equiv.) in 30 mL of dry THF at room temperature under a nitrogen atmosphere. After effervescence had ceased, α,α' -dibromo-*p*-xylene (1.06 g, 4 mmol, 1.0 equiv.) was added dropwise and the resulting mixture was allowed to heat at 60 °C for 4 hours. Excess NaH was carefully quenched by H₂O. After removing all the volatiles from the reaction mixture, water (15 mL) was added and further extracted with EtOAc (2×15 mL). The combined organic layer was washed with brine (15 mL), dried with anhydrous sodium sulfate, and then concentrated. The crude product was purified by passing a short silica column to afford the desired product as a white solid (1.03 g, 74%, m.p. 41 °C). ¹H NMR (CDCl₃, 500 MHz) δ 7.31 (s, 4H), 5.70 (s, 4H), 4.50 (s, 4H), 4.29 (sept, J = 3.5 Hz, 2H), 2.61-2.56 (m, 4H), 2.48-2.44 (m, 4H); ¹³C NMR (CDCl₃, 125 MHz) δ 138.1, 128.6, 127.9, 78.7, 70.7, 39.4. HRMS-ESI (m/z): calculated for C₁₈H₂₂O₂ [M]⁺, 270.1620; Found, 270.1622. Calcd for C₁₈H₂₂O₂: C, 79.96; H, 8.20. Found: C, 79.60; H, 8.04.

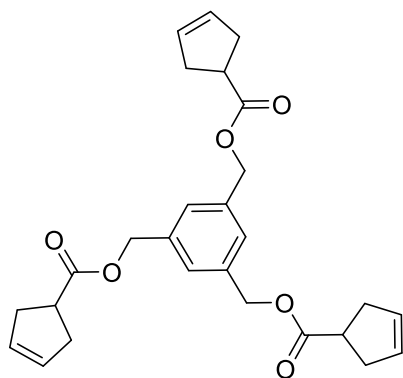
¹H NMR of 2d



¹³C NMR of 2d

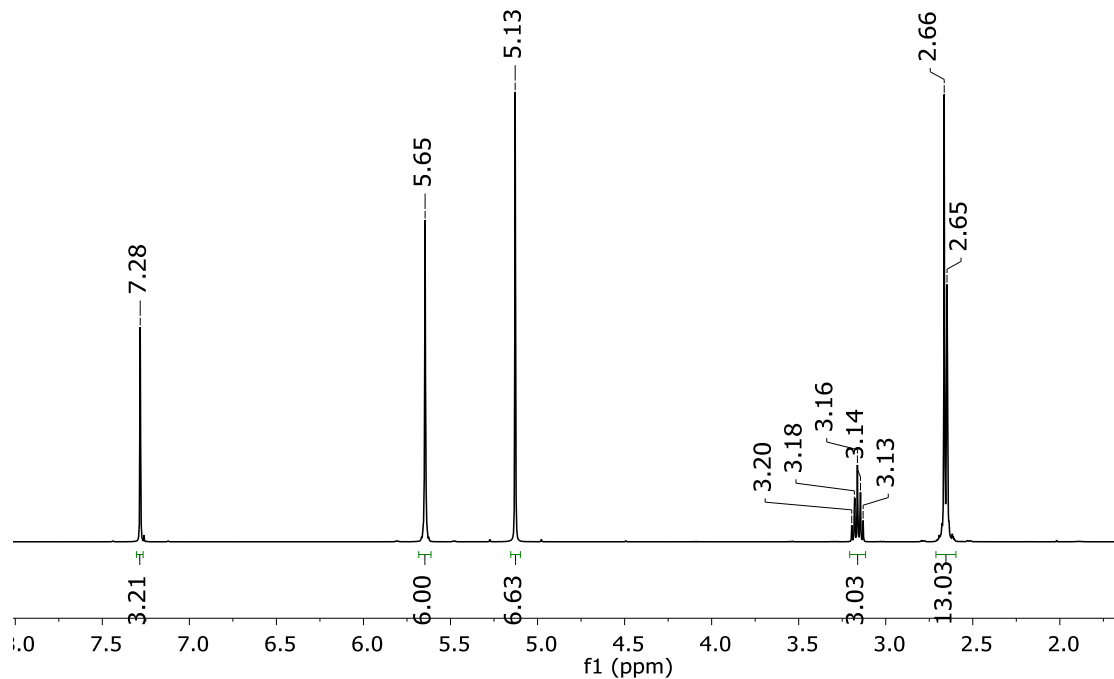


Synthesis of benzene-1,3,5-triyltris(methylene) tris(cyclopent-3-ene-1-carboxylate) (3a)

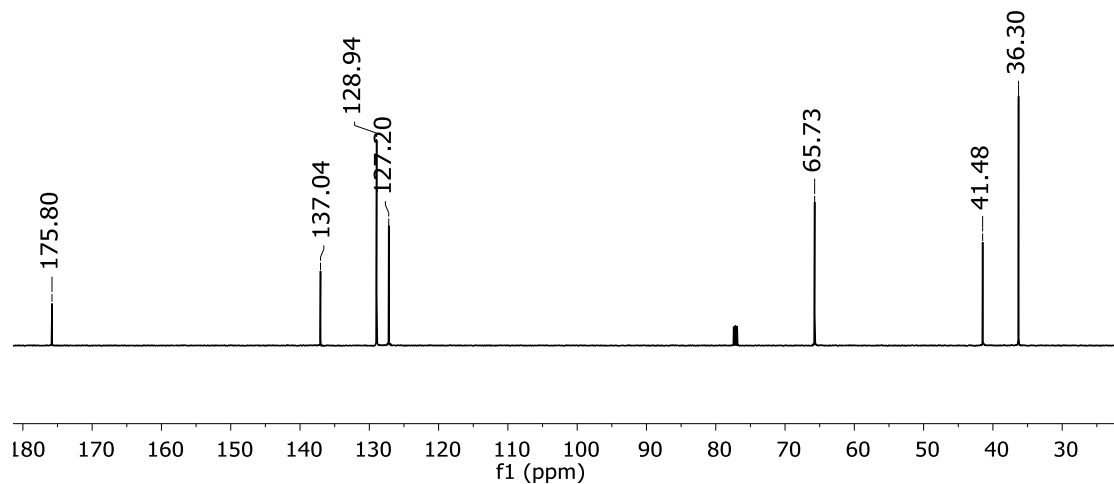


To a mixture of cyclopent-3-enecarboxylic acid (2 g, 17.8 mmol, 4.0 equiv.) and K_2CO_3 (3.70 g, 27.8 mmol, 6 equiv.) in DMF (30 mL) was added 1,3,5-tris(bromomethyl)benzene (1.59 g, 4.46 mmol, 1.0 equiv.). The mixture was stirred at 60 °C for 24 h. The resulting mixture was filtered. The filtrate was concentrated. 20 mL EtOAc was added to the residue and washed with brine (2×15 mL), dried with anhydrous sodium sulfate, and then concentrated. The crude product was purified by flash chromatography to give the desired product as colorless oil (1.40 g, 70%). ¹H NMR ($CDCl_3$, 500 MHz) δ 7.28 (s, 3H), 5.65 (s, 6H), 5.13 (s, 6H), 3.16 (m, 3H), 2.66-2.65 (m, 12H); ¹³C NMR ($CDCl_3$, 125 MHz) δ 175.8, 137.0, 128.9, 127.2, 65.7, 41.5, 36.3. HRMS-ESI (m/z): calculated for $C_{27}H_{31}O_6$ [M+H]⁺, 451.2121; Found, 451.2125.

¹H NMR of 3a



¹³C NMR of 3a



3.7.3 DSC Characterization

Bulk polymerization of 2b: The DSC specimen was encapsulated using Tzero hermetic aluminum pan with 5-15 mg loading of the resulting network polymer (after 24-h bulk polymerization with 0.22 mol % Grubbs II per double bond). Typical DSC measurement was done by heating specimen from -100 °C to 200 °C with a ramping rate of 10 °C/min. For all

samples, the significant exothermic peak was identified as depolymerization peaks, and peak maximum was reported as T_d ; T_g was the midpoint on the thermal curve corresponding to heat flow difference between the extrapolated onset and extrapolated end.

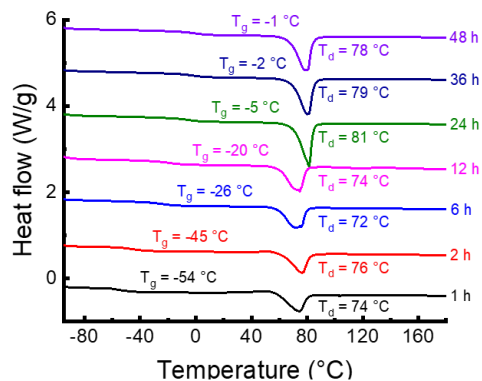


Figure 3.6 DSC curves of the specimen from bulk ROMP of **2b** after different polymerization time at room temperature.

Table 3.3 Depolymerization enthalpy and monomer conversion of **2b** after different polymerization time at room temperature.

Polymerization time (h)	Depolymerization enthalpy ΔH (J/g)	Monomer conversion (%)
48	56.2	89
36	55.5	88
24	54.2	85
12	45.3	79
6	41.8	77
2	35.7	60
1	35.9	56

Depolymerization of network polymers: The sample were prepared from bulk polymerization which was first initiated at 50 °C (for **2a**, **2b**, **2d** and **3a**) or 80 °C (for **2b** and **2c**) for 30 minutes and then cooled to room temperature for 24 hours.

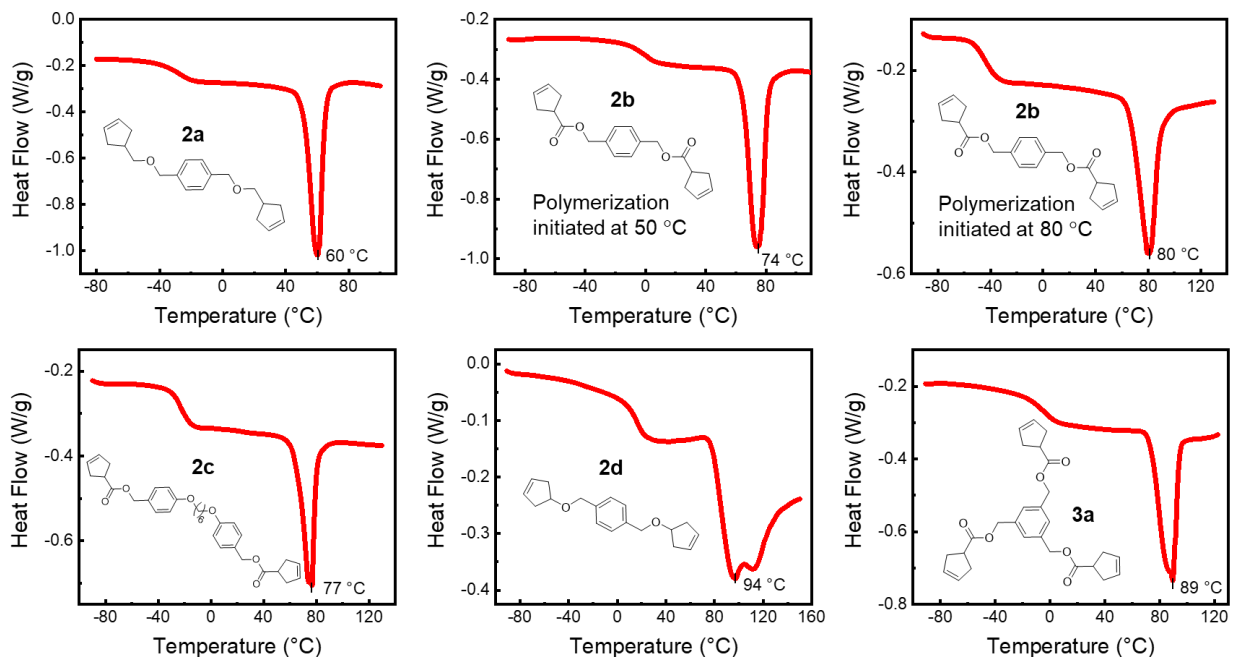


Figure 3.7 Depolymerization peak maximums of polymerization mixture of cyclopentene derivatives **2a-2d** and **3a**.

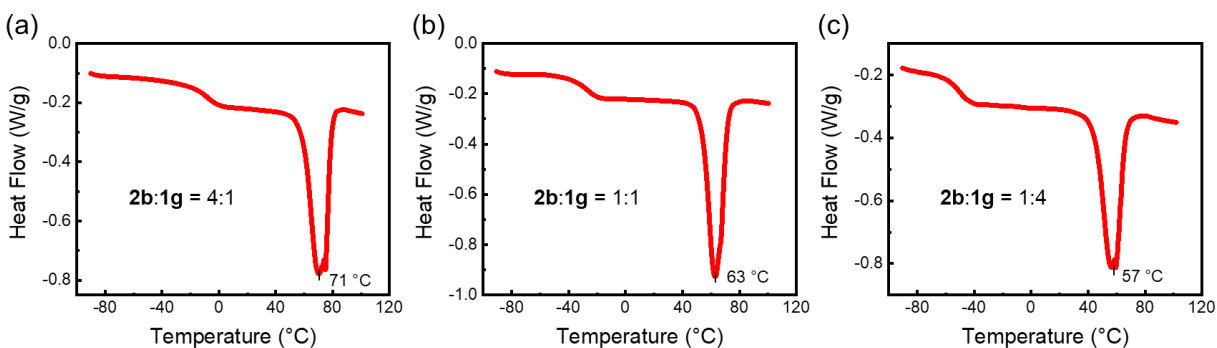


Figure 3.8 Depolymerization peak maximums of copolymerization of **2b** and **1g** at different ratios. The samples were prepared from bulk polymerization which was first initiated at 55 °C for 30 minutes and then cooled to room temperature for 24 hours.

3.7.4 Raman Characterization

The collected spectrum was fitted by Gaussian-Lorentzian, and the monomer conversion was calculated according to the ratio of *trans* C=C to *cis* C=C. Purified network polymer from **2b** consisted of 40% *trans* C=C and 60% *cis* C=C.

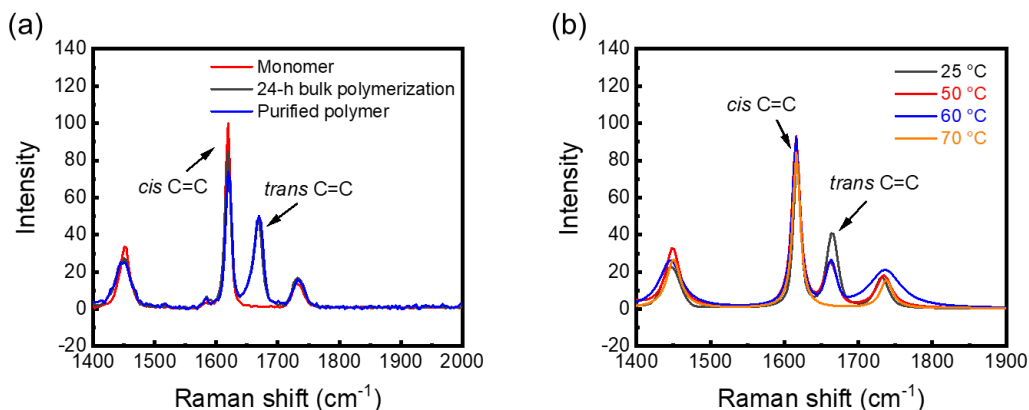


Figure 3.9 (a) Raman spectrum of monomer **2b**, reaction mixture after 24-h bulk polymerization (with Grubbs II loading 0.44 mol %) and purified polymer sample from **2b**. (b) Raman spectrum of reaction mixture (which is from 24-h bulk polymerization) at different temperature for 10 min.

Table 3.4 Monomer conversion of **2b** at different polymerization time determined by Raman and $^1\text{H NMR}$.

Polymerization time (h)	<i>tran</i> : <i>cis</i>	Monomer conversion by Raman (%)	Monomer conversion by $^1\text{H NMR}$ (%)
36	0.48	82	88
24	0.51	85	85
6	0.42	74	77
2	0.30	58	60
1	0.31	60	56

3.7.5 Rheological Characterization

In all cases except the bulk polymerization of **1g** (Figure 3.3 (a)), the subdominant modulus, G'' (loss modulus) and the loss ratio, $\tan(\delta) = G''/G'$, was always less than 0.1 and is omitted for clarity. Oscillatory characterization was performed at 1% strain amplitude and 1 rad/s for all materials. Neat monomers and Grubbs' catalysts (0.22 mol % per double bond) were well mixed before loading on the plates. The polymerization was first initiated at 55 °C for 10 minutes and then cooled to room temperature for 2 hours. This timeframe was chosen for convenience, since over a period of 24 hours (Figure 3.3 (b)), no mixture types showed development of moduli to a steady value. Stress relaxation tests were performed after 2-hour polymerization and minimal relaxation (< 1%) was seen on the timescale of 10 minutes. Stress

relaxation characterization was performed with a step strain of 1%. Complex viscosity after depolymerization at 55 °C of **2b** and **1g** (1:4) was measured at 1 rad/s by increasing the strain amplitude until the torque signal was resolvable.

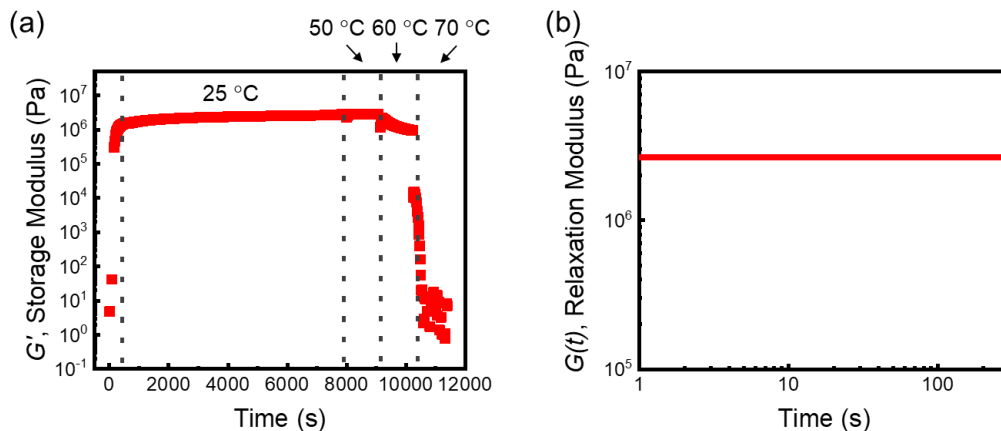


Figure 3.10 (a) Viscoelastic modulus growth and decay of bulk polymerization of **2b** at 1 rad/s. After initiation at 55 °C for 10 minutes and polymerization at 25 °C for 2 hours, slight depolymerization occurred at 60 °C, and prominent depolymerization occurred at 70 °C. (b) Stress relaxation of this sample after 2 h-polymerization at 25 °C.

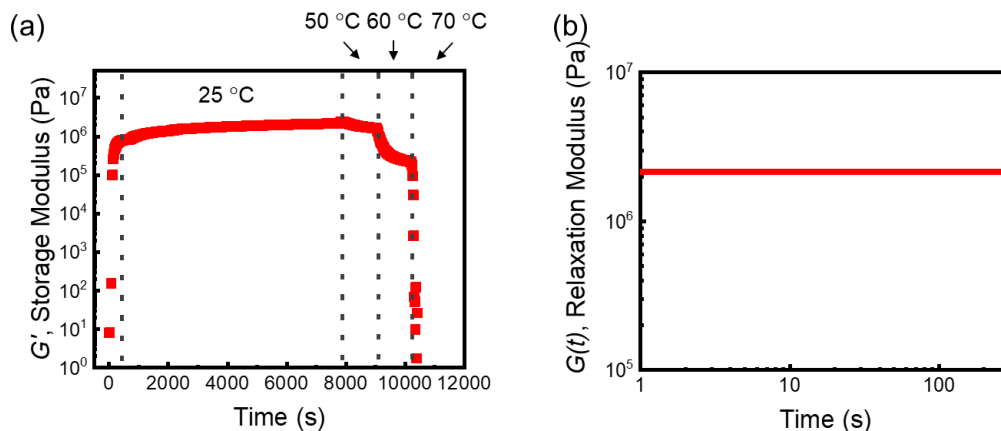


Figure 3.11 (a) Viscoelastic modulus growth and decay of bulk copolymerization of **2b** and **1g** (4:1) at 1 rad/s. After initiation at 55 °C for 10 minutes and polymerization at 25 °C for 2 hours, depolymerization occurred at 60 °C, and full depolymerization occurred at 70 °C. (b) Stress relaxation of this sample after 2 h-polymerization at 25 °C.

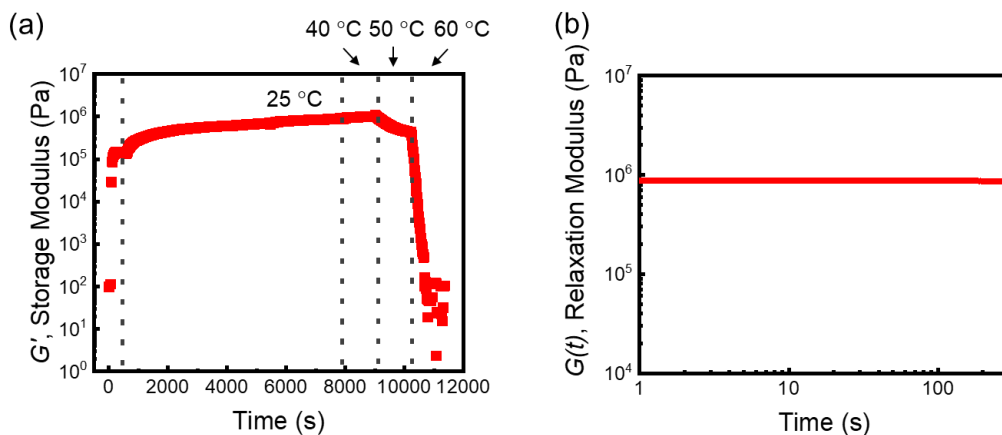


Figure 3.12 (a) Viscoelastic modulus growth and decay of bulk copolymerization of **2b** and **1g** (1:1) at 1 rad/s. After initiation at 55 °C for 10 minutes and polymerization at 25 °C for 2 hours, slight depolymerization occurred at 50 °C, and prominent depolymerization occurred at 60 °C. (b) Stress relaxation of this sample after 2 h-polymerization at 25 °C.

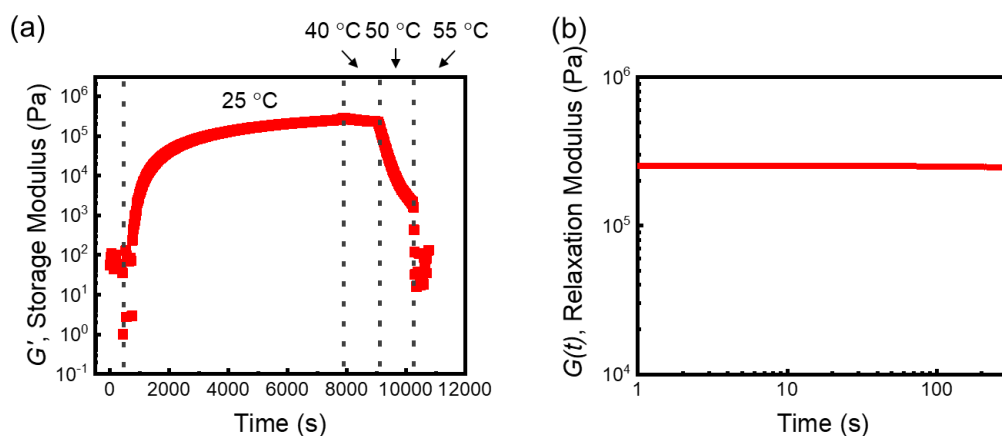


Figure 3.13 (a) Viscoelastic modulus growth and decay of bulk copolymerization of **2b** and **1g** (1:4) at 1 rad/s. After initiation at 55 °C for 10 minutes and polymerization at 25 °C for 2 hours, a large extent of depolymerization occurred at 50 °C and full depolymerization was achieved by further heating to 55 °C. (b) Stress relaxation of this sample after 2 h-polymerization at 25 °C.

3.7.6 Evaluation of Reversibility

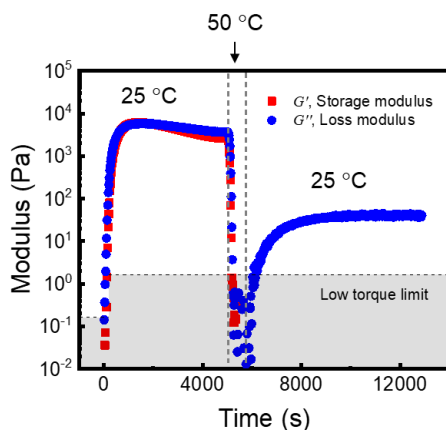


Figure 3.14 Rheological characterization at 1 rad/s of poly(pentenamer) from **1g**. The sample was polymerized at 25 °C for 2 h, heating to 50 °C for 10 min and repolymerized at 25 °C for 2 h.

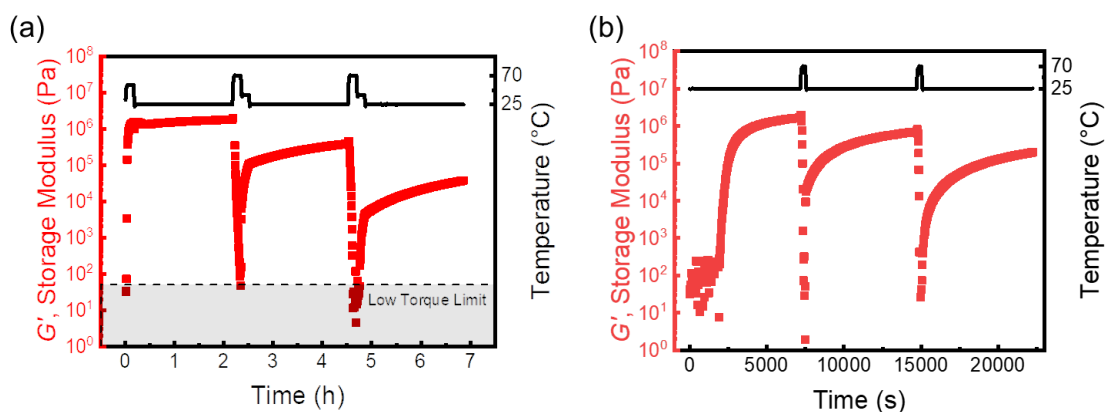


Figure 3.15 Rheological characterization at 1 rad/s of CANs from **2b** at Grubbs II loading of (a) 0.44 mol % and (b) 2.2 mol %. The samples were cycled between 25 °C and 70 °C.

Table 3.5 G' of CANs from **2b** at different catalyst loading.

Cycle	G' with 0.44 mol % cat. (MPa)	G' with 2.2 mol % cat. (MPa)
1	1.2	1.7
2	0.14	0.7
3	0.02	0.2

3.8 Notes and References

Notes:

Portions of this chapter have been published: Liu, H.; Nelson, A. Z.; Ren, Y.; Yang, K.; Ewoldt, R. H.; Moore, J. S. “Dynamic Remodeling of Covalent Networks via Ring-Opening Metathesis Polymerization” *ACS Macro Lett.* **2018**, *7*, 933-937. They are reproduced/adapted with permission. Copyright 2018 American Chemical Society.

References:

- (1) Helmke, K. J.; Heald, R.; Wilbur, J. D. Interplay between Spindle Architecture and Function. *Int. Rev. Cell Mol. Biol.* **2013**, *306*, 83–125.
- (2) Moutinho-Pereira, S.; Debec, A.; Maiato, H. Microtubule Cytoskeleton Remodeling by Acentriolar Microtubule-Organizing Centers at the Entry and Exit from Mitosis in *Drosophila* Somatic Cells. *Mol. Biol. Cell* **2009**, *20*, 2796–2808.
- (3) Stossel, T. P. Cell Surface Actin Remodeling. *J. Cell Sci.* **2006**, *119*, 3261–3264.
- (4) Kloxin, C. J.; Scott, T. F.; Adzima, B. J.; Bowman, C. N. Covalent Adaptable Networks (CANs): A Unique Paradigm in Cross-Linked Polymers. *Macromolecules* **2010**, *43*, 2643–2653.
- (5) Denissen, W.; Winne, J. M.; Du Prez, F. E. Vitrimers: Permanent Organic Networks with Glass-like Fluidity. *Chem. Sci.* **2016**, *7*, 30–38.
- (6) Roy, N.; Bruchmann, B.; Lehn, J.-M. DYNAMERS: Dynamic Polymers as Self-Healing Materials. *Chem. Soc. Rev.* **2015**, *44*, 3786–3807.
- (7) Zou, W.; Dong, J.; Luo, Y.; Zhao, Q.; Xie, T. Dynamic Covalent Polymer Networks: From Old Chemistry to Modern Day Innovations. *Adv. Mater.* **2017**, *29*, 1606100.
- (8) Kloxin, C. J.; Bowman, C. N. Covalent Adaptable Networks: Smart, Reconfigurable and Responsive Network Systems. *Chem. Soc. Rev.* **2013**, *42*, 7161–7173.
- (9) Chen, X. A Thermally Re-Mendable Cross-Linked Polymeric Material. *Science* (80-.). **2002**, *295*, 1698–1702.
- (10) Lu, Y.; Guan, Z. Olefin Metathesis for Efficient Polymer Healing via Dynamic Exchange of Strong Carbon – Carbon Double Bonds. *J. Am. Chem. Soc.* **2012**, *134*, 14226–14231.
- (11) Lu, Y. X.; Tournilhac, F.; Leibler, L.; Guan, Z. Making Insoluble Polymer Networks

- Malleable via Olefin Metathesis. *J. Am. Chem. Soc.* **2012**, *134*, 8424–8427.
- (12) Lee, H. K.; Bang, K. T.; Hess, A.; Grubbs, R. H.; Choi, T. L. Multiple Olefin Metathesis Polymerization That Combines All Three Olefin Metathesis Transformations: Ring-Opening, Ring-Closing, and Cross Metathesis. *J. Am. Chem. Soc.* **2015**, *137*, 9262–9265.
- (13) Soon, H. H.; Wenzel, A. G.; Salguero, T. T.; Day, M. W.; Grubbs, R. H. Decomposition of Ruthenium Olefin Metathesis Catalysts. *J. Am. Chem. Soc.* **2007**, *129*, 7961–7968.
- (14) Ulman, M.; Grubbs, R. H. Ruthenium Carbene-Based Olefin Metathesis Initiators: Catalyst Decomposition and Longevity. *J. Org. Chem.* **1999**, *64*, 7202–7207.
- (15) Wan, F.; Li, C.; Jiang, L.; Li, Y. Synthesis and Characterization of Binuclear Zn(II)-Cyclen Complexes Bridged by α,ω -Bis(4-Methylphenoxy) Alkanes. *Res. Chem. Intermed.* **2012**, *38*, 2085–2096.

Chapter 4: Monomer Design in Frontal Ring-Opening Metathesis Polymerization

4.1 Abstract

Frontal ring-opening metathesis polymerization (FROMP) holds great promises in rapid and low-energy manufacturing of polymer and composite materials. Thus far, only *endo*- and *exo*-dicyclopentadiene (DCPD) have been reported as FROMP monomers. Expanding the scope of monomers not only establishes design principles that strengthen the fundamental understanding of metathesis chemistry but also guides further development of functional materials with tunable properties. In this chapter, we investigated 30 cyclic olefins and characterized their performance in FROMP. Due to the complexity of the FROMP process, limited information on structure-property relationship was obtained by conventional approaches such as linear regression. Thus, we applied machine learning models that utilize monomer structural parameters as inputs and FROMP performance (i.e., frontal velocity and heat released) as outputs. Despite a small data set, the model we developed predicts FROMP performance with reasonable accuracy and identifies structural features that are key determinants in FROMP.

4.2 Introduction

Thermally-initiated frontal polymerization (FP) is a process that forms a confined propagating reaction zone where monomer transforms to polymer. Many FP chemistries have been developed, which enables a wide variety of applications such as out-of-autoclave curing of large composites and cure-on-demand repair.¹⁻⁴ Radical FP is by far the most investigated method due to the high exothermicity of addition polymerization and the readily available monomers and initiators.¹ However, the limiting aspects of radical FP include short pot life when combined with highly reactive monomers and inferior mechanical properties of the resulting polymers. Recently, Robertson et al. demonstrated that phosphite-inhibited FROMP of *endo*-dicyclopentadiene (*endo*-DCPD) substantially extends the pot life up to 30 hours,⁵ which allows manufacturing high-performance thermosets and fiber-reinforced polymer composites (FRPC).⁴ This strategy dramatically reduces, by several orders of magnitude, the energy required for

curing and yields FRPCs with similar mechanical properties to those from conventional autoclave curing.^{4,6,7} Upon a local thermal stimulus, the latent Grubbs' catalyst is initiated to trigger an exothermic reaction which further activates the latent catalyst and drives the polymerization of the available monomer. One characteristic of a successful FROMP is the stable front propagation after removal of the thermal stimulus, which is quantified by constant frontal velocity (v_f) regardless of front position. However, only *endo*- and *exo*-DCPD have been investigated as FROMP monomers.^{4,5,7-9} Studies on other strained monomers will expand the toolbox of FROMP and bring functionalities to the materials with desirable properties.

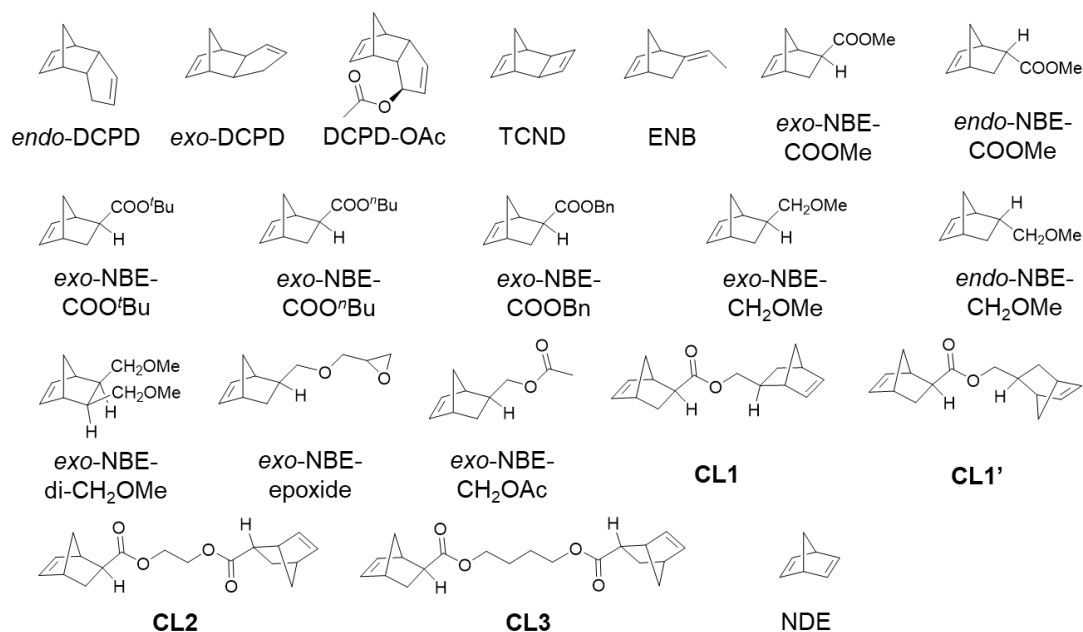
Linear regression is a common statistical tool to study structure-property relationships in both industry and academia.¹⁰ One example is the Hammett equation which describes a linear free-energy relationship relating reaction rates and equilibrium constants.¹¹ Linear regression is fast to model and straightforward to interpret, and thus it's particularly useful when the situation is not extremely complicated. Recently, the models from linear regression analysis have been demonstrated for optimizing reaction selectivity by prediction on catalyst, ligand, and substrate effects.^{12,13} However, it remains challenging for linear regression to predict complex targets which are affected by a larger number of variables. Since machine learning (ML) approaches perform much better at studying complex, highly non-linear relationships, Ahneman et al. built a random forest ML model to accurately predict the yields in C-N cross-coupling reactions. In addition, the model was also successfully applied to sparse training sets and out-of-sample prediction. Inspired by the success of regression analysis on complex organic reactions, we applied linear regression and machine learning methods to quantitatively understand the FROMP process and guide further monomer design.

4.3 Structure-Property Relationship by Linear Regression

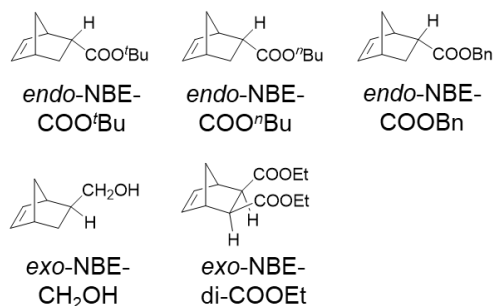
Based on previous understanding of ROMP and FP, the following aspects are crucial to a successful FROMP. First, ring strain (or ΔH) should be sufficient to drive further polymerization and prevent front quenching from heat loss to the surroundings such as the reaction vessel.^{14,15} Second, high polymerization rate is also essential to ensure the propagation at a steady v_f . Third, the monomer is preferably a liquid at room temperature or a low-melting solid (mp < 35 °C) and has a boiling point higher than the front temperature (bp > 150 °C). This ensures maximum

efficiency of FROMP under neat conditions with minimal heat loss due to vaporization. Fourth, the monomer should also be thermally stable at front temperature and chemically compatible with Grubbs' catalyst. Cyclopropene and cyclobutene derivatives possess higher ring strain energy compared to other cycloalkenes, but they are generally thermally unstable and require tedious synthesis on an appreciable scale.¹⁶⁻¹⁸ In addition, functional groups with strong Lewis basicity should be avoided to maintain the reactivity of the catalyst.^{19,20} According to these limiting aspects, we reasoned that norbornene (NBE) derivatives were excellent FROMP monomer candidates owing to their high ring strain and ease of functionalization.^{14,21}

Stable front



Unstable front



No propagation

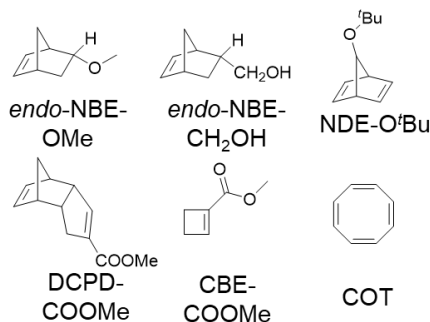


Figure 4.1 FROMP monomers investigated. The categorization was based on FROMP performed in NMR tubes proceeding in a descending mode. Formulation: 500 mg monomer, 100 ppm Grubbs II per NBE C=C, 1.0 equiv. *P*(*O*Bu)₃ and 40 μ L toluene.

To evaluate the reactivity, all FROMP experiments were performed in NMR tubes (Economy 5 mm × 7" L, 100 MHz), proceeding in a descending mode. v_f was measured in the presence of Grubbs II (100 ppm per norbornenyl double bond), 1.0 equiv. P(OBu)₃ and 500 mg neat liquid monomers; heat released (ΔH , J/g) of ROMP was quantified by DSC. As shown in Figure 4.1, we categorized the investigated monomers into three groups: stable front with a constant v_f throughout (Table 4.1), unstable front where v_f decreases over time and FROMP is quenched at some point, and no propagation where FROMP is not observed (Table 4.2). Since v_f depends on boundary conditions,⁴ the results reported here were obtained from the same formulation and reactor geometry. The lowest steady v_f we observed is 0.23 mm/s, and below this value, heat generated from polymerization might not be sufficient to sustain a steady front propagation.

4.3.1 Constitutive Equation

With v_f and ΔH values measured for all monomers that exhibit steady front propagation, we first attempted to build a constitutive equation that describes FROMP reactivity (i.e., v_f) using monomer properties (such as density and ΔH). This equation would be a straightforward and quantitative way to identify the determinants in the FROMP process.

We hypothesized that v_f is proportional to the heat release rate (i.e., heat released per unit volume per unit time). Through dimensional analysis, heat release rate could be expressed as a product of ΔH (J/g), density (g/L), and polymerization rate constant k_{obs} (min⁻¹) as shown below.

$$v_f \propto \frac{\Delta H(\text{J})}{\Delta V(\text{L}) \cdot \Delta t(\text{min})} = \Delta H \left(\frac{\text{J}}{\text{mol}} \right) \cdot \frac{1}{\text{MW} \left(\frac{\text{g}}{\text{mol}} \right)} \cdot \rho \left(\frac{\text{g}}{\text{L}} \right) \cdot k_{\text{obs}} \left(\frac{1}{\text{min}} \right)$$

ΔH (J/g) was obtained from DSC measurements, and it is dependent on molecular weight (MW) which will be discussed with more details in the next section. Direct measurement of k_{obs} at front temperatures is challenging; instead, solution polymerization at 25 °C in *d*₈-THF was performed to determine k_{obs} assuming ROMP is a pseudo-first-order reaction (Figure 4.18). We first selected five NBE derivatives to test the feasibility of the constitutive equation. As shown in Figure 4.2 (a), there is no correlation between v_f and ΔH (J/g). NBE-COOMe and NBE-CH₂OMe release similar amounts of heat upon polymerization, but their v_f values are significantly different presumably due to the distinct polymerization rates. Gratifyingly, after considering the k_{obs} term

and plotting v_f against the heat release rate, it exhibits a much stronger linear correlation (Figure 4.2 (b)). Thus, heat release rate is a more appropriate and accurate parameter to describe v_f .

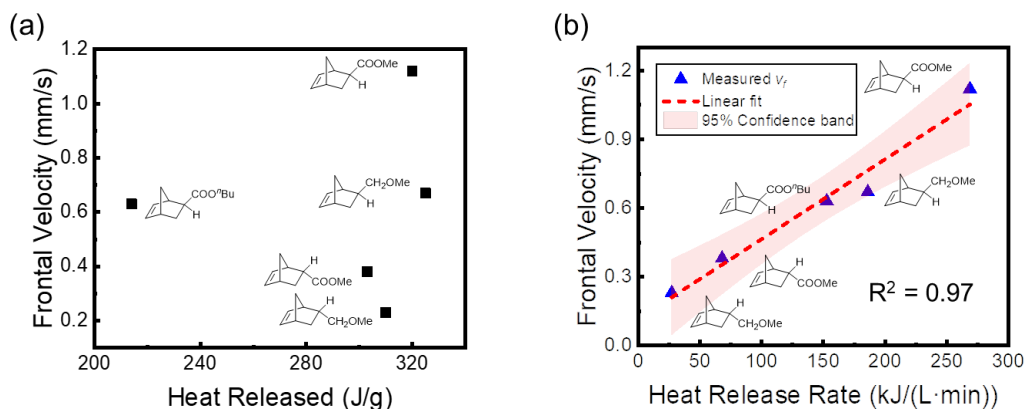


Figure 4.2 (a) Correlation between v_f and heat released (J/g) for selected monomers. (b) Correlation between v_f and heat release rate (kJ/(L·min)) for selected monomers.

Encouraged by the preliminary results, more FROMP monomers with steady v_f values were included. Even though the general trend suggests that a larger ΔH leads to a faster v_f , both plots show quite poor linear correlation (Figure 4.3). Inclusion of k_{obs} shows even worse correlation, implying that k_{obs} values at 25 °C in solution fail to reflect relative polymerization rates at the front temperatures. A more precise method is needed to describe kinetic parameter in the bulk polymerization at high temperatures. In addition, other factors might be missing in the equation such as polarity of the monomer and glass transition temperature (T_g) of the resulting polymer. The polarity of solvents plays a role in the initiation of the catalyst,^{22,23} and thus different functional groups in the monomer could result in disparate FROMP reactivity. Furthermore, with minimum amount of toluene present in FROMP, the mobility of polymerized chains is limited. It potentially retards the polymerization rate and reduces FROMP reactivity, especially in the case where a cross-linked polymer is formed. The effect of cross-linking will be further discussed in Chapter 5.

Due to the complexity of FROMP, a constitutive equation that accurately describes FROMP reactivity by monomer properties is still under investigation. However, some linear correlations were constructed between v_f and MW or thermodynamic properties of the monomer.

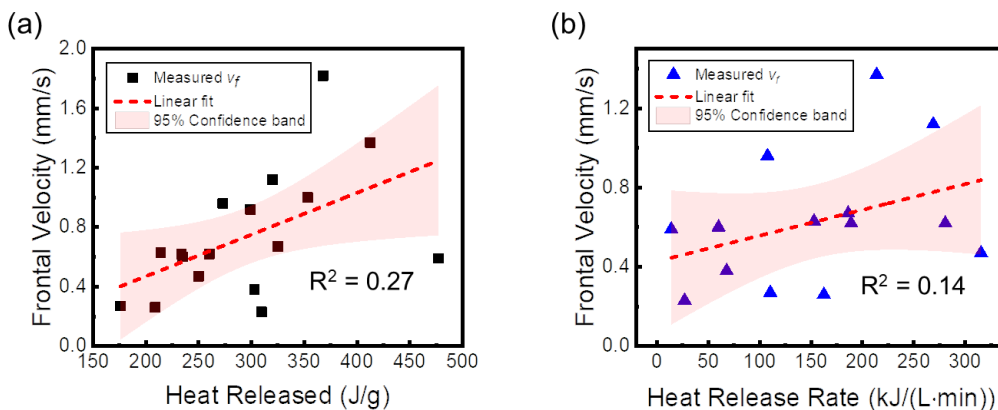


Figure 4.3 (a) Correlation between v_f and heat released (J/g). (b) Correlation between v_f and heat release rate (kJ/(L·min)).

4.3.2 Effect of Molecular Weight

Increasing the size of the substituent has minimum impact on polymerization kinetics,²⁴ but larger MW decreases the energy density (i.e., heat released per unit volume) since non-reactive substituents do not contribute to ΔH . As shown in Figure 4.4, 50% increase in MW from *exo*-NBE-COOMe (152.19 g/mol) to *exo*-NBE-COOBn (228.29 g/mol) leads to 77% reduction in v_f (from 1.12 mm/s to 0.26 mm/s). Similar variation was observed in monomers with other anchor groups. For monomers with the same anchor group, v_f changes linearly over $1/\text{MW}$, which could be employed to estimate v_f of analogous compounds. Therefore, this result supports our hypothesis on the linear relationship between v_f and $1/\text{MW}$ and implies that structurally similar monomers exhibit similar thermodynamic and kinetic behavior.

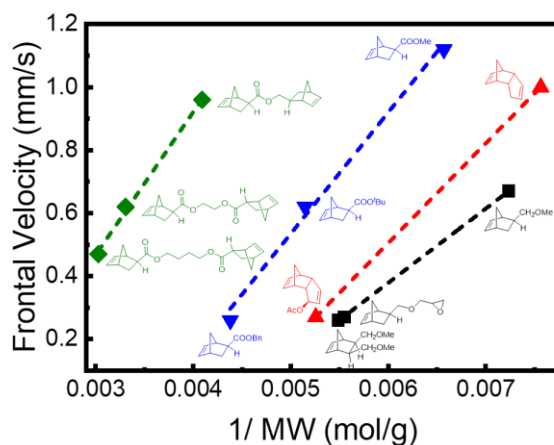


Figure 4.4 v_f dependence on monomer molecular weight. Dashed lines are the linear fit of measured v_f .

4.3.3 Correlation with Thermodynamic Properties

All FROMP experiments discussed so far were performed immediately (< 1 min) after mixing all the compounds. If the mixture is incubated at room temperature for a certain amount of time, spontaneous polymerization would occur. As shown in Figure 4.5 (a), addition of 1.0 equiv. $\text{P}(\text{O}i\text{Bu})_3$ as an inhibitor effectively suppressed ROMP of *endo*-DCPD, so minimum monomer conversion was observed before 2 hours at room temperature. Meanwhile, there was a slight increase in v_f after 30-min incubation, presumably resulting from better catalyst initiation. This is supported by DSC data in Figure 4.5 (b) where the polymerization peak with a longer incubation time became broader and shifted to a lower onset temperature. With the conversion of *endo*-DCPD gradually increasing, v_f decreased accordingly. After 10-h incubation, FROMP was quenched, and monomer conversion reached 50%. This result agrees well with the fact that maximum fiber volume in FRPC is 51%, and above this fraction, heat released would not be sufficient to sustain the front propagation.⁴ All the incubated samples (up to 10 hours at room temperature) before FROMP were fully soluble in *d*₈-THF, which indicates that negligible cross-linking by cyclopentenyl C=C occurred during incubation at room temperature.

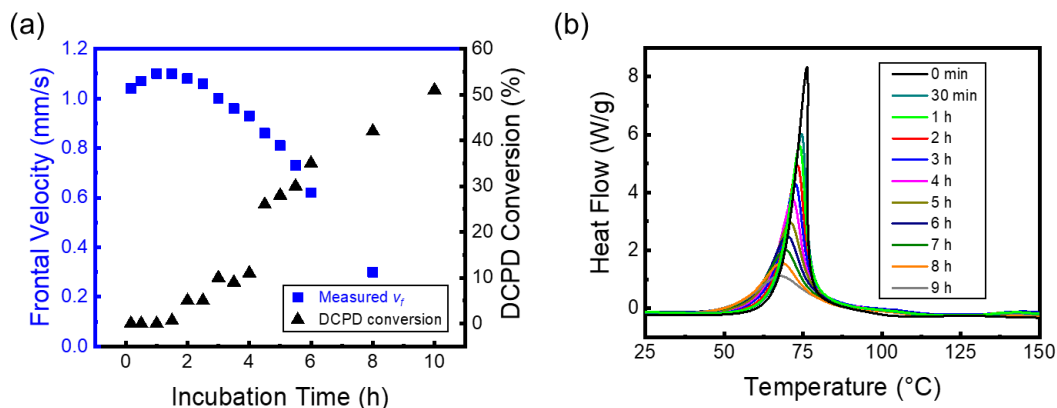


Figure 4.5 (a) v_f and *endo*-DCPD conversion at different incubation time at room temperature. Conversion was measured by ^1H NMR after quenching the mixture by ethyl vinyl ether. (b) ROMP exothermic peaks by DSC at different incubation time.

As illustrated in Figure 4.6 (a), the decrease in v_f over incubation time originates from the less amount of heat generated from polymerization with the increase in monomer conversion. v_f is linearly correlated with ΔH , which agrees well with the constitutive equation discussed earlier.

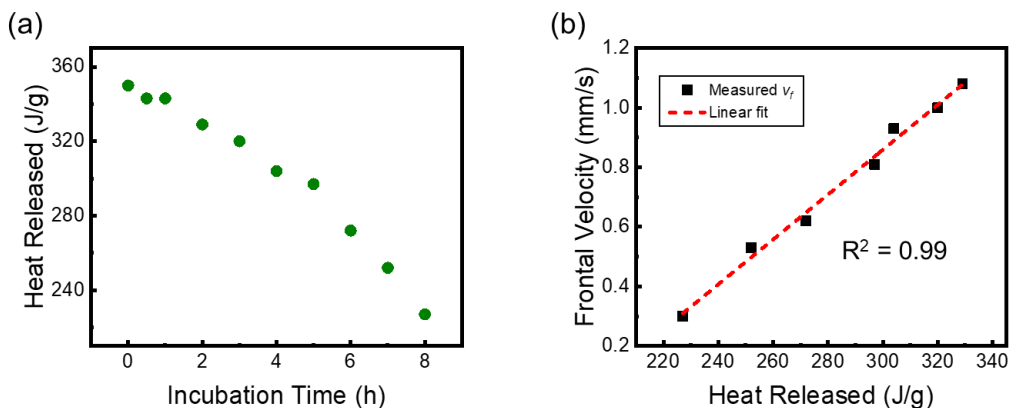


Figure 4.6 (a) ΔH at different incubation time. (b) A linear correlation between v_f and ΔH . The data points included were from incubation after 2 hours.

4.3.4 Effect of Substituents

Other than the substituent size, the stereochemistry and the functional group also dramatically alter FROMP reactivity. *exo*-monomers exhibit much faster v_f than their corresponding *endo*-isomers due to their larger ring strain and a higher rate of polymerization.^{7,15,25} The primary cause is the steric interactions. The *endo*-substituent hinders the approaching of active [Ru] carbenes and monomers from the bottom, and thus *endo*-NBEs usually have slow v_f or even no propagation. Another example is the norbornadiene (NDE) derivative NDE-O^tBu with a bulky substituent on the bridge head. Even though unsubstituted NDE possesses the largest v_f (4.4 mm/s) and ΔH (823 J/g) among all the monomers investigated (Table 4.1), The -O^tBu substituent results in no propagation owing to the unfavorable steric hindrance and formation of the stable chelate structure shown in Figure 4.7 (b).

Due to the excellent functional group tolerance of Grubbs II, ester, ether and epoxide can be frontally polymerized with steady v_f values (Figure 4.1 and Table 4.1). *exo*-NBE-CH₂OH, monomer with an alcohol moiety, showed some propagation, but the irreversible coordination with [Ru] at front temperature significantly retarded the kinetics and led to the front quenching. Previous examples suggest that anchor group effect, originating from the formation of five- or six-membered chelate with [Ru] carbene, steric demands and electronic structure, results in the variance of polymerization kinetics.^{16,17-21} We also observed anchor group effect in FROMP. As shown in Figure 4.7 (a), four different anchor groups were studied. *exo*-NBE-COOMe exhibits a larger v_f (1.12 mm/s) than *exo*-NBE-CH₂OAc (0.92 mm/s), but the former monomer has a smaller MW (152.19 g/mol) than the latter one (166.22 g/mol). To eliminate the effect of MW, v_f

was extrapolated to the same MW as *exo*-NBE-CH₂OAc. The estimated v_f of *exo*-NBE-COOR with a MW of 166.22 g/mol is 0.93 mm/s which is similar to $v_f(\textit{exo}\text{-NBE-CH}_2\text{OAc})$. Based on the monomers we investigated, the reactivity in FROMP decreases in the order of $-\text{COOR} \approx -\text{CH}_2\text{OCOR} > -\text{CH}_2\text{OR} > -\text{OR}$. The thermodynamic property (ΔH) of each monomer except NBE-OMe is similar, so the difference in v_f presumably results from kinetics. This could be well explained by the ability to form a chelate with [Ru] (Figure 4.7 (b)). Formation of a five-membered chelate is more stable than a six-membered chelate, which leads to much lower reactivity of NBE-OMe and NDE-O^tBu. In addition, generation of chelate structure is more favorable with *endo*-isomers, which explains the reactivity difference in *exo*- and *endo*-isomers. Other factors such as the electronic structure and polarity might also contribute to FROMP behavior, but the hypothesis on chelate formation best aligns with the experimental results.

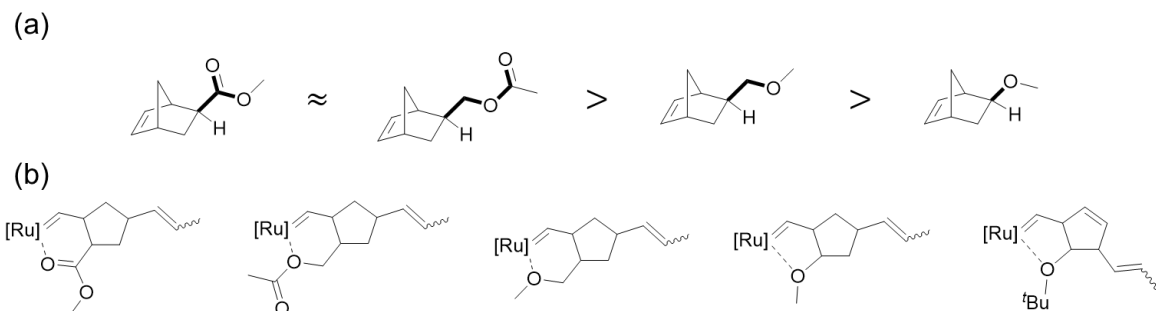


Figure 4.7 (a) Anchor group effect observed in this study. (b) Possible chelate structure with [Ru].

4.4 Structure-Property Relationship by Machine Learning

Owing to the complexity of FROMP with numerous factors interacting, it remains challenging to predict the FROMP performance of unknown structures and identify the principal features of a successful monomer despite some understanding gained in the last section. Constitutive equation discussed earlier is a linear regression that assumes a linear relationship between reaction input (product of ΔH , ρ and k_{obs}) and output (v_f). The selected input variables were based on specific mechanistic hypothesis that v_f is proportional to the heat release rate. ML approaches, however, accept numerous input descriptors without recourse to a mechanistic hypothesis and evaluate functions with greater flexibility to match patterns in data. Thus, we applied ML methods to build a more generalized and quantitative structure-property relationship.

Random forest algorithm, one of the ML methods, is operated by randomly sampling the data and constructing decision trees, which are then aggregated to generate an overall prediction.³¹ Furthermore, this algorithm could achieve enhanced predictive power over other methods using a significantly smaller subset of the training data.³² After some preliminary testing on different models, the random forest algorithm was found to provide significant improvements over linear regression analysis and other ML methods in terms of root mean square error (RMSE) (Table 4.3). Thus, we employed the random forest ML model to train monomers with stable propagation and predict the performance of FROMP.

First, we calculated the equilibrium geometry of the monomer with DFT at the B3LYP/6-31G(d) level using Spartan. From the DFT output files, parameters including vibrational frequency, bond order, atomic charge and dipole moment were extracted to quantitatively describe the molecule. These parameters plus MW and density of the monomer, a total of 103 structural features, were utilized as inputs for ML model. The outputs are ΔH (J/g) and ν_f which are directly related to FROMP performance. To build a model, we employed 17 monomers that possess steady ν_f values with 13 monomers (80%) being the training set and the remaining 4 monomers (20%) as the test set. The model would be accurate when the number of features (103 descriptors) is way higher than the number of experimental data points (17 monomers). As shown in Figure 4.8 (a) and Figure 4.19, the model predicts ΔH fairly well with R^2 of training set and test set 0.94 and 0.74, respectively. However, for ν_f , it only predicts with reasonable accuracy in the range of 0.26-1.37 mm/s. The test set does not converge when ν_f values are too low or too high, resulting from lack of experimental data points outside the range of 0.26-1.37 mm/s. On one hand, obtaining low steady ν_f values (< 0.23 mm/s) is experimentally challenging because the insufficient ΔH would eventually lead to front quenching due to the substantial heat loss to the environment. On the other hand, higher ν_f requires an inherently more strained ring, which is also challenging. The highest ν_f determined (4.4 mm/s) is NDE which has a larger ring strain than norbornene or DCPD. However, NDE evaporates extensively during FROMP owing to its low boiling point (89 °C), which is not regarded as a typical steady FROMP.

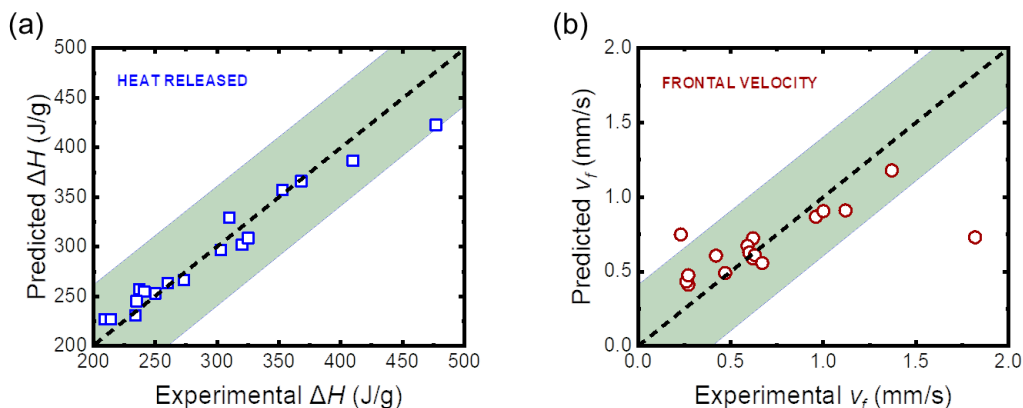


Figure 4.8 (a) Experimental vs predicted results by random forest algorithm for ΔH (J/g). Convergence and best performance at n estimators = 1000 and max depth = 6 with training set $R^2 = 0.94$ and test set $R^2 = 0.74$. (b) Experimental vs predicted plots by random forest algorithm for v_f (mm/s). Convergence and best performance at n estimators = 10000 and max depth = 6 with training set $R^2 = 0.85$. Test set fails to converge at very low or very high v_f values but performs well at intermediate values.

With the predictive model established, we sought to determine whether it could provide some mechanistic insights of FROMP chemistry. Unlike a linear regression model, the random forest model is challenging to interpret directly. Thus, relative importance of the features utilized to construct the model were evaluated. One such measure is the percent increase in the model's RMSE when values for that feature are randomly shuffled and the model is retrained.³³ The top 16 most important features in predicting ΔH and v_f are listed in Figure 4.9. It suggests that descriptors on thermodynamic properties, ratio of bond length (symmetry of the molecule), bond angle and electrostatic interactions are the main contributors to the variance in ΔH and v_f . The identification from the model helps us visualize the trends from a massive number of potential variables. Since numerous correlations could be generated by plotting ΔH or v_f against any DFT-calculated parameter, a few examples are analyzed below to demonstrate how the machine recognizes the patterns. Although one feature is not sufficient to obtain a predictive linear model, the trends obtained by the machine provide some insights into design principles and mechanistic understanding of anchor group effect we observed earlier.

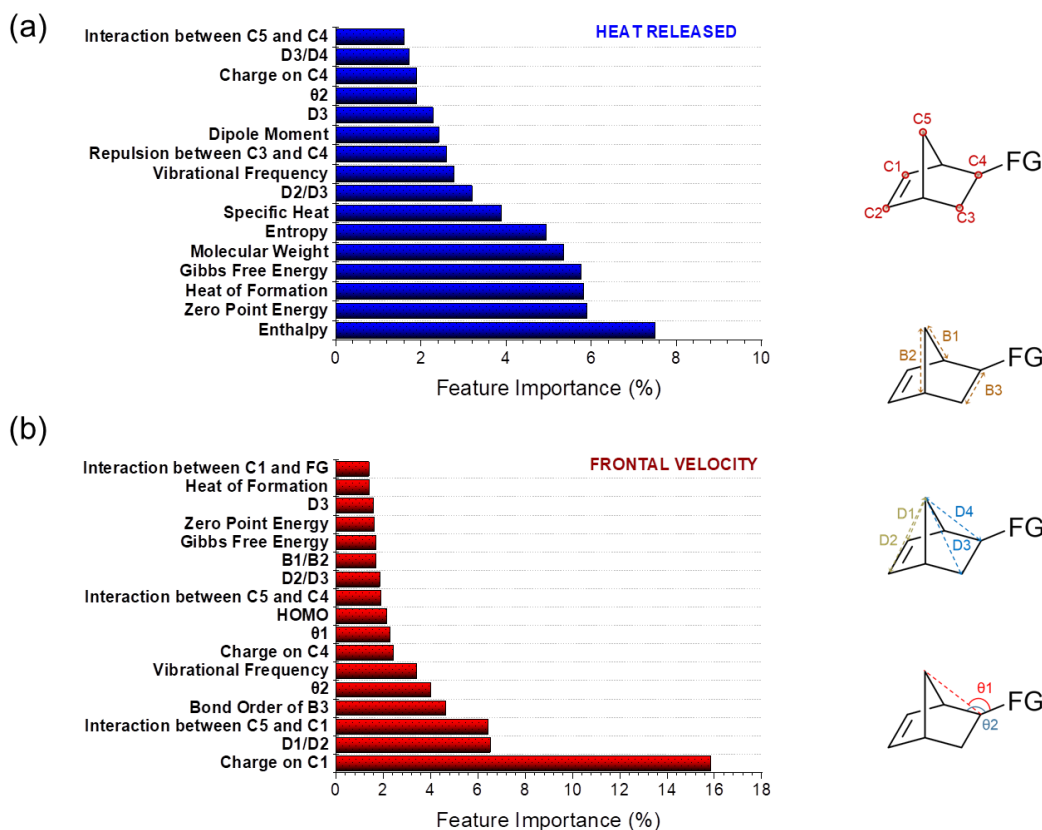


Figure 4.9 The top 16 most important features of the random forest model for predicting (a) ΔH and (b) v_f . C1-C5 represent carbon atoms as indicated; B1 and B2 are bond length; D1-D4 represent the distance between two carbon atoms as indicated; θ is the bond angle as indicated.

We first correlated enthalpy (the top 1 feature) with heat released ΔH (determined by DSC). Enthalpy values were obtained from the equilibrium geometry calculation by DFT and represent the relative energy level of the molecule. In other words, a less negative enthalpy means lower thermodynamic stability of the molecule. As shown in Figure 4.10, monomers with less negative enthalpy values, such as NDE, TCND and ENB, tend to release larger amounts of heat in ROMP. With increased size of the ester substituent, the molecule possesses much smaller enthalpy, and thus has a dramatically lower ΔH value. This implies that an unknown structure with a less negative enthalpy calculated by DFT is more likely to have higher ΔH and be a more reactive FROMP monomer candidate. Similarly, measured v_f values were correlated with atomic charge on C1 and bond angle θ_2 , respectively. Compared to ΔH , v_f is a more complicated property, and the trends are less clear. As illustrated in Figure 4.11, more negative charge on C1 and larger θ_2 tend to afford monomers with lower v_f . In addition, the anchor group effect

observed in the last section is most likely to originate from the difference in electrostatic interaction and bond angle.

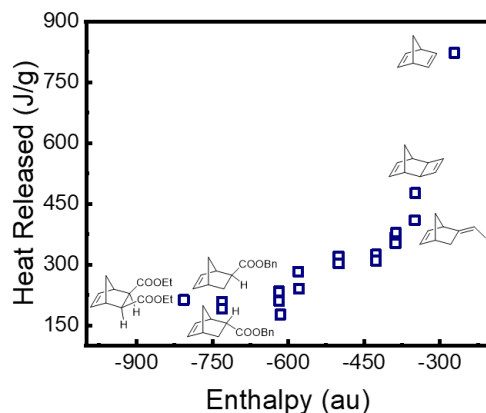


Figure 4.10 Correlation between heat released (determined by DSC) and enthalpy (of the equilibrium geometry calculated by DFT at 298.15 K). 1 au = 2625.5 kJ/mol.

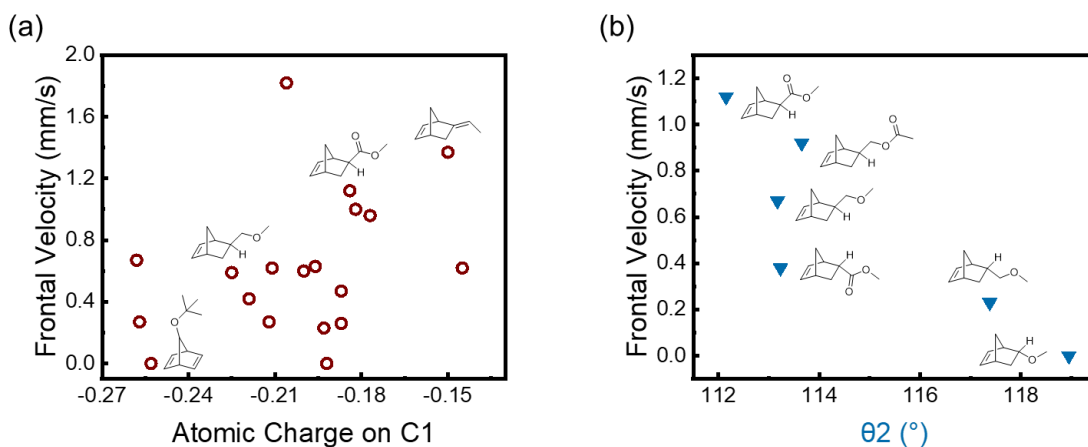


Figure 4.11 (a) Correlation between v_f and atomic charge on C1. (b) Correlation between v_f and bond angle θ_2 . The atomic charge and bond angle values were obtained from DFT calculations.

4.5 Gel Time of Functionalized Monomers

Since thermal initiation and subsequent polymerization occur even at room temperature according to Arrhenius kinetics, the amount of available initiator or monomer will eventually be depleted, making FROMP impossible. As mentioned earlier, phosphite-inhibited FROMP significantly extends the working time up to 30 hours.⁵ Interestingly, the mixture of Grubbs II, phosphite, and *endo*-DCPD would slowly transform from a liquid to a viscoelastic gel at room temperature. The gelation does not result in concomitant spontaneous polymerization, as

observed with other inhibitors such as 4-dimethylaminopyridine. This is remarkable because it allows access to a range of rheological profiles between low-viscosity liquid and free-standing elastomeric gel.⁴ A longer gel time (t_{gel}), corresponding to the crossover of G' and G'' , is desirable for processing purposes. As t_{gel} is directly related to kinetics, we hypothesized that monomers with lower reactivity afford longer gel time. However, DCPD-OAc ($v_f = 0.27$ mm/s) showed a t_{gel} of 1.8 h while *endo*-DCPD has a faster v_f of 1.00 mm/s and a much longer t_{gel} of 4.8 h under the exact same conditions (Figure 4.12). From the DSC traces shown in Figure 4.13, ROMP of DCPD-OAc is initiated at a lower temperature, presumably resulting from the polarity of the acetate group that facilitates the dissociation of the pre-catalyst or phosphite-inhibited catalyst. We also observed similar trends in other functionalized NBE monomers, and the parameters that affect gel time are still under investigation.

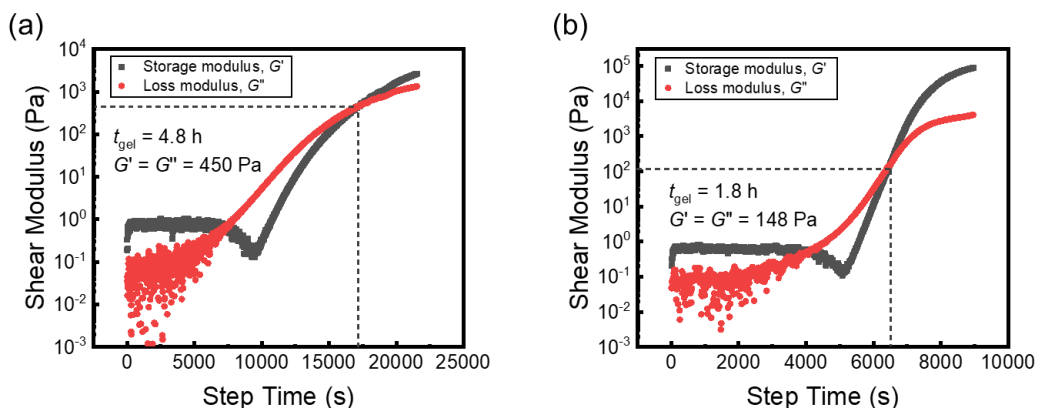


Figure 4.12 Rheological characterization for curing at 25 °C of (a) *endo*-DCPD and (b) DCPD-OAc. t_{gel} is the point where $G' = G''$. Time-sweep measurements were performed with a strain of 0.1% and a frequency of 1 Hz.

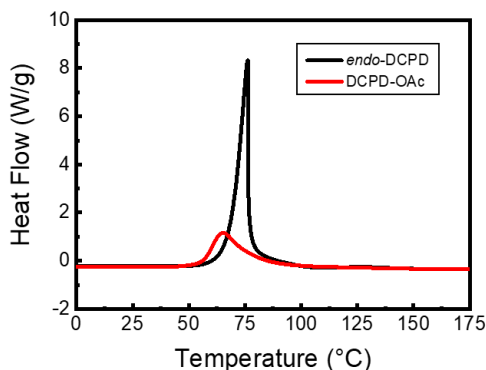


Figure 4.13 Exothermic polymerization peaks of *endo*-DCPD and DCPD-OAc. Ramping rate: 10 °C/min.

4.6 Cross-Linking Mechanism of DCPD

While a few examples of linear polydicyclopentadiene (pDCPD) are reported,^{34–37} the vast majority of pDCPD obtained from ROMP or FROMP appears to be cross-linked. However, the cross-linking mechanism still remains the subject of some debate. The mode of cross-linking is proposed to be generated through two pathways, metathesis of cyclopentene ring and thermally-initiated olefin addition (Figure 4.14). On one hand, due to the low ring strain energy of cyclopentene ring, cross-linking through metathesis reaction is not thermodynamically favorable, especially at high front temperatures. This has been shown in Chapter 2 and Chapter 3. The study on incubation time also suggests that minimum metathesis of cyclopentene ring occurs even after 10-h polymerization at room temperature. On the other hand, radical addition usually requires extensive heating, especially in the case of bulk polymerization where chain mobility restricts the reaction.³⁸ In the FROMP process, even though the front temperature could reach as high as 200 °C depending on the reaction geometry, this high temperature maintains less than a minute and cools back to room temperature quickly. Thus, radical process is less likely to be the principal mode of cross-linking.

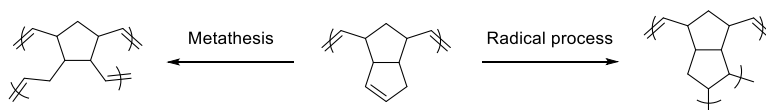


Figure 4.14 Two proposed cross-linking modes in ROMP of DCPD.

The cross-linked structure after FROMP is characterized by its insolubility in common organic solvents and higher T_g (> 100 °C) than linear pDCPD (< 70 °C). To test the feasibility of radical cross-linking, a radical initiator dicumyl peroxide which has a required temperature for 1-h half-life of 135 °C was added to the reaction mixture. As shown in Figure 4.15, addition of 1 mol % initiator did increase the T_g slightly from 102 °C to 107 °C when polymerization was performed at 135 °C for 1 hour. However, a decrease in T_g was observed if the sample was from FROMP experiments because the initiator serves as a plasticizer in the sample. These results imply that thermally initiated radical process makes a minimum contribution to the cross-linking of pDCPD.

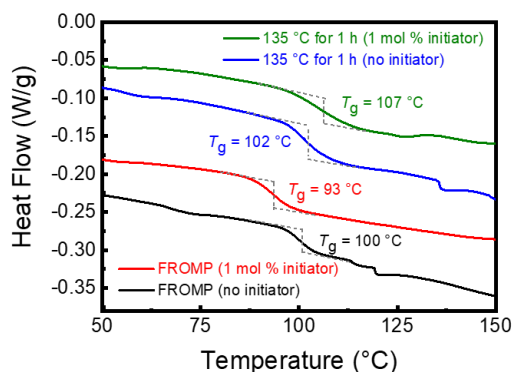


Figure 4.15 Glass transition temperatures of pDCPD samples under different reaction conditions. Green and blue traces represent ROMP of *endo*-DCPD at 135 °C for 1 hour with and without the presence of 1 mol % dicumyl peroxide as the radical initiator, respectively. Red and black traces represent FROMP of *endo*-DCPD with and without the presence of 1 mol % dicumyl peroxide as the radical initiator, respectively. Addition of 1 mol % initiator did not affect v_f . All experiments were performed at 100 ppm Grubbs II loading and 1.0 equiv. $P(OBu)_3$.

Thus, the metathesis of cyclopentene ring might be responsible for the cross-linked structure. However, 5,6-dihydrocyclopentadiene is not able to homopolymerize or copolymerize with another strained monomer even with increased catalyst loading and fast-initiating Grubbs III. We reasoned that even though the equilibrium largely favors ring-closing form, there might exist a small degree (< 5%) of cyclopentene ring-opening that results in a slightly cross-linked polymer (Figure 4.16). Since bulk polymerization of *endo*-DCPD immediately affords a tough material that restricts the movement of polymer chains, ring-opened cyclopentene ring might be stuck in a non-equilibrium state. The mechanical properties of the resulting pDCPD benefits from the small amount of cross-linking; otherwise, the thermoset would be brittle when densely cross-linked. A more detailed structural characterization of pDCPD would benefit the mechanistic understanding of ROMP in the bulk state.

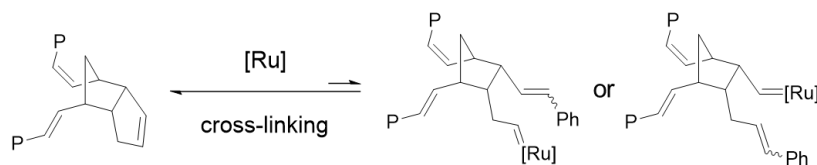


Figure 4.16 Unfavorable metathesis of cyclopentene ring.

4.7 FROMP of TCND

To design a more reactive FROMP monomer, we initially synthesized tricyclo[4.2.1.0^{2,5}]nona-3,7-diene (TCND) which consists of two strained rings, norbornene and cyclobutene. TCND possesses a higher ΔH (477 J/g) and front temperature (186 °C) due to its larger ring strain energy than *endo*-DCPD ($\Delta H = 353$ J/g, front temperature = 150 °C); however, it shows a much slower v_f (0.59 mm/s) than *endo*-DCPD (1 mm/s). One reason is the sluggish kinetics of TCND, characterized by an extremely broad polymerization peak spanning from 30 °C to 150 °C (Figure 4.17 (b)). We also noticed a sharp endothermic peak at 236 °C, corresponding to the boiling point of unreacted TCND. Since ROMP of both rings on TCND affords densely cross-linked polymers, we speculated that the ultra-high cross-linking density immediately freezes the whole system and leads to incomplete monomer conversion. Copolymerization behavior in Figure 4.17 (a) demonstrates that incorporating 5, 10 and 20 wt. % of TCND substantially reduces v_f even below v_f (TCND).

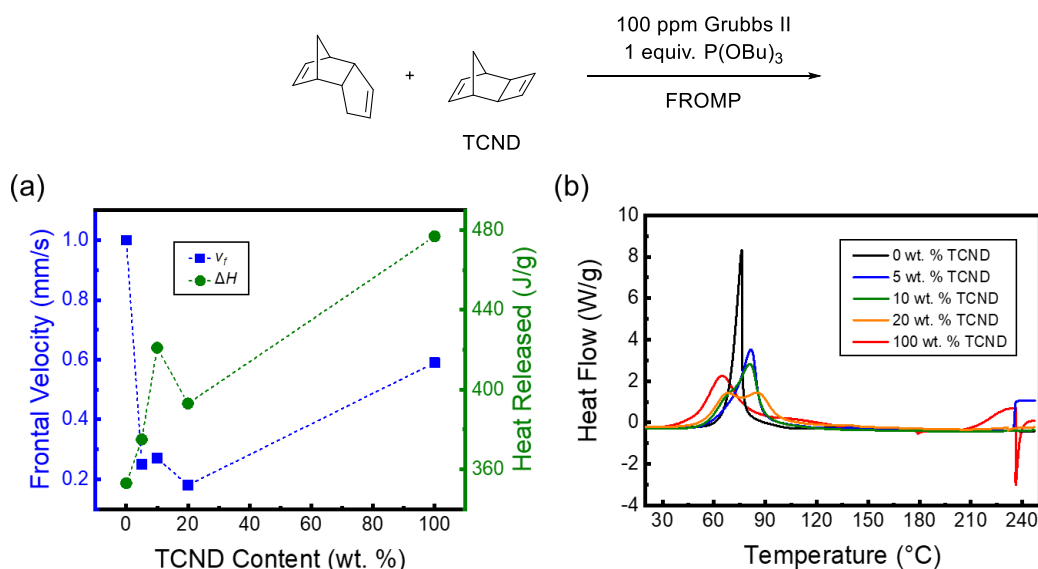


Figure 4.17 (a) Frontal velocity, heat released data and (b) DSC traces of copolymerization of *endo*-DCPD and TCND. FROMP was performed in the presence of 100 ppm Grubbs II catalyst and 1.0 equiv P(OBu)₃ at 20 °C. DSC ramping rate: 10 °C/min.

Low front temperature, incomplete monomer conversion and densely cross-linked structure upon copolymerization could explain the unusual copolymerization behavior, but a more comprehensive mechanistic study is needed. Investigation of cyclobutene derivatives and dihydrodicyclopentadiene would be the first steps to test the hypothesis on the role of cross-

linking. Other characterization methods such as infrared and Raman spectroscopy would also provide useful and quantitative structural information of the resulting polymers.

4.8 Conclusion

We investigated 30 strained monomers to expand the toolbox of FROMP, gain a further fundamental understanding of metathesis chemistry, and guide rational monomer design. We first attempted to build a constitutive equation based on the hypothesis that FROMP reactivity (v_f) is proportional to the heat release rate. Despite a poor linear correlation between v_f and heat release rate for structurally disparate monomers, the effect of molecular weight and anchor group on FROMP shed light on some design principles. Smaller MW results in a higher heat release rate and thus faster v_f . For monomers with different anchor groups, v_f decreases in the order of $-\text{COOR} \approx -\text{CH}_2\text{OCOR} > -\text{CH}_2\text{OR} > -\text{OR}$.

Due to the complexity of FROMP with numerous variables interacting, we applied ML methods to build a more quantitative structure-property relationship to predict the FROMP performance of unknown structures and identify the principal features of a desirable monomer. Random forest algorithm was utilized to build the model with 103 structural parameters of the monomer as inputs and FROMP properties (i.e., ΔH and v_f) as outputs. Models with reasonable predictability were obtained for ΔH and v_f despite a small sample size. Furthermore, important features (such as thermodynamic properties of the molecule, ratio of bond length (symmetry of the molecule), bond angle and electrostatic interactions) were identified to explain the variance in FROMP performance. Gratifyingly, the patterns that ML models recognized agree well with some of the conclusions from our previous structure-property relationship studies.

In addition to expanding the monomer scope, several other aspects were also evaluated such as the substituent effect on gel time, cross-linking mechanism of DCPD and FROMP of a potentially more reactive TCND monomer. These findings all contribute to the fundamental understanding of ROMP and further optimization of materials manufacturing processes.

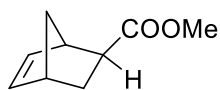
4.9 Experimental Details

4.9.1 Materials and General Methods

Unless otherwise stated, all starting materials and reagents such as *endo*-Dicyclopentadiene (*endo*-DCPD), 5-ethylidene-2-norbornene (ENB), *exo*-5-norbornenecarboxylic acid (*exo*-NBE-COOH), Grubbs II, and P(OBu)₃ were purchased from Sigma-Aldrich without further purification. TCND was synthesized from quadricyclane and *cis*-1,2-bis(phenylsulfonyl)ethylene, followed by reduction using sodium amalgam. DCPD-COOME was provided by Tong Li from University of Victoria. Since *endo*-DCPD is a solid at room temperature, 5 wt. % ENB was added to depress the melting point. All references to *endo*-DCPD herein refer to the 95:5 *endo*-DCPD:ENB solution. ¹H and ¹³C NMR spectra were recorded on a Varian Unity 500 MHz spectrometer or a Carver B500 spectrometer in the VOICE NMR laboratory at the University of Illinois. Chemical shifts are reported in δ (ppm) relative to the residual solvent peak (CDCl₃: 7.26 for ¹H; CDCl₃: 77.16 for ¹³C). Coupling constants (*J*) are reported in Hertz (Hz). Splitting patterns are designated as s (singlet), d (doublet), t (triplet), quint (quintet), sep (septet), dd (doublet of doublets), dt (doublet of triplets), and m (multiplet). High-resolution ESI mass spectra were recorded on a Micromass 70-VSE spectrometer through the Mass Spectrometry Facility, SCS at University of Illinois. The DSC measurement was performed using TA Instrument Q20 Differential Scanning Calorimeter equipped with a Liquid Nitrogen Cooling System (LNCS). Tzero hermetic aluminum pans and lids were used as sample testing containers. Nitrogen was used as sample purge gas and the ramping rate was 10 °C/min. Front temperatures were measured using stainless steel type T thermocouples (Omega Engineering, Model TMQSS-020U). Thermocouple data was collected using a temperature sensor (Phidgets, Model 1048) and recorded using a custom LabVIEW code (National Instruments) at 100 Hz.

4.9.2 Synthesis of Strained Monomers

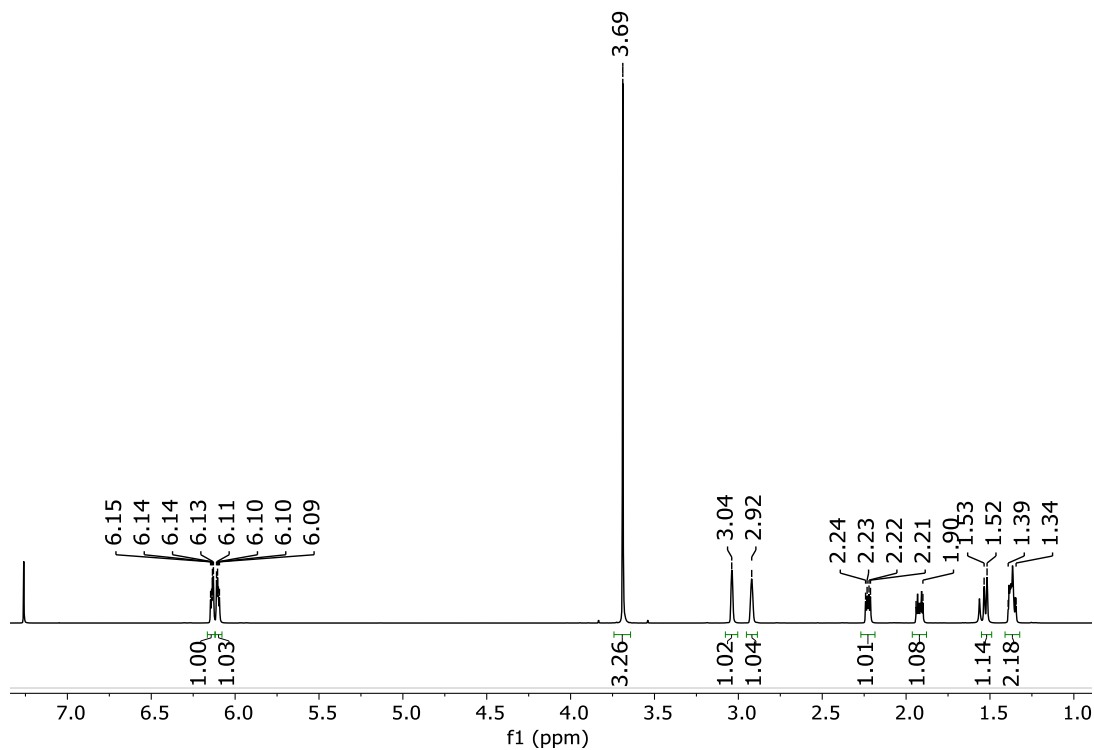
Synthesis of *exo*-Methyl 5-norbornene-2-carboxylate (*exo*-NBE-COOME)



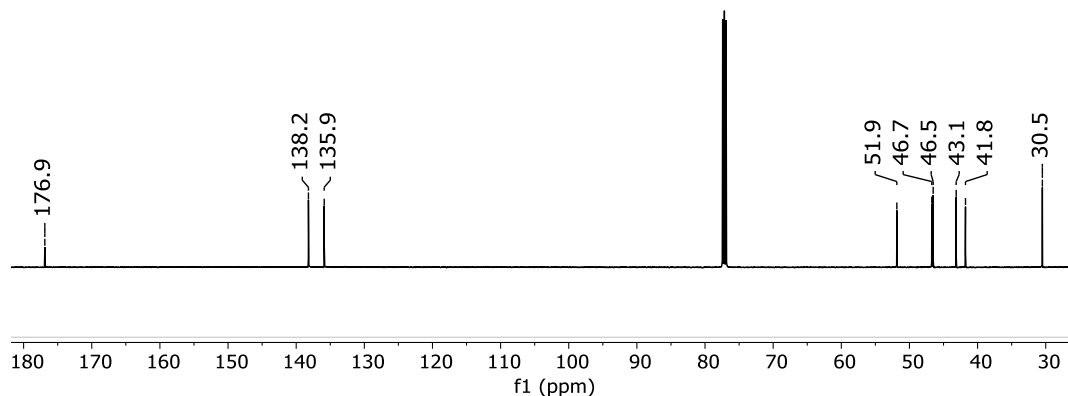
In a solution of *exo*-NBE-COOH (2.5 g, 18 mmol, 1.0 equiv.) in CH₂Cl₂ (2.5 mL), methanol (7.5 mL, 10 equiv.) and H₂SO₄ (0.25 mL) were added. The reaction was allowed

to stir at 70 °C. After the completion of the reaction monitored by TLC, the resulting mixture was concentrated. CH₂Cl₂ (20 mL) was added to the residue and washed with brine (2×15 mL), dried with anhydrous sodium sulfate, and then concentrated. The crude product was further purified by flash chromatography to give the desired compound as a colorless liquid (2.53 g, 92%). ¹H NMR (CDCl₃, 500 MHz) δ 6.14 (dd, *J* = 5.5 Hz and 3 Hz, 1H), 6.10 (dd, *J* = 5.5 Hz and 3 Hz, 1H), 3.69 (s, 3H), 3.04 (s, 1H), 2.92 (s, 1H), 2.23 (dd, *J* = 10.5 Hz and 4.5 Hz, 1H), 1.92 (dt, *J* = 11.5 Hz and 4 Hz, 1H), 1.52 (d, *J* = 8.5 Hz, 1H), 1.39-1.34 (m, 2H); ¹³C NMR (CDCl₃, 125 MHz) δ 176.9, 138.2, 135.9, 51.9, 46.7, 46.5, 43.1, 41.8, 30.5. HRMS-EI (*m/z*): calculated for C₉H₁₂O₂ [M]⁺, 152.0837; Found, 152.0833.

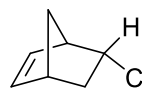
¹H NMR of *exo*-NBE-COOMe



^{13}C NMR of *exo*-NBE-COOMe

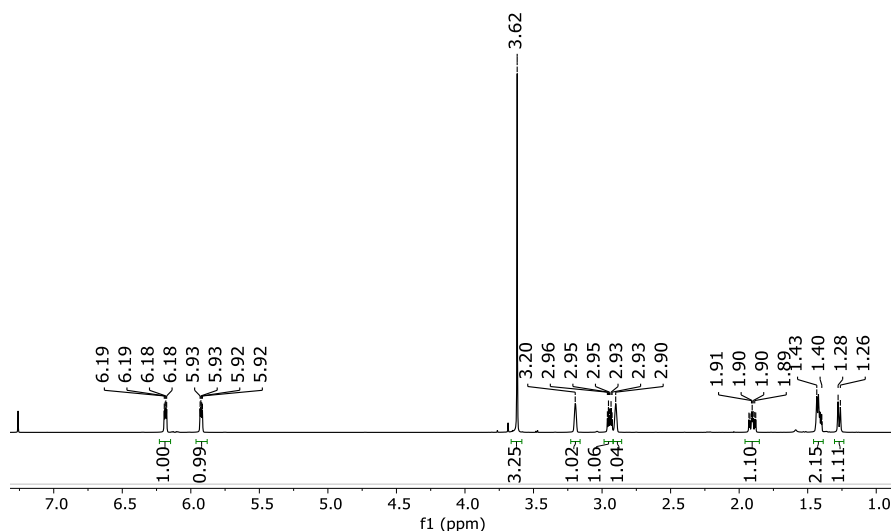


Synthesis of *endo*-Methyl 5-norbornene-2-carboxylate (*endo*-NBE-COOMe)

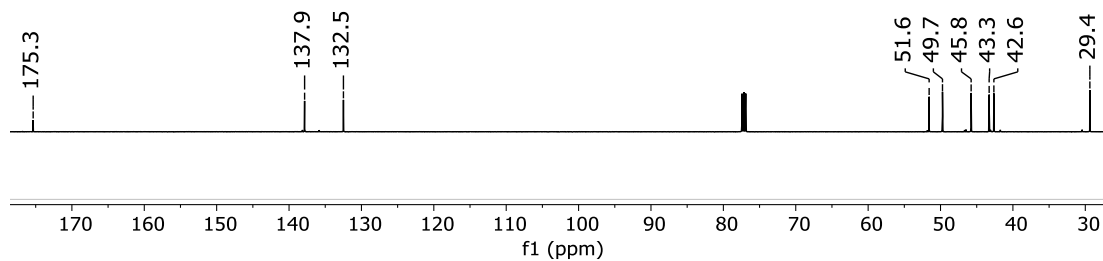


The procedure is the same as *exo*-NBE-COOMe except that the starting material is a mixture of *exo*- and *endo*-NBE-COOH (predominantly *endo*). After the esterification, *endo*-NBE-COOMe was purified from *exo*-isomer by chromatography to afford a colorless liquid (1.13 g, 41%). ^1H NMR (CDCl_3 , 500 MHz) δ 6.18 (dd, $J = 5.6$ and 3.1 Hz, 1H), 5.92 (dd, $J = 5.6$ and 2.8 Hz, 1H), 3.62 (s, 3H), 3.20 (s, 1H), 2.99-2.92 (m, 1H), 2.90 (s, 1H), 1.90 (ddd, $J = 13.0$, 9.4 and 3.7 Hz, 1H), 1.46-1.38 (m, 2H), 1.27 (d, $J = 8.3$ Hz, 1H); ^{13}C NMR (CDCl_3 , 125 MHz) δ 175.3, 137.9, 132.5, 51.6, 49.7, 45.8, 43.3, 42.6, 29.4. HRMS-ESI (m/z): calculated for $\text{C}_9\text{H}_{13}\text{O}_2$ $[\text{M}+\text{H}]^+$, 153.0916; Found, 153.0917.

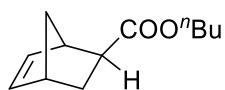
^1H NMR of *endo*-NBE-COOMe



^{13}C NMR of *endo*-NBE-COOMe

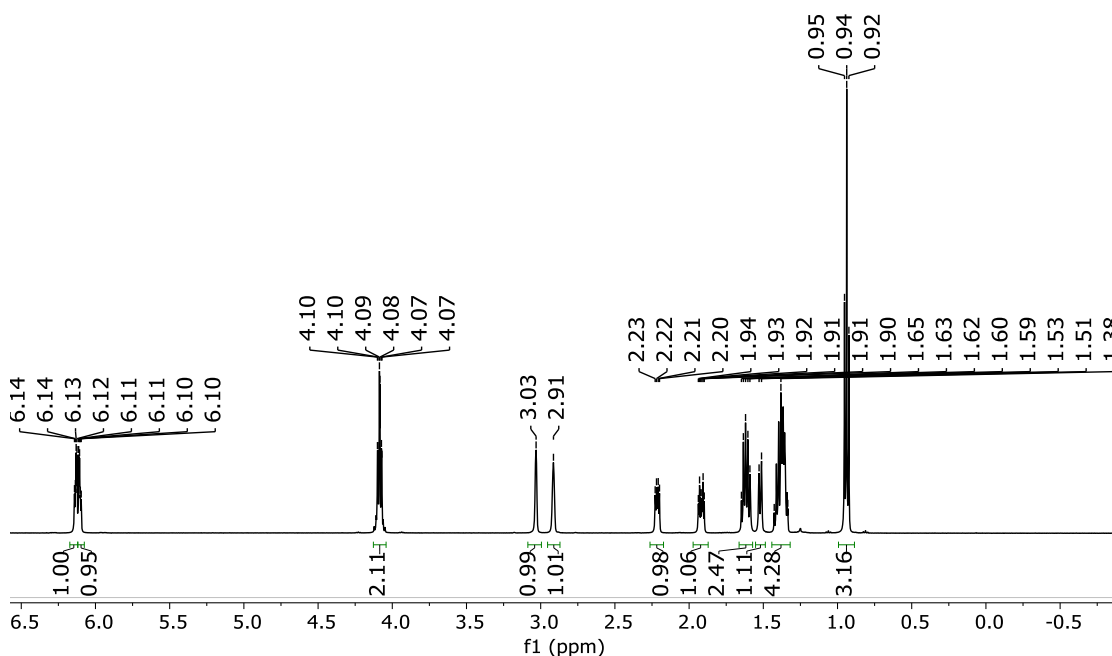


Synthesis of *exo*-ⁿButyl 5-norbornene-2-carboxylate (*exo*-NBE-COOⁿBu)³⁹

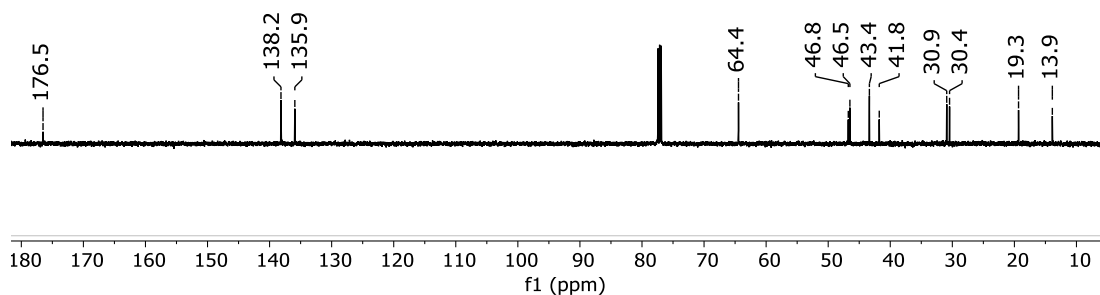


^1H NMR (CDCl_3 , 500 MHz) δ 6.13 (dd, $J = 5.5$ and 2.9 Hz, 1H), 6.10 (dd, $J = 5.5$ and 3.0 Hz, 1H), 4.08 (td, $J = 6.7$ and 1.8 Hz, 2H), 3.03 (s, 1H), 2.91 (s, 1H), 2.21 (dd, $J = 10.2$ and 4.4 Hz, 1H), 1.92 (dt, $J = 11.8$ and 3.9 Hz, 1H), 1.62 (dt, $J = 14.6$ and 6.7 Hz, 2H), 1.52 (d, $J = 8.3$ Hz, 1H), 1.44-1.32 (m, 4H), 0.94 (t, $J = 7.4$ Hz, 3H); ^{13}C NMR (CDCl_3 , 125 MHz) δ 176.5, 138.2, 135.9, 64.4, 46.8, 46.5, 43.4, 41.8, 30.9, 30.4, 19.3, 13.9. HRMS-ESI (m/z): calculated for $\text{C}_{12}\text{H}_{19}\text{O}_2$ [$\text{M}+\text{H}$] $^+$, 195.1385; Found, 195.1386.

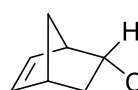
^1H NMR of *exo*-NBE-COOⁿBu



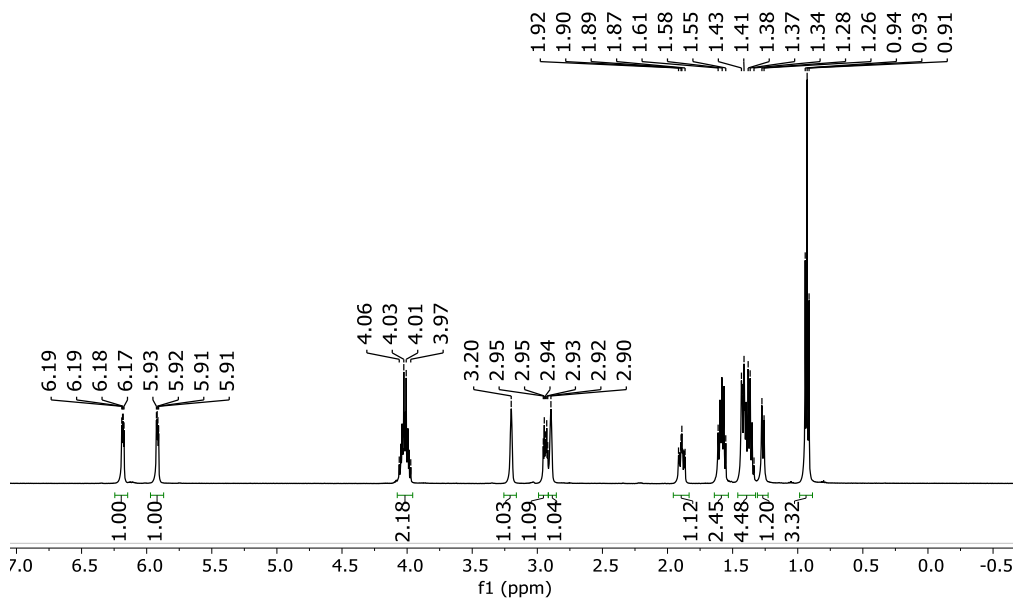
^{13}C NMR of *exo*-NBE-COOⁿBu



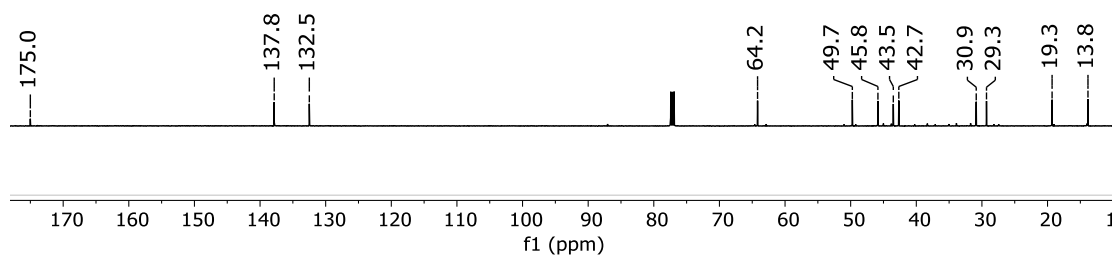
Synthesis of *endo*-ⁿButyl 5-norbornene-2-carboxylate (*endo*-NBE-COOⁿBu)³⁹

 ^1H NMR (CDCl_3 , 500 MHz) δ 6.18 (dd, $J = 5.6$ and 3.0 Hz, 1H), 5.92 (dd, $J = 5.6$ and 2.8 Hz, 1H), 4.02 (qt, $J = 10.8$ and 6.6 Hz, 2H), 3.20 (s, 1H), 2.94 (dt, $J = 9.2$ and 3.9 Hz, 1H), 2.90 (s, 1H), 1.89 (ddd, $J = 12.3$, 9.4 and 3.7 Hz, 1H), 1.64-1.53 (m, 2H), 1.46-1.32 (m, 4H), 1.27 (d, $J = 8.1$ Hz, 1H), 0.93 (t, $J = 7.4$ Hz, 3H); ^{13}C NMR (CDCl_3 , 125 MHz) δ 175.0, 137.8, 132.5, 64.2, 49.7, 45.8, 43.5, 42.7, 30.9, 29.3, 19.3, 13.8. HRMS-ESI (m/z): calculated for $\text{C}_{12}\text{H}_{19}\text{O}_2$ [$\text{M}+\text{H}$] $^+$, 195.1385; Found, 195.1389.

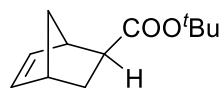
^1H NMR of *endo*-NBE-COOⁿBu



^{13}C NMR of *endo*-NBE-COO^tBu

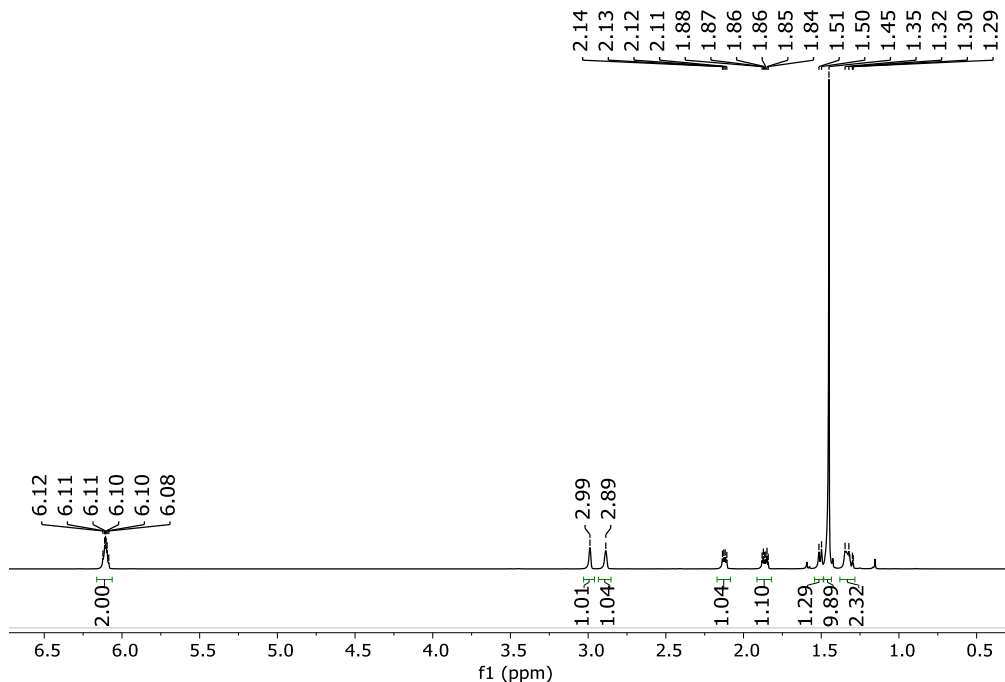


Synthesis of *exo*-^tButyl 5-norbornene-2-carboxylate (*exo*-NBE-COO^tBu)³⁹

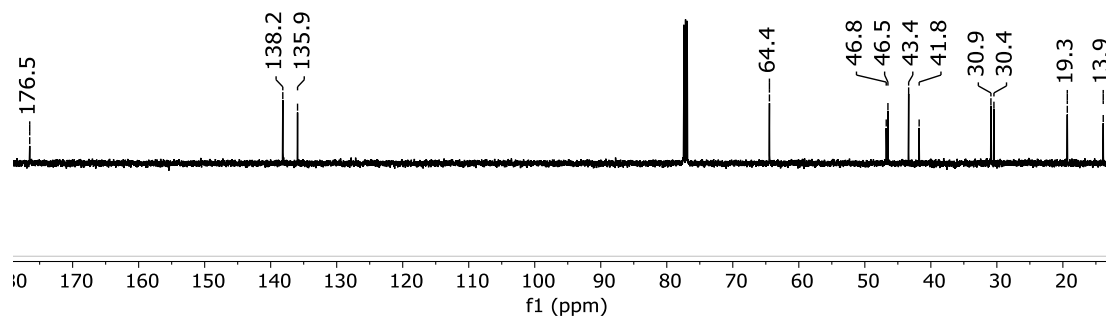


^1H NMR (CDCl_3 , 500 MHz) δ 6.16-6.06 (m, 2H), 2.99 (s, 1H), 2.89 (s, 1H), 2.12 (dd, $J = 9.2$ and 4.7 Hz, 1H), 1.86 (dt, $J = 11.5$ and 3.9 Hz, 1H), 1.51 (d, $J = 8.4$ Hz, 1H), 1.45 (s, 9H), 1.38-1.28 (m, 2H); ^{13}C NMR (CDCl_3 , 125 MHz) δ 176.5, 138.2, 135.9, 64.4, 46.8, 46.5, 43.4, 41.8, 30.9, 30.4, 19.3, 13.9. HRMS-ESI (m/z): calculated for $\text{C}_{12}\text{H}_{19}\text{O}_2$ $[\text{M}+\text{H}]^+$, 195.1385; Found, 195.1381.

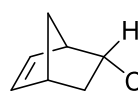
^1H NMR of *exo*-NBE-COO^tBu



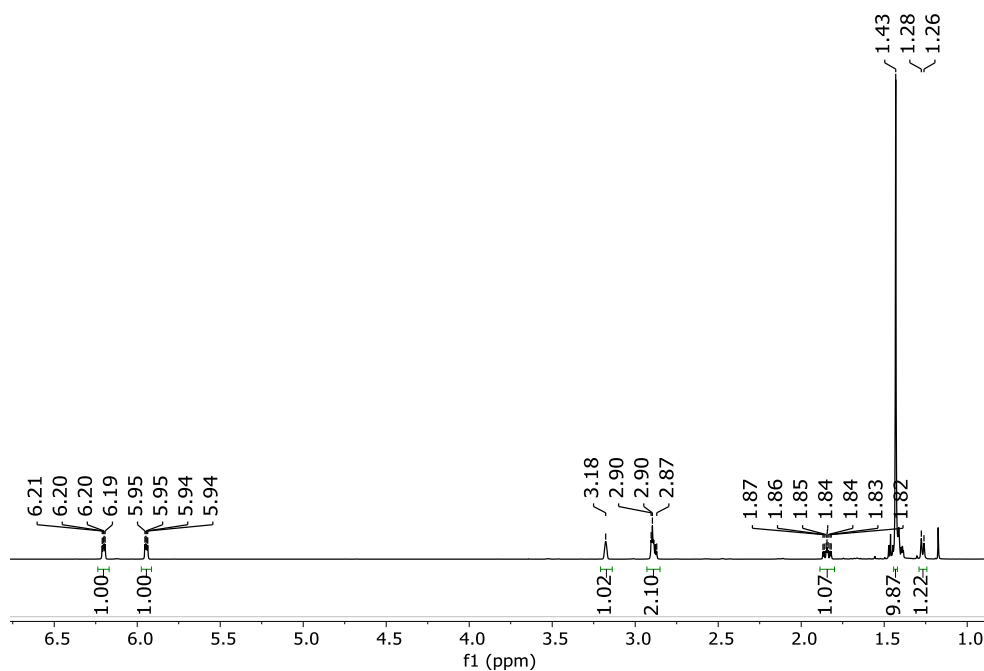
^{13}C NMR of *exo*-NBE-COO^tBu



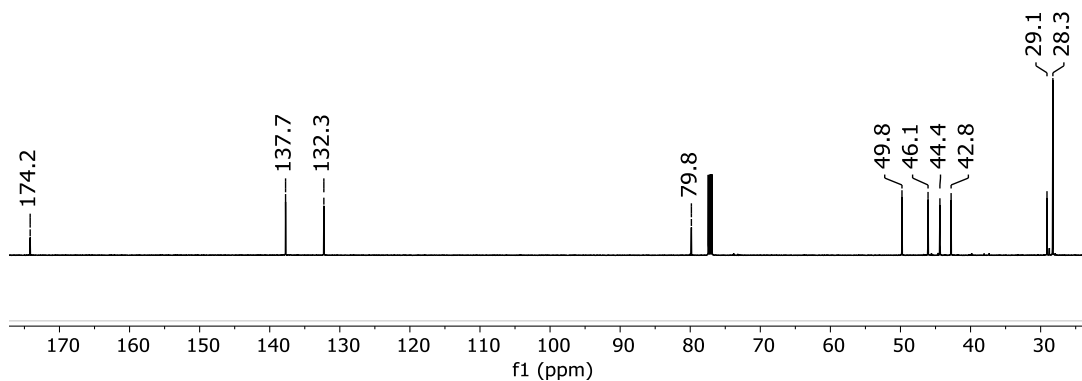
Synthesis of *endo*-^tButyl 5-norbornene-2-carboxylate (*endo*-NBE-COO^tBu)³⁹

 ^1H NMR (CDCl_3 , 500 MHz) δ 6.20 (dd, $J = 5.6$ and 3.0 Hz, 1H), 5.95 (dd, $J = 5.6$ and 2.8 Hz, 1H), 3.18 (s, 1H), 2.93-2.85 (m, 2H), 1.84 (ddd, $J = 12.8$, 9.3 and 3.7 Hz, 1H), 1.43 (s, 9H), 1.27 (d, $J = 8.0$ Hz, 1H); ^{13}C NMR (CDCl_3 , 125 MHz) δ 174.2, 137.7, 132.3, 79.8, 49.8, 46.1, 44.4, 42.8, 29.1, 28.3. HRMS-ESI (m/z): calculated for $\text{C}_{12}\text{H}_{19}\text{O}_2$ [$\text{M}+\text{H}$] $^+$, 195.1385; Found, 195.1387.

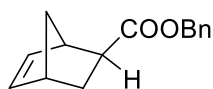
^1H NMR of *endo*-NBE-COO^tBu



^{13}C NMR of *endo*-NBE-COO'Bu

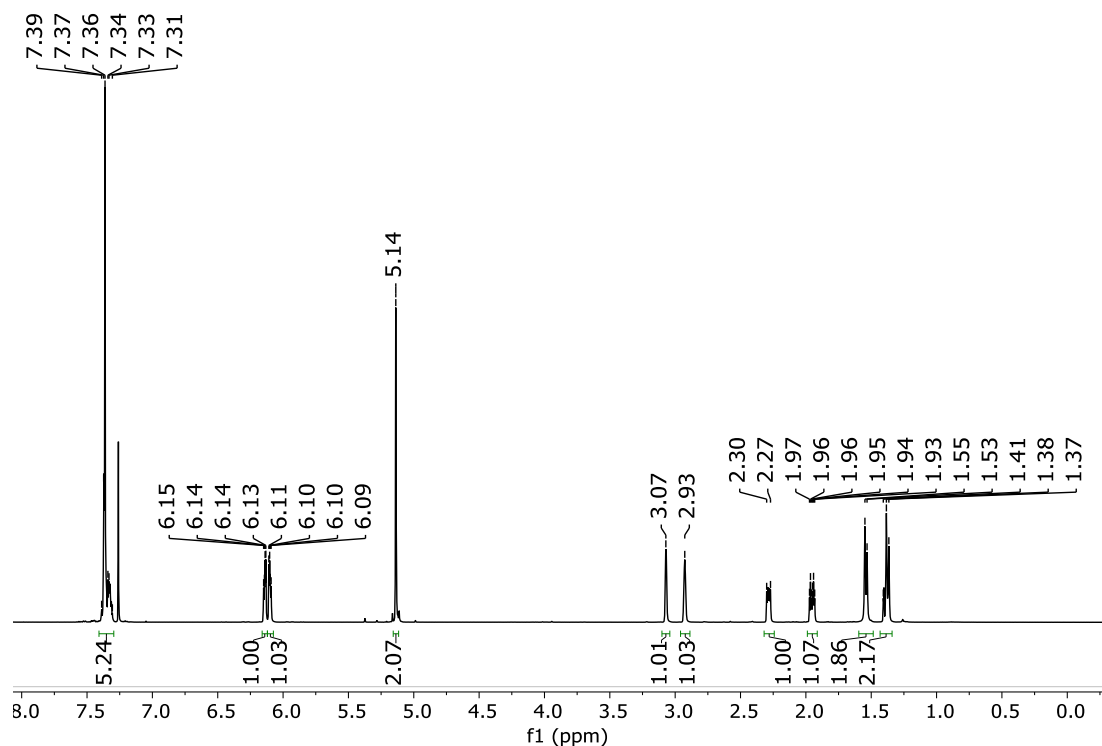


Synthesis of *exo*-Benzyl 5-norbornene-2-carboxylate (*exo*-NBE-COOBn)

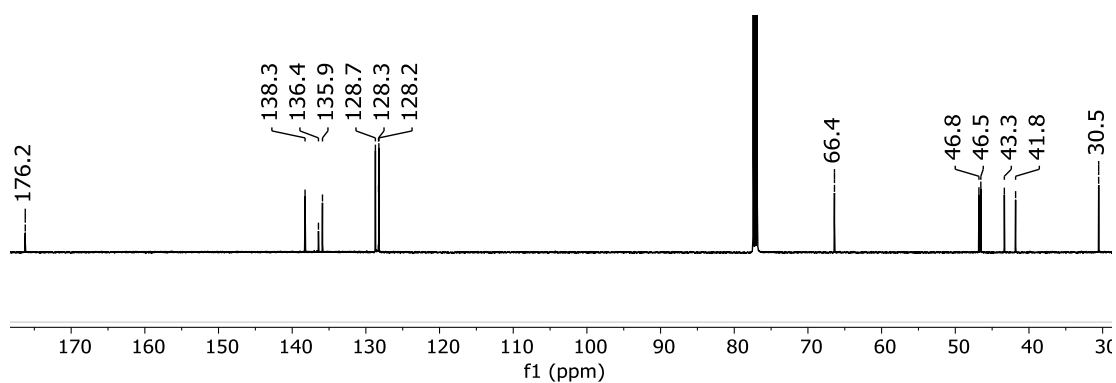


To a mixture of *exo*-NBE-COOH (2.5 g, 18 mmol, 1.0 equiv.) and K_2CO_3 (4.97 g, 36 mmol, 2 equiv.) in acetone (50 mL) was added benzyl bromide (2.16 g, 12.6 mmol, 0.7 equiv.). The mixture was stirred at 60 °C for 8 h. The resulting mixture was filtered. The filtrate was concentrated. 20 mL EtOAc was added to the residue and washed with brine (2×15 mL), dried with anhydrous sodium sulfate, and then concentrated. The crude product was purified by flash chromatography to give the desired product as colorless oil (3.1 g, 75%). ^1H NMR (CDCl_3 , 500 MHz) δ 7.41-7.29 (m, 5H), 6.14 (dd, $J = 5.5$ and 2.9 Hz, 1H), 6.10 (dd, $J = 5.5$ and 3.0 Hz, 1H), 5.14 (s, 2H), 3.07 (s, 1H), 2.93 (s, 1H), 2.28 (ddd, $J = 8.6$, 4.5 and 2.0 Hz, 1H), 1.95 (dt, $J = 12.0$ and 4.0 Hz, 1H), 1.54 (d, $J = 8.1$ Hz, 2H), 1.43-1.34 (m, 2H); ^{13}C NMR (CDCl_3 , 125 MHz) δ 176.2, 138.3, 136.4, 135.9, 128.7, 128.3, 128.2, 66.4, 46.8, 46.5, 43.3, 41.8, 30.5. HRMS-ESI (m/z): calculated for $\text{C}_{15}\text{H}_{17}\text{O}_2$ [$\text{M}+\text{H}$] $^+$, 229.1229; Found, 229.1238.

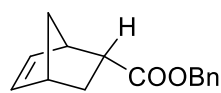
^1H NMR of *exo*-NBE-COOBn



^{13}C NMR of *exo*-NBE-COOBn



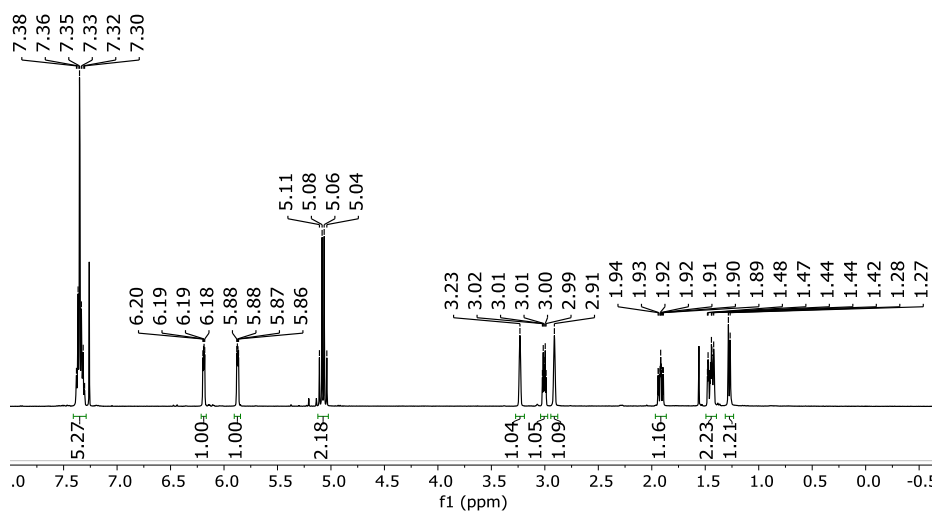
Synthesis of *endo*-Benzyl 5-norbornene-2-carboxylate (*endo*-NBE-COOBn)



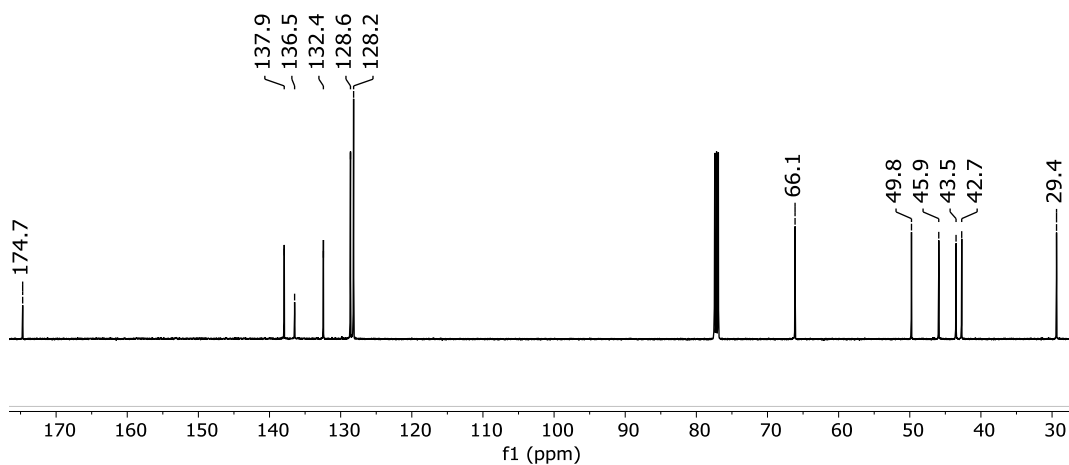
The procedure is the same as *exo*-NBE-COOBn except that the starting material is a mixture of *exo*- and *endo*-NBE-COOH (predominantly *endo*). After the esterification, *endo*-NBE-COOBn was purified from *exo*-isomer by chromatography to afford a colorless liquid (1.57

g, 38%). ^1H NMR (CDCl_3 , 500 MHz) δ 7.41-7.29 (m, 5H), 6.19 (dd, $J = 5.5$ and 3.1 Hz, 1H), 5.87 (dd, $J = 5.6$ and 2.7 Hz, 1H), 5.13-5.02 (m, 2H), 3.23 (s, 1H), 3.01 (dt, $J = 8.8$ and 3.9 Hz, 1H), 2.91 (s, 1H), 1.92 (ddd, $J = 12.6$, 9.4 and 3.7 Hz, 1H), 1.50-1.39 (m, 2H), 1.28 (d, $J = 8.2$ Hz, 1H); ^{13}C NMR (CDCl_3 , 125 MHz) δ 174.7, 137.9, 136.5, 132.4, 128.6, 128.2, 66.1, 49.8, 45.9, 43.5, 42.7, 29.4. HRMS-ESI (m/z): calculated for $\text{C}_{15}\text{H}_{16}\text{O}_2\text{Na}$ $[\text{M}+\text{Na}]^+$, 251.1048; Found, 251.1049.

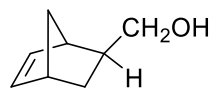
^1H NMR of *endo*-NBE-COOBn



^{13}C NMR of *endo*-NBE-COOBn

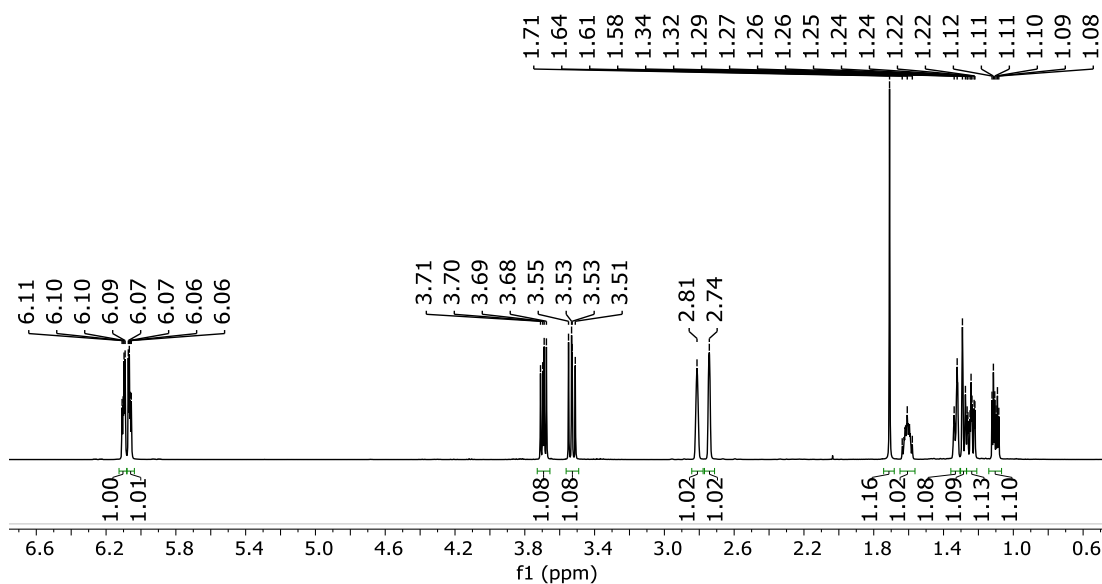


Synthesis of *exo*-5-norbornene-2-methanol (*exo*-NBE-CH₂OH)⁴⁰

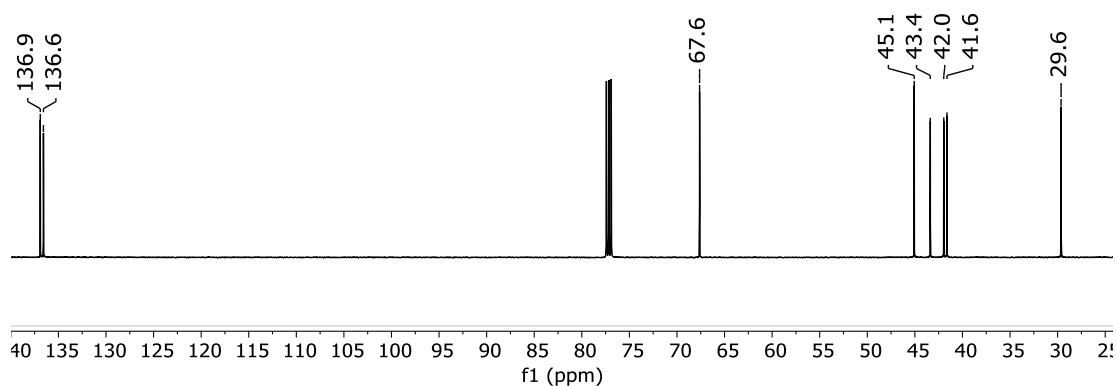


¹H NMR (CDCl₃, 500 MHz) δ 6.10 (dd, *J* = 5.6 and 3.1 Hz, 1H), 6.06 (dd, *J* = 5.6 and 2.9 Hz, 1H), 3.69 (dd, *J* = 10.5 and 6.4 Hz, 1H), 3.53 (dd, *J* = 10.6 and 8.8 Hz, 1H), 2.81 (s, 1H), 2.74 (s, 1H), 1.71 (s, 1H), 1.65-1.56 (m, 1H), 1.33 (d, *J* = 8.6 Hz, 1H), 1.28 (d, *J* = 8.6 Hz, 1H), 1.24 (ddd, *J* = 11.1, 8.4 and 2.3 Hz, 1H), 1.10 (dt, *J* = 11.6, 3.9 Hz, 1H); ¹³C NMR (CDCl₃, 125 MHz) δ 136.9, 136.6, 67.6, 45.1, 43.4, 42.0, 41.6, 29.6. HRMS-ESI (*m/z*): calculated for C₈H₁₃O [M+H]⁺, 125.0966; Found, 125.0964.

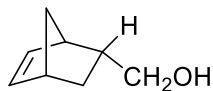
¹H NMR of *exo*-NBE-CH₂OH



¹³C NMR of *exo*-NBE-CH₂OH

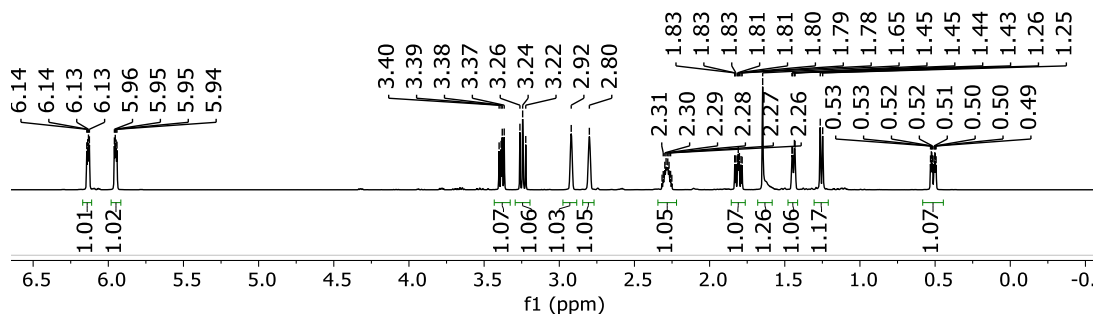


Synthesis of *endo*-5-norbornene-2-methanol (*endo*-NBE-CH₂OH)

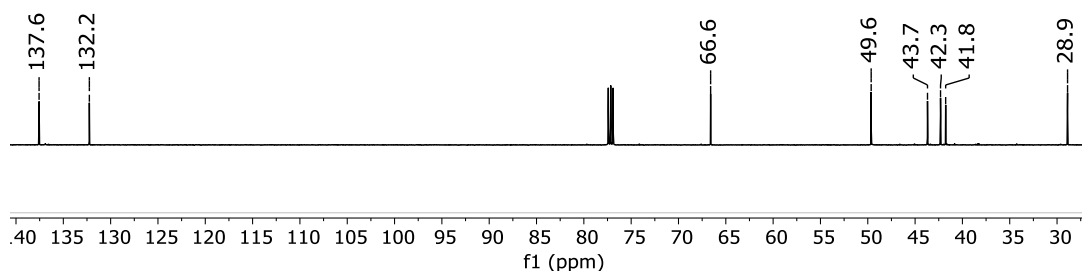


To an ice-cold solution of *endo*-NBE-COOMe (3 g, 19.7 mmol, 1.0 equiv.) in 50 mL dry THF, a solution of LiAlH₄ (1.12 g, 29.6 mmol, 1.5 equiv.) in 12 mL dry THF was dropwise added. The resulting reaction mixture was stirred overnight at room temperature. The reaction was then quenched by slow addition of saturated NH₄Cl solution. The suspension was filtered through Celite, concentrated and extracted with EtOAc. The final product is a colorless oil (2.4 g, 96%). ¹H NMR (CDCl₃, 500 MHz) δ 6.13 (dd, *J* = 5.6 and 3.0 Hz, 1H), 5.95 (dd, *J* = 5.6 and 2.9 Hz, 1H), 3.38 (dd, *J* = 10.5 and 6.5 Hz, 1H), 3.29-3.19 (m, 1H), 2.92 (s, 1H), 2.80 (s, 1H), 2.28 (tq, *J* = 9.2 and 4.0 Hz, 1H), 1.86-1.76 (m, 1H), 1.65 (s, 1H), 1.44 (dd, *J* = 8.2 and 2.2 Hz, 1H), 1.26 (d, *J* = 8.1 Hz, 1H), 0.51 (ddd, *J* = 11.6, 4.3 and 2.7 Hz, 1H); ¹³C NMR (CDCl₃, 125 MHz) δ 137.6, 132.2, 66.6, 49.6, 43.7, 42.3, 41.8, 28.9. HRMS-ESI (*m/z*): calculated for C₈H₁₃O [M+H]⁺, 125.0966; Found, 125.0963.

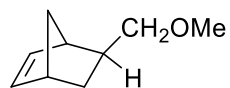
¹H NMR of *endo*-NBE-CH₂OH



¹³C NMR of *endo*-NBE-CH₂OH

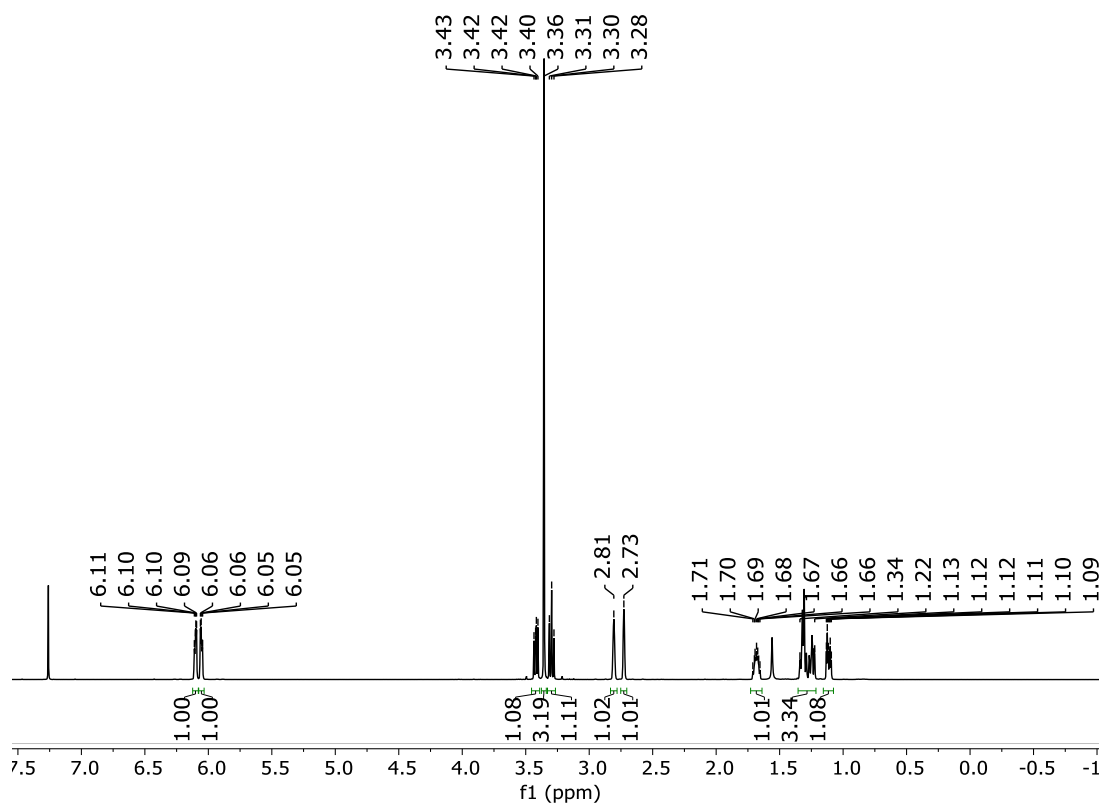


Synthesis of *exo*-5-(methoxymethyl)bicyclo[2.2.1]hept-2-ene (*exo*-NBE-CH₂OMe)⁴¹

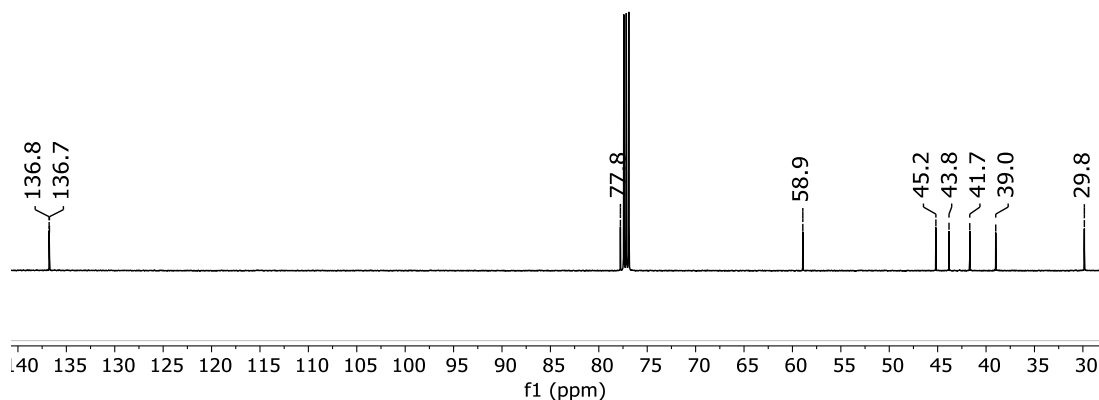


¹H NMR (CDCl₃, 500 MHz) δ 6.10 (dd, *J* = 5.5 Hz and 2.5 Hz, 1H), 6.05 (dd, *J* = 5.5 Hz and 2.5 Hz, 1H), 3.42 (dd, *J* = 9.5 Hz and 6 Hz, 1H), 3.36 (s, 3H), 3.30 (t, *J* = 9 Hz, 1H), 2.81 (s, 1H), 2.73 (s, 1H), 1.68 (sep, *J* = 5 Hz, 1H), 1.34-1.22 (m, 3H), 1.11 (dt, *J* = 12 Hz and 3.5 Hz, 1H); ¹³C NMR (CDCl₃, 125 MHz) δ 136.8, 136.7, 77.8, 58.9, 45.2, 43.8, 41.7, 39.0, 29.8. HRMS-EI (*m/z*): calculated for C₉H₁₄O [M]⁺, 138.1045; Found, 138.1043.

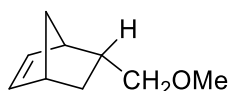
¹H NMR of *exo*-NBE-CH₂OMe



^{13}C NMR of *exo*-NBE-CH₂OMe

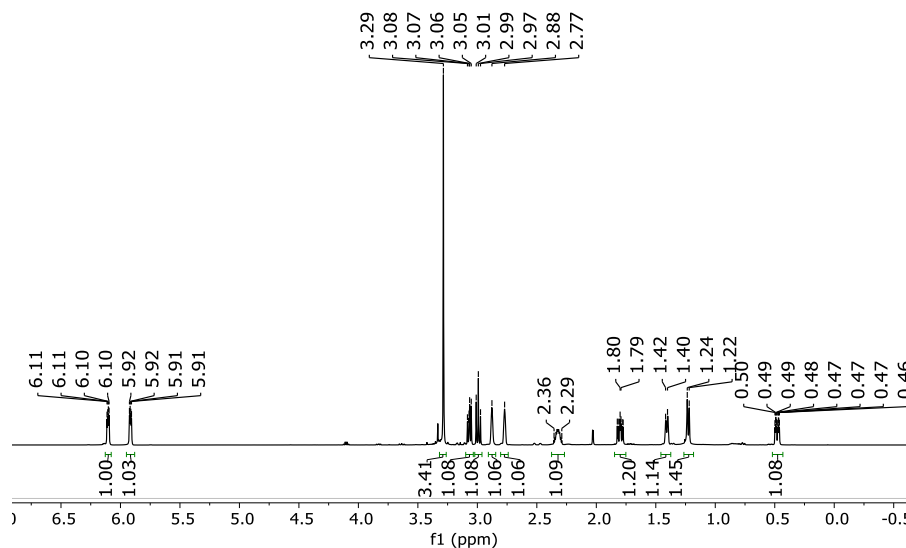


Synthesis of *endo*-5-(methoxymethyl)bicyclo[2.2.1]hept-2-ene (*endo*-NBE-CH₂OMe)

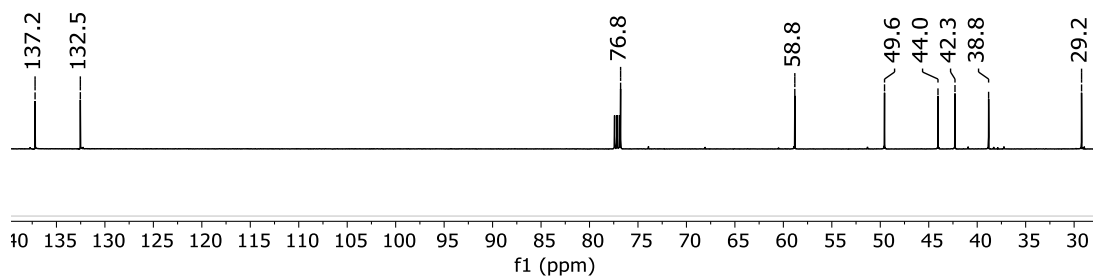


The procedure is the same as *exo*-NBE-CH₂OMe except that the starting material is *endo*-NBE-CH₂OH. ^1H NMR (CDCl₃, 500 MHz) δ 6.10 (dd, $J = 5.6$ and 3.0 Hz, 1H), 5.92 (dd, $J = 5.6$ and 2.9 Hz, 1H), 3.29 (s, 3H), 3.07 (dd, $J = 9.2$ and 6.7 Hz, 1H), 2.99 (t, $J = 9.0$ Hz, 1H), 2.88 (s, 1H), 2.77 (s, 1H), 2.32 (dh, $J = 13.1$ and 4.0 Hz, 1H), 1.80 (ddd, $J = 12.8$, 9.2 and 3.8 Hz, 1H), 1.46-1.37 (m, 1H), 1.23 (d, $J = 8.1$ Hz, 1H), 0.48 (ddd, $J = 11.6$, 4.3 and 2.7 Hz, 1H); ^{13}C NMR (CDCl₃, 125 MHz) δ 137.2, 132.5, 76.8, 58.8, 49.6, 44.0, 42.3, 38.8, 29.2. HRMS-EI (m/z): calculated for C₉H₁₅O [M+H]⁺, 139.1123; Found, 139.1123.

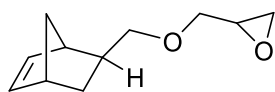
^1H NMR of *endo*-NBE-CH₂OMe



^{13}C NMR of *endo*-NBE-CH₂OMe

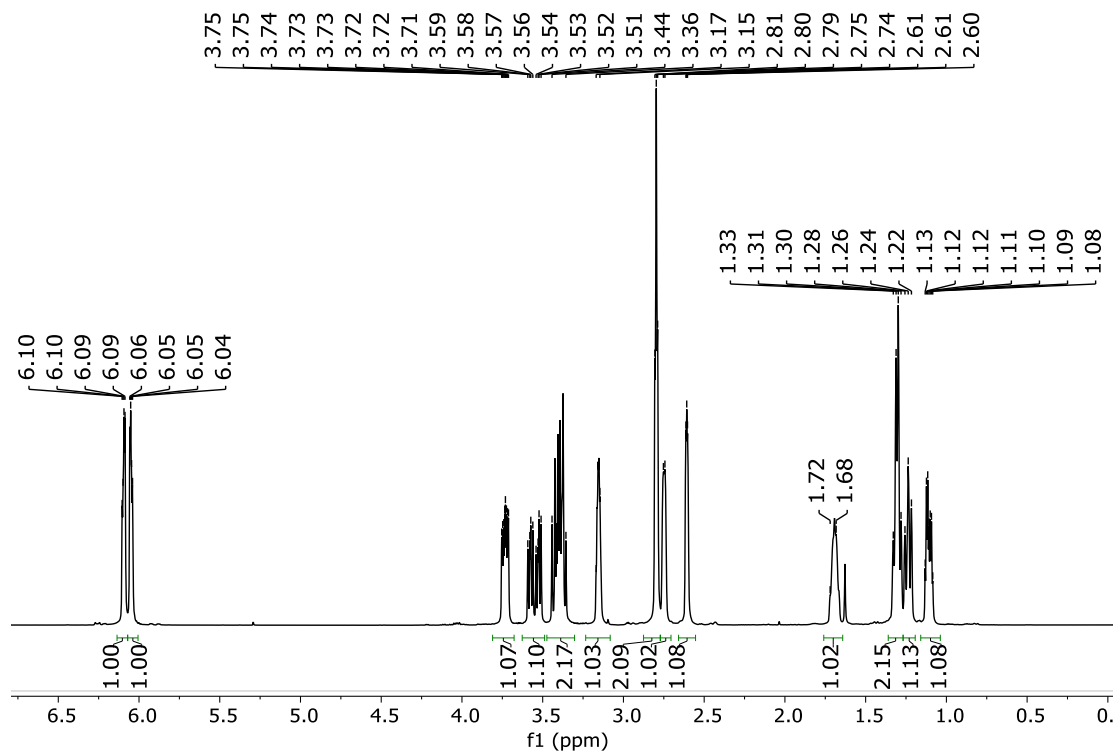


Synthesis of *exo*-2-(((bicyclo[2.2.1]hept-5-en-2-yl)methoxy)methyl)oxirane (*exo*-NBE-epoxide)

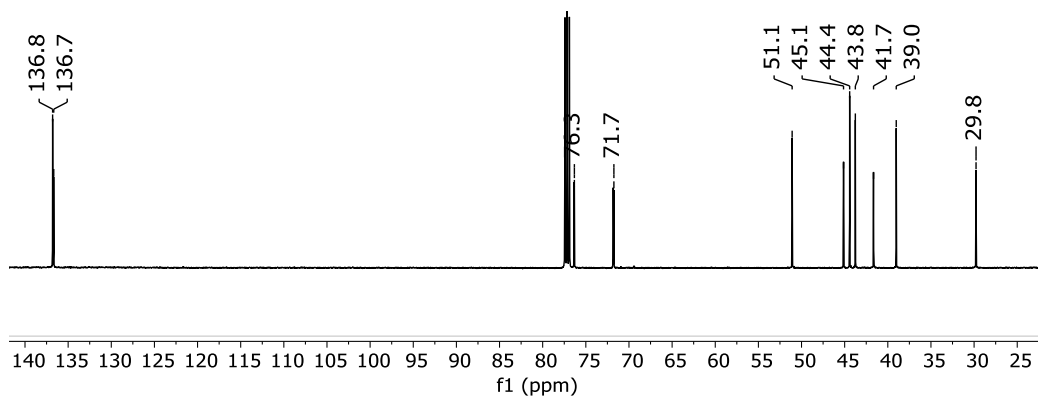


To a mixture of tetrabutylammonium bromide (52.2 mg, 0.16 mmol, 0.02 equiv.), epichlorohydrin (923 mg, 9.7 mmol, 1.2 equiv.) and 2 mL 50 wt. % NaOH aqueous solution, *exo*-NBE-CH₂OH (1 g, 8.1 mmol, 1.0 equiv.) was added dropwise. After 30 min, the reaction was quenched by ice water, extracted with EtOAc and purified by column to afford a colorless liquid (0.91 g, 63%). ^1H NMR (CDCl₃, 500 MHz) δ 6.10 (dd, $J = 5.9$ and 3.1 Hz, 1H), 6.05 (dd, $J = 5.7$ and 3.0 Hz, 1H), 3.73 (ddd, $J = 11.5$, 6.4 and 3.0 Hz, 1H), 3.55 (ddd, $J = 25.5$, 9.3 and 6.2 Hz, 1H), 3.47-3.30 (m, 2H), 3.15 (dt, $J = 6.3$ and 3.2 Hz, 1H), 2.80 (t, $J = 4.5$ Hz, 2H), 2.75 (dd, $J = 6.8$ and 2.9 Hz, 1H), 2.61 (dt, $J = 4.6$ and 2.1 Hz, 1H), 1.76-1.64 (m, 1H), 1.30 (q, $J = 8.6$ Hz, 2H), 1.24 (t, $J = 10.1$ Hz, 1H), 1.11 (dq, $J = 11.7$ and 3.9 Hz, 1H); ^{13}C NMR (CDCl₃, 125 MHz) δ 136.8, 136.7, 76.3, 71.7, 51.1, 45.1, 44.4, 43.8, 41.7, 39.0, 29.8. HRMS-ESI (m/z): calculated for C₁₁H₁₇O₂ [M+H]⁺, 181.1229; Found, 181.1226.

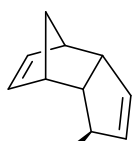
^1H NMR of *exo*-NBE-epoxide



^{13}C NMR of *exo*-NBE-epoxide



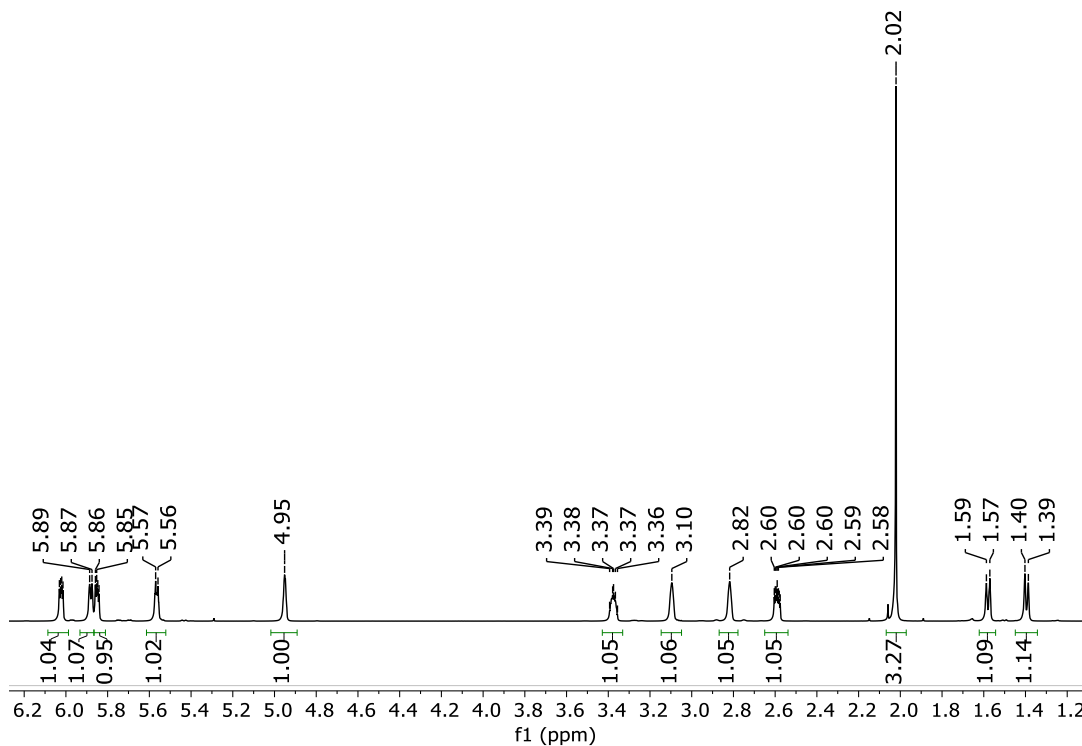
Synthesis of *endo*-DCPD-OAc⁴²



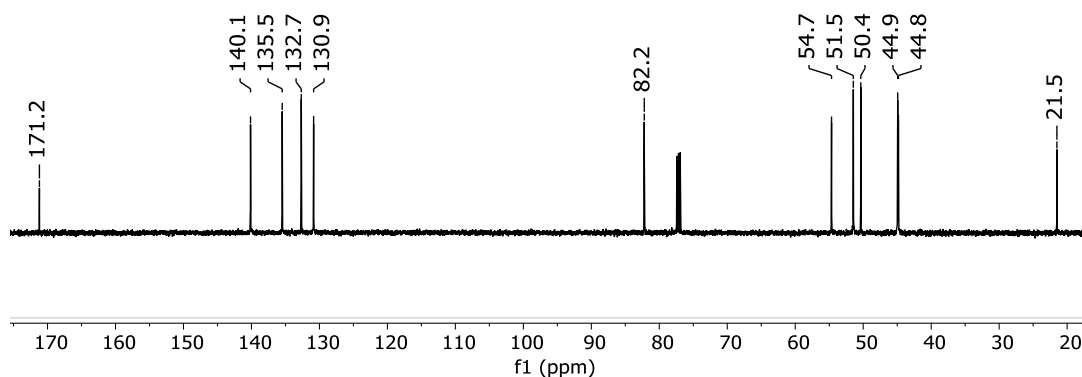
^1H NMR (CDCl_3 , 500 MHz) δ 6.02 (dd, $J = 5.6$ and 2.9 Hz, 1H), 5.88 (d, $J = 5.6$ Hz, 1H), 5.85 (dd, $J = 5.6$ and 3.0 Hz, 1H), 5.56 (dt, $J = 5.6$ and 2.1 Hz, 1H), 5.02-4.89 (m, 1H),

3.43-3.33 (m, 1H), 3.10 (s, 1H), 2.82 (s, 1H), 2.59 (ddd, $J = 7.2, 4.3$ and 2.3 Hz, 1H), 2.02 (s, 3H), 1.58 (d, $J = 8.2$ Hz, 1H), 1.39 (d, $J = 8.2$ Hz, 1H); ^{13}C NMR (CDCl_3 , 125 MHz) ^{13}C NMR (126 MHz, CDCl_3) δ 171.2, 140.1, 135.5, 132.7, 130.9, 82.2, 54.7, 51.5, 50.4, 44.9, 44.8, 21.5.

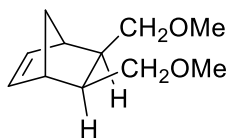
^1H NMR of *endo*-DCPD-OAc



^{13}C NMR of *endo*-DCPD-OAc

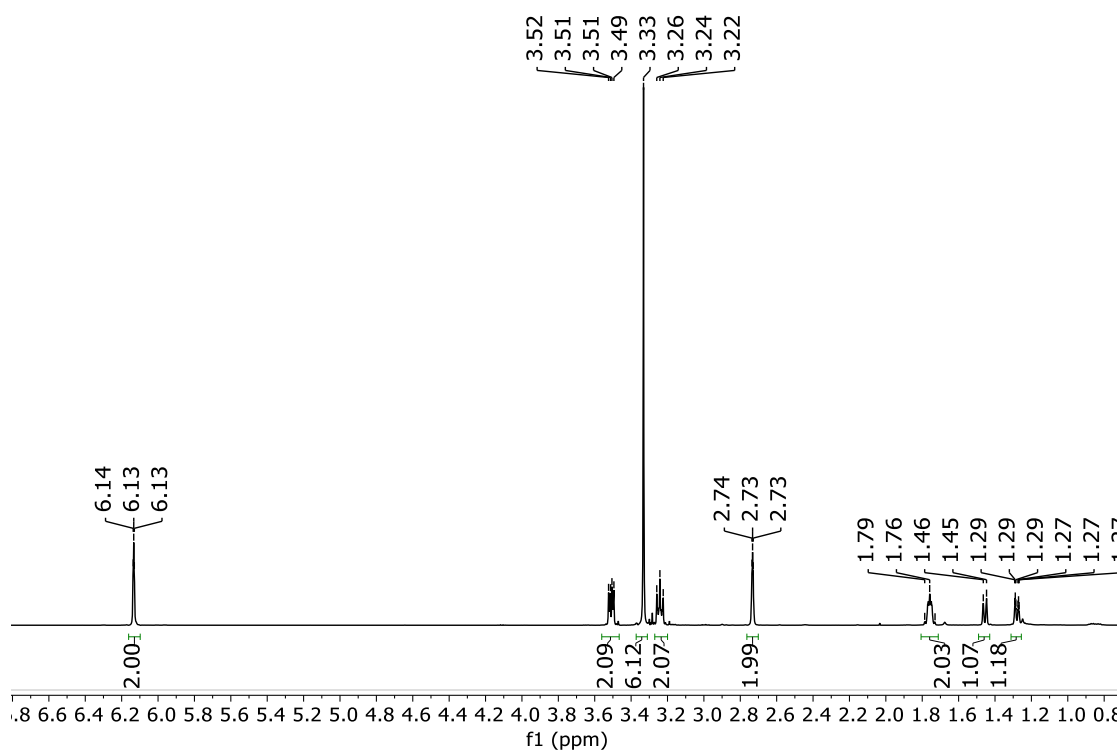


Synthesis of *exo,exo*-NBE-di-CH₂OMe⁴¹

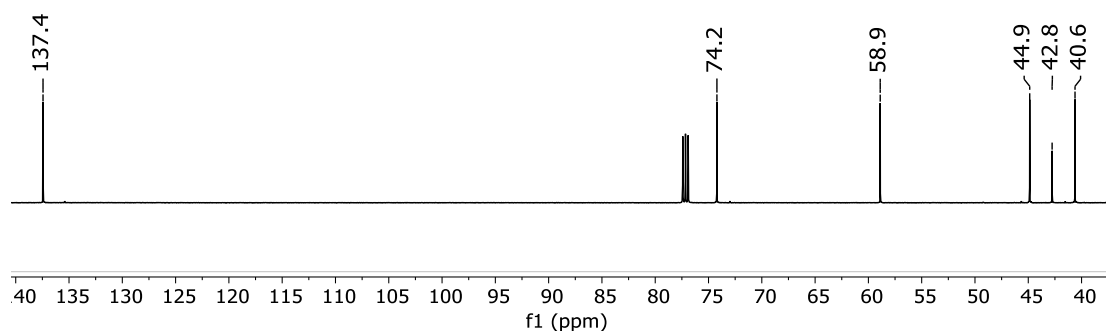


¹H NMR (CDCl₃, 500 MHz) δ 6.16-6.10 (m, 2H), 3.56-3.47 (m, 2H), 3.33 (s, 6H), 3.28-3.20 (m, 2H), 2.73 (p, *J* = 1.7 Hz, 2H), 1.80-1.71 (m, 2H), 1.46 (d, *J* = 8.9 Hz, 1H), 1.28 (dt, *J* = 8.8 and 1.7 Hz, 1H); ¹³C NMR (CDCl₃, 125 MHz) δ 137.4, 74.2, 58.9, 44.9, 42.8, 40.6. HRMS-ESI (*m/z*): calculated for C₁₁H₁₈O₂Na [M+Na]⁺, 205.1204; Found, 205.1198.

¹H NMR of *exo,exo*-NBE-di-CH₂OMe

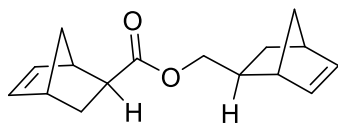


¹³C NMR of *exo,exo*-NBE-di-CH₂OMe



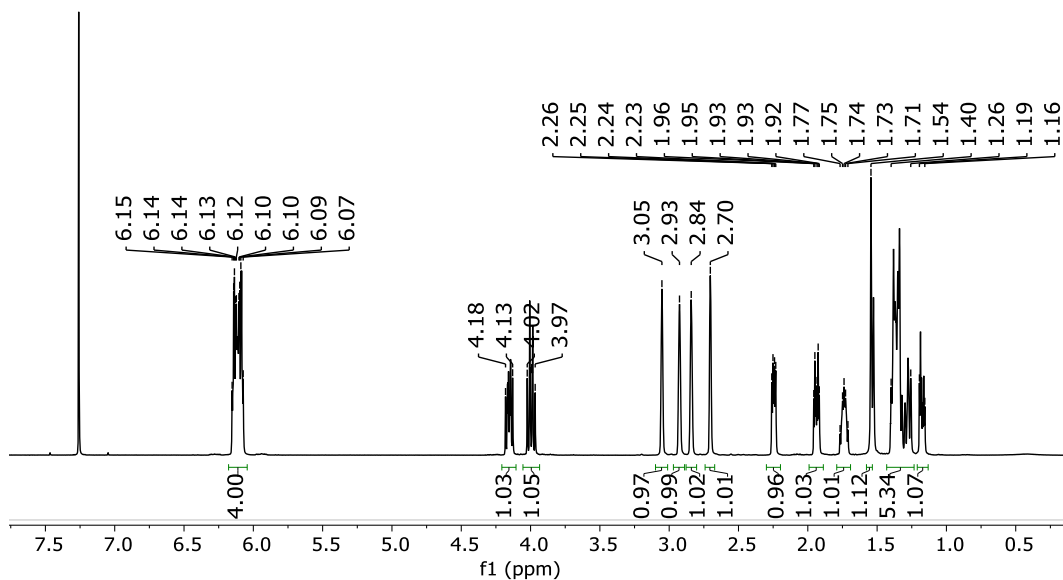
Synthesis of dinorbornenyl cross-linkers: These *exo, exo*-cross-linkers were obtained through two steps, converting *exo*-NBE-COOH to acyl chloride, followed by nucleophilic addition of the corresponding alcohol. Under N₂ atmosphere, 4 mL oxalyl chloride was added to *exo*-NBE-COOH (2.5 g, 1.05 equiv.). After complete dissolution of the solids, two drops of anhydrous DMF was added. The reaction was allowed to stir overnight at room temperature. The mixture was then concentrated by rotary evaporator to remove excess amount of oxalyl chloride. CHCl₃ (3 mL) was added to the residue and concentrated again. This was repeated three times to remove as much oxalyl chloride as possible. The resulting crude *exo*-NBE-COCl (yellowish oil) was dissolved in 20 mL CH₂Cl₂ and placed in an ice bath. A solution of alcohol (1.0 equiv. *exo*-NBE-CH₂OH for **CL1** and 0.5 equiv. diol for **CL2&CL3**) and NEt₃ (1.2 equiv.) in 10 mL CH₂Cl₂ was added. The reaction was warmed to room temperature and stirred under N₂ for 4 hours. TLC analyses indicated the reaction to be complete. The reaction mixture was extracted with CH₂Cl₂ and brine, dried with anhydrous sodium sulfate, and then concentrated. The crude product was purified by flash chromatography to give the desired compound as a colorless liquid.

Synthesis of CL1

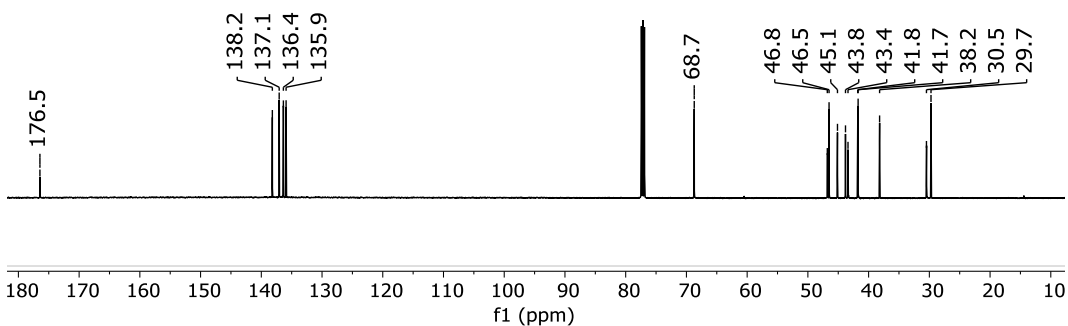


Colorless liquid (3.8 g, 90%). ¹H NMR (CDCl₃, 500 MHz) δ 6.15-6.07 (m, 4H), 4.18-4.13 (m, 1H), 4.00 (dt, *J* = 10.5 Hz and 9 Hz, 1H), 3.05 (s, 1H), 2.93 (s, 1H), 2.84 (s, 1H), 2.70 (s, 1H), 2.24 (dd, *J* = 10 Hz and 4.5 Hz, 1H), 1.94 (dt, *J* = 12 Hz and 4 Hz, 1H), 1.77-1.71 (m, 1H), 1.54 (d, *J* = 9 Hz, 1H), 1.40-1.26 (m, 5H), 1.18 (dt, *J* = 12 Hz and 4 Hz, 1H); ¹³C NMR (CDCl₃, 125 MHz) δ 176.5, 138.2, 137.1, 136.4, 135.9, 68.7, 46.8, 46.5, 45.1, 43.8, 43.4, 41.8, 41.7, 38.2, 30.5, 29.7. HRMS-EI (*m/z*): calculated for C₁₆H₂₀O₂ [M]⁺, 244.1463; Found, 244.1473.

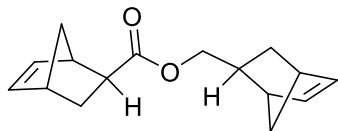
¹H NMR of CL1



¹³C NMR of CL1



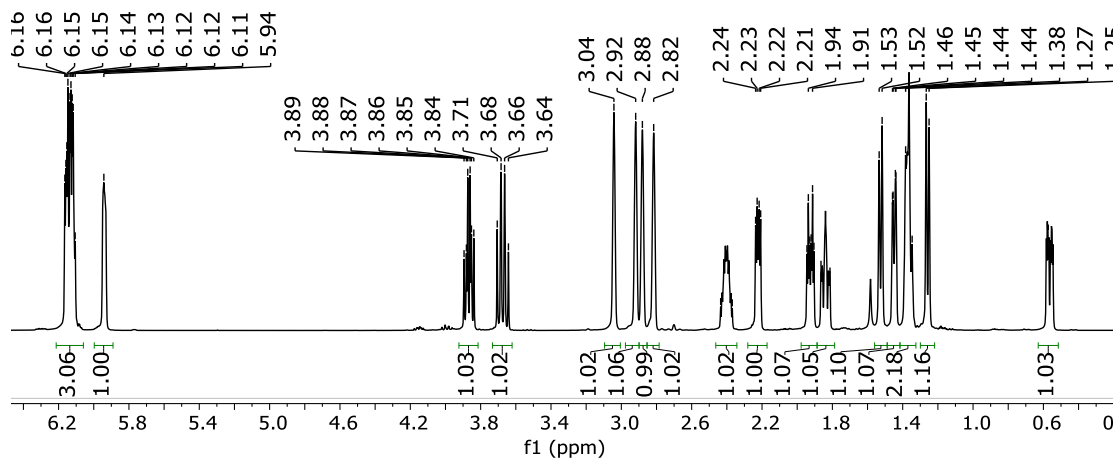
Synthesis of CL1'



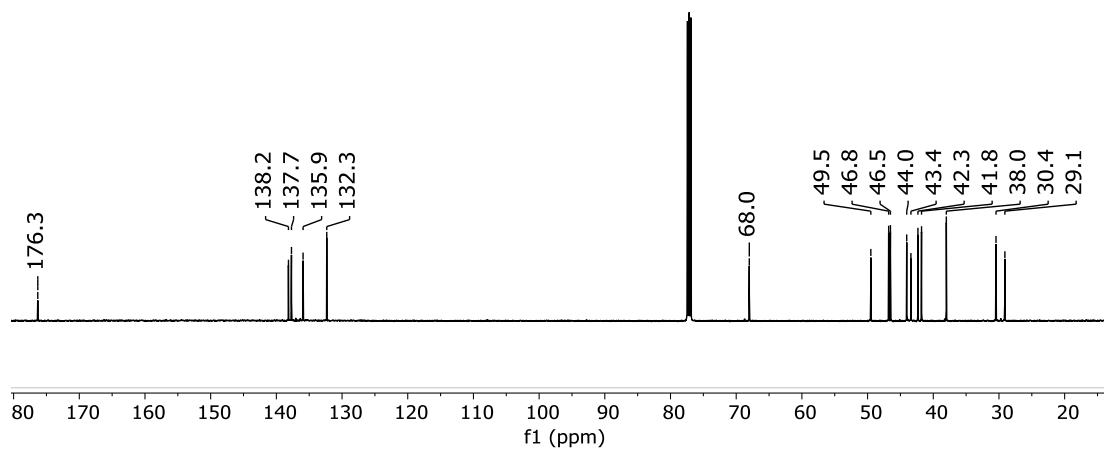
Colorless liquid (3.5 g, 83%). ¹H NMR (CDCl₃, 500 MHz) δ 6.13 (dtd, *J* = 12.1, 5.6 and 2.9 Hz, 3H), 5.94 (dd, *J* = 6.3 and 2.8 Hz, 1H), 3.87 (td, *J* = 10.5 and 6.7 Hz, 1H), 3.73-3.62 (m, 1H), 3.04 (s, 1H), 2.92 (s, 1H), 2.88 (s, 1H), 2.82 (s, 1H), 2.40 (dddd, *J* = 13.6, 9.5, 7.0 and 3.9 Hz, 1H), 2.22 (dd, *J* = 10.0 and 4.4 Hz, 1H), 1.92 (dt, *J* = 11.8 and 4.0 Hz, 1H), 1.89-1.79 (m, 1H), 1.53 (d, *J* = 8.4 Hz, 1H), 1.49-1.42 (m, 1H), 1.36 (d, *J* = 18.5 Hz, 2H), 1.26 (d, *J* = 8.1 Hz, 1H), 0.56 (ddd, *J* = 11.7, 4.5 and 2.6 Hz, 1H); ¹³C NMR (CDCl₃, 125 MHz) δ

176.3, 138.2, 137.7, 135.9, 132.3, 68.0, 49.5, 46.8, 46.5, 44.0, 43.4, 42.3, 41.8, 38.0, 30.4, 29.1.
 HRMS-ESI (m/z): calculated for $C_{16}H_{21}O_2$ [$M+H$] $^+$, 245.1542; Found, 245.1543.

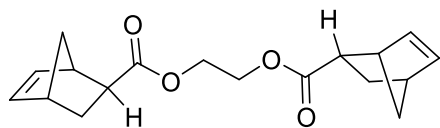
1H NMR of CL1'



^{13}C NMR of CL1'



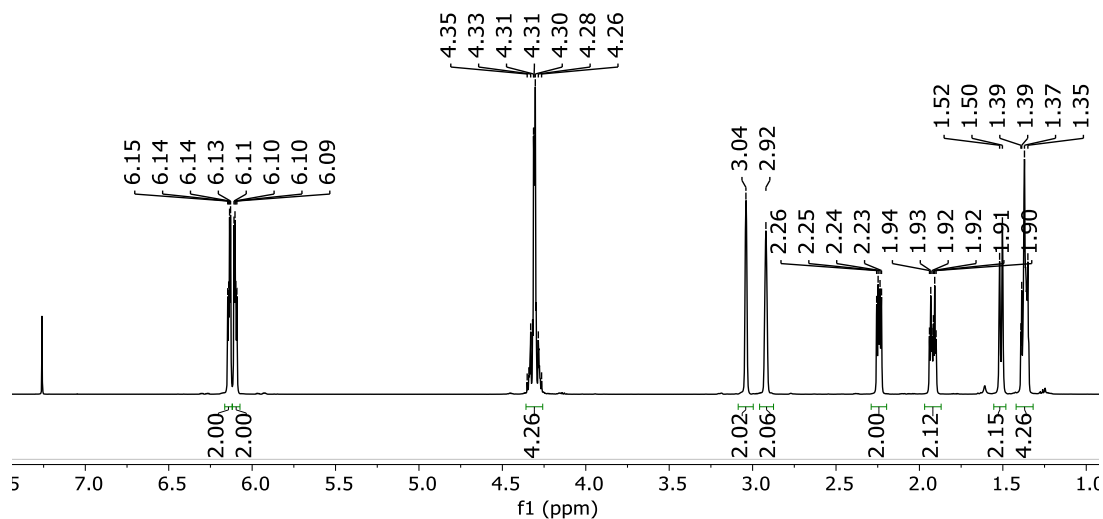
Synthesis of CL2



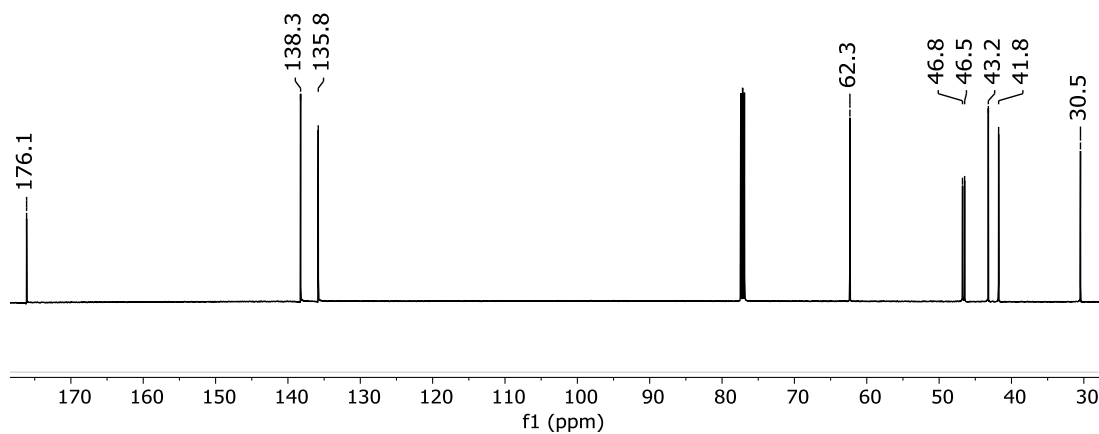
Colorless liquid (1.6 g, 61%). 1H NMR (CDCl₃, 500 MHz) δ 6.14 (dd, $J = 5.5$ Hz and 2.5 Hz, 2H), 6.10 (dd, $J = 5.5$ Hz and 2.5 Hz, 2H), 4.35-4.27 (m, 4H), 3.04 (s, 2H), 2.92 (s, 2H), 2.24 (dd, $J = 10$ Hz and 4 Hz, 2H), 1.92 (dt, $J = 12$ Hz and 4 Hz, 2H), 1.51 (d, $J = 8$ Hz, 2H), 1.39-1.34 (m, 4H); ^{13}C NMR (CDCl₃, 125 MHz) δ 176.1, 138.3, 135.8,

62.3, 46.8, 46.5, 43.2, 41.8, 30.5. HRMS-ESI (m/z): calculated for $C_{18}H_{22}O_4Na$ $[M+Na]^+$, 325.1416; Found, 325.1411.

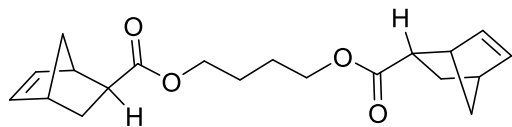
1H NMR of CL2



^{13}C NMR of CL2



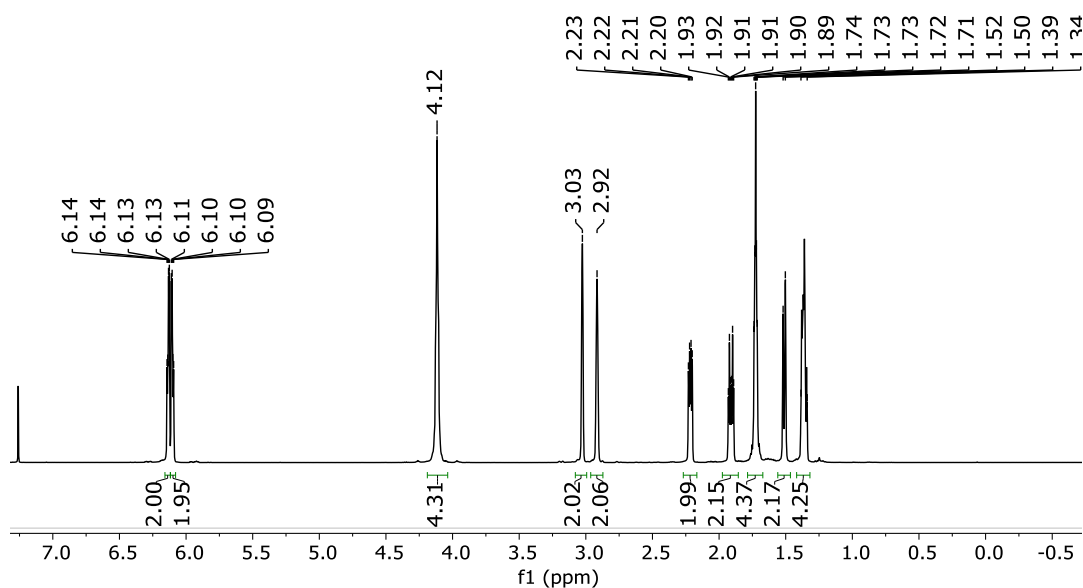
Synthesis of CL3



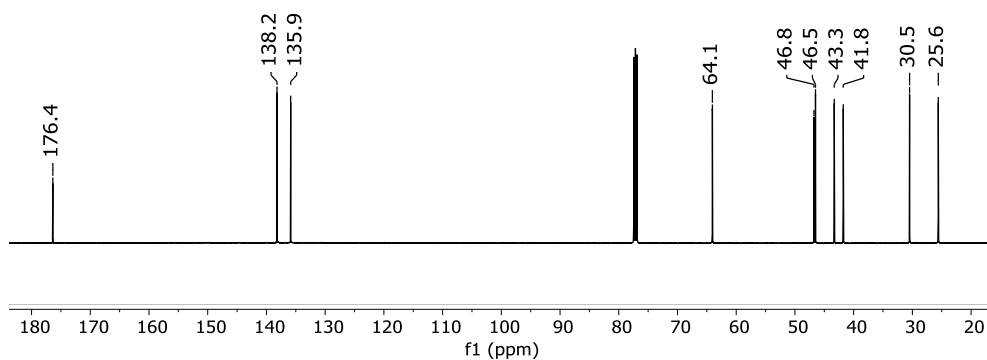
Colorless liquid (1.7 g, 60%). 1H NMR (CDCl₃, 500 MHz) δ 6.13 (dd, $J = 5.5$ Hz and 3 Hz, 2H), 6.10 (dd, $J = 5.5$ Hz and 3 Hz, 2H), 4.12 (s, 4H), 3.03 (s, 2H), 2.92 (s, 2H), 2.22 (dd, $J = 9.5$ Hz and 4.5 Hz, 2H), 1.91 (dt, $J = 11.5$ Hz and 4 Hz, 2H), 1.73 (quint, $J = 3$ Hz, 4H), 1.51 (d, $J = 8.5$ Hz, 2H), 1.39-1.34 (m, 4H); ^{13}C NMR (CDCl₃,

125 MHz) δ 176.4, 138.2, 135.9, 64.1, 46.8, 46.5, 43.3, 41.8, 30.5, 25.6. HRMS-ESI (m/z): calculated for $C_{20}H_{27}O_4$ $[M+H]^+$, 331.1909; Found, 331.1913.

1H NMR of CL3



^{13}C NMR of CL3



4.9.3 Frontal Velocity Measurement

Instead of 13×100 mm test tubes as reported in previous examples, we performed all FROMP experiments in NMR tubes (Economy 5 mm \times 7" L, 100 MHz) in this study. The frontal velocities (v_f) obtained with NMR tubes are the same or slightly lower (especially for less reactive monomers) compared to those obtained in test tubes. The formulation is Grubbs II (100 ppm per norbornenyl double bond), 1.0 equiv. $P(OBu)_3$ (dissolved in 40 μ L dry toluene) and 500 mg neat liquid monomers. The catalyst/phosphite solution was freshly made and then added to

500 mg monomers. After thoroughly mixing and rapidly transferring to an NMR tube, a soldering iron was applied near the surface of the liquid. FROMP proceeded in a descending mode with the thermocouple positioned roughly 1 cm from the top of the liquid surface. Once frontal propagation started, the soldering iron was removed. v_f was calculated from the slope of the linear fitting of the front position against time. To avoid v_f acceleration introduced by the thermocouple on propagation, v_f calculations only included the region without the thermocouple.

4.9.4 DSC Characterization

After thoroughly mixing catalyst/phosphite solution with the monomers for FROMP experiments, 5-15 mg of the mixture was immediately transferred to a hermetic aluminum pan and placed in a pre-cooled DSC (to prevent simultaneous polymerization before data collection). Heat released data (ΔH) was obtained by integrating the exothermic peak.

Table 4.1 Molecular weight, v_f and ΔH of monomers with a steady front propagation.



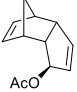

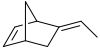
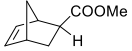
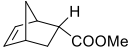
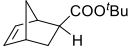
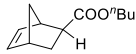
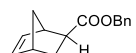
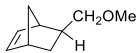
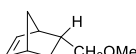
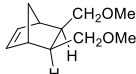
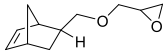
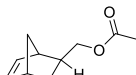
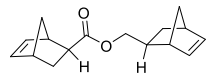
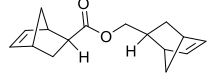
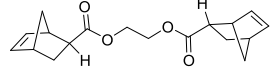
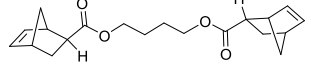

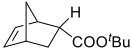
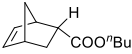
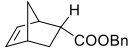
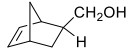
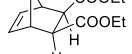
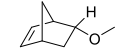
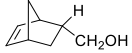
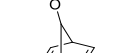

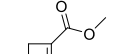
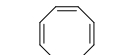
Monomer	Molecular weight (g/mol)	v_f (mm/s)	ΔH (J/g)
	132.21	1.00	353
	132.21	1.82	368
	190.24	0.27	177
	118.18	0.59	477
	120.20	1.37	410
	152.19	1.12	320
	152.19	0.42	303
	194.27	0.62	234

Table 4.1 (cont.) Molecular weight, v_f and ΔH of monomers with a steady front propagation.

Monomer	Molecular weight (g/mol)	v_f (mm/s)	ΔH (J/g)
	194.27	0.63	214
	228.29	0.26	209
	138.21	0.67	325
	138.21	0.23	310
	182.26	0.26	283
	180.25	0.27	241
	166.22	0.92	299
	244.33	0.96	273
	244.33	0.60	235
	302.37	0.62	260
	330.42	0.47	250
	92.14	4.40 ^a	823

^a The front temperature is much higher than the boiling point (89 °C) of NDE. Front propagates while NDE evaporates with extensive void formation, which is not typical in FROMP.

Table 4.2 Molecular weight and ΔH of monomers without a steady front propagation.

Monomer	Molecular weight (g/mol)	FROMP behavior	ΔH (J/g)
	194.27	Unstable front	211
	194.27	Unstable front	233
	228.29	Unstable front	191
	124.18	Unstable front	358
	238.28	Unstable front	213
	124.18	No propagation	379
	124.18	No propagation	320
	164.24	No propagation	14
	190.24	No propagation	50
	112.13	No propagation	80
	104.15	No propagation	9

4.9.5 Kinetic Experiments

In a glove box, Grubbs II (1.0 equiv.) was dissolved in 0.6 mL d_8 -toluene in a screw-cap NMR tube. Monomer (300 equiv.) in 0.2 mL d_8 -toluene was then added to the catalyst solution to make a final catalyst concentration of 0.6 mM, and the NMR tube was immediately inserted to the instrument with the temperature pre-set to 20 °C. Array experiments were programmed to obtain ^1H spectra at different time points. k_{obs} values were determined from the slope plotting $\ln([M]/[M]_0)$ against time. An example of norbornadiene was shown below.

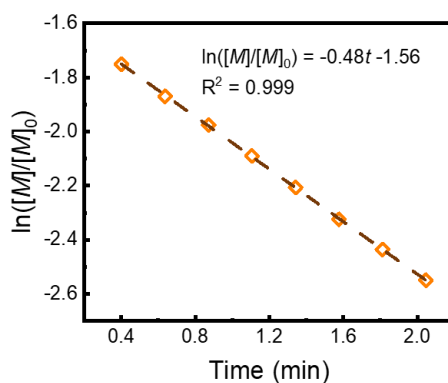


Figure 4.18 k_{obs} of ROMP of norbornadiene at 20 °C in d_8 -toluene determined by 1H NMR.

Table 4.3 k_{obs} values for FROMP monomers.

Monomer				
k_{obs} (min^{-1})	0.48	0.58	0.75	0.20
Monomer				
k_{obs} (min^{-1})	0.67	0.14	0.77	0.68
Monomer				
k_{obs} (min^{-1})	0.53	0.09	0.34	0.22
Monomer				
k_{obs} (min^{-1})	0.87	1.06		

4.9.6 Machine Learning Model

The predictive accuracy of an array of ML methods were evaluated using 80% of the heat released data as a training set to predict the remaining 20% test set.

Table 4.4 Molecular weight and ΔH of monomers without a steady front propagation.

Classifier	Training Set R ²	Test Set R ²	Test Set RMSE
k Nearest Neighbor Regression	0.6710	-5.5888	64.7976
Support Vector Regression	-0.0359	-9.0958	80.2093
Bayesian Ridge Regression	0.8738	-6.7140	70.1122
Linear Regression	1	-13.5426	96.2668
Random Forest Regression	0.9369	0.7355	12.9834

Random forest regressor with scikit-learn package was used for ML model. The 103 features as input data are listed as follows:

MW: Molecular Weight; RO: Density; VF: Vibrational Frequency with highest intensity; DB: Bond order of DB; SBG: Bond order of the breaking side 1; SB: Bond order of the breaking side 2; TC1: Top C charge 1; TC2: Top C charge; TC3: Top C charge 3; GC1: DB C charge 11; GC2: DB C charge 12; GC3: Double bond C charge 13; SC1: Double bond C charge 21; SC2: Double bond C charge 22; SC3: Double bond C charge 23; CG1: Group side C charge 11, CG2: Group side C charge 12; CG3: Group side C charge 13; CNG1: Group side C charge 21, CNG2: Group side C charge 22; CNG3: Group side C charge 23; C-ONG: Distance between top C and group side DB C; C-OG: Distance between top C and off-group side DB C; C-G: Distance between top C and group side C1; C-NG: Distance between top C and group side C 2; TA: Top angle in the ring; AIR: Angle formed by the strained ring; AWG: Angle of the group with the ring; TD1: Top C bond length 1; TD2 : Top C bond length 2; BR1: Bond length on DB side 1; BR2: Bond length on DB side 2; BR3: Bond length on DB side 3; ANG: Angle formed by top C and group at the ring; RN: Repulsion between C atoms on the group side (estimate of strain); DSTN: Distortion of the top triangle; R1: C-ONG/C-OG; R2: C-G/C-NG; R3: C-G/C-ONG; R4: C-NG/C-OG; R5: TD1/TD2; MBO1: Bond order group side 1; MBO2: Bond order group side 2; MBO3: Bond order group side 3; MBL1: Bond length group side 1; MBL2: Bond length group side 2; MBL3: Bond length group side 3; HUMO;LUMO; CHG11: Charge of group1; CHG12: Charge o group 2; CHG13: Charge of group 3; CHG21: Charge of other group 1; CHG22: Charge of other group

2; CHG23: Charge of other group 3; CHG31: CHG11+CHG12 1; CHG32: CHG11+CHG12 2; CHG33: CHG11+CHG12 3; REP2: Repulsion between top C and C attached to group; T-SC11: TC1*GC1; T-SC12: TC2*GC2; T-SC13: TC3*GC3; T-CG1:TC1*CG1; T-CG2: TC2*CG2; T-CG3: TC3*CG3; T-SG1: TC1*SC1; T-SG2: TC2*SC2; T-SG3: TC3*SC3; T-NG1: TC1*CNG1; T-NG2: TC2*CNG2; T-NG3: TC3*CNG3; T-G1: TC1*CHG11; T-G2: TC2*CHG12; T-G3: TC3*CHG13; T-G+1: TC1*CHG21; T-G+2: TC2*CHG22; TG+3: TC3*CHG23; G-SC11: CHG11*GC1; G-SC12: CHG12*GC2 ;G-SC13: CHG13*GC3; G-SC21: CHG11*SC1; G-SC22: CHG12*SC2; G-SC23: CHG13*SC3; G-CG1: CHG11*CG1; G-CG2: CHG12*CG2; G-CG3: CHG13*CG3; G-NG1: CHG11*CNG1; G-NG2: CHG12*CNG2; G-NG3: CHG13*CNG3; G-G11: CHG11*CHG11; G-G12: CHG12*CHG12; G-G13: CHG13*CHG13; G-G+1: CHG11*CHG21; G-G+2: CHG12*CHG22; G-G+3: CHG13*CHG23; BG: Band gap; BBE: Heat of Formation; DM: Dipole Moment; ZPE: Zero point energy; DHH: Enthalpy; DS: Entropy; DG: Gibbs free energy; CV: Specific heat

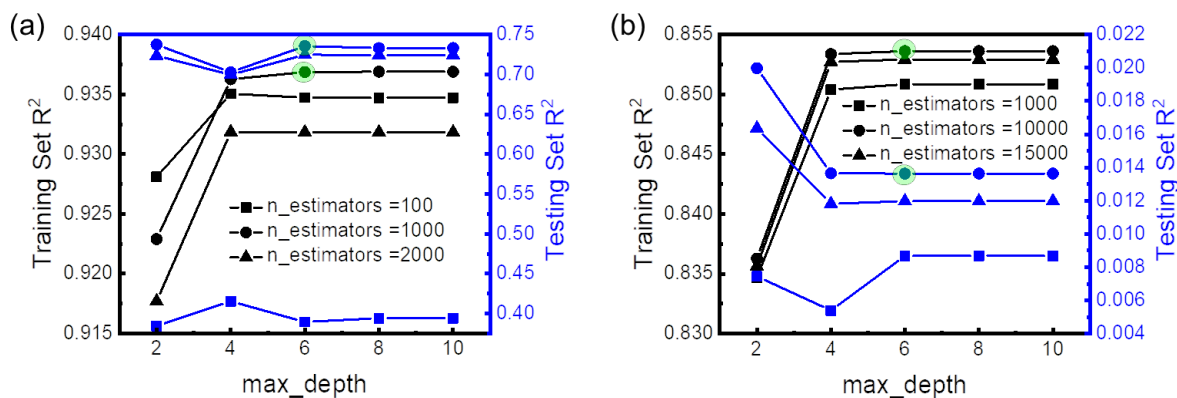


Figure 4.19 Parameters tuning for convergence in predictive model of (a) heat released and (b) frontal velocity. $n_estimators$ represents the number of trees in the forest. Usually the higher the number of trees the better to learn the data. However, adding a lot of trees can slow down the training process considerably. max_depth represents the depth of each tree in the forest. The deeper the tree, the more splits it has and it captures more information about the data.

4.9.7 Gel Time Measurement

Gel time was measured by a TA Instruments AR-G2 rheometer equipped with 25-mm-diameter parallel aluminum plates and a solvent trap. The formulation is similar to FROMP experiments (100 ppm Grubbs II, 1.0 equiv. P(OBu)₃) except that 5 wt.% ENB was added to DCPD-OAc to eliminate the contribution from ENB. Time-sweep measurements were performed at 25 °C with a strain of 0.1% and a frequency of 1 Hz.

4.10 References

- (1) Pojman, J. A. *Frontal Polymerization*; Elsevier B.V., **2012**; Vol. 4.
- (2) Davtyan, S. P.; Berlin, A. A.; Tonoyan, A. O. Advances and Problems of Frontal Polymerization Processes. **2011**, *1*, 56–92.
- (3) Scognamillo, S.; Bounds, C.; Luger, M.; Mariani, A.; Pojman, J. A. Frontal Cationic Curing of Epoxy Resins. *J. Polym. Sci. Part A Polym. Chem.* **2010**, *48*, 2000–2005.
- (4) Robertson, I. D.; Yourdkhani, M.; Centellas, P. J.; Aw, J. E.; Ivanoff, D. G.; Goli, E.; Lloyd, E. M.; Dean, L. M.; Sottos, N. R.; Geubelle, P. H.; et al. Rapid Energy-Efficient Manufacturing of Polymers and Composites via Frontal Polymerization. *Nature* **2018**, *557*, 223–227.
- (5) Robertson, I. D.; Dean, L. M.; Rudebusch, G. E.; Sottos, N. R.; White, S. R.; Moore, J. S. Alkyl Phosphite Inhibitors for Frontal Ring-Opening Metathesis Polymerization Greatly Increase Pot Life. *ACS Macro Lett.* **2017**, *6*, 609–612.
- (6) Mol, J. C. Industrial Applications of Olefin Metathesis. *J. Mol. Catal. A Chem.* **2004**, *213*, 39–45.
- (7) Robertson, I. D.; Pruitt, E. L.; Moore, J. S. Frontal Ring-Opening Metathesis Polymerization of Exo-Dicyclopentadiene for Low Catalyst Loadings. *ACS Macro Lett.* **2016**, *5*, 593–596.
- (8) Mariani, A.; Fiori, S.; Chekanov, Y.; Pojman, J. A. Frontal Ring-Opening Metathesis Polymerization of Dicyclopentadiene. *Macromolecules* **2001**, *34*, 6539–6541.
- (9) Ruiu, A.; Sanna, D.; Alzari, V.; Nuvoli, D.; Mariani, A. Advances in the Frontal Ring Opening Metathesis Polymerization of Dicyclopentadiene. *J. Polym. Sci. Part A Polym. Chem.* **2014**, *52*, 2776–2780.
- (10) Draper, N. R.; Smith, H. *Applied Regression Analysis*, Third edit.; Wiley, **1998**.
- (11) Hammett, L. P. The Effect of Structure upon the Reactions of Organic Compounds. Benzene Derivatives. *J. Am. Chem. Soc.* **1937**, *59*, 96–103.
- (12) Milo, A.; Bess, E. N.; Sigman, M. S. Interrogating Selectivity in Catalysis Using Molecular Vibrations. *Nature* **2014**, *507*, 210–214.
- (13) Milo, A.; Neel, A. J.; Toste, F. D.; Sigman, M. S. A Data-Intensive Approach to Mechanistic Elucidation Applied to Chiral Anion Catalysis. *Science* **2015**, *347*, 737–743.
- (14) Sutthasupa, S.; Shiotsuki, M.; Sanda, F. Recent Advances in Ring-Opening Metathesis

- Polymerization, and Application to Synthesis of Functional Materials. *Polym. J.* **2010**, *42*, 905–915.
- (15) Slugovc, C. The Ring Opening Metathesis Polymerisation Toolbox. *Macromol. Rapid Commun.* **2004**, *25*, 1283–1297.
- (16) Schleyer, P. V. R.; Williams, J. E.; Blanchard, K. R. The Evaluation of Strain in Hydrocarbons. The Strain in Adamantane and Its Origin. *J. Am. Chem. Soc.* **1970**, *92*, 2377–2386.
- (17) Elling, B. R.; Su, J. K.; Xia, Y. Ring-Opening Metathesis Polymerization of 1,2-Disubstituted Cyclopropenes. *Chem. Commun.* **2016**, *52*, 9097–9100.
- (18) Maughon, B. R.; Grubbs, R. H. Ruthenium Alkylidene Initiated Living Ring-Opening Metathesis Polymerization (ROMP) of 3-Substituted Cyclobutenes. *Macromolecules* **1997**, *30*, 3459–3469.
- (19) Slugovc, C.; Stelzer, F. *Handbook of Metathesis*; Robert H. Grubbs, Ed.; Wiley-VCH: Weinheim, **2004**.
- (20) Wilson, G. O.; Porter, K. A.; Weissman, H.; White, S. R.; Sottos, N. R.; Moore, J. S. Stability of Second Generation Grubbs' Alkylidenes to Primary Amines: Formation of Novel Ruthenium-Amine Complexes. *Adv. Synth. Catal.* **2009**, *351*, 1817–1825.
- (21) Michael A. Tallon. *Handbook of Maleic Anhydride Based Materials: Syntheses, Properties and Applications*; Musa, O. M., Ed.; Springer: Switzerland, **2016**.
- (22) Bielawski, C. W.; Grubbs, R. H. Increasing the Initiation Efficiency of Ruthenium-Based Ring-Opening Metathesis Initiators: Effect of Excess Phosphine. *Macromolecules* **2001**, *34*, 8838–8840.
- (23) Walker, R.; Conrad, R. M.; Grubbs, R. H. The Living ROMP of *Trans* -Cyclooctene. *Macromolecules* **2009**, *42*, 599–605.
- (24) Lenev, D. A.; Ashirov, R. V.; Semakin, S. V.; Bozhenkova, G.; Kiselev, S. A.; Verpoort, F.; Lyapkov, A. A. Reactivity of Norbornene Esters in Ring-Opening Metathesis Polymerization Initiated by a N-Chelating Hoveyda II Type Catalyst. *RSC Adv.* **2016**, *6*, 5177–5183.
- (25) Rule, J. D.; Moore, J. S. ROMP Reactivity of Endo- and Exo-Dicyclopentadiene. *Macromolecules* **2002**, *35*, 7878–7882.
- (26) Czelusniak, I.; Heywood, J. D.; Kenwright, A. M.; Khosravi, E. Investigation of Factors

- Affecting Ruthenium Complexation in ROMP Reactions of Oxygen-Containing Norbornene Derivatives Using Grubbs First Generation Initiator. *J. Mol. Catal. A Chem.* **2008**, *280*, 29–34.
- (27) Haigh, D. M.; Kenwright, A. M.; Khosravi, E. Nature of the Propagating Species in Ring-Opening Metathesis Polymerizations of Oxygen-Containing Monomers Using Well-Defined Ruthenium Initiators. *Macromolecules* **2005**, *38*, 7571–7579.
- (28) Slugovc, C.; Demel, S.; Riegler, S.; Hobisch, J.; Stelzer, F. The Resting State Makes the Difference: The Influence of the Anchor Group in the ROMP of Norbornene Derivatives. *Macromol. Rapid Commun.* **2004**, *25*, 475–480.
- (29) Kumar, D. R.; Lidster, B. J.; Adams, R. W.; Turner, M. L. Mechanistic Investigation of the Ring Opening Metathesis Polymerisation of Alkoxy and Alkyl Substituted Paracyclophanedienes. *Polym. Chem.* **2017**, *8*, 3186–3194.
- (30) Radzinski, S. C.; Foster, J. C.; Chapleski, R. C.; Troya, D.; Matson, J. B. Bottlebrush Polymer Synthesis by Ring-Opening Metathesis Polymerization: The Significance of the Anchor Group. *J. Am. Chem. Soc.* **2016**, *138*, 6998–7004.
- (31) Breiman, L. E. O. *Machine Learning*; Schapire, R. E., Ed.; Kluwer Academic Publishers: Netherlands., **2001**.
- (32) Ahneman, D. T.; Estrada, J. G.; Lin, S.; Dreher, S. D.; Doyle, A. G. Predicting Reaction Performance in C–N Cross-Coupling Using Machine Learning. *Science* **2018**, *360*, 186–190.
- (33) Hastie Trevor; Tibshirani, R.; Friedman, J. *The Elements of Statistical Learning*; Springer-Verlag, **2009**.
- (34) Davidson, T. A.; Wagener, K. B. The Polymerization of Dicyclopentadiene: An Investigation of Mechanism. *J. Mol. Catal. A Chem.* **1998**, *133*, 67–74.
- (35) Abadie, M. J.; Dimonie, M.; Couve, C.; Dragutan, V. New Catalysts for Linear Polydicyclopentadiene Synthesis. *Eur. Polym. J.* **2000**, *36*, 1213–1219.
- (36) Dumrath, C.; Dumrath, A.; Neumann, H.; Beller, M.; Kadyrov, R. Practical Ruthenium Catalysts for the Synthesis of Cyclic Olefin Oligomers, Polymers, and Their Hydrogenated Derivatives. *ChemCatChem* **2014**, *6*, 3101–3104.
- (37) Goetz, A. E.; Boydston, A. J. Metal-Free Preparation of Linear and Cross-Linked Polydicyclopentadiene. *J. Am. Chem. Soc.* **2015**, *137*, 7572–7575.

- (38) Cuthbert, T. J.; Li, T.; Speed, A. W. H.; Wulff, J. E. Structure of the Thermally Induced Cross-Link in C -Linked Methyl Ester-Functionalized Polydicyclopentadiene (f PDCPD). *Macromolecules* **2018**, *51*, 2038–2047.
- (39) Wright, S. W.; Hageman, D. L.; Wright, A. S.; McClure, L. D. Convenient Preparations of T-Butyl Esters and Ethers from t-Butanol. *Tetrahedron Lett.* **1997**, *38*, 7345–7348.
- (40) Vrabel, M.; Kölle, P.; Brunner, K. M.; Gattner, M. J.; López-Carrillo, V.; De Vivie-Riedle, R.; Carell, T. Norbornenes in Inverse Electron-Demand Diels-Alder Reactions. *Chem. - A Eur. J.* **2013**, *19*, 13309–13312.
- (41) Drouin, S. D.; Zamanian, F.; Fogg, D. E. Multiple Tandem Catalysis: Facile Cycling between Hydrogenation and Metathesis Chemistry. *Organometallics* **2001**, *20*, 5495–5497.
- (42) Gong, L.; Liu, K.; Ou, E.; Xu, F.; Lu, Y.; Wang, Z.; Gao, T.; Yang, Z.; Xu, W. ROMP of Acetoxy-Substituted Dicyclopentadiene to a Linear Polymer with a High Tg. *RSC Adv.* **2015**, *5*, 26185–26188.

Chapter 5: Non-Monotonic Acceleration in Frontal Ring-Opening Metathesis Copolymerization

5.1 Abstract

Copolymerization in FROMP allows for systematic modification of materials properties while maintaining the benefits of the current DCPD system such as low cost of the monomer and excellent mechanical properties of the resulting pDCPD. While the copolymerization reactivity and copolymer properties generally exhibit monotonic dependence on monomer composition that is predicted by the mixing rule, we discovered that copolymerization with a dinorbornenyl (di-NBE) cross-linker does not conform to the rule. As the comonomer content increases, the FROMP reaction shows a non-monotonic increase in frontal velocity. At low di-NBE comonomer loadings, the cross-linked structure renders proximity of reactive NBE and affords higher NBE C=C concentration, facilitating the approach of active carbenes and accelerating the polymerization. As di-NBE comonomer wt. % increases to a point where cross-linking density is too high, polymerization is retarded owing to the reduced mobility of propagating chains. We studied the behavior of a series of comonomers and found that the non-monotonic trend only exists in copolymerization with di-NBE cross-linkers and becomes less evident when the cross-linker possesses a larger molecular weight. This copolymerization system provides a new strategy to tune physical properties (such as cross-linking density) and simultaneously improve the efficiency in FROMP-based materials manufacturing.

5.2 Introduction

As discussed in Chapter 4, FROMP has great potential in manufacturing large parts of high-performance thermosets and FRPCs.¹ *endo*-DCPD is an excellent monomer in FROMP owing to its high strain energy and commercial availability, and the resulting pDCPD is a cross-linked polymer with superior mechanical properties.¹⁻³ Despite the advantages of *endo*-DCPD, there are still challenges in the current system, including poor interfacial shear strength in FRPCs and low cross-linking density of pDCPD.¹ One approach to mitigate this problem is by copolymerization with other functional monomers.

Copolymerization is a common strategy to tailor polymeric materials with desired properties by modifying the chemical structure and comonomer feed ratio. In radical FP, copolymerization has been largely explored to synthesize functional materials,^{4,5} interpenetrating networks,⁶ gradient polymers,⁷ hydrogels,^{8,9} and consolidants.¹⁰ v_f becomes systematically-controlled as it is a monotonic function of the comonomer composition, initiator concentration and initial reactant temperature.^{1,15–17} Copolymerization in FROMP, however, is underexplored due to the limited availability of functionalized monomers with adequate amount of ring strain. Since FROMP is directly related to the amount of heat released upon ring opening, we envisioned that NBE derivatives are excellent comonomer candidates as they possess similar ring strain and ring structure as *endo*-DCPD.¹³ Thus, copolymerization of *endo*-DCPD with NBE-based monomers would systematically modify the properties (such as mechanical and interfacial properties) of pDCPD without sacrificing v_f . Here we studied the copolymerization behavior in FROMP and discovered an unusual non-monotonic increase in v_f upon copolymerizing with di-NBE monomers, which contradicts the intuitive understanding of the mixing rule.

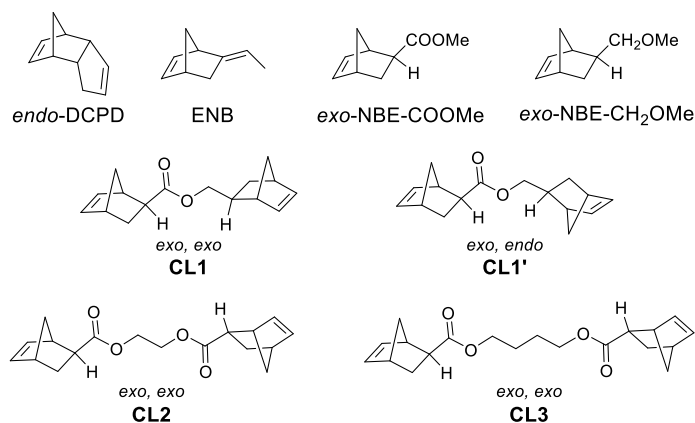


Figure 5.1 Monomers investigated in the copolymerization study.

The mixing rule is an empirical approach for the prediction of properties of multi-component system over a wide range of chemical composition. In materials science, the “rule of mixtures” is commonly used as a simple method that yields acceptable predictions compared to experimental values.¹⁴ The mixtures’ property is predicted to have an upper bound defined by the weighted arithmetic mean (WAM) and a lower bound based on the weighted harmonic mean (WHM) of each individual component. Thus, properties of binary mixtures, such as v_f , as well as density, modulus and conductivity,¹⁵ lie between the corresponding properties of the pure components. In free-radical frontal copolymerization, while v_f shows monotonic dependence on

composition,^{11,12} exceptions have been noted. Pojman et al. observed an interesting relationship in a system of binary FP reactions which consisted of free-radically polymerized diacrylate and an amine-cured epoxy. v_f exhibited a minimum or maximum value at intermediate compositions.^{6,16} They suggested that this behavior is related to the independent mechanism of each polymerization, and boron trichloride from amine-cured epoxy affected the decomposition of the peroxide initiator. Another example is the frontal thiol-ene polymerization where v_f reached a maximum value at a thiol:ene ratio of 1:1 due to the complete consumption of both monomers.^{17,18} For copolymerization in FROMP, the above scenarios on independent mechanisms and stoichiometry are not expected when two comonomers are both strained rings. Intuitively, the weighted means are able to predict FROMP performance (such as v_f) with acceptable accuracy. Thus, monomers that homopolymerize at a v_f comparable or even faster than $v_f(\text{endo-DCPD})$ in FROMP are ideal candidates for copolymerization.

5.3 Design of Cross-Linkers

As discussed in Chapter 4, v_f is sensitive to the functional group that attaches to the NBE ring (Table 5.1). Ester as an anchor group is expected to perform more efficiently than ether in FROMP. We envisioned that a di-NBE (**CL1**) with $-\text{COOR}$ or $-\text{CH}_2\text{OCOR}$ as the linker would propagate at a v_f around 1.00 mm/s. Gratifyingly, **CL1** polymerizes at $v_f = 0.96$ mm/s, which makes it an ideal cross-linker in FROMP since it modulates cross-linking density without adversely affecting v_f .

Table 5.1 v_f and ΔH of investigated monomers.

Monomer	<i>endo</i> -DCPD	ENB	<i>exo</i> -NBE-COOMe	<i>exo</i> -NBE-CH ₂ OMe
v_f (mm/s) ^a	1.00 ± 0.03	1.37 ± 0.05	1.12 ± 0.06	0.67 ± 0.03
ΔH (J/g) ^b	353 ± 5	420 ± 7	320 ± 10	325 ± 5
Monomer	CL1	CL1'	CL2	CL3
v_f (mm/s) ^a	0.96 ± 0.06	0.60	0.62 ± 0.04	0.47 ± 0.04
ΔH (J/g) ^b	273 ± 7	235	260 ± 5	250 ± 8

^a FROMP was performed in NMR tubes and proceeded in a descending mode. v_f was measured with the formulation of 100 ppm second generation Grubbs' catalyst (Grubbs II) per norbornenyl C=C, 1.0 equiv. $P(\text{OBu})_3$ and 500 mg neat liquid monomers.

^b ΔH (J/g) was measured by DSC with a ramping rate of 10 °C/min. The error bar was obtained from three trials.

Instead of an ester linkage, we also synthesized the analogue with an amide linker since amide functionality which exhibits superior thermal stability and mechanical properties after polymerization. However, this amide cross-linker is a solid with poor solubility in DCPD (< 10 wt. % incorporation of amide cross-linker), which drastically limits its potential in copolymerization.

5.4 Mixing Rule in Copolymerization

For copolymerization in FROMP, we initially studied the v_f dependence by varying the weight percentage of ENB upon copolymerizing with *endo*-DCPD. With v_f and ΔH values obtained from homopolymerization (Chapter 4), the predicted WAM and WHM were calculated as $w_A E_A + w_B E_B$ and $(w_A / E_A + w_B / E_B)^{-1}$, respectively.¹⁴ w represents the weight percentage, and E represents the corresponding property of each individual component.

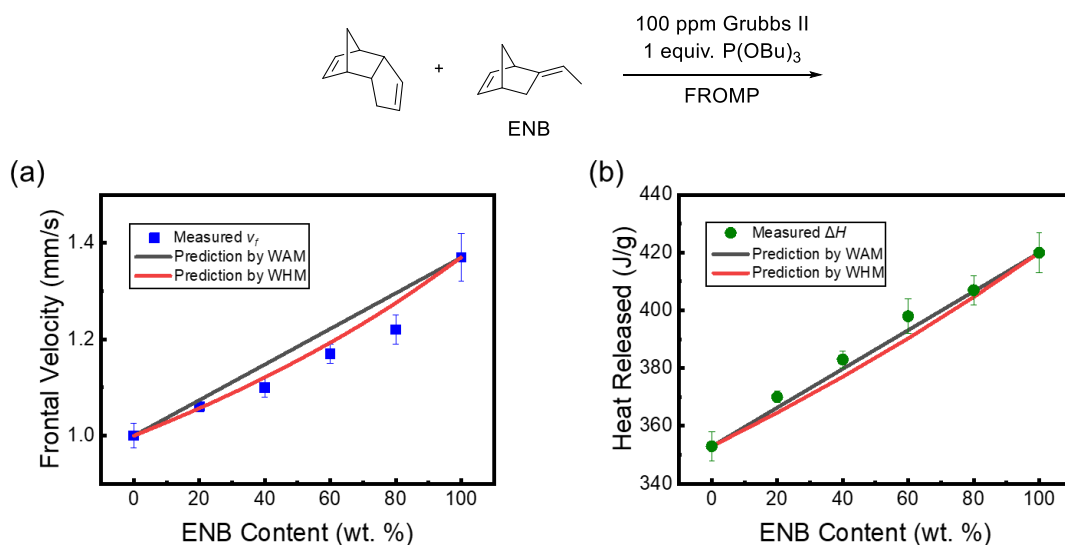


Figure 5.2 (a) Frontal velocity and (b) heat released data of copolymerization of *endo*-DCPD and ENB. FROMP was performed in the presence of 100 ppm Grubbs II catalyst and 1.0 equiv. P(OBu)₃ at 20 °C. WAM and WHM represent weighted arithmetic mean and weighted harmonic mean, respectively.

As expected, v_f shows a steady increase as ENB loading increases (Figure 5.2 (a)). The same trend was observed with ΔH as v_f is directly related to the amount of heat generated during FROMP (Figure 5.2 (b)). Although v_f exhibits a slight negative deviation from WHM of each individual monomer, similar to the observation in previous frontal radical copolymerization,¹¹ the weighted means predict the copolymerization performance with acceptable errors.

5.5 Copolymerization with Cross-Linkers

However, upon copolymerization of **CL1** and *endo*-DCPD, v_f exhibits a non-monotonic behavior as the content of **CL1** increases while ΔH decreases with much less deviation from WAM or WHM (Figure 5.3 (a) and 5.3 (b)). The highest v_f was observed to be 1.4 mm/s at 40 wt. % loading of **CL1** which is 40% higher than v_f of each individual monomer. Similar observations were made when **CL1'** was employed as a comonomer. Despite a much lower reactivity due to one *endo*-NBE ring, copolymerization of *endo*-DCPD and **CL1'** ($v_f = 0.6$ mm/s) exhibits a non-monotonic increase in v_f and an apparent deviation from WAM and WHM (Figure 5.10 and Figure 5.12). As expected, copolymerization with **CL1** increases the cross-linking density of the resulting thermosets. Introducing 10 and 20 wt. % of **CL1** elevates T_g from 100 °C to 116 °C and 138 °C, respectively (Figure 5.18).

To understand the unusual non-monotonic behavior of **CL1**, we proposed several hypotheses. It is known that v_f is affected by the front temperature,¹ so the temperature profile was measured at different **CL1** compositions. However, as shown in Figure 5.3 (c), the front temperature does not show a strong correlation with v_f . Thus, the non-monotonic increase in v_f does not result from generating more heat nor elevating the front temperature by introducing **CL1** into FROMP. We noticed that as the wt. % of **CL1** increases, the exothermic peak becomes broader and polymerization initiates at an earlier temperature as shown in Figure 5.3 (d). We then hypothesized that the increase in v_f results from a better initiation of the catalyst upon mixing with ester-functionalized monomers.

To test this hypothesis, *exo*-NBE-COOME was employed as a comonomer. It was selected because it not only polymerizes at a lower temperature than *endo*-DCPD, but also contains an ester functional group that might contribute to the v_f increase. As shown in Figure 5.4 (b), the DSC curve of copolymerization shifts to a lower temperature with broadening of the peak shape as the comonomer wt. % increases. Even though pure *exo*-NBE-COOME possesses a higher v_f than *endo*-DCPD, it does not exhibit any evident acceleration in v_f (Figure 5.4 (a)) as observed with **CL1** under the same FROMP conditions. Similar observation was made in the copolymerization of *endo*-DCPD and *exo*-NBE-CH₂OME where v_f shows monotonic dependence on composition (Figure 5.11 and Figure 5.13). Overall, neither more efficient catalyst initiation nor the ester functional group is the origin of non-monotonic behavior.

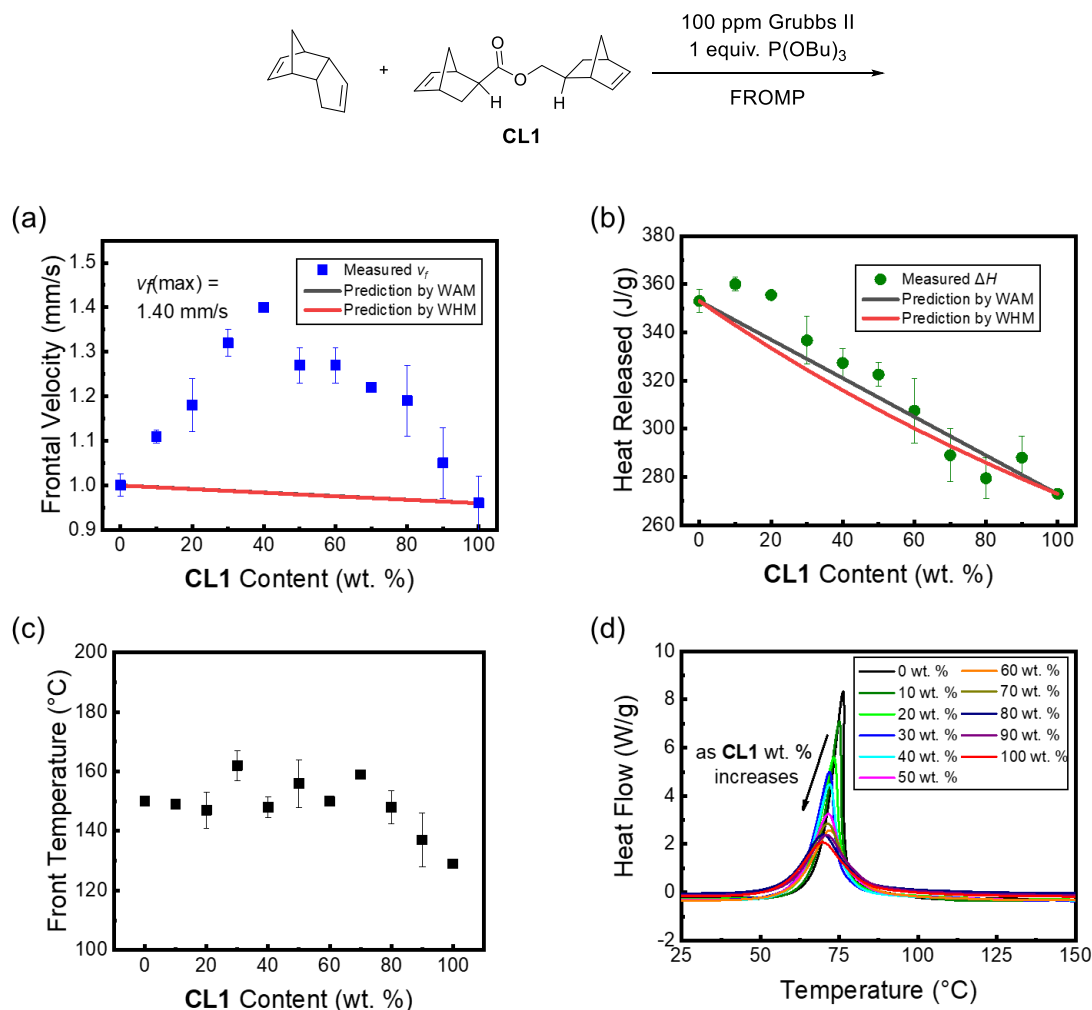


Figure 5.3 (a) Frontal velocity, (b) heat released, (c) front temperature and (d) DSC traces of copolymerization of *endo*-DCPD and **CL1**. FROMP was performed in the presence of 100 ppm Grubbs II catalyst per norbornenyl C=C and 1.0 equiv. $P(\text{OBu})_3$ at 20 $^{\circ}\text{C}$. WAM and WHM represent weighted arithmetic mean and weighted harmonic mean, respectively.

Since the non-monotonic increase was only observed with di-NBE cross-linker, we further tested **CL2** which can be regarded as the “dimer” of *exo*-NBE-COOMe as its MW doubles. Despite the lower v_f of **CL2** (0.62 mm/s), its copolymerization with *endo*-DCPD shows similar non-monotonic behavior with the maximum v_f observed at 40 wt. % (Figure 5.5 (a) and Figure 5.14). This implies that v_f shows acceleration when two NBE rings are physically linked together. This physical link leads to a higher neat NBE C=C concentration ($[M]_{\text{neat}}$) which is calculated as density divided by MW per NBE moiety. To be more specific, even though **CL2** and *exo*-NBE-COOMe have almost the same MW per NBE, the former monomer possesses a higher $[M]_{\text{neat}}$ (7.6 mol/L) than the latter one (7.1 mol/L) because **CL2** has a larger density (1.15 g/mL). Thus, for the same total mass, comonomer with a higher $[M]_{\text{neat}}$ affords more reactive

C=C bond per unit volume, which accelerates the front propagation. This is further supported by copolymerization with **CL3** which has a larger MW but similar $[M]_{\text{neat}}$ (6.9 mol/L) as *exo*-NBE-COOMe. A steady decrease in v_f was observed when **CL3** was copolymerized with *endo*-DCPD (Figure 5.5 (b), Figure 5.15). Among all the cross-linkers investigated, **CL1** has the largest $[M]_{\text{neat}}$ of 9.0 mol/L, and thus it exhibits the largest deviation from the weighted means.

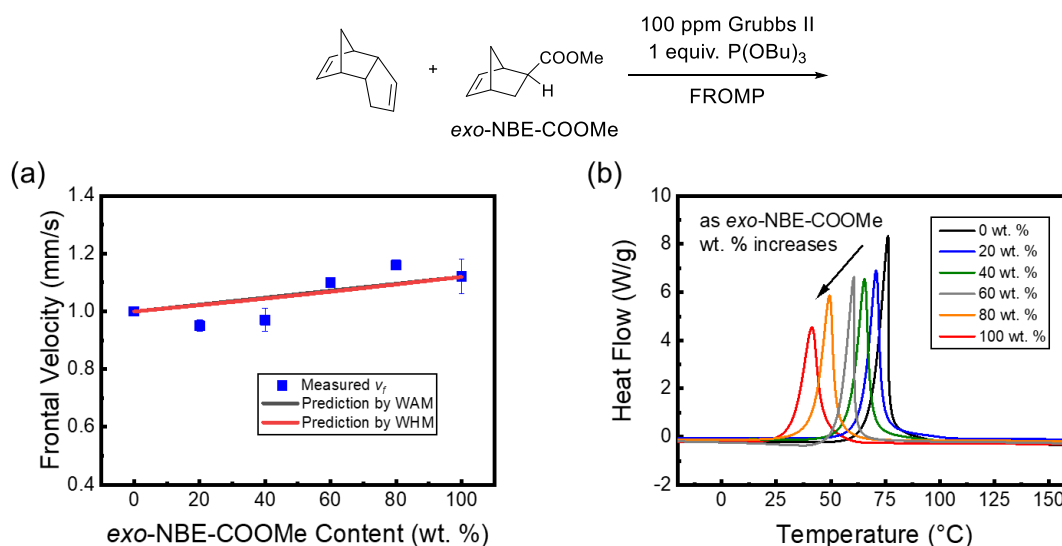


Figure 5.4 (a) Frontal velocity and (b) DSC traces of copolymerization of *endo*-DCPD and *exo*-NBE-COOMe. FROMP was performed in the presence of 100 ppm Grubbs II catalyst and 1.0 equiv. $P(OBu)_3$ at 20 °C. WAM and WHM represent weighted arithmetic mean and weighted harmonic mean, respectively.

Table 5.2 Molecular weight, density and $[M]_{\text{neat}}$ of comonomers.

Monomer	<i>endo</i> -DCPD	ENB	<i>exo</i> -NBE-COOMe	CL1	CL1'	CL2	CL3
MW (g/mol)	132.21	120.19	152.19	244.33	244.33	302.37	330.42
ρ (g/mL) ^a	0.99	0.89	1.08	1.10	1.10	1.15	1.14
$[M]_{\text{neat}}$ (mol/L) ^b	7.5	7.4	7.1	9.0	9.0	7.6	6.9

^a Density was measured three times and reported as the average value with the standard deviation less than 0.01 g/mL. ^b $[M]_{\text{neat}}$ is calculated as ρ / MW per NBE C=C bond.

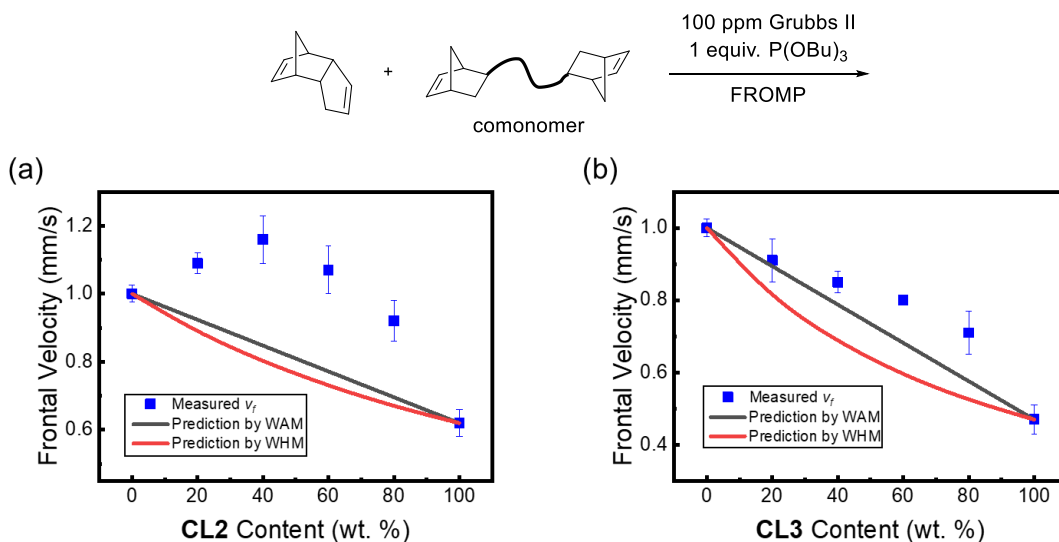


Figure 5.5 Frontal velocity of copolymerization of (a) *endo*-DCPD and **CL2**, (b) *endo*-DCPD and **CL3**. FROMP was performed in the presence of 100 ppm Grubbs II catalyst and 1.0 equiv $P(OBu)_3$ at 20 °C. WAM and WHM represent weighted arithmetic mean and weighted harmonic mean, respectively.

5.6 Role of Cross-Linking

While $[M]_{\text{neat}}$ is a key determinant for the v_f acceleration, the degree of cross-linking also greatly contributes to the non-monotonic dependence. In copolymerization with ENB ($[M]_{\text{neat}}$ of 7.4 mol/L), v_f deviates negatively from WAM and WHM, while **CL3** with even lower $[M]_{\text{neat}}$ of 6.9 mol/L exhibits a positive deviation. This suggests that cross-linking renders close proximity of two NBE rings, which allows for a more rapid approach of propagating Ru carbene. To eliminate the effect of concentration, toluene was employed as a solvent to fix the total NBE C=C bond concentration at 7.1 mol/L when copolymerizing *endo*-DCPD and **CL1**, the non-monotonic dependence on composition is still observed albeit with a much smaller deviation from WAM and WHM (Figure 5.6 and Figure 5.16). Toluene molecules act as diluents and weaken the proximity effect by cross-linking.

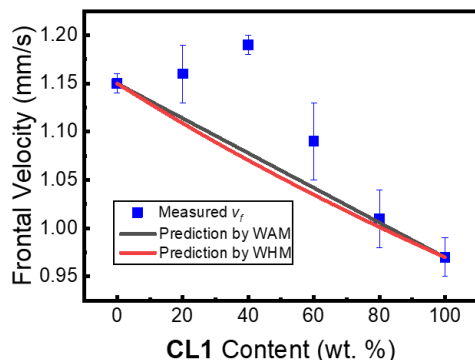
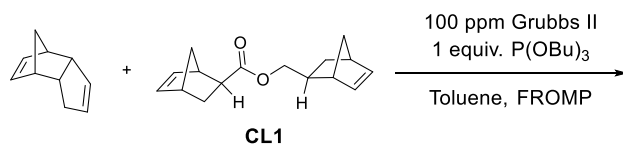


Figure 5.6 Frontal velocity of copolymerization of *endo*-DCPD and **CL1** in toluene solution with NBE C=C concentration of 7.11 M. FROMP was performed in the presence of 100 ppm Grubbs II catalyst and 1.0 equiv. P(OBu)₃ at 20 °C. WAM and WHM represent weighted arithmetic mean and weighted harmonic mean, respectively.

While lower loading of the cross-linker promotes the reactivity of FROMP, higher cross-linking density reduces the mobility of propagating chains and decelerates the polymerization. This phenomenon has been previously observed, especially in bulk polymerization where diffusion is one key factor.^{25–27} In the case of copolymerization of *endo*-DCPD and di-NBE (**CL1** or **CL2**), deceleration effect due to the limited chain mobility dominates over the proximity effect when the cross-linker loading is larger than 40 wt. %. As *endo*-DCPD generates some degree of cross-linking itself by ring-opening of cyclopentenyl ring, we further copolymerized **CL1** and ENB which homopolymerizes to a linear structure. As shown in Figure 5.7 and Figure 5.17, it exhibits similar non-monotonic dependence on **CL1** wt. %, but the maximum v_f shifts to 60 wt. %. Since homopolymerization of ENB does not contribute to cross-linking, higher loading of **CL1** is required to reach the threshold where high cross-linking density adversely affects the reactivity.

The effect of cross-linking degree on v_f is further supported by the concentration dependence study in homopolymerization. Unlike **CL1** that forms a highly cross-linked polymer, *endo*-DCPD only cross-links to a small degree due to the unfavorable ring-opening of low-strain cyclopentene ring.^{28,29} As shown in Figure 5.8, FROMP of *endo*-DCPD demonstrates a linear relationship between v_f and NBE C=C concentration with $R^2 = 0.996$. This correlation also supports our hypothesis in Chapter 4 that v_f is proportional to heat released per unit volume.

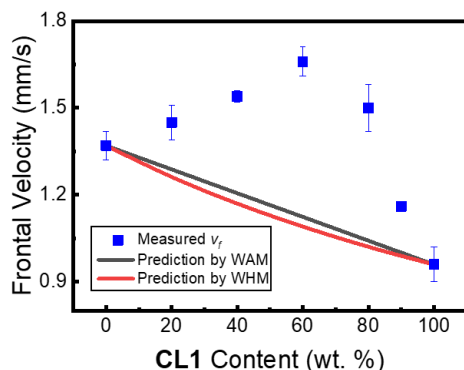
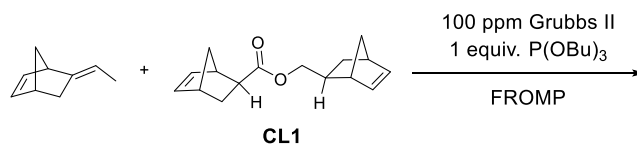


Figure 5.7 Frontal velocity of copolymerization of ENB and CL1. FROMP was performed in the presence of 100 ppm Grubbs II catalyst and 1.0 equiv. $P(OBu)_3$ at 20 °C. WAM and WHM represent weighted arithmetic mean and weighted harmonic mean, respectively.

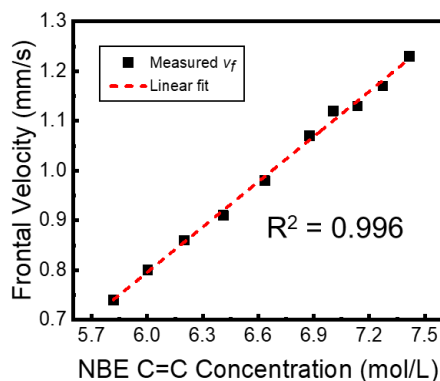


Figure 5.8 Concentration dependence of *endo*-DCPD in FROMP. A linear relationship was observed between v_f and NBE C=C concentration.

However, FROMP of **CL1** reaches a maximum v_f of 1.04 mm/s at 7.7 mol/L C=C concentration (Figure 5.9 (a)). We reasoned that beyond this critical point, the high cross-linking density in **CL1** system limits the accessibility of active propagating chains and decelerates FROMP. At lower concentration, a linear relationship similar to *endo*-DCPD, was also observed (Figure 5.9 (b)). While cross-linking modulates the rate of propagation, it does not affect thermodynamic properties, and thus ΔH exhibits monotonic dependence as predicted by weighted means in all cases.

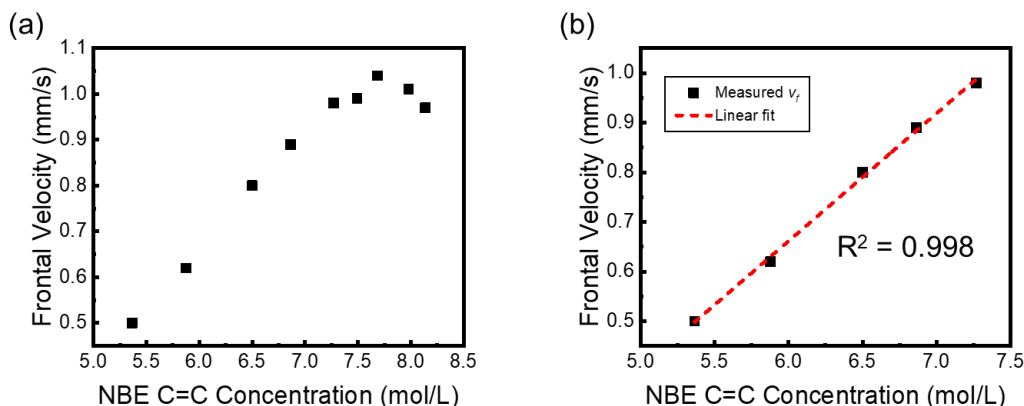


Figure 5.9 (a) Concentration dependence of CLI in FROMP. (b) Linear relationship at lower NBE C=C concentration.

5.7 Conclusion

We investigated the copolymerization behavior in FROMP and discovered the non-monotonic increase in v_f as the content of di-NBE comonomer increases. The v_f increase does not correlate with the change in ΔH , front temperature and kinetic properties. Instead, this unusual behavior results from higher $[M]_{\text{neat}}$ of di-NBEs and the nature of the cross-linked structure which accelerates the propagation of active [Ru] species. With cross-linking density further increasing, the limited chain mobility decelerates the propagation. As far as we are aware, this phenomenon has not been observed in other FP systems where monomers polymerize with the same mechanism. With v_f accelerated by copolymerization, it offers a potential approach to increase fiber content and simultaneously improve the interfacial and mechanical properties in FRPC manufacturing.¹ FROMP with di-NBE comonomers opens up new possibilities for more rapid, energy-efficient fabrication of thermosets and composite materials with tunable properties.

5.8 Experimental Details

5.8.1 Materials and General Methods

Unless otherwise stated, all starting materials and reagents such as *endo*-Dicyclopentadiene (*endo*-DCPD), 5-ethylidene-2-norbornene (ENB), *exo*-5-norbornenecarboxylic acid (*exo*-NBE-COOH), Grubbs II, and $\text{P}(\text{O}i\text{Bu})_3$ were purchased from

Sigma-Aldrich without further purification. Since *endo*-DCPD is a solid at room temperature, 5 wt. % ENB was added to depress the melting point. All references to *endo*-DCPD herein refer to the 95:5 *endo*-DCPD:ENB solution. The DSC measurement was performed using TA Instrument Q20 Differential Scanning Calorimeter equipped with a Liquid Nitrogen Cooling System (LNCS). Tzero hermetic aluminum pans and lids were used as sample testing containers. Nitrogen was used as sample purge gas and the ramping rate was 10 °C/min. Front temperatures were measured using stainless steel type T thermocouples (Omega Engineering, Model TMQSS-020U). Thermocouple data was collected using a temperature sensor (Phidgets, Model 1048) and recorded using a custom LabVIEW code (National Instruments) at 100 Hz.

5.8.2 Frontal Velocity Measurement

FROMP experiments were performed in NMR tubes (Economy 5 mm × 7" L, 100 MHz) at 20 °C. The formulation is Grubbs II (100 ppm per NBE C=C), 1.0 equiv. P(OBu)₃ (dissolved in 40 μL dry toluene) and 500 mg neat liquid monomers. The catalyst/phosphite solution was freshly made and then added to 500 mg monomers. After thoroughly mixing and rapidly transferring to an NMR tube, a soldering iron was applied near the surface of the liquid. FROMP proceeded in a descending mode with the thermocouple positioned roughly 1 cm from the top of the liquid surface. Once frontal propagation started, the soldering iron was removed. v_f was calculated from the slope of the linear fitting of the front position against time. To avoid v_f acceleration introduced by the thermocouple on propagation, v_f calculations only included the region without the thermocouple. Due to the low boiling point of toluene, there was bubble formation especially at the beginning of FROMP. v_f measurement was generally taken in the bubble-free region and not affected by vaporization of toluene. WAM and WHM represent weighted arithmetic mean and weighted harmonic mean, respectively.

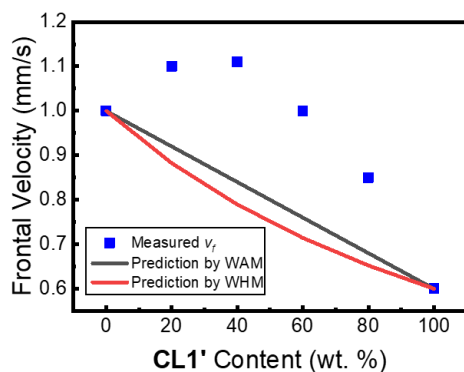


Figure 5.10 Frontal velocity of copolymerization of endo-DCPD and CL1'.

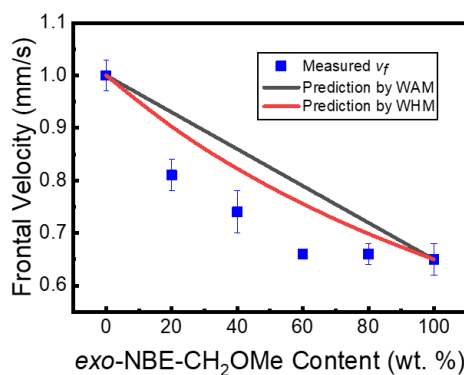


Figure 5.11 Frontal velocity of copolymerization of endo-DCPD and exo-NBE-CH₂OMe.

5.8.3 DSC Characterization

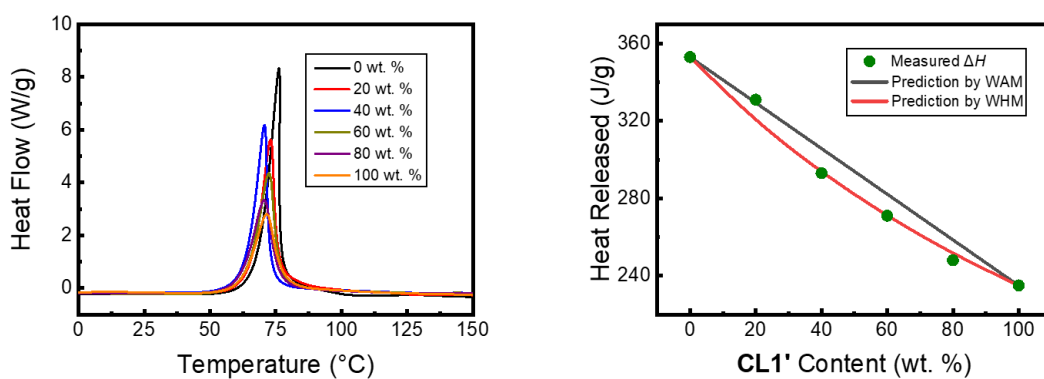


Figure 5.12 DSC traces (left) and heat released data (right) of copolymerization of endo-DCPD and CL1'.

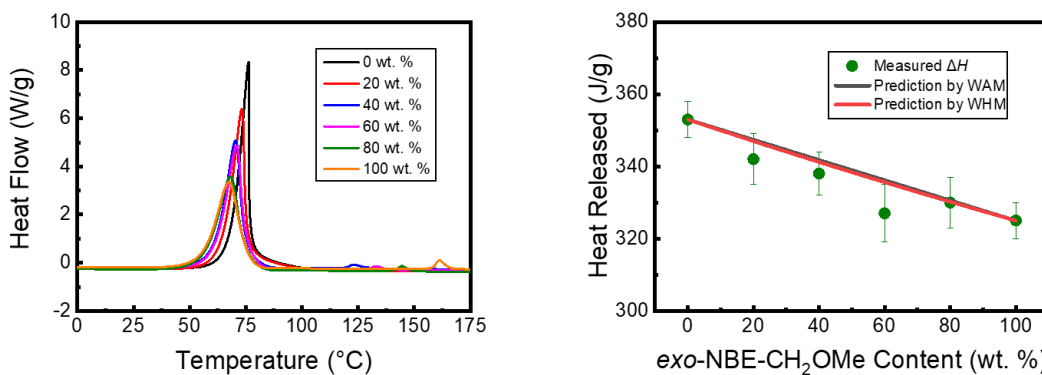


Figure 5.13 DSC traces (left) and heat released data (right) of copolymerization of endo-DCPD and exo-NBE-CH₂OMe.

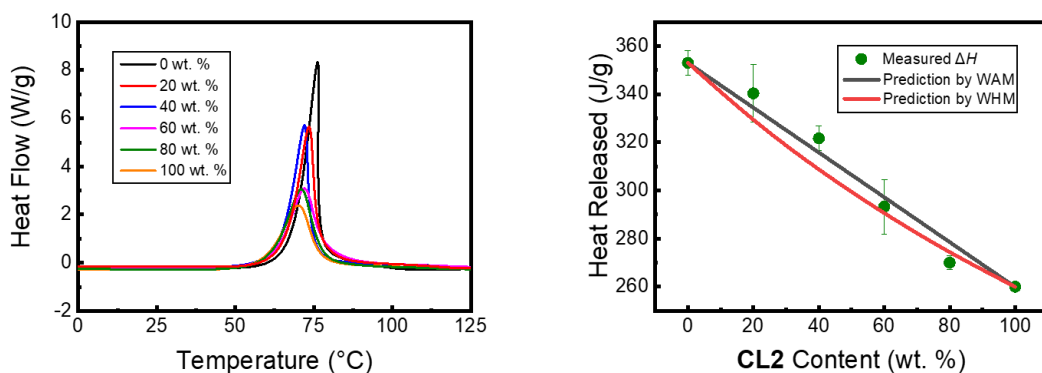


Figure 5.14 DSC traces (left) and heat released data (right) of copolymerization of endo-DCPD and CL2.

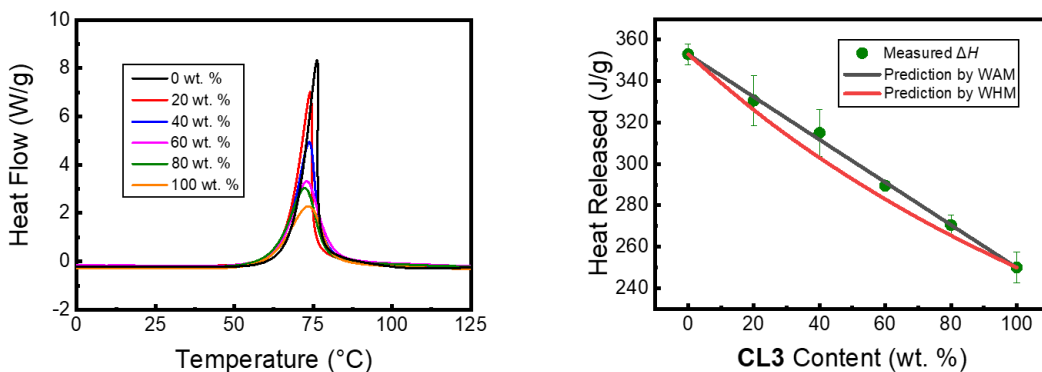


Figure 5.15 DSC traces (left) and heat released data (right) of copolymerization of endo-DCPD and CL3.

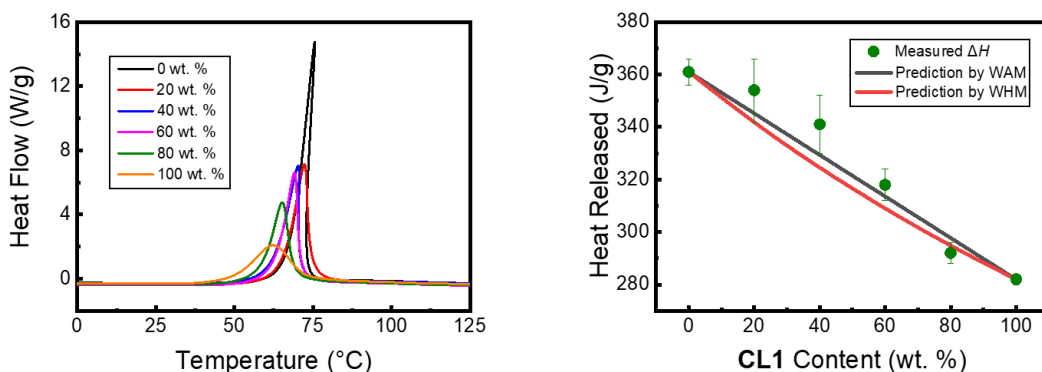


Figure 5.16 DSC traces (left) and heat released data (right) of copolymerization of endo-DCPD and CL1 in toluene solution with norbornenyl double bond concentration of 7.11 M.

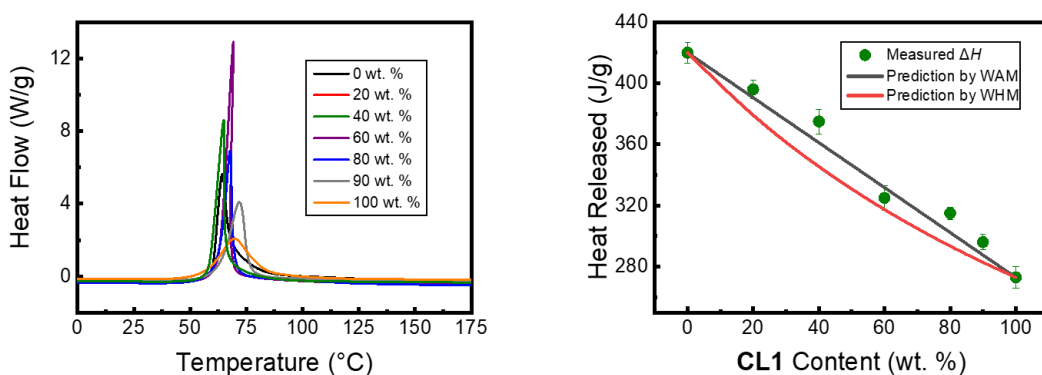


Figure 5.17 DSC traces (left) and heat released data (right) of copolymerization of ENB and CL1.

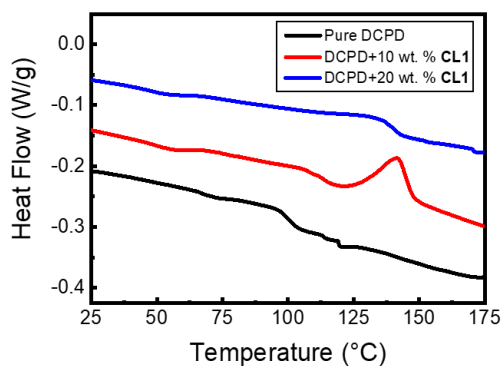


Figure 5.18 T_g of thermoset samples with different CL1 content. The sample for T_g measurement was taken from the part without the thermocouple. Then it was subjected to ramp scans from -50 to 200 °C at 10 °C/min.

5.9 References

- (1) Robertson, I. D.; Yourdkhani, M.; Centellas, P. J.; Aw, J. E.; Ivanoff, D. G.; Goli, E.; Lloyd, E. M.; Dean, L. M.; Sottos, N. R.; Geubelle, P. H.; et al. Rapid Energy-Efficient Manufacturing of Polymers and Composites via Frontal Polymerization. *Nature* **2018**, *557*, 223–227.
- (2) Mol, J. C. Industrial Applications of Olefin Metathesis. *J. Mol. Catal. A Chem.* **2004**, *213*, 39–45.
- (3) Robertson, I. D.; Pruitt, E. L.; Moore, J. S. Frontal Ring-Opening Metathesis Polymerization of Exo-Dicyclopentadiene for Low Catalyst Loadings. *ACS Macro Lett.* **2016**, *5*, 593–596.
- (4) Szalay, J.; Nagy, I.; Bányai, I.; Deák, G.; Bazsa, G.; Zsuga, M. High Temperature Copolymerization of Styrene and Maleic Anhydride in Propagating Polymerization Front. *Macromol. Rapid Commun.* **1999**, *20*, 315–318.
- (5) Hu, T.; Chen, S.; Tian, Y.; Pojman, J. A.; Chen, L. Frontal Free-Radical Copolymerization of Urethane-Acrylates. *J. Poly. Sci. Part A. Polym. Chem.* **2006**, *44*, 3018–3024.
- (6) Pojman, J. A.; Elcan, W.; Khan, A. M.; Mathias, L. Binary Frontal Polymerization: A New Method to Produce Simultaneous Interpenetrating Polymer Networks (SINs). *J. Polym. Sci. Part A Polym. Chem.* **1997**, *35*, 227–230.
- (7) Nuvoli, D.; Alzari, V.; Pojman, J. A.; Sanna, V.; Ruiu, A.; Sanna, D.; Malucelli, G.; Mariani, A. Synthesis and Characterization of Functionally Gradient Materials Obtained by Frontal Polymerization. *ACS Appl. Mater. Interfaces* **2015**, *7*, 3600–3606.
- (8) Scognamillo, S.; Alzari, V.; Nuvoli, D.; Illescas, J.; Marceddu, S.; Mariani, A. Thermoresponsive Super Water Absorbent Hydrogels Prepared by Frontal Polymerization of N-Isopropyl Acrylamide and 3-Sulfopropyl Acrylate Potassium Salt. *J. Polym. Sci. Part A Polym. Chem.* **2011**, *49*, 1228–1234.
- (9) Yan, Q. Z.; Zhang, W. F.; Lu, G. D.; Su, X. T.; Ge, C. C. Frontal Polymerization Synthesis of Starch-Grafted Hydrogels: Effect of Temperature and Tube Size on Propagating Front and Properties of Hydrogels. *Chem. - A Eur. J.* **2006**, *12*, 3303–3309.
- (10) Vicini, S.; Mariani, A.; Princi, E.; Bidali, S.; Pincin, S.; Fiori, S.; Pedemonte, E.; Brunetti, A. Frontal Polymerization of Acrylic Monomers for the Consolidation of Stone. *Polym. Adv. Technol.* **2005**, *16*, 293–298.

- (11) Perry, M. F.; Volpert, V. A.; Lewis, L. L.; Nichols, H. A.; Pojman, J. A. Free-Radical Frontal Copolymerization: The Dependence of the Front Velocity on the Monomer Feed Composition and Reactivity Ratios. *Macromol. Theory Simulations* **2003**, *12*, 276–286.
- (12) Pujari, N. S. Frontal Polymerization: Synthesis of Homo and Copolymers. **2007**.
- (13) Rule, J. D.; Moore, J. S. ROMP Reactivity of Endo- and Exo-Dicyclopentadiene. *Macromolecules* **2002**, *35*, 7878–7882.
- (14) Donald R. Askeland, Pradeep P. Fulay, W. J. W. *The Science and Engineering of Materials*; **2010**; Vol. sixth edit.
- (15) Kim, H. S.; Hong, S. I.; Kim, S. J. On the Rule of Mixtures for Predicting the Mechanical Properties of Composites with Homogeneously Distributed Soft and Hard Particles. *J. Mater. Process. Technol.* **2001**, *112*, 109–113.
- (16) Pojman, J. A.; Griffith, J.; Nichols, H. A. Binary Frontal Polymerization: Velocity Dependence on Initial Composition. *E-Polymers* **2004**, No. 013, 1–7.
- (17) Pojman, J. A.; Varisli, B.; Perryman, A.; Edwards, C.; Hoyle, C. Frontal Polymerization with Thiol-Ene Systems. *Macromolecules* **2004**, *37*, 691–693.
- (18) Devadoss, D. E.; Pojman, J. A.; Volpert, V. A. Mathematical Modeling of Thiol-Ene Frontal Polymerization. *Chem. Eng. Sci.* **2006**, *61*, 1261–1275.

Chapter 6: Summary and Outlook

6.1 Summary

This dissertation presents ROMP monomer design that enables two different applications, dynamic remodeling and rapid manufacturing. The polymerization behavior is modulated by rational selection of ring size and incorporation of substituents. We systematically investigated structure-property relationships to probe how subtle structural variation dramatically alters the overall performance, which not only strengthens the fundamental understanding of ROMP chemistry but also guides functional materials design.

In Chapter 2, we systematically studied the polymerization-depolymerization behavior of low-strain cyclopentene derivatives in equilibrium ROMP. To quantify the depolymerizability, T_c values of monosubstituted cyclopentenes in both solution and bulk polymerization were determined by VT-NMR and DSC, respectively. We found that a bulky substituent at the homoallylic position greatly reduces ring strain and T_c , allowing the resulting polyentenamer to depolymerize under solvent-free conditions at elevated temperatures ranging from 40-100 °C. The depolymerization behavior could be fine-tuned by selecting anchor groups with a decreasing T_c in the order of $-OR > -COOR > -CH_2OR$.

With the feasibility assessed by systematic T_c studies, thermally reversible networks were developed in Chapter 3 based on di- or trifunctional cyclopentene derivatives. The depolymerizability of the network polymer is readily modulated either by incorporating different anchor groups or copolymerizing with a low- T_c cyclopentene derivative. Therefore, the neat liquid monomers undergo ROMP at room temperature to afford mechanically robust network polymers (G' in MPa region) with high yields; the resulting polymers fully depolymerize to a free-flowing liquid (viscosity of 10^{-2} Pa·s) at slightly elevated temperatures. This process is triggered solely by a mild thermal stimulus and is reversible for several cycles, characterized by DSC and rheological tests. Although the reversibility is limited by the catalyst lifetime, moderate recovery efficiency was achieved by copolymerization.

While ROMP of low-strain monomers is a delicate equilibrium, highly strained cyclic olefins polymerize rapidly and release large amounts of heat which could be employed as the

energy source for FROMP. We examined 30 strained monomers and expanded the toolbox of FROMP in Chapter 4. To build a quantitative structure-property relationship, linear regression analysis was first utilized based on the hypothesis that v_f is proportional to the heat release rate. Even though it did not perform well for structurally disparate monomers, linear relationships between v_f and monomer properties (such as MW and ΔH) were observed. In addition, anchor group plays a significant role with v_f decreasing in the order of $-\text{COOR} \approx -\text{CH}_2\text{OCOR} > -\text{CH}_2\text{OR} > -\text{OR}$. Since FROMP is a complicated process where numerous factors interact, machine learning approaches were further applied. Models based on 17 monomers that possess steady v_f values were constructed with reasonable predictability, and important features that determine FROMP performance were also identified. Some of the patterns recognized by the ML models agree well with our conclusions from previous structure-property relationship studies. Furthermore, it suggests that electrostatic interactions, bond angles and dipole moment might be the origin of the anchor group effect.

Chapter 5 investigates the copolymerization behavior in FROMP. Usually, the mixture property lies between the corresponding properties of pure components. However, a non-monotonic increase in v_f was observed in copolymerization with di-NBE cross-linkers, which contradicts the intuitive understanding of the mixing rules. After examining the copolymerization behavior of a series of monomers such as mono-NBE derivatives and di-NBE cross-linkers with different MW, we believe the degree of cross-linking is mainly responsible for this unusual behavior. As the loading of di-NBE increases, the cross-linked structure brings the reactive C=C to proximity, which increases the effective C=C concentration and accelerates the front propagation. When the cross-linking density becomes too high with di-NBE wt. % further increasing, limited chain mobility would retard the polymerization. In addition, molarity of C=C of the cross-linker also plays a role in v_f acceleration. The copolymerization study not only provides a strategy to systematically modify materials physical properties (such as interfacial shear strength and mechanical properties) but also contributes to fundamental understanding of FROMP.

6.2 Outlook

FROMP enables rapid, energy-efficient fabrication of thermoset and composite materials, which is applicable to a variety of manufacturing technologies. Further advancements require precise control over FROMP performance such as v_f and rheological profiles. Fundamental understanding with the aid of modeling would greatly benefit the application of monomer study to functional materials design.

Other than thermodynamic, kinetic, and physical properties of a monomer, cross-linking degree is one crucial parameter that modulates FROMP behavior based on the conclusions from Chapter 4 and 5. The ability to form cross-links could either be a promoter or an inhibitor in FROMP. Since cross-linking density directly determines the mechanical properties, a model that quantitatively describes the correlation between v_f and cross-linking degree would allow accurate prediction on FROMP performance and development of functional materials with tunable mechanical properties.

Understanding how monomer structures affect gel time (or pot life) is also important, especially when it comes to FRPC manufacturing. From the monomers we investigated so far, incorporating substituents on the ring substantially shortens the gel time, and *endo*-DCPD has the longest gel time. As there is no clear correlation between v_f and gel time, fundamental understanding of DCPD gel formation and its microstructure is essential towards the engineering of functionalized composite materials with controllable rheological profiles.

Many functionalized molecules have been proven to be excellent FROMP monomer candidates in Chapter 4, and our next step is to apply these monomers to functional materials manufacturing. Some success has been achieved in improving the interfacial shear strength by employing a norbornene derivative with an epoxide moiety. Similarly, other modifications on material properties such as hydrophilicity would be accomplished by installing the desirable functionality on the monomer.